ARL-SR-0511 ● Nov 2025

DEVCOM
ARMY RESEARCH LABORATORY

Proceedings of the 2025 DoD Basic Research Conference

Dashiell L.P. Vitullo, Chase T. Ellis, Mahesh R. Neupane,
Luke A. Baldwin, and Maureen E. Kperogi

NOTICES

Disclaimers

ARL-SR-0511 ● Nov 2025

Proceedings of the 2025 DoD Basic Research Conference

Dashiell L.P. Vitullo
Technical Lead, DEVCOM Army Research Laboratory

Chase T. Ellis
Technical Committee, U.S. Naval Research Laboratory

Mahesh R. Neupane
Technical Committee, DEVCOM Army Research Laboratory Army Research Office

Luke A. Baldwin
Technical Committee, Air Force Research Laboratory

Maureen E. Kperogi
Conference Chair, DoD Basic Research Office

REPORT DOCUMENTATION PAGE

1. REPORT DATE	2. REPORT TYPE	3. DATES COVERED: START DATE	END DATE
November 2025	Special Report	5 AUG 2025	8 AUG 2025

4. TITLE AND SUBTITLE
Proceedings of the 2025 DoD Basic Research Conference

5a. CONTRACT NUMBER	5b. GRANT NUMBER	5c. PROGRAM ELEMENT NUMBER

5d. PROJECT NUMBER	5e. TASK NUMBER	5f. WORK UNIT NUMBER

6. AUTHOR(S)
Dashiell L.P. Vitullo, Chase T. Ellis, Mahesh R. Neupane, Luke A. Baldwin, and Maureen E. Kperogi

7. PERFORMING ORGANIZATION NAME(S) AND ADDRESS(ES)	8. PERFORMING ORGANIZATION REPORT NUMBER
DEVCOM Army Research Laboratory ATTN: FCDD-RLA-NB Aberdeen Proving Ground, MD 21005	ARL-SR-0511

9. SPONSORING/MONITORING AGENCY NAME(S) AND ADDRESS(ES)	10. SPONSOR/MONITOR'S ACRONYM(S)	11. SPONSOR/MONITOR'S REPORT NUMBER(S)

12. DISTRIBUTION/AVAILABILITY STATEMENT
DISTRIBUTION STATEMENT A. Approved for public release: distribution unlimited.

13. SUPPLEMENTARY NOTES

14. ABSTRACT
The collected abstracts herein constitute the Proceedings of the 2025 DoD Basic Research Conference.

15. SUBJECT TERMS
Proceedings, DoD Basic Research, 2025

16. SECURITY CLASSIFICATION OF: a. REPORT	b. ABSTRACT	C. THIS PAGE	17. LIMITATION OF ABSTRACT	18. NUMBER OF PAGES
UNCLASSIFIED	UNCLASSIFIED	UNCLASSIFIED	UU	191

19a. NAME OF RESPONSIBLE PERSON	19b. PHONE NUMBER *(Include area code)*
Dashiell L.P. Vitullo	(520) 691-5034

STANDARD FORM 298 (REV. 5/2020)
Prescribed by ANSI Std. Z39.18

Contents

Preface

The 2025 DoD Basic Research Conference showcased groundbreaking research, facilitated collaboration, and informed researchers about opportunities in basic research.

Conference Chair: Dr. Maureen Erinne Kperogi

Creation of the conference technical program and editing of this document were overseen by the Technical Committee (membership listed above).

The conference featured 16 topics, each with a topic lead and some with a supporting topic committee:

Topic	**Topic Lead**	**Topic Committee**
Biological Sciences	Rasha Rammamieh	Aarti Gautam
Synthetic Biology and Bionanotechnology	Michael Goodson	Svetlana Harbaugh, Jorge Chavez, Amy Breedon
Materials Sciences and Discovery	John Lyons	Latha Nataraj
Additive Manufacturing	Jian Yu	Alexander Butler
AI & Data Science	Dan Cassenti	Ruoting Yang, Tung-Duong Tran-Luu, Marvin Conn, Jesse Milzman
Quantum Science & Technologies	Brian Kirby	Daniel Jones
Robotics and Manufacturing	Sean Donegan	
Ultra-Wide Band Gap	Elias Garratt	John Lyons, Mihee Ji, David Storm
Power & Energy	Christopher Chiara	
Electromagnetic Sciences	Henrique Schmitt	
Emerging Electronics	Blair Connelly	
Optics and Photonics	Sang-Yeon Cho	Chase Ellis
Social Sciences	Alex Wind	Laura Steckman, Michael Natali
Weapons Sciences and Directed Energy	Christopher Crouse	Kelsea Miller
Acoustics	Caleb Sieck	Carl Hart, Vijaykumar Peddinti
Mathematical Science	Philip Buskohl	

1. Topic: Biological Sciences

1.1 Session: Biological Sciences for Military Applications

Compact, Electronically-Readable Point-of-Care Immunoassays

David A. Kidwell* and Kevin Le+

*U.S. Naval Research Laboratory, Washington, DC 20375
+ NOVA Research, Inc., Alexandria, VA 22308, USA
Corresponding Author Email: David.A.Kidwell6.civ@us.navy.mil
Keywords: Lateral-flow immunoassay, LFIA, Point-Of Care diagnostics, POC

Lateral-Flow Immunoassays (LFIAs) are nearly ideal point-of-care technology. They are portable, rapid, self-contained, inexpensive to manufacture, can detect diverse species and diseases, and require no power to operate. They are widely used as pregnancy, HIV, or influenza tests, and most recently for detection of COVID-19. However, typical LFIAs are not quantitative nor are they sufficiently sensitive to diagnose a disease in the early stages. We have developed a form of LFIAs that can be electronically read with inexpensive and portable readers the size of home glucometers. This system leverages our proven methodology of using catalytic nanoparticle labels with LFIA technology[1] yielding a 500-fold improvement in sensitivity over commercial LFIAs using gold nanoparticles. Our electronic readable system is known as fcLFIA™ or the fuel cell Lateral Flow ImmunoAssay and adopts the principles of fuel cells to provide signal transduction.[2] The catalytic nanoparticle labels used as the biological labels, once captured, complete the fuel cell and the electrons produced are easily measured. Our system is unique in that the fcLFIA actually produces power that is measured, rather than imposing an outside potential and measuring some redox reaction at the capture electrode. The signal is robust, long-lived, and requires only a simple volt meter-like detection system for digitization. Thus, the platform can be quite small and low-power, potentially even solar powered. The principles behind our fcLFIA™ platform, its design, representative data, and its potential to deliver meaningful diagnostic sensitivity in the same simple format as a LFIA will be presented.

[1] S.P. Mulvaney, D.A. Kidwell, J.N. Lanese, R.P. Lopez, M.E. Sumera, and E. Wei, “Catalytic Lateral Flow Immunoassays (cLFIA): Amplified Signal in a Self-Contained Assay Format”, *Sens. Bio-Sens. Res.*, **30** (2020) 100390.

[2] David Kidwell, “Compact, Electronically-Readable Point-of-Care Immunoassays”, US-20230288412-A1, 09-14-2023.

Phase Separation as a Design Paradigm for Engineering Adaptive Biological Materials

Youngchan Kim

U.S. Naval Research Laboratory, Washington, DC 20375
Email: youngchan.kim2.civ@us.navy.mil
Keywords: Biomolecular condensates, phase separation, intrinsically disordered proteins, coarse-grained model.

Biomolecular phase separation drives the formation of dynamic, membraneless structures in living systems. These condensates offer a blueprint for engineering adaptive biological materials that respond to environmental cues, self-organize, and reconfigure in real time. Intrinsically disordered proteins (IDPs), through weak, multivalent interactions, are key drivers of this behavior. Understanding the sequence determinants of phase separation and molecular basis of condensate material properties is essential for designing programmable biomolecular systems. Our work investigates the phase behavior and material properties of condensates using molecular simulations of sequence-specific coarse-grained IDP models. We show that tuning sequence composition — and specifically, charge patterning — modulates multivalent interactions, enabling control over condensate formation, morphology, and viscoelasticity. These phase-separated systems can exhibit programmable compartmentalization, stress responsiveness, and tunable mechanical properties—features critical for materials intended to operate in extreme or unpredictable environments. This framework establishes phase separation as a design paradigm for creating soft, self-healing, or responsive biological materials tailored to DoD needs for adaptable, resilient, and multifunctional platforms.

Understanding the Robustness and Persistence of Dynamic Structures Formed by Ant Self-Assemblages

Michael L. Mayo[1,*], Kevin R. Pilkiewicz[1], Audrey B. Harrison[1], and Anne M. Mayo[1]

[1]Environmental Laboratory, U.S. Army Corps of Engineers, 3909 Halls Ferry Rd, Vicksburg, MS 39180
**Corresponding Author Email: Michael.L.Mayo@erdc.dren.mil*

Keywords: Collective Motion, Complex Systems, Structural Self-Assembly, Critical Behavior

A remarkable phenomenon of nature is that organisms self-organize into complex structures that function in a wide range of inhospitable environments. One example involves the raft-like self-assemblages of the fire ant *Solenopsis invicta* (Insecta: Formicidae), which exhibit tether-like protrusions at the boundary wherein individuals bind to each other and form a structural mass (**Fig. 1**). Tethers grow and shrink as individuals detach into the free-moving layer of the raft's surface. A cycle of renewal at the raft periphery results from individuals transitioning between the free and bound structural states in a process called "treadmilling," which itself persists for several hours until the ants eventually become inactive and the entire raft degrades. This begs the question of how individual behavior (via treadmilling) affects the overall lifetime of an ant self-assemblage. More precisely, we suspect that ant rafts represent a "metastable" state, i.e., constantly on the verge of collapse until the ants rearrange themselves into a new configuration with an extended lifetime. This idea is consistent with the Bak-Tang-Wiesenfeld theory of "self-organized criticality" (SOC) and may explain the formation of metastable structures that are not "finely tuned" to a specific parameter value, but rather emerge from a wide range of initial conditions and are therefore robust to perturbations. Whether ant self-assemblages are critically metastable remains an open question, but oscillatory behavior (such as tether growth and contraction) has been linked before to SOC theory. Here we conduct an experimental investigation of ant self-assemblages by recording video of the dynamically evolving structure of self-assembled ant rafts over a broad range of timescales (minutes to hours) and use tracking software to isolate the trajectories of individual ants as they traverse the surface layer of the raft. We then aim to develop agent-based models with local interaction rules inspired by our findings that can reproduce the kind of dynamic self-organized structures exhibited by fire ants. This 6.1 basic research project supports Army priority research areas of Autonomy and Materials by Design.

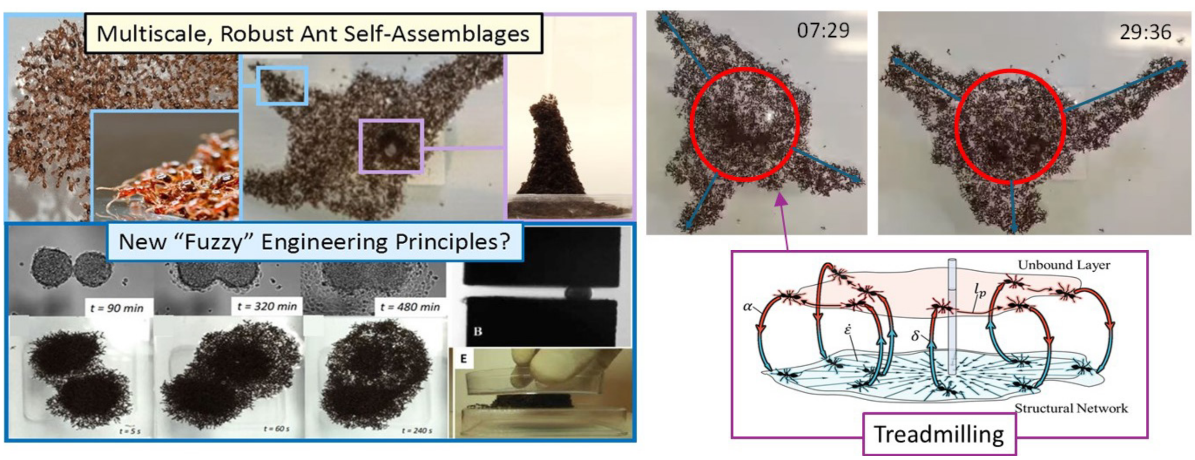

Fig. 1 – Materials degrade over time, but ant self-assemblages demonstrate a persistence of function in harsh conditions. (Left) Understanding how these systems actively renew and heal their structure could lead to breakthroughs in self-healing, or synthetic "active matter" materials. (Right) Dynamic treadmilling alters boundaries and contributes to structural persistence via ant renewal.

Funding: Funding was provided by the U.S. Army Engineer Research and Development Center (ERDC) through the Installations and Operational Environment (IOE) 6.1 basic research program. Opinions, interpretations, conclusions, and recommendations are those of the author and are not necessarily endorsed by the U.S. Army.

Plug Equilibration Enzyme Kinetic (PEEK) Assay Development for Rapid Down-Selection of Bioprospected Isolates

Joseph M. Pennington IV [1,^] and Rebecca L. Renberg [1,^,*]

[1]DEVCOM Army Research Laboratory, Biological & Biotechnology Sciences Division, 2800 Powder Mill Road, Adelphi, MD 20783
^ authors contributed equally to the work
**Corresponding Author Email: rebecca.l.renberg.civ@army.mil*
Keywords: enzyme kinetics, bioprospecting, assay development

The Department of Defense has a strong interest in circular manufacturing efforts to upcycle waste materials reducing the sustained logistical burden on forward deployments. Bioprospecting efforts at DEVCOM ARL are identifying novel organisms that metabolize polymeric material through deep sequencing and metagenomics analysis. Sequencing and enzymatic analysis, however, is time- and labor- intensive requiring 16+ weeks to screen, isolate, and identify an isolate of interest. To expediate this screening, we have developed a technically simplistic, yet powerful, assay to potentially identify isolates of interest prior to species identification for polymer-degradation studies. The plug equilibration enzyme kinetic (PEEK) assay directly quantifies the enzymatic activity from an agar plug in a high-throughput 96-well format without the need for organism outgrowth or enzymatic purification. Through development of the PEEK assay, we have reduced the time required to identify priority isolates from 16 to 8 weeks, significantly reducing the timeline to discovery.

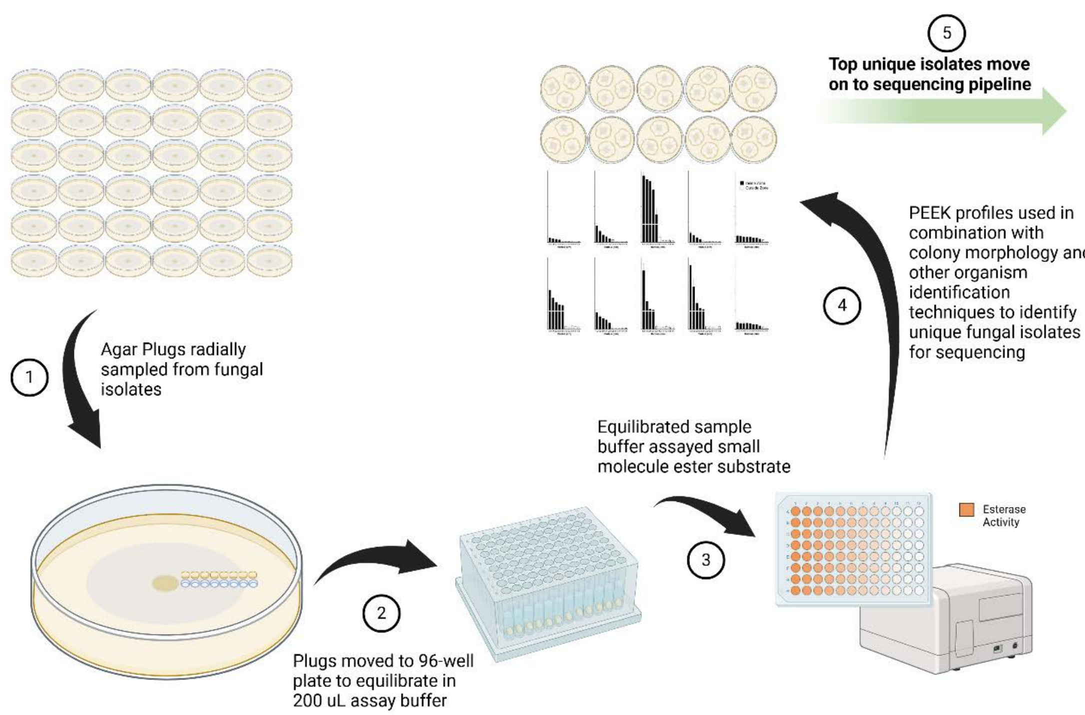

Fig. 1 - Overview of the PEEK Assay Workflow.

Volatile Compound Emission Signatures as Sentinels of Permafrost Thaw in Arctic Environments

Morgan Conrady[1,*], Thomas Douglas[2], Gwendolyn Reeser[1], Ryan Busby[1], Kyoo Jo[1], and Donald Cropek[1]

[1]Construction Engineering Research Laboratory, Engineer Research and Development Center, 2902 Newmark Drive, Champaign, IL, 61822

[2]Cold Regions Research and Engineering Laboratory, Engineer Research and Development Center, Building 4070, 9th Avenue, Fort Wainwright, AK, 99703

**Corresponding Author Email: Morgan.W.Conrady@usace.army.mil*

Keywords: permafrost; volatile compounds; arctic environments; emission signature; thermokasrst

Permafrost is soil, rock, ice, and organic matter that has remained at 0ºC or lower for two or more years.[1] It is primarily found in the Northern Hemisphere underlying 24% of North America, and a significant portion of Alaska (85%) and Canada (50%).[2] Permafrost thickness varies in the environment as latitudes and locations change across permafrost covered areas.[3] The seasonally thawed active layer sits above the near surface permafrost layer (~45 cm) (Fig. 1). Snow, ice, and permafrost all contain frozen forms of water in cold Arctic regions that are both ubiquitous and intimately connected to vegetation and soil conditions. We hypothesized that frozen aqueous sinks store significant hydrophilic biogenic chemicals which could potentially be used to detect the condition and status of these environments. When changes occurred to these aqueous sinks from permafrost thaw, the fate of these chemicals could potentially be used to detect these changes. We collected a variety of samples including permafrost cores, thermokarst, surface vegetation, and snow *in situ* from the Engineer Research and Development Center (ERDC) Permafrost Tunnel and Farmer's Loop research sites in Interior Alaska. We used direct injection into a gas chromatography- mass spectrometry (GC-MS) system to examine volatile samples. Military operations require knowledge of soil and environmental conditions during maneuvers and in operational planning. Of particular interest is soil strength as this is a fundamental condition that regulates viable types of maneuvers. This research provides breakthrough information to improve Army awareness of cold region surface soil and vegetation conditions. Additionally, this information provides knowledge of how permafrost affects the environment and vice versa by identifying chemicals that are stored and released during natural environmental processes.

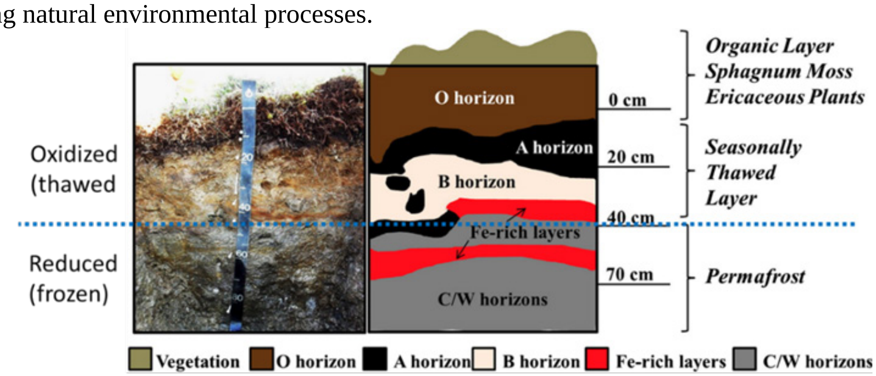

Fig. 1 – Oxidized and reduced soil and permafrost layers. Note the seasonally thawed active layer is present at ~45cm and is readily identifiable by the transition from oxidized to reduced conditions.[4]

Funding: This work was funded by the U.S. Army Engineer Research and Development Center Installations and Operational Environment 6.1 Basic Research Program.

References:

[1] J. Obu, " How Much of the Earth's Surface is Underlain by Permafrost?" *JGR Earth Surface*, vol 126, no. 5, p. 1, Apr. 2021, doi: e2021JF006123.
[2] S.L. Smith, V.E. Romanovsky, A.G. Lewkowicz, C.R. Burn, M. Allard, G.D. Clow, K. Yoshikawa, J. Throop. "Thermal state of permafrost North America: a contribution to the international polar year." Permafrost and Periglacial Processes, vol. 21, no. 2, p. 117, Apr. 2010, doi: 10.1002/ppp.690.
[3] M. Stieglitz, S.J. Dérv, V.E. Romanovsky, T.E. Osterkamp. "The role of snow cover in the warming of arctic permafrost." Geophysical Research Letters, vol. 30, no. 13, p. 1721, Jul. 2003, doi: 10.1029/2003GL017337.
[4] A.J. Barker, T.A. Douglas, A.D. Jacobson, J.W. McClelland, A.G. Ilgen, M.S. Khosh, G.O. Lehn, T.P. Trainor. "Late season mobilization of trace metals in two small Alaska arctic watersheds as a proxy for landscape scale permafrost active layer dynamics. Chemical Geology, vol. 381, p. 180, May 2014.

Exploiting Cross-Kingdom Communication: Amplifying Plant-Microbe Signaling Pathways for Desired Output

Alice Goldstein-Plesser[1], Kory Rankin[1], Anna Ulanova[,2], Franz Lichtner[1,*]
[1]*USACE Engineer Research Development Center, Cold Regions Research Engineering Laboratory, 72 Lyme Road, Hanover, NH 03755*
[2]*ORISE, 1299 Bethal Valley Road, Oak Ridge, TN 37830*
**Corresponding Author Email: franz.j.lichtner@usace.army.mil*
Keywords: plant-microbe interactions, volatile organic compounds, signaling

Plants and their associated microbes constitutively produce volatile organic compounds (VOCs), and can change VOC profiles when triggered by injury, environmental stress, or pathogen presence[1], [2], [3]. However, the scale of the impact of leaf associated microbiota (phylosphere) on plant VOC signaling is unknown. By characterizing this complex interaction between plants and the phylosphere at the regulatory and chemical level, this cross-kingdom communication may be exploited to effectively amplify signals of environmental change. **We hypothesize that phylosphere manipulation via microbial inoculation will both change the VOC profile of plants, and that this manipulation can be hijacked to amplify signals of specific environmental changes.** We first established a model system using the environmental bacterium *Bacillus subtilis* and tested its capacity to establish a phylosphere community on three different plant species. We then used this model system to test the change in VOC production of plants with or without phylosphere amendment, showing that VOC production was impacted phylosphere amendments. We expanded this work to use the plant-microbe system to measure environmental changes in the form of rare earth elements (REE) in the soil. Due to raising concern and interest in REE availability, we tested the capacity of our model plant-microbe system to respond to three different REEs (Lanthanum, Cerium, and Yttrium) dosed into the soil. We are continuing to characterize the genetic regulation of VOC and the impacts microbes have on signaling pathways. This work has demonstrated that VOC profiles from plants can be both manipulated by bacterial amendment and may be used to highlight environmental shifts of interest.

Funding: DoD Army Basic Research 6.1 Installations Operations and Environment

References:

[1] Y. T. Cheng, L. Zhang, and S. Y. He, “Plant-Microbe Interactions Facing Environmental Challenge,” *Cell Host Microbe*, vol. 26, no. 2, pp. 183–192, Aug. 2019, doi: 10.1016/j.chom.2019.07.009.

[2] F. O. Chagas, R. de C. Pessotti, A. M. Caraballo-Rodríguez, and M. T. Pupo, “Chemical signaling involved in plant–microbe interactions,” *Chem. Soc. Rev.*, vol. 47, no. 5, pp. 1652–1704, 2018, doi: 10.1039/C7CS00343A.

[3] Y. Yang, J. Shah, and D. F. Klessig, “Signal perception and transduction in plant defense responses.,” *Genes Dev.*, vol. 11, no. 13, pp. 1621–1639, Jul. 1997, doi: 10.1101/gad.11.13.1621.

2. Topic: Synthetic Biology and Bionanotechnology

Vampire Amoebae as Fungal Biocontrol Agents: Genomics and Comparative Transcriptomics of Mycophagy

Presenter: Gabriel Schuler

Authors: Robert Jones[1], Rebecca Renberg[1], & Gabriel Schuler[1]

[1]*DEVCOM Army Research Laboratory, 2800 Powder Mill Road, Adelphi, MD 20783*

Filamentous fungi are diverse group of organisms known to biofoul and degrade a wide range of materials. For decades the MIL-STD-810 has been used by the US Military to test fungal growth and potential impact on military materials and equipment. Many filamentous fungi are resistant to antifungal compounds and cleaning agents due to their protective cell wall and diverse biochemical pathways. A potential solution to stop fungal biofouling on materiel is to develop antifungals from natural fungal predators. Fungal predators like the Vampyrellids, colloquially known as vampire amoebae, have evolved unique feeding strategies to overcome the defense mechanisms of filamentous fungi. We tested the ability of multiple predatory amoebas to feed on and stop the growth of filamentous fungi. We demonstrated that the amoeba *Cryptodifflugia oviformis* is effective at killing all five MIL-STD-810 fungi. To better understand the molecular mechanisms of mycophagy we sequenced genomic DNA of three protist species shown to feed on filamentous fungi, *Cryptodifflugia oviformis, Deuteramoeba mycophaga*, and *Platyreta germanica,* using Oxford Nanopore Technologies (ONT) long read sequencing. Each of these cultures contained multiple strains of unidentified prokaryotes, therefore we treated each culture as a low diversity metagenome. We developed a fully automated bioinformatic pipeline to filter, assemble, and annotate the eukaryotic genomes from metagenomic ONT sequencing. To further elucidate the molecular toolkit of fungivorous predation, we performed a comparative transcriptomic analysis on the top fungal predator, *Cryptodifflugia oviformis*, at different stages of fungal predation. We identified and analyzed putative genes associated with fungal phagocytosis and found them consistent with predation on prokaryotes in model amoeba systems.

Programmable Whole-Cell Biosensors: Engineering Bacterial Transcription Factors for Precision Small Molecule Detection in E. coli

Hyunjung A. Kim[1,*], Charlie Johnson[2], Edward Perkins[1] and Inyup Paik[2,3]
[1]U.S. Army Corps of Engineers, Engineering Research and Development Center, Construction and Engineering Research Laboratory, 2902 Newmark Dr., Champaign, IL, 61822
[2]University of Texas at Austin, 2515 Speedway, Austin, TX 78712
[3]U.S. Army Corps of Engineers, Engineering Research and Development Center, Environmental Laboratory, 3909 Halls Ferry Rd, Vicksburg, MS 39180
**Corresponding Author Email: Hyunjung.A.Kim@usace.armys.mil*
Keywords: biosensor, transcription factor, small molecule, genetic circuits

Whole-cell biosensors offer a powerful platform for detecting small molecules with high specificity and adaptability. In this work, we present a framework for engineering E. coli-based biosensors using bacterial transcription factors engineered to respond to a target analyte. By repurposing and optimizing native bacterial transcription factors, we constructed genetic circuits capable of converting molecular binding events into quantifiable outputs as green fluorescence. We demonstrate potential of the tunability, dynamic range, and specificity of our sensors across a few small molecule targets, highlighting their potential for environmental monitoring, diagnostics, and metabolic engineering. This platform provides a foundation for rapidly deployable, programmable biosensors tailored to real-world detection challenges.

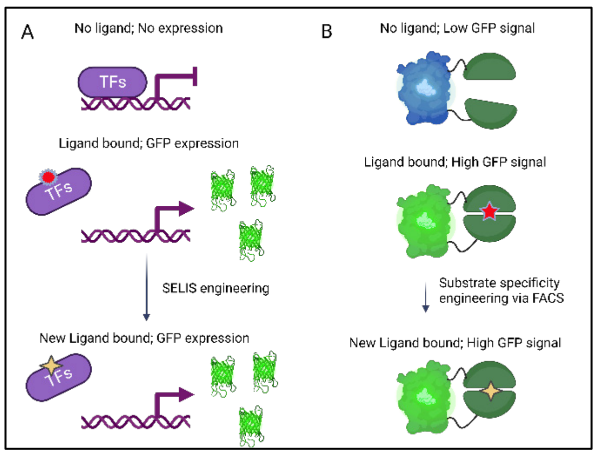

Fig. 1 – high throughput biosensor platform via E. coli whole cell for small molecule detection.

Design, Synthesis and Functional Validation of Fusion Cold Resistant Recombinant Lysozymes

Ping Gong[1,*], Xiao Luo[1], Natalie Barker[1] , Alexis Thompson[1,2], Andrew Maxwell[3] and Tim Schutt[1]

[1]Environmental Laboratory, [3]Information Technology Laboratory, U.S. Army Engineer Research and Development Center, 3909 Halls Ferry Road, Vicksburg, MS 39180

[2]Oak Ridge Institute for Science and Education, 1299 Bethel Valley Rd, Oak Ridge, TN 3783

**Corresponding Author Email: Ping.Gong@usace.army.mil*

Keywords: Fusion protein, cold resistance, lysozyme, biosynthesis, protein purification, functional assay.

The performance of enzyme-based biosensors in cold environments is often hindered by enzyme instability and reduced catalytic efficiency. To address this, we propose to engineer synthetic cold-tolerant lysozymes by fusing cold-sensitive wild-type enzymes (lysozymes as an example [1]) with antifreeze protein (AFP) domains [2]. Specifically, a lysozyme can be fused with an AFP ice-binding domain (IBD) via flexible peptide linkers at either the N- or the C-terminus. The fusion protein is subject to in silico modeling using AlphaFold [3], docking with a ligand (small substrate molecule) and molecular dynamic simulation to evaluate in silico its structural and functional properties. This approach allows for high-throughput ranking of thousands of fusion candidates in evaluating the gain-of-function potential of domain fusion for cold adaptation. Several lysozyme families were selected based on the availability of high-resolution crystal structures and prior success in heterologous expression using an *E. coli* cellular system. Fusion constructs were screened for structural integrity, foldability, and flexibility to prioritize high-confidence designs. Selected constructs were codon-optimized, cloned into T7-inducible *p*ET vectors, expressed in *E. coli* BL21, and purified using size exclusion chromatography and affinity columns. Protein expression and purity were verified using an Agilent Bioanalyzer. Enzymatic activity of purified lysozymes was confirmed individually using the EnzChek™ Lysozyme Assay Kit, whereas the AFP property was validated by determining the growth rates of *E. coli* expressing AFP at low temperatures. Initial results indicate that independently expressed lysozymes and AFPs retained their respective functions post-expression and purification. Ongoing work focuses on producing and validating the fusion proteins to confirm dual functionality. If successful, this study would demonstrate the feasibility of engineering lysozymes with cold tolerance without compromising catalytic activity. These results provide critical evidence for engineering new features into a protein and support broader applications in biosensing and synthetic biology under extreme conditions.

Funding: This work was supported by the Army Basic Research Program.

References:

[1] I. Inoue, M. Rechsteiner, "On the relationship between the metabolic and thermodynamic stabilities of T4 lysozymes. Measurements in Escherichia coli", J Biol Chem., Nov. 1994; vol. 269, no. 46, 29241-6.

[2] C. Wang, S. Pakhomova, M. E. Newcomer, B. C. Christner, B. H. Luo, "Structural basis of antifreeze activity of a bacterial multi-domain antifreeze protein", PLOS ONE, 2017, vol. 12, no. 11, e0187169.

[3] A. W. Senior, R. Evans, J. Jumper, et al., "Improved protein structure prediction using potentials from deep learning", Nature, Jan. 2020, vol. 577, 706–710.

Analog Epigenetic Memory Revealed by Targeted Chromatin Editing

Sebastian Palacios[1,2,3†], Simone Bruno[1,4†], Ron Weiss[2], Elia Salibi[1], Isabella Goodchild-Michelman[2], Andrew Kane[2], Katherine Illia[2,3] and Domitilla Del Vecchio[1,2*]

[1]Department of Mechanical Engineering, MIT, Cambridge, MA 02139
[2]Department of Biological Engineering, MIT, Cambridge, MA 02139
[3]Institute for Medical Engineering and Science, MIT, Cambridge, MA 02139
[4]Department of Data Science, Dana-Farber Cancer Institute, Boston, MA 02215
**Corresponding Author Email: ddv@mit.edu*
Keywords: synthetic biology, epigenetics, cellular memory, systems biology

Cells store information in the chromatin state by means of chemical modifications to DNA and histones that self-propagate through cell divisions and time. Although these modifications can keep gene expression silenced over generations, whether and how they maintain any other gene expression state remains unknown. Here, we found that chromatin modifications can maintain a wide range of gene expression levels over time, a phenomenon that we call analog epigenetic memory. We engineered a genomic reporter and epigenetic effectors to monitor with clonal resolution the gene expression dynamics following targeted perturbations to the chromatin state. Any gene expression level resulting from these perturbations stably persisted over time along with a distinct grade of DNA methylation. Altering the DNA methylation grade directly or interfering with DNA methylation maintenance resulted in permanent loss of gene expression memory. This identifies DNA methylation as the chief chromatin mark enabling analog epigenetic memory of gene expression. Consistent with the experiments, our chromatin modification model indicates that analog memory requires that the positive feedback between DNA methylation and Histone H3 Lysine 9 trimethylation (H3K9me3) is sufficiently weak. Our discovery will lead to a deeper understanding of epigenetic memory and to new tools for synthetic biology.

Funding: National Science Foundation, MODULUS Award Number 2027949, Vannevar Bush Faculty Fellowship ONR Award Number N00014-25-1-2053

Leveraging Cell-Free Synthetic Biology and AI for Scalable Point-of-care Diagnostics, Biomanufacturing, and Materials

David Garcia[1*]

[1]*Applied Synthetic Biology and Olfaction Branch, DEVCOM Chemical Biological Center, Ricketts Point Rd, Gunpowder, MD 21010*
**Corresponding Author Email: david.c.garcia62.ctr@army.mil*
Keywords: "Synthetic Biology", "Cell-free" "Machine Learning", "Biosensing", "Biocatalysts".

Cell-free synthetic biology is a powerful tool that enables transcription and translation through cell-free protein synthesis (CFPS), as well as biocatalytic transformations via cell-free metabolic engineering (CFME), using the membrane-free cytoplasmic contents of the cell. By circumventing the constraints of cellular physiology and evolutionary pressures, cell-free systems offer a modular approach to biological transformations, allowing for the rapid characterization of individual biological components with precise control over the chemical environment. These tools redefine how we engineer biological systems for applications in health, materials, and energy. However, the fundamental knowledge and high-throughput techniques necessary to select ideal biocatalysts, reaction conditions, and production platforms are limited. In this talk, I will share my research addressing these bottlenecks to improve the function of cell-free synthetic biology towards scalable applications (Fig. 1). First, we demonstrate the ability to rapidly optimize robust point-of-care diagnostics by leveraging a 384-well solid matrix format, acoustic liquid handling, and machine vision to improve the heat-resistance of freeze-dried cell-free biosensors[1]. Second, we showcase a framework to characterize and scale cell-free metabolism by developing a novel co-culturing technique for extract production and addressing batch-to-batch variability using high-throughput Design of Experiments and machine learning methods[2]. Lastly, I will share our recent progress integrating cell-free biological prototyping with large language models to accelerate the production of novel melanin materials and investigate the substrate scope and promiscuity of biological catalysts.

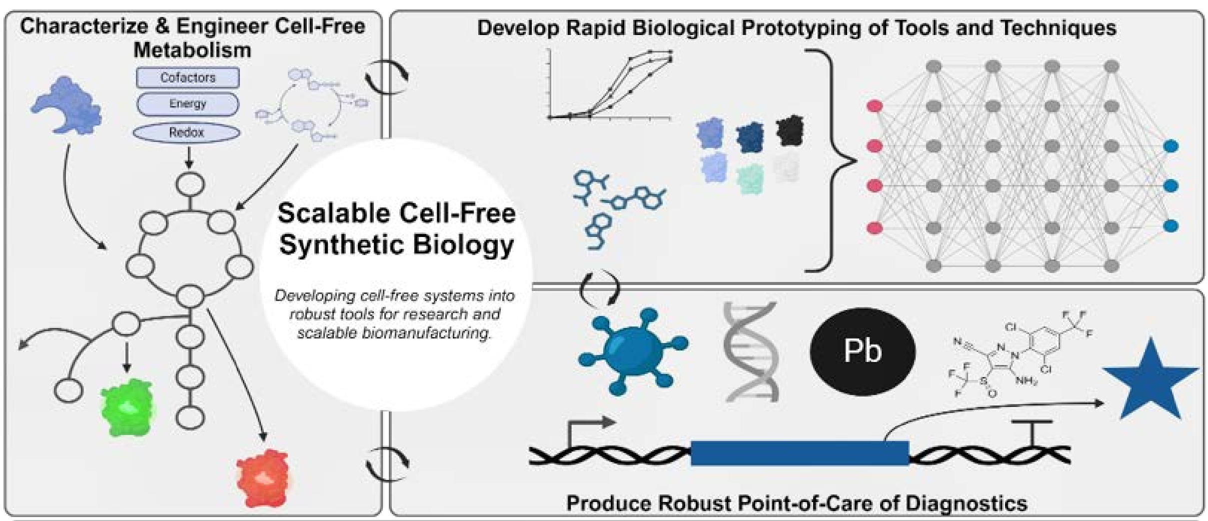

Fig. 1 – Understanding the systems level characteristics of cell-free synthetic biology enables cell-free biomanufacturing, not just in regards to the kinds of molecules we can produce, but also in our ability to reliably produce globally useful tools like biosensors, as well as our ability to enable more and more ambitious research through rapid biological prototyping.

References:

[1] D. C. Garcia, J. P. Davies, K. Rhea, M. Lee, and M. W. Lux, "Cell-Free Optimized Production of Protoporphyrin IX," bioRxiv
[2] D. C. Garcia, J. P. Davies, C. E. Davidson, D. A. Phillips, A. E. Miklos, and M. M. Lux, "High-Throughput Optimization of Paper-Based Cell-Free Biosensors," *bioRxiv*

Solution Blow Spinning of Cell-Free Functionalized Polymer Fibers

Jennifer Lee[1,2*], Susan Kozawa[2,3], Stephen Blum[2], Kris Van de Voorde[2], Marilyn Lee[2]
[1]*Defense Threat Reduction Agency, 8725 John J. Kingman Rd, Ft. Belvoir, VA 22060*
[2]*DEVCOM Chemical Biological Center, 8198 Blackhawk Rd, Aberdeen Proving Ground, MD 21010*
[3]*Oak Ridge Institute for Science and Education, 1299 Bethel Valley Rd, Oak Ridge, TN 37830*
**Corresponding Author Email: jennifer.a.lee80.civ@army.mil*
Keywords: cell-free protein synthesis, solution blow spinning, polymer, fibers, detection, sensing

Cell-free protein synthesis (CFPS) is a versatile synthetic biology platform that can be programmed to perform diverse functions by changing the DNA input into the system. Warfighter relevant functions include biomanufacturing, drug development, metabolic engineering, decontamination, and sensing. A key advantage of CFPS systems is their ability to be lyophilized for shelf storage and subsequently rehydrated in situ for on-demand field use [1].

While lyophilized CFPS systems have been traditionally implemented in tubes or on paper matrices, these configurations can be sensitive to environmental conditions like humidity, limiting their field application to controlled environments. Embedding CFPS systems into polymers offers a promising approach to expand their utility into more practical form factors that can be integrated into equipment, protecting the CFPS systems from environmental elements while providing versatile capabilities (Fig. 1).

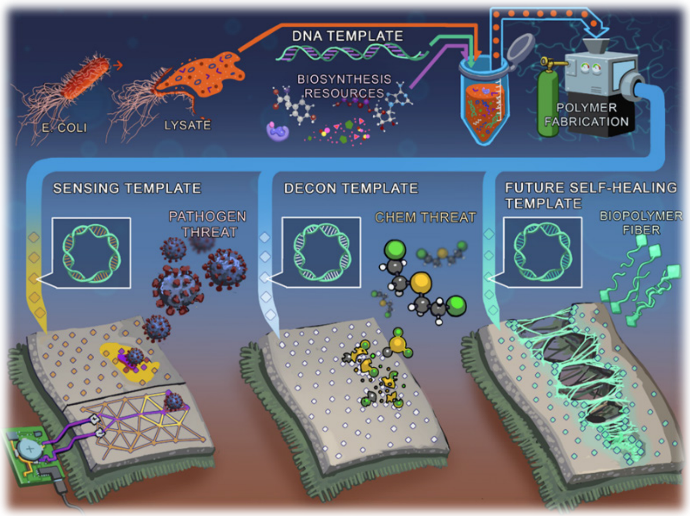

Fig. 1 – Cartoon depicting potential warfighter-relevant functionality of CFPS enabled polymer materials.

Our group has previously demonstrated that CFPS systems are tolerant to certain solvents and maintain functionality after being embedded in solvent-cast polymer films [2,3]. The presented work extends these findings by investigating the feasibility of embedding CFPS systems into polymer fibers, with potential end products including functionalized textiles, wipes, and filters. Solution blow spinning (SBS), a scalable technique using compressed air to pull fibers from polymer solutions, was employed to create non-woven fiber mats from polymer solutions containing lyophilized CFPS reactions. Polymer candidates include a range of hydrophobic and hydrophilic polymers, examining how processing conditions and polymer selection influence stability and activity of CFPS in nanofibers.

In this work we characterized fiber properties using scanning electron microscopy, energy dispersive x-ray analysis, and nuclear magnetic resonance spectroscopy. CFPS activity was assessed through colorimetric and fluorescent assays, including microscopy and video analysis. Biothreat detection capabilities were demonstrated using an RNA toehold switch sensor to detect genetic material. Additionally, we successfully spun fibers onto commercial off-the-shelf masks, illustrating the potential application of CFPS-embedded polymer fibers in practical contexts.

Funding: Funding was provided by the U.S. Army via the Chemical Biological Advanced Materials Manufacturing Program (PE 0601102A Project VR9) at the Combat Capabilities Development Command Chemical Biological Center.

References:

[1] Pardee, K.; Green, A.A.; Ferrante, T.; Cameron, D.E.; DaleyKeyser, A.; Yin, P.; Collins, J.J., Paper-based synthetic gene networks. *Cell* **2014,** *159* (4), pp 940-954.
[2] Lee, M.S.; Lee, J.A.; Biondo, J.R.; Lux, J.E.; Raig, R.M.; Berger, P.N.; Bernhards, C.B.; Kuhn, D.L.; Gupta, M.K.; Lux, M.W., Cell-Free Protein Expression in Polymer Materials. *Acs Synthetic Biology* **2024,** *13* (4), pp 1152-1164.
[3] Lee, M.S.; Raig, R.M.; Gupta, M.K.; Lux, M.W., Lyophilized Cell-Free Systems Display Tolerance to Organic Solvent Exposure. *ACS Synth Biol* **2020,** *9* (8), pp 1951-1957.

Peptide Based Liquid-Liquid Coacervates for Biosensing, Degradation Resistance, and as Biofoundries

Christopher M. Green[1], Angelica Rose-Galvan[1], Victoria Segal[1], Joyce C. Breger[1], Isabella Tiboni[2], Drew P. Lysne[1], Rein V. Ulijn[3], Igor L. Medintz[1], Sebastián A. Díaz[1,*]

[1]*Center for Bio/Molecular Science and Engineering, Code 6900, U.S. Naval Research Laboratory, Washington, DC 20375, United States*
[2]*U.S. Naval Research Laboratory Historically Black Colleges and Universities/Minority Institutions Internship Program, Washington, DC, 20002 USA*
[3] *Advanced Science Research Center (ASRC) at the Graduate Center City University of New York 85 St. Nicholas Terrace New York, New York 10031, United States*

**Corresponding Author Email: sebastian.a.diaz2.civ@us.navy.mil*
Keywords: DNA nanotechnology, Peptide Coacervates, Biosensing, Cell-free biosynthesis

Nature utilizes various materials such as peptides, nucleotides, and lipids to create order within complex environments such as cell interiors. Imitating nature, we combine DNA nanotechnology with peptide nanotechnology, specifically peptide based liquid-liquid phase separations, to access advanced functionalities. Peptide-based liquid-liquid phase separated domains, also known as coacervates, are neither pure homogenous liquid phase nor a heterogenous aggregate, displaying varying degrees of order.[1] Coacervates are of keen interest in cell biology, where they function as membraneless organelles, dynamically colocalizing enzymes and other biomolecules (e.g. RNA) to enhance translation and other operations. We recently demonstrated that sequestration of DNA biosensors within coacervates allows for i) a greater than 20-fold reduction of the limit of detection within coacervates when compared to control buffer solutions; ii) an increase in the kinetics, equilibrium was reached more than 4-times faster in coacervates; and iii) enhancement in the dye fluorescent quantum yields within the coacervates, resulting in greater signal-to-noise.[2] We have also found that coacervates protect DNA from nuclease degradation while subsequently allowing for release from the coacervate upon proper stimuli, which could have implications for nucleotide delivery applications. We hypothesize that the strong peptide-DNA interaction within the coacervates inhibits degradation and have preliminary evidence that this can be applied to other biological moieties, e.g. enzymes. In a third demonstration, enzymatic cascades are sequestered into coacervates improving product flux through the system by exploiting enzyme stabilization and intermediate channeling.

References

[1] Sheehan, et al., "Peptide-Based Supramolecular Systems Chemistry", **Chem. Rev.**, *121*, 13869, (2021).

[2] Green, et al., "Sequestration within peptide coacervates improves the fluorescence intensity, kinetics, and limits of detection of dye-based DNA biosensors", **Commun. Chem.**, *7*, 49, (2024).

Funding: Support from the OUSD RE in the form of a LUCI fellowship. R.V.U. acknowledges funding from Office of Naval Research for the Vannevar Bush Faculty Fellowship.

3. Topic: Materials Sciences and Discovery

3.1 Session: Semiconductors

Effective Doping Strategies for the Halide Perovskites

John L. Lyons[1,*], Michael Swift[1], Michael H. Stewart[2], Barbara A. Marcheschi[2], Paul D. Cunningham[3], Nicholas V. Proscia[3], and John P. Murphy[3], and Sarah Brittman[3]

[1]Center for Computational Materials Science, U.S. Naval Research Laboratory, Washington, DC 20375
[2]Optical Sciences Division, U.S. Naval Research Laboratory, Washington, DC 20375
[3]Electronics Division, U.S. Naval Research Laboratory, Washington, DC 20375
**Corresponding Author Email: john.l.lyons27.civ@us.navy.mil*
Keywords: "Halide perovskites, doping, first-principles calculations"

The halide perovskites, such as cesium lead bromide and methylammonium lead iodide, are high-performing light emitters and absorbers. For these applications, greater control over electrical conductivity would be a great benefit. This talk will provide an overview of our theoretical and experimental efforts aimed at controllably doping the halide perovskites to achieve the desired optical and electrical properties.

Despite their successes achieved as photovoltaic materials, effective strategies for controllably doping the halide perovskites are still lacking. It has proven difficult to achieve high and controllable *p*-type carrier concentrations in some cases, and reliable *n*-type-doping strategies have not been developed. In this work, possible dopants are first evaluated in the halide perovskites using first-principles calculations based on a hybrid functional with spin-orbit coupling. This approach not only leads to accurate predictions for band structure and crystal structures [1], but also provides a better description of dopant properties. We assess whether dopant impurities (such as Ag, Na, and Cu for acceptors, and Bi, Sc, and Y for donors) can act as shallow dopants on the proper substitutional site, and whether other configurations of these impurities might lead to compensation of potential electrical conductivity. Among the p-type dopants considered, sodium and silver are identified as the most promising acceptors for achieving p-type conductivity, and optimum chemical potential conditions for these dopants are identified [2]. Turning to donor doping, we find that common n-type dopants such as Bi are deep [3]. We demonstrate the validity of our first-principles calculations by comparing with optical measurements of Bi-doped $CsPbBr_3$ crystals [4]. Bi donors are found to give rise to characteristic near-infrared luminescence, in good agreement with theoretical predictions. While Bi is a deep donor in the halide perovskites, yttrium and scandium are identified as promising donor dopants that are capable of yielding n-type conductivity in a variety of halide perovskite systems [3].

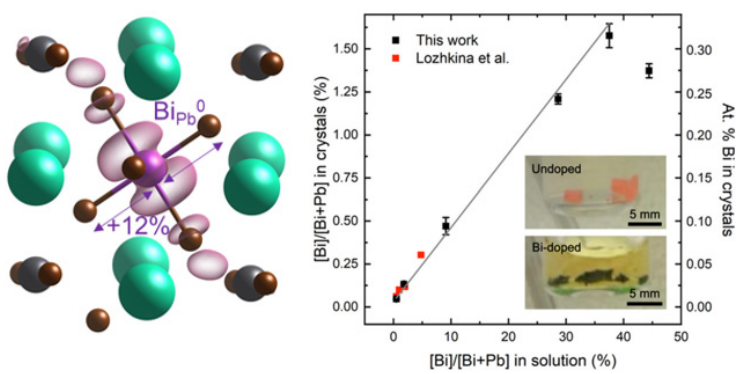

Fig. 1 – (Left) structure of bismuth donors in $CsPbBr_3$, with the spin isosurfaces (in pink) indicating deep behavior. Pb atoms are in gray, Br in brown, and Cs are green. At right, Bi concentration in doped crystals is plotted against the amount of Bi in solution.

Funding: This work was supported by the ONR/NRL 6.1 Basic Research Program.

References:

[1] M. W. Swift and J. L. Lyons, "Lone-pair stereochemistry induces ferroelectric distortion and the Rashba effect in inorganic halide perovskites", Chem. Mater., vol. 35, no. 21, Nov. 2023, 9370.
[2] J. L. Lyons and M. W. Swift, "Trends for acceptor dopants in lead halide perovskites", J. Phys. Chem., vol. 127, no. 26, June 2023, 12735.
[3] J. L. Lyons, "Effective donor dopants for lead halide perovskites," Chem. Mater., vol. 33, no. 15, July 2021, 6200.
[4] S. Brittman, B. T. Jones, M. H. Stewart, B. A. Marcheschi, P. D. Cunningham, N. V. Proscia, C. T. Ellis, J. P. Murphy, K. Sendgikoski, T. H. Brintlinger, and J. L. Lyons, "Near-infrared photoluminescence from bismuth, a deep defect in cesium lead bromide perovskite," Appl. Phys. Lett., vol. 126, no. 3, Jan. 2025, 032103.

Unveiling Ferroelectric Transitions in Inorganic Halide Perovskites with a Machine-Learning Interatomic Potential

Michael W. Swift[1,*] and Noam Bernstein[1]
[1]*Center for Computational Materials Science, U.S. Naval Research Laboratory, Washington, D.C. 20375 USA.*
**Corresponding Author Email: michael.w.swift5.civ@us.navy.mil*
Keywords: Halide Perovskites, Ferroelectricity, Machine Learning, Interatomic Potentials, Molecular Dynamics

We employ a machine-learning interatomic potential (MLIP), trained on hybrid DFT data, to efficiently simulate ferroelectricity in inorganic halide perovskites. Molecular dynamics simulations using this potential accurately capture the lone-pair-driven ferroelectric distortions, revealing the temperatures and pressures at which the ferroelectric/paraelectric phase transitions occur. These results highlight the power and versatility of MLIPs for accelerated atomistic materials simulations.

Inorganic halide perovskites, CsMX_3 (with M = Sn, Pb and X = I, Br), are promising materials for various optoelectronic applications, including low-SWaP-C sensors for DoD-relevant mobile platforms [1]. Recent work highlights the role of the metal cation lone pair in driving ferroelectric distortions, with intriguing implications for spintronics and nanocrystal optoelectronics leveraging bright excitons [2]. However, accurately modeling the structural and electronic properties of these materials, particularly those arising from the metal cation lone pair, requires computationally expensive methods like hybrid density functional theory (DFT) with spin-orbit coupling. This computational cost limits the accessible length and time scales of simulations, hindering the study of phenomena like ferroelectric phase transitions. In this work, we employ a MACE machine-learning interatomic potential (MLIP) [3], starting with the MACE-MP-0 foundation model [4] and fine-tuned to a modestly sized hybrid-DFT dataset, to investigate the ferroelectric-to-paraelectric phase transition in CsMX_3 perovskites as a function of temperature and pressure. Our MLIP accurately reproduces the lone-pair-driven ferroelectric distortions previously predicted for these materials [2]. Using molecular dynamics simulations with the MLIP, we explore the temperature and pressure dependence of the ferroelectric order parameter and characterize the phase transitions. This approach enables efficient large-scale simulations of these technologically relevant materials, paving the way for a deeper understanding of their finite-temperature behavior and the role of the lone pair in driving ferroelectricity.

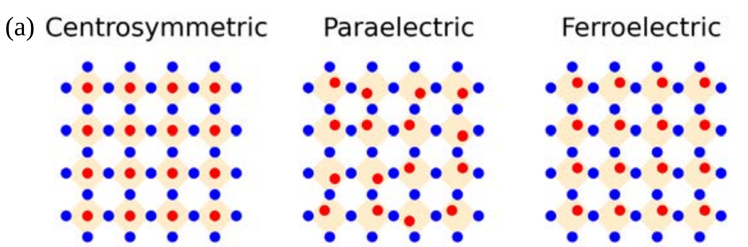

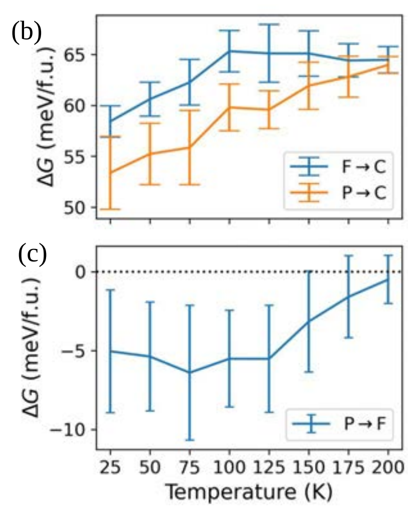

Fig. 1: (a) Illustration showing the centrosymmetric phase (C), disordered local moments (paraelectric phase P), and ordered local moments (ferroelectric phase F) (b) Phase transition simulation in CsSnI3, showing the free-energy change going from F to C (blue) and P to C (orange). (c) The difference gives the free-energy change from P to F, shown in blue. The paraeletric-ferroelectric phase transition occurs near 200 Kelvin.

Funding: This work was supported by the ONR/NRL 6.1 Basic Research Program.

References:

[1] M. A. Becker *et al.*, “Bright triplet excitons in caesium lead halide perovskites,” Nature, vol. 553, no. 7687, Jan 2018, pp. 189-193
[2] M. W. Swift and J. L. Lyons, “Lone-Pair Stereochemistry Induces Ferroelectric Distortion and the Rashba Effect in Inorganic Halide Perovskites,” Chem. Mater., vol. 35, no. 21, Nov. 2023, pp 9370-9377
[3] I. Batatia, D. P. Kovacs, G. Simm, C. Ortner, and G. Csányi, “MACE: Higher order equivariant message passing neural networks for fast and accurate force fields,” Adv. Neural Inf. Process. Syst., vol. 35, November 2022, pp 11423-11436
[4] I. Batatia *et al.*, “A Foundation Model for Atomistic Materials Chemistry”, Dec. 2023, arXiv:2401.00096.

Basal Plane Dislocation Mitigation in SiC via Etching and Growth Interrupts

R.L. Myers-Ward[1,*], N.A. Mahadik[1], D.A. Scheiman[1], J.R. Hajzus[1] and S.T. White[2]
[1]U.S. Naval Research Laboratory, Washington, DC 20375
[2]National Research Council, Washington, DC 20001
**Corresponding Author Email: rachael.l.myers-ward.civ@us.navy.mil*
Keywords: Extended defects, silicon carbide, power electronics material

Basal plane dislocations (BPD) in SiC are high-voltage bipolar device killers that source Shockley-type stacking faults in the presence of an electron-hole plasma and cause forward voltage drifts in bipolar devices [1]. It has been imperative to develop ways to prevent the expansion of these extended defects, where multiple research groups have been successful in mitigating their propagation from the substrate into the epitaxial layer [2-5]. We will report a new process to mitigate the BPD expansion at power densities up to 13 $kWcm^{-2}$ UV excitation using a H_2 etch before the buffer layer growth, followed by a H_2 growth interrupt prior to the low doped epitaxial layer growth. Comparisons of H_2 etching to Ar annealing along with using H_2 versus Ar during growth interrupts to prevent BPD expansion with the goal of understanding the mechanism of the suppression of BPD expansion will be presented.

SiC epitaxial layers were grown using a horizontal hot-wall CVD reactor with SiH_4 (2% in H_2) and C_3H_8 on 4° off-axis substrates toward the [11-20] that are known to have BPDs. A H_2 etch or Ar anneal was performed before the buffer layer (BL; n-type ~ $2x10^{18}$ cm^{-3}) growth while a growth interrupt in H_2 or Ar was conducted prior to the intentionally low doped (n-type ~ $5x10^{15}$ cm^{-3}) drift layer. The H_2 etch or Ar anneal was carried out at 1665 °C and 70 mbar for 50 min. During the growth interrupt, the sample was cooled to 1000 °C in either 80 slm H_2 or 5 slm Ar at 100 mbar. Ultraviolet photoluminescence (UVPL) imaging was used to image the samples before and after UV stressing up to 13 $kWcm^{-2}$. The film thickness was evaluated by Fourier transform infrared analysis, quality by X-ray diffraction and doping concentration via Hg probe CV measurements.

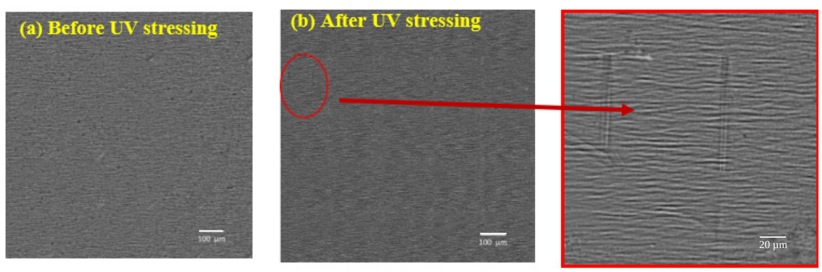

Fig. 1 – UVPL images of epitaxial sample with Ar anneal before BL and growth interrupt in Ar before drift layer (a) before stressing (no BPD in epilayer) and (b) after UV stressing at 1 $kWcm^{-2}$, showing a BPD that expanded from the substrate.

The H_2 etch and H_2 growth interrupt prevents BPDs from expanding under UV stress of 13 $kWcm^{-2}$ and it is believed that the H_2 treatment specifically inhibits this expansion. To confirm the role of H_2, we performed a growth using an Ar anneal at 1665 °C instead of a H_2 etch and the growth interrupt was conducted in an Ar atmosphere instead of H_2. The sample was UV stressed up to 1000 Wcm^{-2} and it was found that four BPD expanded from the substrate into the epilayer, see Fig 1. For comparison, a sample grown with a double H_2 etch (before the buffer layer growth and drift layer) and a sample grown with a H_2 etch plus H_2 growth interrupt did not produce faulting at the same power density. We will present detailed parametric results of samples grown with various etching/ annealing, growth interrupts, anneal times, buffer layer thickness, gas flow rates and interrupt temperature, both in H_2 and Ar.

References:

[1] J.P. Bergman, *et. al.*, Mater. Sci. Forum Vol. 353-356, 299 (2001).
[2] N.A. Mahadik *et.al.*, Mater Sci Forum 858, 233 (2016).
[3] R. E. Stahlbush, et *al.*, Appl. Phys. Lett. 94, 041916 (2009).
[4] M. Kato, *et al.*, Sci. Rep., 12, 18790 (2022).
[5] N.A. Mahadik *et. al.*, Appl. Phys. Lett., 100, 042102 (2012).

Controlling the Crystalline Nature of PEALD Thin Films Through Understanding of Plasma Characteristics

P. Litwin[1,*], M. Currie[2], N. Nepal[2], M. Sales[1], D. Boris[2], M. Johnson[2], S. Walton[2], V. Wheeler[2]

[1] NRC Research Associateship Program, 2101 Constitution Ave. NW, Washington, DC 20418
[2] U.S. Naval Research Laboratory, National Academy of the Sciences, 4555 Overlook Ave SW, Washington, DC 20375
**Corresponding Author Email: peter.m.litwin.ctr@us.navy.mil*
Keywords: Vanadium Oxide, Plasma-enhanced Atomic Layer Deposition

Plasma-enhanced atomic layer deposition (PEALD) utilizes a plasma-based reactant step increasing the complexity of the deposition process compared to thermal ALD. The plasma-based reactant step introduces a flux of energetic particles (ions, fast neutrals, electrons, photons, etc.) directed towards the surface of the growing thin film, which helps reduce the energetic barriers to high growth rates or crystallinity at low temperatures. Understanding the role that these energetic species play in the deposition process potentially enables better tunability of the growth conditions for a given application. For example, during the plasma step, careful control of the power, pressure, gas flow mixture, and substrate bias all enable control over the magnitude of the ion energy flux density delivered to the sample surface. The consequence of this is a greater level of control over the properties of the deposited material. This has been experimentally observed in previous studies, namely in the control of the crystalline phase of various compounds. For example, through alteration of the gas chemistry, flow rate, and pressure used during the reactant half-step it has been shown that the rutile and anatase phases of TiO_2 and the α- and β-phases of Ga_2O_3 could be selectively deposited [1, 2].

In this work, we investigate methods to vary the properties of the plasma in our PEALD system. We use a suite of characterization techniques, including optical emission spectroscopy (OES) and Langmuir probe measurements, to examine how various plasma conditions (power, pressure, and gas flow ratio) impact the ion flux, plasma potential, and atomic O concentrations produced in our Kurt J. Lesker 150 LX PEALD system. As a testbed, we deposit vanadium oxide and report on how the changing properties of the plasma impact the properties of the deposited thin films. We find that through alteration of the pressure in the system during the plasma process, the films can be selectively deposited in an amorphous or crystalline manner. We correlate this change in crystallinity with the change in the energy flux density delivered to the material surface during deposition. From this, we estimate the critical energy flux density necessary for crystallization of vanadium oxide films deposited in our PEALD system. Lastly, we discuss these results more broadly and consider the applicability of these findings to other material systems.

References:

[1] V. D. Wheeler et al., Phase Control of Crystalline Ga_2O_3 Films by Plasma-Enhanced Atomic Layer Deposition Chemistry of Materials, vol. 32, no. 3, pp. 1140–1152, Feb. 2020.

[2] J. R. Avila et al., Impact of Growth Conditions on the Phase Selectivity and Epitaxial Quality of TiO_2 Films Grown by the Plasma-Assisted Atomic Layer Deposition, Chemistry of Materials, vol. 31, no. 11, pp. 3900–3908, Jun. 2019.

Exploring the Mechanisms of Turing-like Nanoparticle Pattern Formation under Electron Beam Irradiation

Camila Faccini de Lima[1], Thilini Umesha Dissanayake[1], and Taylor Woehl[1,*]
[1]*Department of Chemical and Biomolecular Engineering, University of Maryland College Park, College Park, MD 20742*
**Corresponding Author Email: tjwoehl@umd.edu*
Keywords: Self-assembly, nanoparticles, Liquid-Phase TEM, radiolysis.

Self-assembly is a fundamental feature in Nature for the creation of sophisticated structures starting from individual building blocks. The driving force for self-assembly is reduction in global free energy of a solution of building blocks, where they arrange into spatial patterns due to attractive interparticle forces. Biomolecular interactions in cells have been a primary source of inspiration for the self-assembly of synthetic soft matter and nanomaterials as an effective bottom-up strategy for developing functional materials with optical, electromagnetic, and biological functionalities[1,2,3] with applications in drug delivery, catalysis, electronics, among others. Conventional self-assembly of synthetic systems is conducted at- or near-equilibrium and often results in isotropic, closed-packed structures. Precise control over interparticle interactions via delicate biomolecules and complex nanoparticle synthesis is required to tune the resulting self-assembled structure. In contrast, self-assembly in biological systems occurs far from equilibrium, where reaction-diffusion phenomena underpin the formation of countless structures including lipid bilayers, and even shells, tubules and fibers[4,5]. The spatial patterns formed through reaction-diffusion instability (RDI), known as Turing patterns, emerge from initially homogeneous systems *via* activation and inhibition reactions coupled with diffusion[6]. Local self-activation and long ranged inhibition reactions amplify small random concentration perturbations to form spot, stripe, and labyrinth patterns.

We have shown that nanopatterns akin to Turing patterns emerge in a nanoparticle-polymer system at a solid-liquid interface. The nanoparticle-polymer system is exposed to chemical radicals generated by irradiating the solvent with a high energy electron beam, which also enables high spatial resolution dynamic imaging using liquid phase transmission electron microscopy (LPTEM). The formation of nanoparticle patterns, such as spots, labyrinths, and stripes was modulated by electron dose rates and the concentration of the linking molecule, 1-Ethyl-3-(3-dimethylaminopropyl)carbodiimide (EDC). Spot patterns predominantly formed at lower EDC concentrations and lower dose rates, transitioning into labyrinth-like structures at intermediate to high dose rates. Notably, nanoparticle string patterns emerged at higher EDC concentrations and moderate electron dose rates due to reduced nanoparticle mobility facilitated by stronger amide coupling reactions anchoring nanoparticles to the surface. We demonstrate that the nanopattern formation requires gold nanoparticles and involves electron beam-induced radical reactions with siloxane polymers. Inclusion of a radical scavenger, tert-butanol, prevented pattern formation, highlighting the critical role of hydroxyl radicals. These observations underscore a three-component reaction-diffusion mechanism comprising hydroxyl radicals, gold nanoparticles, and siloxane polymers. Finally, we use computational simulations to explore the impacts of irradiation conditions and temperature on the radiolysis chemistry of the system, specifically on the concentration distribution of the reactants implicated in pattern formation. We propose that temperature can be used to tune the diffusion coefficients of the components involved in the RDI reactions, acting as an easily accessible turning knob for pattern emergence and type.

Funding: This material is based upon work supported by the Air Force Office of Science and Research under award no. #FA9550-24-1-0275.

References:

[1] D. Philp and J. F. Stoddart, "Self-assembly in natural and unnatural systems," *Angew. Chem. Int. Ed. Engl.*, vol. 35, pp. 1154–1196, 1996.
[2] R. Klajn, J. F. Stoddart, and B. A. Grzybowski, "Nanoparticles functionalised with reversible molecular and supramolecular switches," *Chem. Soc. Rev.*, vol. 39, no. 6, pp. 2203–2237, 2010.
[3] S. Mann, "Self-assembly and transformation of hybrid nano-objects and nanostructures under equilibrium and non-equilibrium conditions," *Nature Mater.*, vol. 8, pp. 781–792, 2009.
[4] D. Hayakawa et al. "Geometrically programmed self-limited assembly of tubules using DNA origami colloids", *Proc. Natl. Acad. Sci.* vol. 119 no. 43 pp e2207902119, 2022.
[5] A.C. Mendes, et al. "Self-assembly in nature: using the principles of nature to create complex nanobiomaterials." *Wiley interdiscip. rev. Nanomed and nanobiotechnol.* vol. 5, no. 6, 2013.
[6] A.M. Turing, "The Chemical Basis of Morphogenesis" *Phil. Trans. R. Soc. Lond. B* vol. 237 no. 641 pp 37-72, 1952.

3D Lattices of Infrared Plasmonic and Excitonic Colloidal Nanocrystals

Sarah Brittman[1,*], Paul D. Cunningham[1], Veronica R. Policht[1], Todd H. Brintlinger[1], Patrick Y. Yee[2], Nadeemullah A. Mahadik[1], Frederick L. Beyer[3], Chase T. Ellis[1], and Janice E. Boercker[1]

[1]U.S. Naval Research Laboratory, 4555 Overlook Ave., SW, Washington, DC 20375

[2]Jacobs, 7740 Milestone Parkway, Suite 400, Hanover, MD 21076

[3]DEVCOM Army Research Laboratory, 6300 Rodman Road, Aberdeen Proving Ground, MD 21005

**Corresponding Author Email: sarah.f.brittman.civ@us.navy.mil*

Keywords: exciton, plasmon, infrared, colloidal nanocrystal, superlattice

Semiconductor colloidal nanocrystals have immense potential to contribute to efficient and inexpensive infrared optoelectronics [1]. Current devices made from colloidal nanocrystals contain films of nanocrystals that lack long-range order. Controlling the periodic arrangement of these nanocrystals into 3D arrays, often called nanocrystal superlattices, has the potential to generate engineered metamaterials that exhibit properties not achievable in natural semiconductors or in films of disordered nanocrystals. Their features are also an order of magnitude smaller than those of conventional, top-down fabricated metamaterials. The current size of individual ordered domains in these nanocrystal superlattices (analogous to grain size in polycrystalline materials), however, is typically microscopic, so the field lacks detailed structure-property relationships. To address this challenge, we have created microscale domains of binary nanocrystal ordered solids of infrared plasmonic $Cu_{2-x}S$/PbS core/shell and excitonic PbS nanocrystals by engineering the surface chemistry of our nanocrystals (Fig. 1) [2, 3]. We then directly correlated photoluminescence micro-spectroscopy performed air-free with transmission electron microscopy of the binary superlattices and single-component PbS superlattices. The PbS nanocrystals within the binary superlattices were still nearly as luminescent as their counterparts in single-component PbS superlattices, and they exhibited photoluminescence decay dynamics 30 times faster, suggesting that both the radiative and non-radiative decay rates have been accelerated. A pronounced redshift of 80 meV was also observed in the emission from the binary superlattices, relative to that of the single-component PbS superlattices. The magnitude of this shift suggests an interaction between the plasmonic and excitonic nanocrystals. Our correlated measurements also discerned two distinct photoluminescence behaviors among the population of measured binary superlattices. As our capabilities in nanocrystal assembly and correlated microscopy continue to improve, we envision that combining such correlated measurements with optical modeling will enhance our understanding of multicomponent nanocrystal superlattices and allow us to engineer desired properties such as bright and fast infrared emission.

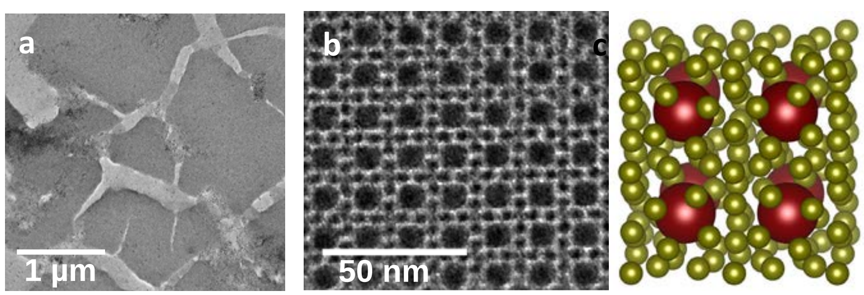

Fig. 1 – a) Scanning electron micrograph of domains of infrared binary nanocrystal superlattices. b) Transmission electron micrograph of the arrangement of the nanocrystals within the superlattices. c) Diagram of the structure of the binary superlattice where red spheres are the larger plasmonic $Cu_{2-x}S$/PbS nanocrystals and gold spheres are the smaller excitonic PbS nanocrystals.

References:

[1] M. Allen, et al. "Image Sensors and Cameras Based on Colloidal Quantum Dots (CQD) for Visible-to-SWIR Detection," In *Proc. SPIE Infrared Tech. Appl. L*, Jun. 2024, 13046OD.

[2] S. Brittman, et al. "Binary Superlattices of Infrared Plasmonic and Excitonic Nanocrystals," *ACS Appl. Mater. Inter.*, vol. 12, no. 21, May 2020, 24271.

[3] P. Y. Yee, et al. "$Cu_{2-x}S$/PbS Core/Shell Nanocrystals with Improved Chemical Stability," *Chem. Mater.*, vol. 33, no. 17, Aug. 2021, 6685.

Leveraging Plasmon Rulers: High-Throughput Anti-Icing Screening with Gold Nanoparticles

Eunkeu Oh,[1,*] Popular Pandey,[1,2] Young C. Kim,[3] Paul Johns,[1] Kimihiro Susumu,[1] Sang Ho Lee[1,4], Michael H. Stewart[1]

[1]*Optical Sciences Division, U.S. Naval Research Laboratory, Washington, DC 20375, USA*

[2]*American Society for Engineering Education, Washington, DC 20036, USA*

[3]*Center for Materials Physics and Technology, U.S. Naval Research Laboratory, Washington, DC 20375, USA*

[4]*Amentum, Amentum Technology Inc. 2551 Dulles View Dr. Herndon, VA 20171, USA*
**Corresponding Author Email: eunkeu.oh2.civ@us.navy.mil*
Keywords: anti-icing, plasmon rulers, gold nanoparticle. High-throughput

A standardized and robust colorimetric method for evaluating anti-icing efficacy using a gold nanoparticle (AuNP) plasmon ruler assay for high-throughput screening (HTS) of anti-icing reagents is developed. We showed that dithiolate-grafted AuNPs act as a plasmon molecular ruler to measure the interparticle distance of AuNPs during freezing.[1] Our optimized AuNP probe demonstrated high colloidal stability and superior buffer resilience, making it suitable for various types of target molecules, including chemicals, proteins, and organometals, with a large dynamic sensing range. We explored how localized surface plasmon resonance peak of AuNP correlate with ice crystal growth and use it to evaluate the anti-icing efficacy of reagents. Molecular dynamics and numerical simulations were carried out to understand the effects of ligand on the surface of AuNP during cooling and to calculate the apparent interparticle distance of AuNPs during ice formation and its changes in the presence of anti-icing reagents. By implementing a dose-response analysis and IC50 calculation, we proposed a new tool to quantify AuNP-based colorimetric assay for standardized HTS of anti-icing efficacy. Our results, validated against established ice recrystallization inhibition and dynamic ice shaping measurements, were analyzed using machine learning to study dynamic changes in ice size and shape over time. Finally, we will show that specific ligand-modified AuNPs exhibit remarkable stability in harsh buffer environments and endure multiple lyophilization cycles, significantly increasing their shelf life, versatility, and applicability in previously untested environments.

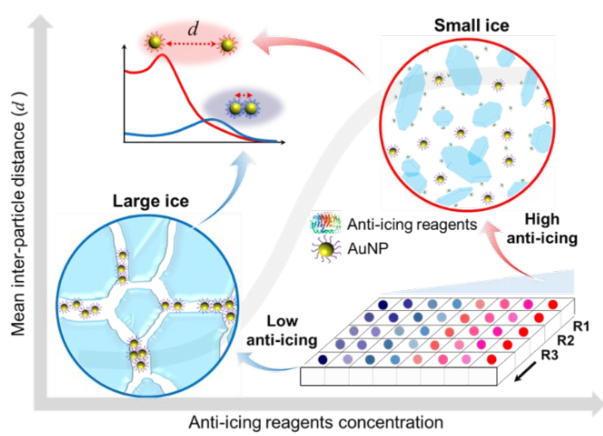

Fig. 1 – High throughput AuNP-based colorimetric assay for screening anti-icing efficacy of reagents. This study demonstrates a standardized and robust colorimetric method for evaluating anti-icing efficacy using a gold nanoparticle (AuNP) plasmon ruler assay–that measures changes in the interparticle distance “d” of AuNPs during freezing–for high-throughput screening of anti-icing reagents.

References:

[1] E. Oh et al., “Systematic Development of Plasmon Ruler using Dithiolate-Grafted Gold Nanoparticle for High-throughput Screening of Anti-icing Activity,” ACS ANM, ASAP 2025

Thin Conductive Cu Films by Post-Reduction of Atomic Layer Deposited CuO

Meg Sales[1,*], Neeraj Nepal[2], Peter M. Litwin[1], David R. Boris[2], Scott G. Walton[2], and Virginia D. Wheeler[2]

[1]NRC Research Associateship Program, Washington, DC 20001

[2]U.S. Naval Research Laboratory, Washington, DC 20375

**Corresponding Author Email: maria.g.sales.ctr@us.navy.mil*

Keywords: Cu thin films, CuO, ALD, plasma reduction

Interconnect applications in microelectronics have helped spur the need to develop robust and scalable atomic layer deposition (ALD) processes for copper (Cu). For this application space, the unique advantage of ALD is being able to conformally coat high aspect ratio via structures due to its self-saturating nature and precise thickness control. Reported ALD recipes for pure Cu typically rely on reactions between a metal-organic Cu precursor and a reducing reactant, including different chemical compounds for thermal ALD or a reducing plasma for plasma-enhanced ALD (PEALD). However, these conventional Cu ALD processes have very low growth rates of 0.1-0.5 Å/cycle, at best. As is typical of other metal ALD recipes, traditional ALD of metallic Cu requires the deposition of at least 20-40 nm in order to achieve full grain coalescence and a conductive film.

In this work, we report on an alternative way of obtaining conductive Cu films through the use of an in-situ plasma reduction. Initially, copper (II) oxide, or CuO, is deposited by PEALD at a substrate temperature of 150 °C, using copper(I)-N,N'-di-sec-butylacetamidinate ($[Cu(^{s}Bu\text{-}amd)]_2$) and Ar/O_2 plasma as precursors. The growth rate for this CuO recipe is 0.3 Å/cycle, which is higher than what is obtained for pure Cu using the same precursor (0.1 Å/cycle). Grown CuO films have a low concentration of incorporated ligands and a smooth surface morphology. Following CuO ALD, the CuO film is exposed to reducing plasma pulses containing a mixture of Ar and H_2 gas. This reduction with Ar/H_2 plasma exposure is performed in-situ, without removing the CuO sample from the ALD reactor. To characterize the films, spectroscopic ellipsometry (SE), X-ray photoelectron spectroscopy (XPS), atomic force microscopy (AFM), and contactless sheet resistance measurements were performed.

In this talk, we will discuss various parameters in the Ar/H_2 reducing plasma, such as total exposure time, pulse lengths, and number of reducing plasma cycles, and investigate how they affect key properties of the resultant Cu film, such as chemistry, morphology, and resistivity. Additionally, we report on utilizing supercycles of CuO ALD and reducing plasma pulses to grow thicker (30 nm) Cu films with low resistivity. To date, our most optimal CuO-then-post-reduction procedure yielded a 30 nm Cu film with a root mean square (RMS) roughness of 3.3-3.5 nm and a resistivity of 3.8 μΩ cm, which is only a factor of 2 greater than for bulk Cu.

In situ CVD of Graphene for SiC Thin Film Transfer

D. J. Pennachio[1)], J. R. Hajzus[1)], J. M. Woodward[1)], R. L. Myers-Ward[1)]
[1)] U.S. Naval Research Laboratory, Washington, DC 20375, USA
Email: Daniel.J.Pennachio2.civ@us.navy.mil
Keywords: Silicon Carbide, Remote Epitaxy, Graphene, 2D Materials

Remote epitaxy (RE) is a thin film growth technique that incorporates a release layer into the material stack, allowing for transfer of the deposited material with minimal defects [1]. Transferred 2D two-dimensional (2D) material, such as graphene, is commonly used for a release layer, but the transfer step can degrade the film and increase process complexity. To avoid this, we examine *in situ* graphitic carbon growth on SiC substrates before subsequent SiC epitaxy in the same chemical vapor deposition (CVD) RE process. RE SiC and subsequent SiC epilayer transfer is desired since isolated SiC membranes are excellent for quantum photonics and SiC substrate reuse can provide significant cost savings. Despite these benefits, the high-temperature hydrogen-containing CVD environment can damage graphene, making RE difficult under standard SiC growth conditions [2].

This study established growth windows for *in situ* graphene via propane-based hot wall CVD. This propane-based graphene growth enables an efficient transition to subsequent SiC deposition using established SiC growth conditions since it shares a similar hydrogen ambient to standard SiC CVD. Growing at 1620 °C in 20 slm H_2 with 20 sccm propane flow produced predominantly monolayer (ML) graphene films on on-axis 6H-SiC(0001) substrates with minimal defects found in Raman spectral maps. Films grown on 4° off-axis 4H-SiC(0001) substrates were multilayer (6 ML) graphitic carbon despite experiencing the same conditions as the on-axis substrates. This optimized graphene growth condition was used for subsequent RE attempts to study the effect of SiC precursor dose, C/Si ratio, and growth rate on epilayer crystallinity and graphene barrier damage. SiC crystalline quality appeared correlated to growth rate, with lower growth rates producing smoother films with fewer polytype inclusions. Single-crystalline, polytype-pure SiC epilayers was achieved on 4° off-axis CVD graphene/4H-SiC(0001). Effects of initial SiC growth parameters on the graphitic carbon release layer were explored via cross-sectional transmission electron microscopy (TEM) and attempts at epilayer transfer. Some growth interfaces exhibited non-uniform multilayer graphitic carbon, motivating further study of this growth system to improve boundary uniformity and SiC epilayer quality.

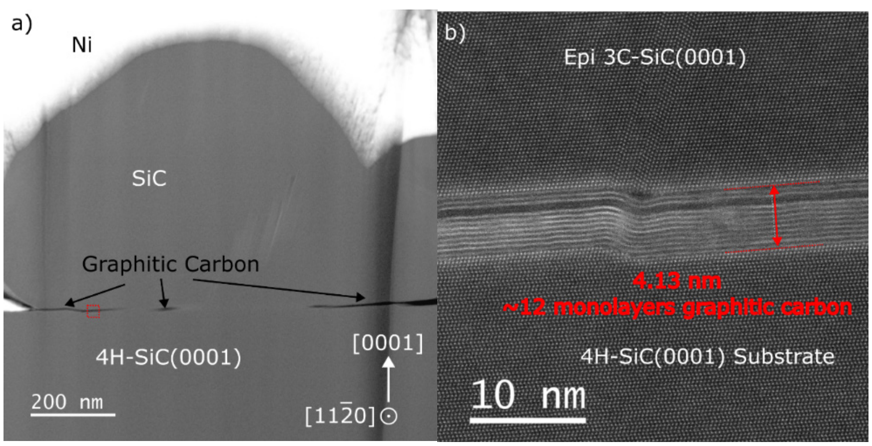

Fig. 1: a) A HAADF-STEM cross section of a 3C-SiC(0001)/graphitic carbon/4H-SiC(0001) heterostructure where the graphitic carbon was grown in situ directly before the SiC epilayer. b) A MAADF-STEM image of the interface region highlighted by the red square in a), showing the film's epitaxial alignment to the substrate and layered structure of the graphitic carbon.

[1] Kim, Y., Cruz, S., Lee, K. et al. Nature 544, 340–343 (2017).
[2] Pennachio, D. J., Hajzus, J. R., & Myers-Ward, R. L. JVST B, 43(2). (2025).

Exploring the Mechanisms of Turing-like Nanoparticle Pattern Formation under Electron Beam Irradiation

Camila Faccini de Lima[1], Thilini Umesha Dissanayake[1], and Taylor Woehl[1,*]
[1]*Department of Chemical and Biomolecular Engineering, University of Maryland College Park, College Park, MD 20742*
**Corresponding Author Email: tjwoehl@umd.edu*
Keywords: Self-assembly, nanoparticles, Liquid-Phase TEM, radiolysis.

Self-assembly is a fundamental feature in Nature for the creation of sophisticated structures starting from individual building blocks. The driving force for self-assembly is reduction in global free energy of a solution of building blocks, where they arrange into spatial patterns due to attractive interparticle forces. Biomolecular interactions in cells have been a primary source of inspiration for the self-assembly of synthetic soft matter and nanomaterials as an effective bottom-up strategy for developing functional materials with optical, electromagnetic, and biological functionalities[1,2,3] with applications in drug delivery, catalysis, electronics, among others. Conventional self-assembly of synthetic systems is conducted at- or near-equilibrium and often results in isotropic, closed-packed structures. Precise control over interparticle interactions via delicate biomolecules and complex nanoparticle synthesis is required to tune the resulting self-assembled structure. In contrast, self-assembly in biological systems occurs far from equilibrium, where reaction-diffusion phenomena underpin the formation of countless structures including lipid bilayers, and even shells, tubules and fibers[4,5]. The spatial patterns formed through reaction-diffusion instability (RDI), known as Turing patterns, emerge from initially homogeneous systems *via* activation and inhibition reactions coupled with diffusion[6]. Local self-activation and long ranged inhibition reactions amplify small random concentration perturbations to form spot, stripe, and labyrinth patterns.

We have shown that nanopatterns akin to Turing patterns emerge in a nanoparticle-polymer system at a solid-liquid interface. The nanoparticle-polymer system is exposed to chemical radicals generated by irradiating the solvent with a high energy electron beam, which also enables high spatial resolution dynamic imaging using liquid phase transmission electron microscopy (LPTEM). The formation of nanoparticle patterns, such as spots, labyrinths, and stripes was modulated by electron dose rates and the concentration of the linking molecule, 1-Ethyl-3-(3-dimethylaminopropyl)carbodiimide (EDC). Spot patterns predominantly formed at lower EDC concentrations and lower dose rates, transitioning into labyrinth-like structures at intermediate to high dose rates. Notably, nanoparticle string patterns emerged at higher EDC concentrations and moderate electron dose rates due to reduced nanoparticle mobility facilitated by stronger amide coupling reactions anchoring nanoparticles to the surface. We demonstrate that the nanopattern formation requires gold nanoparticles and involves electron beam-induced radical reactions with siloxane polymers. Inclusion of a radical scavenger, tert-butanol, prevented pattern formation, highlighting the critical role of hydroxyl radicals. These observations underscore a three-component reaction-diffusion mechanism comprising hydroxyl radicals, gold nanoparticles, and siloxane polymers. Finally, we use computational simulations to explore the impacts of irradiation conditions and temperature on the radiolysis chemistry of the system, specifically on the concentration distribution of the reactants implicated in pattern formation. We propose that temperature can be used to tune the diffusion coefficients of the components involved in the RDI reactions, acting as an easily accessible turning knob for pattern emergence and type.

Funding: This material is based upon work supported by the Air Force Office of Science and Research under award no. #FA9550-24-1-0275.

References:

[1] D. Philp and J. F. Stoddart, "Self-assembly in natural and unnatural systems," *Angew. Chem. Int. Ed. Engl.*, vol. 35, pp. 1154–1196, 1996.
[2] R. Klajn, J. F. Stoddart, and B. A. Grzybowski, "Nanoparticles functionalised with reversible molecular and supramolecular switches," *Chem. Soc. Rev.*, vol. 39, no. 6, pp. 2203–2237, 2010.
[3] S. Mann, "Self-assembly and transformation of hybrid nano-objects and nanostructures under equilibrium and non-equilibrium conditions," *Nature Mater.*, vol. 8, pp. 781–792, 2009.
[4] D. Hayakawa et al. “Geometrically programmed self-limited assembly of tubules using DNA origami colloids”, *Proc. Natl. Acad. Sci.* vol. 119 no. 43 pp e2207902119, 2022.
[5] A.C. Mendes, et al. “Self-assembly in nature: using the principles of nature to create complex nanobiomaterials.” *Wiley interdiscip. rev. Nanomed and nanobiotechnol.* vol. 5, no. 6, 2013.
[6] A.M. Turing, “The Chemical Basis of Morphogenesis” *Phil. Trans. R. Soc. Lond. B* vol. 237 no. 641 pp 37-72, 1952.

Extrinsic Effects on Interlayer Exciton Dynamics in $MoSe_2/WSe_2$ Heterostructures

Ibrahim Boulares[1,*], Owen Vail[1], Robert Boyd[2], Mattew Chin[1], and Sina Najmaei[1]

[1]DEVCOM Army Research Laboratory, 2800 Powder Mill Rd, Adelphi, MD 20783
[2]Department of Material Science and Engineering, University of Wisconsin-Madison, 1509 University Avenue, Madison, WI 53706
**Ibrahim.Boulares.civ@army.mil*
Corresponding Author Email: Ibrahim.Boulares.civ@army.mil
Keywords: Optics, transmission metal dichalcogenides (TMDs), interlayer exciton

We investigate the effects of fabrication processes on the charge transfer dynamics of the interlayer exciton in TMD heterostructures via time-resolved photoluminescence and transient absorption spectroscopy.

Interlayer exciton properties in two-dimensional transition metal dichalcogenides (TMD) are of great interest due to their large binding energies and long lifetimes. These properties provide an opportunity in ultra-low power bosonic functionality for dissipationless computing, unprecedented long lifetime BECs at high temperatures, and passive electromagnetic sensors. However, realization of such novel optoexcitonic functionality requires a fundamental understanding of the charge population balance resulting from the formation of the interlayer exciton as well as the extrinsic effects, such as defects, interface quality, twist angle, *etc*.

Interlayer excitons are bound electron – hole pairs bound by the electrostatic Coulomb force where the charges are spatially separated by insulating layers and reside across two semiconducting layers, minimizing recombination. This configuration occurs naturally in TMD heterostructures that have a type-II band alignment and homobilayers with an out-of-plane electric field. For example, in an $MoSe_2/WSe_2$ heterostructure, the interlayer exciton is composed of an electron in the conduction band of the $MoSe_2$ layer bound across the interface to a hole in the WSe2 valence band; the energy spacing of that pairing results in luminescence at ~935 nm (1.35 eV). The interlayer exciton formation, in ultra-clean samples, is very efficient due to the rapid (< 50 fs) charge transfer process [1], significantly faster than the intralayer exciton decay time. In comparison, chemical vapor deposition (CVD) grown heterostructures show a significantly larger charge transfer time (< 150 fs), which may be due to defects [2]. A strong Coulomb interaction between the holes and electrons, manifested in the large exciton binding energy (~100-350 meV) [3], exists because the layer separation (~0.7 nm) is smaller than the Bohr radius of the intralayer exciton (~1-3 nm) [4,5]. The fact that the electrons and holes are located across an interface gives rise to an out-of-plane electric dipole whose properties are very sensitive to the quality of the interface and distance between the two semiconducting layers. For instance, using an AFM tip to controllably squeeze contaminants (squeegee) out from between 2D layers and their substrates, showed a significant improvement in the interlayer emission signal [6]. Additionally, transient absorption spectroscopy measurements show the hole transfer time in the interlayer exciton formation process increases by 3 orders of magnitude when inserting a 1nm hBN layer between MoSe2 and WSe2 monolayers [7]. Others report the lifetime of the interlayer exciton varies by 2 orders of magnitude when inserting an hBN bilayer between MoSe2-WSe2 monolayers [8]. Such results indicate the sensitivity of the interlayer exciton in TMDs on extrinsic factors. Here, we show the effects of fabrication processes via exfoliation, on the charge transfer dynamics on the interlayer exciton in TMD heterostructures via time-resolved photoluminescence and transient absorption spectroscopy.

References:

[1] Hong, X., *et al*., "Ultrafast charge transfer in atomically thin MoS_2/WS_2 heterostructures," Nat. Nano. 9,682 (2014)
[2] Yu, Y., *el al*,. "Ultrafast formation and dynamics of interlayer exciton in a large-area CVD-grown WS2/WSe2 heterostructure," J. Phys.: Condens. Mat. .30, 495701 (2018)
[3] Jiang, Y., *et al*., "Interlayer exciton formation, relaxation, and transport in TMD van der Waals heterostructures," Light Sci Appl. 10, 72 (2021)
[4] Qiu, DY., *el al*., "Optical spectrum of MoS2: many-body effects and diversity of exciton states," Phys Rev Lett. 111, 216805 (2013)
[5] Berkelbach, T., *el al*., "Theory of neutral and charged excitons in monolayer transition metal dichalcogenides," Phys. Rev. B 88, 045318 (2013)
[6] Rosenberger, M. R., *el al*., "Nano-"Squeegee" for the Creation of Clean 2D Material Interfaces," ACS Appl. Mater. Interfaces, 10, 10379 (2018)
[7] Yoon, Y., *el al*., "Charge Transfer Dynamics in MoSe2/hBN/WSe2 Heterostructures," Nano Lett. 22,24 (2022)
[8] Mahdikhanysarvejahany, F., *el al*., "Interlayer exciton flow in hBN separated MoSe2/WSe2 heterostructures," Bullet. of the APS (2023)
[9] L. Zhang, L. *el al*., "Twist-angle dependence of moiré excitons in WS2/MoSe2 heterobilayers," Nat. Comms. 11,5888 (2020)

Highly Efficient Spin-Orbit Torque Switching in Bi_2Se_3/Fe_3GeTe_2 van der Waals Heterostructures

Connie H. Li[1,*], M. Lohmann[1], D. Wickramaratne[1], J. Moon[1], M. Noyan[1], H.-J. Chuang[1], B. T. Jonker[1]

[1]*Naval Research Laboratory, 4555 Overlook Ave. SW, Washington, DC 20375*

**Corresponding Author Email: connie.h.li.civ@us.navy.mil*

Keywords: topological insulator, 2D ferromagnet, magnetization switching, spin-orbit torque, spintronics

Spin-orbit torque (SOT) switching of ferromagnets enables energy-efficient, reliable non-volatile memories. SOT is generated in a spin-generating layer that effectively separates the read and write path in a magnetic tunnel junction (MTJ) based memory bit cell. This greatly enhances the endurance of the memory cell since the write current no longer flows through the tunnel barrier but instead through a separate low-resistance path. A successful switch of the ferromagnet using SOT can be achieved with shorter write pulses, reducing the overall energy needed.

Topological insulators (TIs) have shown great potential as the spin-generating layer, due to the intrinsic spin-momentum locking of their surface states. However, these states can be destroyed when interfaced with ferromagnetic metals. Van der Waals (vdW) heterostructures with weakly interacting interface can potentially alleviate this issue. However, fully molecular beam epitaxy (MBE) grown TI/2D ferromagnet structures have shown strong interlayer interactions, where only partial switching are achieved with high current densities.

Here we fabricate vdW heterostructures with MBE grown bulk-insulating Bi_2Se_3 and exfoliated 2D ferromagnet Fe_3GeTe_2 with perpendicular magnetic anisotropy (PMA). We achieve full magnetization switching at a critical current density of $1.2x10^6$ A/cm^2, the lowest for switching PMA magnets, with a large SOT efficiency comparable to the highest values reported for Bi_2Se_3 [1]. Density functional theory (DFT) calculations reveal weak interlayer interactions, suppressing proximity induced magnetic moment on Bi_2Se_3, preserving its spin texture. This enables direct access to the TI surface states where the spins are singly degenerate with significant net in-plane polarization [1]. Our results highlight the clear advantage of all-vdW heterostructures with weak interlayer interactions that can enhance SOT efficiency and minimize critical current density, an important step towards realizing next generation low-power non-volatile memory and spintronic devices.

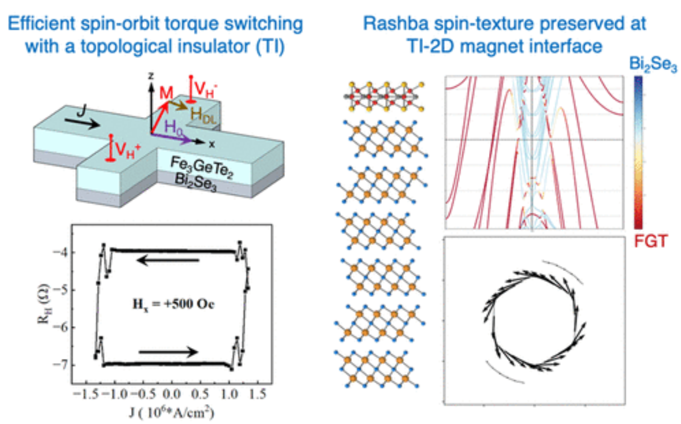

Fig. 1 – Left panel: schematic diagram and measurement geometry of spin-orbit torque switching of Fe_3GeTe_2 2D magnet from topological insulator Bi_2Se_3 (top), and switching results (bottom). Right pane: calculated bands of Bi_2Se_3/Fe_3GeTe_2 heterostructure, indicating spin-momentum locked TI surface states at the interface.

Funding: This research was supported by the Naval Research Laboratory (NRL) base programs and Office of the Undersecretary of Defense (Research & Engineering) ARAP program.

References:

[1] M. Lohmann, D. Wickramaratne, J. Moon, M. Noyan, H.-J. Chuang, B. T. Jonker, and C. H. Li, “Highly Efficient Spin−Orbit Torque Switching in Bi_2Se_3/Fe_3GeTe_2 van der Waals Heterostructures”, *ACS Nano* **18**, 680 (2024).

Highly Efficient Spin-Orbit Torque Switching using Bulk-Insulating Topological Insulator Bi_2Se_3

Mehmet A. Noyan[1†*], Xiaohang Zhang[1,2†], Jisoo Moon[1], Enrique Cobas[1], Mark Lohmann[1], Qiang Zou[3], Lian Li[3], Michael Weinert,[4] Berend T. Jonker[1], Olaf M. J. van 't Erve[1], and Connie H. Li[1*]

[1] Magnetoelectronic Materials & Devices, Materials Science & Technology Division, Naval Research Laboratory, Washington D. C. 20375 USA
[2] Nova Research, Inc., Alexandria, VA 22308 USA
[3] Department of Physics and Astronomy, West Virginia University, Morgantown, WV 26506 USA
[4] Department of Physics and Astronomy, University of Wisconsin, Milwaukee, WI 53202 USA
[†] These authors contributed equally.
[*]Corresponding author. E-mail: mehmet.a.noyan.civ@us.navy.mil, connie.h.li.civ@us.navy.mil
Keywords: spin-orbit torque, topological insulator, magnetization switching, molecular beam epitaxy

Topological insulators (TIs) have shown great potential for efficient spin-orbit torque (SOT) switching of adjacent ferromagnets due to spin-momentum locking of their surface states. However, a substantial bulk-conducting channel in many TIs limits their full potential for low-power operations. Here we synthesize bulk-insulating Bi_2Se_3 on $(BiIn)_2Se_3/In_2Se_3$ buffer layers by molecular beam epitaxy (as confirmed by transport and angle-resolved photoemission spectroscopy (ARPES) measurements), and compare their SOT efficiency to bulk-conducting Bi_2Se_3 films using Kerr rotation and second harmonic Hall measurements. For the bulk-insulating Bi_2Se_3, we find a 4-fold reduction in critical current density for switching of an adjacent NiFe layer and a 5-10-fold enhancement in SOT efficiency, unambiguously demonstrating that Fermi level tuning can significantly enhance switching performance. This is attributed to the current flowing predominantly through the top TI surface state layer, where the generated spins are in close proximity to the NiFe interface. In addition, our TI/FM heterostructures are grown entirely *in situ* without air exposure, where the clean interface can facilitate *strong hybridization* and the formation of interface states, or "descendent states" that exhibit spin-momentum locking, leading to enhanced SOT efficiency for both structures.

Rapid Down-Selection of InAs Plasma Surface Treatments Using *in situ* Spectroscopic Ellipsometry

John P. Murphy[1,*],Glenn Jernigan[1], and Jill A. Nolde[1]
[1]Electronics Science and Technology Division, U.S. Naval Research Laboratory,4555 Overlook Ave SW, Washington, D.C. 20375
**Corresponding Author Email: john.p.murphy399.civ@us.navy.mil*
Keywords: III-V, Indium Arsenide, Critical Points, Plasma Passivation, Surface States.

The surface of InAs has proven to be a particularly difficult to clean and passivate, which becomes a significant problem in its use in infrared optoelectronics. Formation of native oxides on surfaces and sidewalls of InAs is practically unavoidable when processing devices and leads to a high density of surface states which leaves surfaces degenerately n-type. Surface treatments and passivation methods to mitigate these surface states are typically evaluated ex situ through x-ray photoelectron spectroscopy (XPS), capacitance-voltage characteristics or fabrication of an example device; all of which are time-consuming and expose surfaces to interim environmental conditions with a high-likelihood of reforming poor interfaces, which limits the overall number of treatments that can be reasonably explored when developing new processes for surface control. In situ spectroscopic ellipsometry (SE) allows real time process control in plasma-enhanced atomic layer deposition systems and allows for the optimization of surface quality prior to interface passivation. Analysis of critical points in the pseudo dielectric function to assess surface quality of InAs has been established [1] and demonstrated on InAs surfaces using remote plasma treatments [2]. In this study, critical points in the pseudo dielectric function of InAs are utilized to track the efficacy of plasma surface cleaning while exploring the parameter space of both Ar and Ar:H2 plasmas. The chemical and morphological nature of InAs surfaces are elucidated using XPS, via air-free transfer, and followed by atomic force microscopy (AFM) in ambient to assess the evolution of surface morphology. Changes in tracked critical points can be correlated to the surface quality measured via XPS and AFM, demonstrating the utility in this method to rapidly assess surface treatments to InAs surfaces within the broad parameter space of non-equilibrium plasmas utilized in atomic layer processing. Initial results have already demonstrated the utility of this method in the evaluation of Ar:H2 plasmas, seen in the figure below. Monitoring the E2 critical point during plasma treatment readily showed the formation of metallic indium droplets on the surface with greater speed and sensitivity than XPS. Utilizing in situ SE to monitor critical points during plasma surface treatments provides a unique ability to rapidly progress in the field of passivation of InAs-based optoelectronics, and more broadly III-V optoelectronics.

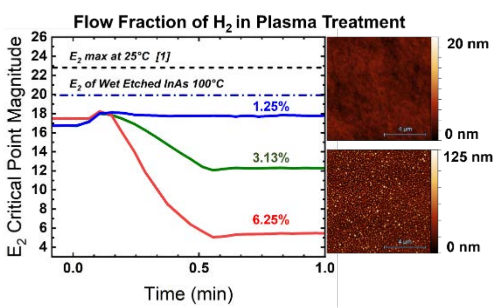

Fig. 1: (left) Transient curves of critical point (E2) at 100 °C during plasma exposure with increasing flow fractions of hydrogen in an Argon:Hydrogen remote plasma surface clean, with target values (dashed lines) from the literature [1] and this studying using established wet-chemical techniques. (right) Atomic force micrographs of the resultant surfaces showing the rapid deterioration of the surface into metallic indium droplets in the 6.25% sample (bottom right), and the absence of indium metal beads on the 1.25% sample (top-right).

Funding: This work was supported by the NRL Jerome and Isabella Karle Distinguished Scholar Fellowship Program.

References

[1] D.E. Aspnes and A.A. Studna, Phys. Rev. B. 27(2), 985-1009 (1983).
[2] M. Losurdo et al., J. Electrochem. Soc. 156 H263 (2009).

Conductivity Mismatch in Topological-Insulator-Based Spintronic Terahertz Emitters

Nicholas S. Sirica,[1*] Jon K. Gustafson[1], Mehmet A. Noyan,[1] Enrique D. Cobas,[1] Connie H. Li[1], and Olaf M. J. van 't Erve[1]

[1]*Materials Science & Technology Division, U.S. Naval Research Laboratory, Washington, D.C. 20375, USA*

**Corresponding Author Email: nicholas.s.sirica.civ@us.navy.mil*

Keywords: Topological Insulator, Spintronics, Terahertz Emission, Nonlinear Optics

Terahertz emission from magnetic heterostructures comprised of surface engineered 3D topological insulators, are compared. Despite an enhancement in spin-orbit torque efficiency, a ~ 5-fold reduction in the terahertz emission amplitude is observed. Such discrepancy between reciprocal measurements of spin-charge conversion is understood to result from a conductivity mismatch across the interface.

Terahertz (THz) emission has emerged as a powerful spectroscopic technique to sensitively probe the electronic symmetry and conversion efficiency in spin-orbit torque devices, through measuring the inverse, spin-to-charge conversion process in magnetic heterostructures.

Here, we report THz emission from magnetic heterostructures comprised of surface engineered Bi_3Se_3 to assess how the position of the chemical potential affects the resultant emission properties. The emission spectra of bare topological insulator (TI) films reflect the *3m* point group symmetry of Bi_2Se_3, while that from magnetic heterostructures follows from the magnetic dipole symmetry of ultrafast demagnetization. Bulk-insulating Bi_2Se_3 heterostructures show a ~ 5-fold reduction in the terahertz emission amplitude as compared to their bulk-conducting counterparts (Fig. 1). This is attributed to a conductivity mismatch across the $Ni_{80}Fe_{20}/Bi_2Se_3$ interface brought on by the low carrier density and high sheet resistance of the bulk-insulating film. Tunnel junctions and Kramers-Weyl semimetals are proposed as an effective strategy to enhance the degree of spin polarization injected across the interface, providing a promising future direction for designing THz spintronic emitters using advanced, functional materials beyond elemental heavy metals.

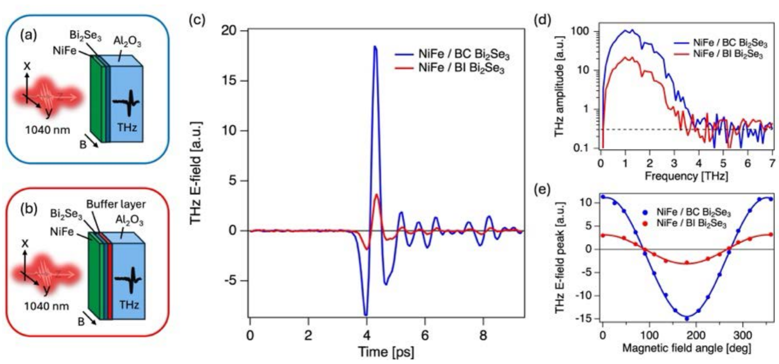

Fig. 1 – Sketch of the THz spintronic emitters (a) $Ni_{80}Fe_{20}$ (8.0 nm)/bulk-conducting (BC-) Bi_2Se_3 (8 QL) and (b) $Ni_{80}Fe_{20}$ (8.0 nm)/bulk-insulating (BI-) Bi_2Se_3 (8 QL). (c) THz waveforms generated from $Ni_{80}Fe_{20}$/BC-Bi_2Se_3 (blue trace) and $Ni_{80}Fe_{20}$/BI-Bi_2Se_3 (red trace) under a saturating magnetic field (0.2 T) applied perpendicular to THz polarization and propagation directions. (d) The corresponding power spectra of the time-domain traces in (e), where noise floor is denoted by the dotted gray line. (e) THz peak amplitude from $Ni_{80}Fe_{20}$/BC-Bi_2Se_3 (blue circles) and $Ni_{80}Fe_{20}$/BI-Bi_2Se_3 heterostructures (red circles) as a function of applied, in-plane magnetic field angle (ϕ). Solid lines show a $\sin(\phi)$ dependence to the experimental data.

Tunable Surface Topographic Control Through Nanofabrication

Sungmin Hong[1,*], Kyoo Jo[1], Donald Cropek[1], Yin Song[1], Anne McCarthy[1], Anna Kim[1], Dale Landas[1]

[1] U.S. Army Engineer Research and Development Center, Construction Engineering Research Laboratory, 2902 Newmark Dr, Champaign, IL 61822, U.S.A

**Corresponding Author Email: Sungmin.Hong@usace.army.mil*

Keywords: Help searches find your abstract. E.g. "Optics, robotics, rubidium".

We present a transformative material platform that enables dynamic, reversible control of surface properties through magnetically responsive micro/nanostructures embedded in soft elastomers. Utilizing bottom-up fabrication in combination with dissolvable template nanoimprinting lithography (DT-NIL), we fabricate stimuli-responsive surface architectures capable of modulating their geometry in response to external magnetic fields. While numerous studies have sought to emulate the multifunctionality of natural surfaces, most engineered systems remain fundamentally static in design and fail to respond effectively to environmental stimuli. True multifunctional structures that can actively reconfigure in real time. Our approach directly addresses this gap by enabling a tunable 4D micro/nanostructure array whose surface topography can be precisely transformed on demand. The topographical modulation is governed by a coordinated triad of parameters: applied magnetic field strength, embedded nanoparticle magnetization, and the mechanical modulus of the elastomer matrix. Through systematic investigation of the relationships among these variables, we achieve finely controlled, reversible changes in surface structure and function. These adaptive surfaces can rapidly transition between multiple states to exhibit tailored interfacial properties, such as hydrophobic/hydrophilic switching and bactericidal activity. The proposed system directly supports critical DoD applications, including anti-icing, corrosion resistance, chemical/biological shielding, and scalable camouflage via optical surface modulation. By enabling on-demand and localized surface reconfiguration, this platform opens a new frontier in responsive interface engineering, with broad implications for defense, biomedical, and soft robotics applications.

Modulating Magnetic Couplings: Computational Chemistry towards Designing a Quantum Spin Liquid Material

Timothy C. Schutt,[1] Ashlyn M. Koval,[1] Gilbert K. Kosgei,[1] P. U. Ashvin Iresh Fernando,[1] Glen R. Jenness,[1] and Manoj K. Shukla[1]

[1]U.S. Army Engineer Research and Development Center, Environmental Laboratory, 3909 Halls Ferry Road, Vicksburg, MS 39180, USA

**Corresponding Author Email: timothy.c.schutt@erdc.dren.mil*

Keywords: QSL, MD, DFT, Quantum Materials, Ionic Liquids

Materials with stable support of quantum spin liquid states are a promising avenue to enable quantum computing, communications, and encryption technologies. The ruthenate, α-$RuCl_3$, has been theorized to be able to achieve the quantum spin liquid state due do its unique electronic spin properties and geometric frustration at the electronic level. Ionic Liquids (IL) and organic intercalants have the potential to modulate structural features of the crystal lattice in the c axis. The third order magnetic coupling terms are associated with inter-layer Ruthenium pairs.[1] Thus inter layer spacing changes topological surface effects with potential to fine-tune the properties of α-$RuCl_3$. It is possible that intercalants that respond to external stimuli, such as cis-trans isomerization of asobenzenes, might permit real-time control of the spacing as depicted in Fig. 1. We have employed molecular dynamics modeling to screen combinations of molecular species for their interactions with α-$RuCl_3$ surfaces and intercalation. Synthesis and testing of the top IL pairs was shown to achieve the structural effect predicted *in silico*.[2] IL-templating at the crystal surface as well as consistent expansion of the c-lattice parameter. Modeled and experimental properties that result from the structural changes suggest the potential to impact quantum state access of the material.

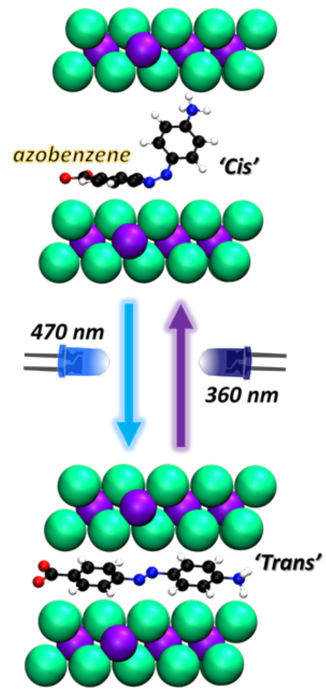

Fig. 1. Depiction of dynamic spacing the α-$RuCl_3$ layers and thus modulating the third order magnetic coupling term.

Funding: Basic research funding under the Installation and Operational Environments (IOE) Program of the United States Army Corps of Engineers and the Environmental Security Technology Certification Program of the Department of Defense by the USAERDC.

References:

[1] Ashlyn M. Koval, Glen R. Jenness, Timothy C. Schutt, Gilbert K. Kosgei, P. U. Ashvin I. Fernando, and Manoj K. Shukla, "Periodic DFT calculations to compute the attributes of a quantum material: honeycomb ruthenium trichloride," ***Phys. Chem. Chem. Phys.***, 2024,**26**, 19369-19379.

[2] P. U. A. I. Fernando, G. K. Kosgei, T. C. Schutt, J. Jernberg,mA. M. Koval, T. L. Thornell and A. N. Kimble. "Efficient microwave-assisted synthesis of 1-hexylpyridin-1-ium bromide: Anion exchange to acetate and fundamentals tools to probe its interaction with $RuCl_3$", J. Mol. Liq., 2024, 397, 124080.

Material Resistance to Erosion Caused by Ship-Scale Cavitation

Joel Hartenberger[1,*], Jin-Keun Choi[1], Geoffrey Warberg[2], Amir Hadadzadeh[2], and Thad Michael[1]

[1]NSWC Carderock Division, 9500 MacArthur Blvd., West Bethesda, MD 20007

[2]The University of Memphis, 3270 Alumni Ave., Memphis, TN 38152

**Corresponding Author Email: joel.d.hartenberger.civ@us.navy.mil*

Keywords: Cavitation, Erosion, Damage, Coatings

Cavitation erosion damages fluid systems, including pumps and propellers, yet remains poorly understood, especially at large scale. Navy propellers and rudders can suffer from damage when water changes phase from liquid to vapor and then back to liquid. This work describes a series of well-controlled, ship-scale experiments that were performed to better understand this complex process. A variety of metals, coatings, and a polymer were installed in a 2.1 m by 3 m hydrofoil and subjected to intense cavitation at speeds ranging from 12.9–18 m/s until they experienced local plastic deformations (i.e. pitting). The data are compared across a range of parameters and with results from the small-scale ASTM G134 testing method. Preliminary results reveal that, for bare metals, the pitting produced by a ship-scale sheet cavity are larger and develop more slowly than pitting produced using the ASTM G134 testing method. Pitting rates for bare metal test specimens relate strongly with flow speed but the erosion of coated metal test specimens appears to relate more strongly with exposure time.

Cavitation occurs when the local pressure in a liquid is reduced below the vapor pressure at the local temperature, resulting in a phase change from liquid to gas. When a subsequent increase in the local pressure causes the gas to change back to the liquid phase, strong pressure waves and liquid jets are created. When this occurs near a surface, local plastic deformation and even material loss may occur. This is known as cavitation erosion. Fig. 1 shows an example of pitting that developed due to cavitation on a soft Aluminum test specimen (Aluminum 1100-H112).

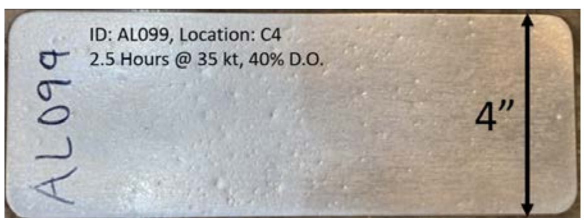

Fig. 1 – Pitting on an Aluminum test specimen caused by a large sheet cavity at 35 knots.

To measure cavitation erosion at ship-scale conditions, experiments were performed in the US Navy's William B. Morgan Large Cavitation Channel which has a test section that is approximately 3 m wide, 3 m high, and 13 m long. Material samples were installed in the Office of Naval Research HiFoil [1], a hydrofoil with a 3 m span and 2.1 m chord and has a pressure distribution similar to the pressure side of a propeller. Ten types of materials and coatings were measured during this testing. Measurements were made at nominal speeds of 13, 14, 16, and 18 m/s with a typical sheet cavity length of approx. 50 percent of the HiFoil chord length. The surface of the material samples was measured with an optical profilometer before and after exposure to cavitation. In addition to the large-scale erosion test, small scale erosion testing was performed using the ASTM G134 method [2]. Metallic materials were characterized by measuring several material properties prior to erosion testing. Preliminary results for Aluminum show that the ship-scale cavitation produced pits that are ~20x larger at a rate ~1000x slower than the ASTM G134 testing method. Coated metal specimens tested for longer durations showed more damage than those tested for shorter durations at higher speeds. The presentation will provide pitting results for several metals and coatings and discuss the underlying factors affecting the erosion rates and failure mechanisms of the various materials tested.

Funding: This work was supported by the Office of Naval Research under grants N0001423WX01969 and N0001425WX00002 supervised by Dr. Julie Young, program officer.

References:

[1] Bourgoyne, D., S. Ceccio, D. Dowling, W. Brewer, S. Jessup, J. Park, and R. Pankajakshan, “Hydrofoil Turbulent Boundary Layer Separation at High Reynolds Numbers,” Proceedings of the *23rd Symposium on Naval Hydrodynamics*, Val de Reuil, France, September 2000.

[2] “Standard Test Method for Erosion of Solid Materials by Cavitating Liquid Jet”, ASTM Designation: G134 – 17, ASTM International, West Conshohocken, PA, 2023.

The Development of a Smoothed Particle Hydrodynamics Framework for Cohesive Soil and Coarse Aggregate Interactions in a Simulated California Bearing Ratio Test

Stubblefield, G.G.[1,*]

[1]U.S. Army Engineer Research and Development Center, 3909 Halls Ferry Rd, Vicksburg, MS 39180
**Corresponding Author Email: George.G.Stubblefield.@usace.army.mil*
Keywords: Smoothed Particle Hydrodynamics, Pavements, Aggregates, Numerical Analysis

The California bearing ratio (CBR) test is commonly used to determine base layer strength by measuring the penetration resistance of a sample and comparing the results to an ideal crushed rock. The size and angularity of the constitutive elements in the base course greatly influence the CBR. Large, angular pieces of aggregate interlock and resist deformation more effectively than small, smooth pieces of aggregate. A computer model should be able to account for shape characteristics of pieces of aggregate and their corresponding interaction to mobilize shear strength under loading. In addition, the layer of soil underneath the base course behaves more as one homogeneous body, since the constitutive elements are significantly smaller than in the aggregate. Therefore, the computer model should also simulate the behavior of cohesive soil in the subgrade.

To accurately model a pavement structure, researchers typically turn to one of two paths to simulate how pavement layers deform under applied loads. The first path describes the interaction between layers, treating each layer as one whole body. Computational schemes such as the layered elastic theory or the finite element method are well suited at capturing the behavior of bodies under low amounts of deformation. However, these approaches fail to capture the behavior of very small bodies, such as individual pieces of aggregate, or large deformation directly underneath a CBR piston. The second path describes the interaction between individual particles, without lumping together pieces of aggregate into one whole layer. Computational schemes such as the discrete element method are well suited for describing behavior between aggregate pieces, but are inadequate for describing subgrades, which behave more like whole bodies.

The Vibrational Entropy of High Entropy Alloys

Brent Fultz[1 *] and Kyle Hunady[1]
[1]Dept. Applied Phys. Materials Sci., California Institute of Technology, 1200 E. Calif. Blvd, Pasadena, CA 91125
*Corresponding Author Email: btf@caltech.edu
Keywords. entropy, vibrational entropy, HEA, calorimetry

Measurements of heat capacity by calorimetry were used to find changes in the vibrational entropy as components are added to concentrated multicomponent alloys. These changes in vibrational entropy alter significantly the entropies of high entropy alloys.

There is enormous international interest in "high-entropy alloys" (at least 23,674 publications to date), with a particular focus on their mechanical properties at high temperatures. These concentrated, multicomponent alloys have a high configurational entropy that helps stabilize them for service at high temperatures. However, their stability depends on the total thermodynamic entropy, and their vibrational entropy is typically an order-of-magnitude larger than their configurational entropy. What is not known, however, is how the vibrational entropy is altered as more components are added to a HEA.

We are measuring vibrational and electronic entropies by precision calorimetry over a temperature range of 2 to 400 K (where configurational entropy remains unchanged), using a PPMS system [1]. We start with equiatomic alloys such as CoCrFeNi and add components such as Al. Instead of increasing the entropy as expected by $\Delta S = k_B \ln n$, where k_B is Boltzmann's constant and n is the number of components in the equiatomic alloy, we find that the effect of Al is a decrease of vibrational entropy by an amount equivalent to decreasing n by 2. This correlates in part with the change of crystal structure from fcc to bcc. Fig. 1b shows examples.

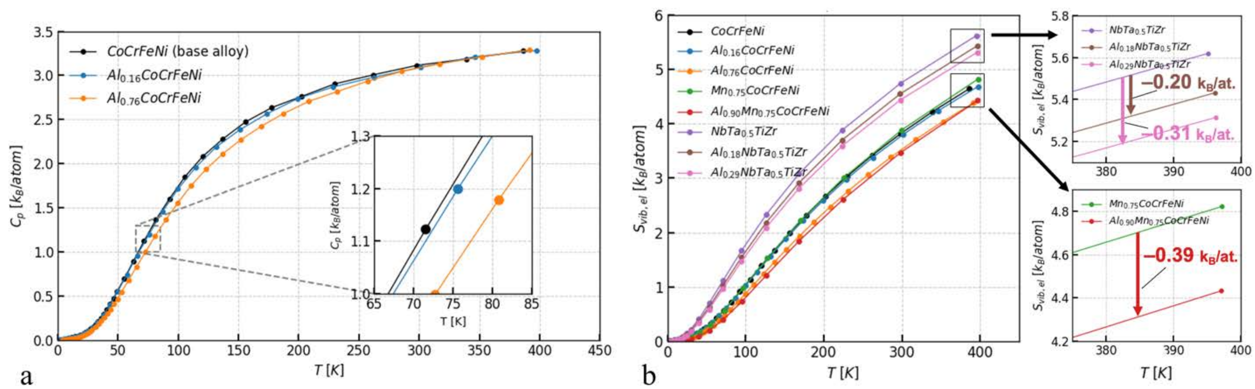

Fig. 1 (a) Calorimetry data $C_P(T)$ on CoCrFeNi compared to CoCrFeNi-Al with two Al concentrations. (b) Entropy vs. T from integrating $C_P/T\, dT$ as in panel a. The right inset shows a decrease in entropy at 390 K with Al additions.

Configurational entropy is expected to be reduced if there is chemical short-range order (SRO) in the alloy, but does vibrational entropy also change with SRO? This work involves preparing multicomponent alloys with high SRO by rapid quenching from the liquid or by high-energy ball milling. Subsequent annealing near 500°C causes changes in SRO as the chemical elements become mobile and redistribute. Mössbauer spectrometry shows that Al atoms migrate to Ni neighbors where they have a lower chemical potential than near Fe atoms.

Our goal is to find rules to estimate the vibrational entropy in concentrated, multicomponent alloys. We are using ideas from Hume-Rothery, with differences in metallic radii, the enthalpies of compound formation (through electronic structure calculations [2]), and we include the atomic mass for vibrational dynamics. Emerging rules, which require further measurements, are 1) vibrational entropy decreases when adding components of larger metallic radii and lower masses, and 2) vibrational entropy decreases with SRO owing to stronger and stiffer chemical bonds.

Funding: This work was supported by the Air Force Office of Scientific Research grant FA9550-25-1-0093.

References

[1] Quantum Design relaxation calorimeter product description. https://qdusa.com/products/ppms.html
[2] K. Persson, "Materials Project" (Compare B2 AlFe to AlNi). https://next-gen.materialsproject.org

Grain Boundary Failure and Strengthening in Entropy Stabilized $(MoNbTaVW)C_5$ Ceramic

Bradley T De Gregorio[1,*], Zoey Warecki[1], James A Wollmershauser[1], Heonjune Ryou[2], Kevin Anderson[1], Lavina Backman[3], Keith Knipling[1], and Evgeniya Lock[1]

[1]*Materials Science and Technology Division, U.S. Naval Research Laboratory, 4555 Overlook Ave. SW, Washington, DC 20375*

[2]*APEX Applied Science and Engineering, 1120 Benfield Blvd. Ste. D, Millersville, MD 21108*

[3]*Spacecraft Engineering Division, U.S. Naval Research Laboratory, 4555 Overlook Ave. SW, Washington, DC 20375*

**Corresponding Author Email: bradley.t.degregorio.civ@us.navy.mil*

Keywords: Hypersonic, High entropy materials, Entropy stabilized ceramic

Nanoscale electron microscopy confirms the presence of deleterious oxide films in a sintered high entropy ceramic. We show that adding a pre-treatment step eliminates the oxides and improves flexural strength.

Development of new materials based on the high entropy stabilization paradigm have resulted in new high strength and high temperature resistance materials, often with additional favorable properties of thermal shock resistance and low reactivity [1]. The configurational entropy of a multicomponent, solid solution system is stable at roughly equimolar composition. Entropy stabilized ceramics have demonstrated exceptional stability and resistance [2,3]. Here we investigate $(MoNbTaVW)C_5$ produced using two different sintering protocols, designated “Molly3” and “Molly8”. The Molly8 sintering protocol includes an additional step to remove surface oxides from the constituent grains before sintering at 1900 °C. Flexural strength tests demonstrated a significant difference between the two samples, with Molly 8 at 360 MPa and Molly3 at 270 MPa.

Secondary electron images reveal a well-polished surface in the Molly8 sample but an irregular surface on the Molly3 sample. Transmission electron microscopy (TEM) characterization was performed using a JEOL F200 at NRL, operated at 200 keV, along with energy dispersive x-ray spectroscopy (EDS) to map out the distribution of any oxide phases. Within the low-strength Molly3 sample, thin oxide films (~10 nm thick) were present along almost all grain boundaries, some of which have opened into gaps. In contrast, grain boundaries in the high-strength Molly8 sample are coherent, with no oxide films observed. Oxygen mapping with EDS confirmed the composition of the grain boundary films in the Molly3 sample. The cation content of the films are variable, some showing high Ta/W concentrations, while others contain high Nb/Mo. These data establish that the low strength of the Molly3 sample is caused by retained surface oxides on the sintered powders, as seen in other entropy stabilized systems [4], and the efficacy of including a pre-treatment step to remove oxides during the sintering protocol in order to the maintain high strength properties of entropy stabilized ceramics.

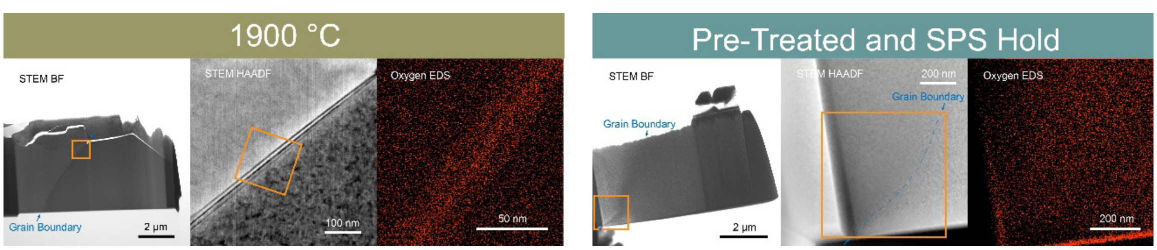

Fig. 1 – Transmission electron microscopy (TEM) imaging and energy dispersive x-ray spectroscopy (EDS) mapping of grain boundaries in the Molly3 (left) and Molly8 (right) samples. The Molly3 sample contains oxide films along the grain boundaries, while these oxides are absent in the high-strength Molly8 sample.

References:

[1] C. Oses et al., “High entropy ceramics,” S. Nat. Rev. Mat., vol. 5, 2020, pp. 295-309.
[2] E. Castle et al., “Processing and properties of high-entropy ultra-high temperature carbides,” Sci. Rep., vol. 8, 2018, Art. No. 8609.
[3] P. Sarker et al., “High-entropy high-hardness metal carbides discovered by entropy descriptors,” Nat. Comm., vol. 9, 2018, Art. No. 4980.
[4] C. Li et al., “Mechanical response and grain boundary behavior of (HfNbTaTiZr)C high-entropy carbide ceramics and its constituent binary carbides,” Surf. Interfac., vol. 52, 2024, Art. No. 104982.

Properties of NiMnGa Shape Memory Alloys for Magnetoelectric Composites

Margo Staruch[1,*], Pavan Chaitanya[2], and Ravi Hadimani[2]

[1]Materials Science and Technology Division, U.S. Naval Research Laboratory, 4555 Overlook Ave. SW, Washington DC 20375

[2]Virginia Commonwealth University, 907 Floyd Ave, Richmond, VA 23284

**Corresponding Author Email: margo.l.staruch.civ@us.navy.mil*

Keywords: ferromagnetic, shape memory alloy, magnetoelectric

Shape memory alloys (SMAs) are a class of materials that will return to a pre-determined shape after heating, reversing any deformations by undergoing an austenitic-martensitic phase transition. Ferromagnetic SMA phases have also been well-established to give rise to large strains of >1% with applied magnetic fields that can shift twin boundaries. These large strains are of interest for many applications including actuators and hermetically sealed joints, and recently have also been considered as the magnetic element in magnetoelectric (ME) composites.[1,2] ME composites conventionally use the magnetostrictive effect in ferromagnets coupled to a piezoelectric material to induce an electric field with an applied magnetic field, with numerous applications including energy harvesting, magnetic field sensing, and electrical stimulation of the brain. However, to achieve these strains requires understanding of the interplay of magnetic fields, stress, and temperature in controlling the response and optimizing the magnetoelectric coupling coefficient α_{ME}. Although $Ni_{50}Mn_{50-x}Ga_x$ SMAs are commercially available, an in-depth understanding of the as-received materials does not yet exist. In this work, we have focused on how to control the magnetostriction and phase transitions by comparing two different COTS $Ni_{50}Mn_{28}Ga_{22}$ bars. The temperature and magnetic field dependence of the magnetization and the strain will be presented, and the narrow window of compressive stress needed to achieve the magnetically-induced phase transition will be discussed. Lastly, in composite heterostructures of the NiMnGa bar and a piezoelectric PVDF polymer, magnetoelectric coupling coefficients of up to 8 mV/cm Oe have been measured without the large 6% strains, and are expected to increase by two orders of magnitude.

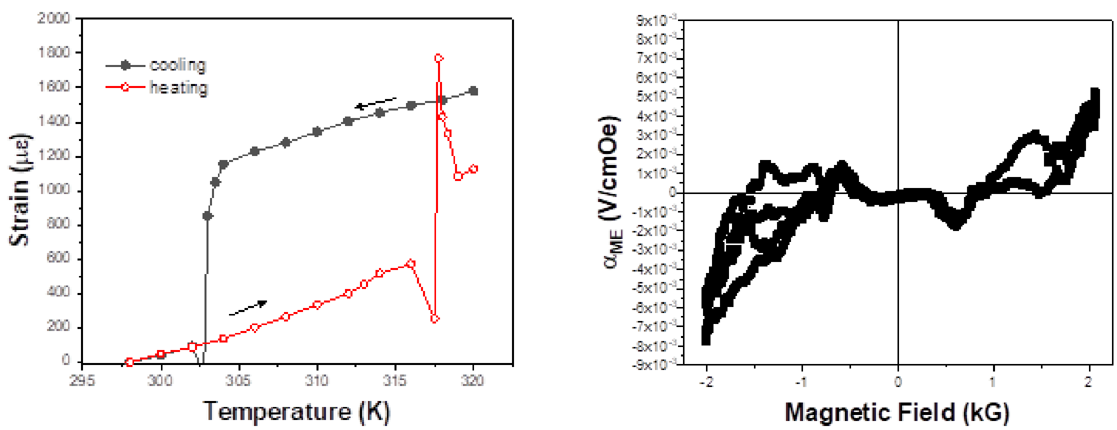

Fig. 1 – (a) Strain versus temperature through the phase transition and (b) the magnetoelectric coupling coefficient versus applied magnetic field for a NiMnGa/PVDF heterostructure.

References:

[1] Z. Zhou et al., "The memory effect of magnetoelectric coupling in FeGaB/NiTi/PMN-PT multiferroic heterostructure" Sci. Rep. vol. 6, 20450 (2016)

[2] S.Y. Chen et al., "Converse magnetoelectric effect in ferromagnetic shape memory alloy/piezoelectric laminate" Appl. Phys. Lett. 95, 022501 (2009)

Thermal Stability of FeCo-Ag Multilayer Thin Films for use in Magnetoelectric Heterostructures for Low SWAP-c Magnetic Field Sensors

Thomas Mion[1*], Margo Staruch[1], Konrad Bussmann[1], and Peter Finkel[1]
[1]*Materials Science and Technology Division, U.S. Naval Research Laboratory, Washington, DC 20375*
**Corresponding Author Email: Thomas.R.Mion.CIV@US.NAVY.MIL*
Keywords: Iron Cobalt, Magnetic multilayers, Thermal stability, Thin film

This investigation studies the thermal and stress properties of FeCo/Ag multilayer thin films prepared by sputter deposition for their potential applications in magnetoelectric heterostructure devices [1,2]. We show rapid thermal annealing of the FeCo/Ag multilayers is robust until annealing temperatures reach 300 – 400 C where a breakdown of the Ag leads to an increased coercive field, and annealing >400 C is severely detrimental to the soft magnetism of the system as the Ag layers deteriorate. X-ray diffraction and reflectometry measurements yield consistent results showing an increased grain size and breakdown of the Ag layers.

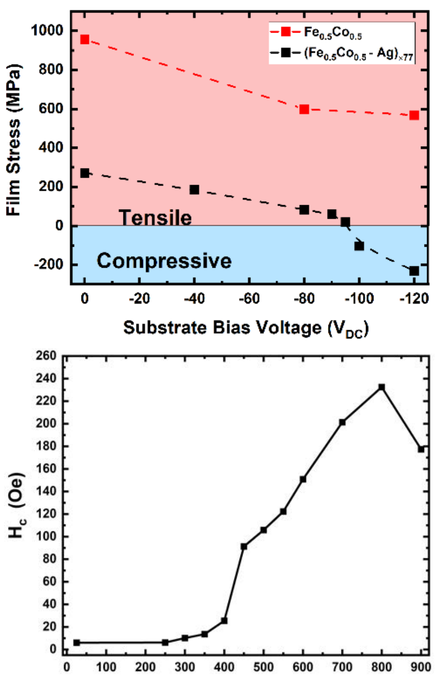

Fig. 1 – Top- Control of as-grown $Fe_{0.5}Co_{0.5}$ and $Fe_{0.5}Co_{0.5}$-Ag multilayer film stress through application of a DC bias voltage during deposition **Bottom-** Trend of the intrinsic coercive field of the $Fe_{0.5}Co_{0.5}$-Ag multilayer after annealing and re-measurement at room temperature.

Physical deposition via magnetron sputtering makes it possible to create layers of repeating materials as well as apply a bias DC electric field to the sample plate. By depositing a small (~8 nm) layer of $Fe_{0.5}Co_{0.5}$ and a subsequent layer of nonmagnetic material this breaks the continuity of magnetic domains in the +z direction restricting the magnetization to be in-plane, and while concomitantly applying a bias DC electric field it is possible to reduce the coercive field and stress of the film. It is currently unknown how a thin film of $Fe_{0.5}Co_{0.5}$-Ag multilayer will be affected when placed in high temperature atmospheres which are often required for device processing and packaging. From the binary phase diagrams, it is known that Ag is immiscible with either Fe or Co at temperatures up to 770 C, thus theoretically there will be no mixing occurring between the Ag and Fe or Ag and Co. Though it is not known if a diffusive process will allow the degradation of the interlayer Ag thus promoting grain formation and growth of magnetic domains.

Fig. 1-Top shows the control of stress in $Fe_{0.5}Co_{0.5}$ and $Fe_{0.5}Co_{0.5}$-Ag multilayer films with an applied DC voltage bias applied to the stage during deposition. A tensile to compressive crossover takes place at ~ -95V. This ability enables excellent control of the film properties for development of microelectromechanical systems (MEMS) device development for magnetic field sensors. Magnetic measurements of the post annealed samples show an increase of the corecive field (H_c) when annealing temperatures were above 250 C. Between 300 – 400 C an increase of H_c from ~6 Oe to ~20 Oe can bee seen in **Fig. 1-Bottom**. A large increase of H_c to ~90 Oe is found when the annealing temperature is above 400 C. The annealing temperature range of 450 – 500 C shows a linear correlation with the increasing cericive field. Because this multilayer structure owes it's low coercive field to the incorporation of the 3 nm Ag layers, it is reasonable to assume eventhough the Ag is imiscible with Fe and Co there is likely some degredation of this multilayer structure. As the temperature increases the Ag seperating the FeCo layers begins to break down allowing out-of-plane crystallite growth thereby negating the usefullness of the multilayer structure. Ag is only imiscible with Fe and Co up to 770 C, which is why when the annealing temperature is >800 C we can see a reduction of H_C in **Fig. 1-Bottom** as an additional alloy phase begins to form.

Funding: Research provided here was performed with funding from the Office of Naval Research through the U.S. Naval Research Laboratory basic research project.

References:

[1] G. Srinivasan, "Magnetoelectric Composites" vol. 40, pp. 153–178, Jul. 2010, doi: 10.1146/ANNUREV-MATSCI-070909-104459.
[2] M. Fiebig, "Revival of the magnetoelectric effect," J Phys D Appl Phys, vol. 38, no. 8, p. R123, Apr. 2005, doi: 10.1088/0022-3727/38/8/R01.

Resolving Femtometer Displacement and Corresponding Quasi-Static Strain via Grazing Excidence Optical Diffraction Experiments (GEODE)

Andrew J. Birnbaum[1,*], John C. Steuben[1], Anna K. Rawlings[1], Scott A. Mathews[2], Benjamin D. Graber[1], and Athanasios Iliopoulos[1]

[1] Code 6394,U.S. Naval Research Laboratory, 4555 Overlook Ave. SW, Washington, DC 20375

[2] Code 6364, U.S. Naval Research Laboratory, 4555 Overlook Ave. SW, Washington, DC 20375

**Corresponding Author Email: andrew.j.birnbaum.civ@us.navy.mil*

Keywords: Strain measurement, diffraction, grazing excidence.

Although strain measurement via optical diffraction is conceptually simple and well understood, it has thus far been limited with respect to strain resolution. This work, based on a simple one-dimensional diffraction grating, builds on prior optical diffraction techniques to significantly extend the resolution with which strain may be measured. A new approach, termed grazing excidence optical diffraction experiment (GEODE) is introduced, demonstrating an ultimate strain resolution of ~800 picostrain, under true quasi-static loading conditions, i.e., without any signal averaging. To our knowledge, this is the finest strain resolution reported to date for a true quasi-static measurement. This technique, in which the diffracted beam propagates close to 90º with respect to the surface normal, allows the separation of strain signals and rigid body rotation. It also allows a variety of noise reduction techniques, employing multiple beams and multiple wavelengths. However, it presents interesting challenges in data acquisition and data processing, due to the distorted profile of the diffracted beam. In addition to presenting proof-of-principle data, this talk will include discussion of image acquisition techniques, data processing, and multi-beam noise reduction.

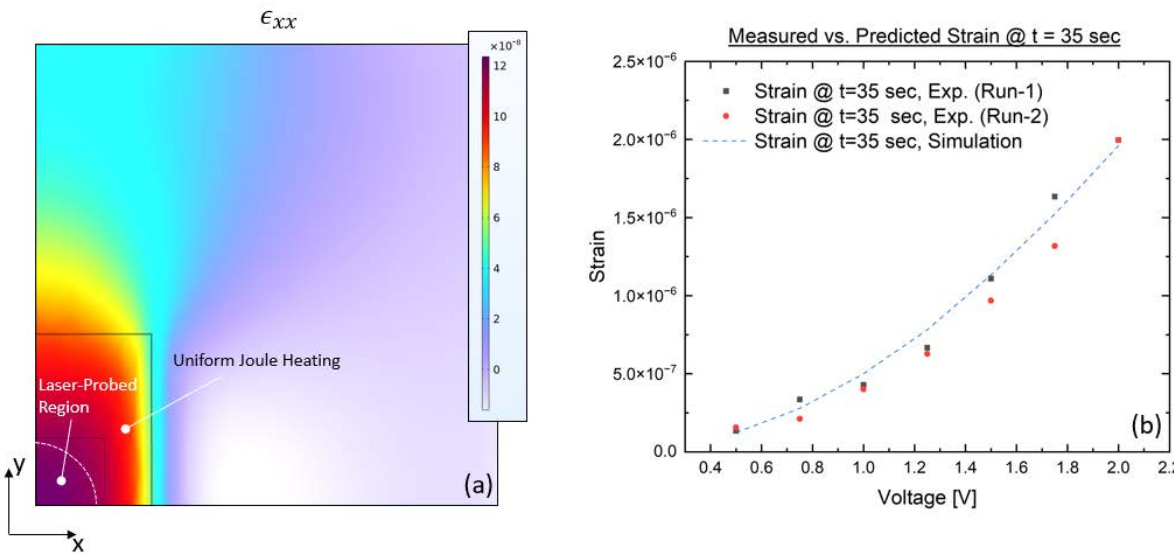

Fig. 1 – (a) Representative contour plot for normal strain, ϵ_{xx} as predicted via the COMSOL Multiphysics model, and (b) comparison of FEM predictions against GEODE-measured values

Funding: This work was funded by the Office of Naval Research, through the NRL 6.1 Base Program.

Experimental and Numerical Fatigue Analysis of Imperfect Octet Lattices

Attilio Arcari[1,*], Nicole A. Apetre[2]
[1]Center for Corrosion Science and Engineering, [2]Materials Science and Technology Division
[1,2]U.S. Naval Research Laboratory, 4555 Overlook Avenue SW, Washington, DC, 20375
**Corresponding Author Email: attilio.arcari.civ@us.navy.mil*
Keywords: metamaterials, fatigue life, durability and reliability of metamaterials, laser bed powder fusion, PA2200 - Polyamide 12.

While metamaterials created by additive manufacturing exhibit enhanced multiphysics properties compared to traditional solid materials, their durability and damage tolerance are critical concerns. This study addresses these concerns by examining the fatigue behavior of octet-cell lattice metamaterials. An initial state of damage is introduced in the coupon by removing one of the nodes of the metamaterial structure located in the center of the sample geometry, therefore severing all connected struts. While sample stiffness remained unaffected, the fatigue life of the samples was reduced by almost one order of magnitude with respect to the sample without the center damage. These structures were 3D-printed using PA2200 nylon via laser powder bed fusion. Experimental measurements of fatigue life are compared with computational simulations to analyze damage progression and ultimate failure mechanisms.

Prior work [1,2] examined the fatigue life of metallic and polymeric metamaterials through numerical and experimental approaches. Numerically, the fatigue life of Ti-6Al-4V octet and Kelvin lattices was predicted as a function of relative density. Experimentally, the completely reversed low-cycle fatigue life of PA2200 octet metamaterials with varying strut thicknesses was measured and correlated with normalized effective stiffness degradation. Analysis of sequential fatigue failures of struts within the metamaterial structure identified nodes in the sample's core volume as the critical connection points for structural integrity. Additionally, the analysis of pre-damaged samples was successful in identifying the critical nodes in the samples where fatigue failures started from. A methodology to assess the fatigue life of imperfect lattices is sought in the current work, to develop an understanding of the effects of stress concentrators caused by deviations from a perfect lattice on fatigue life.

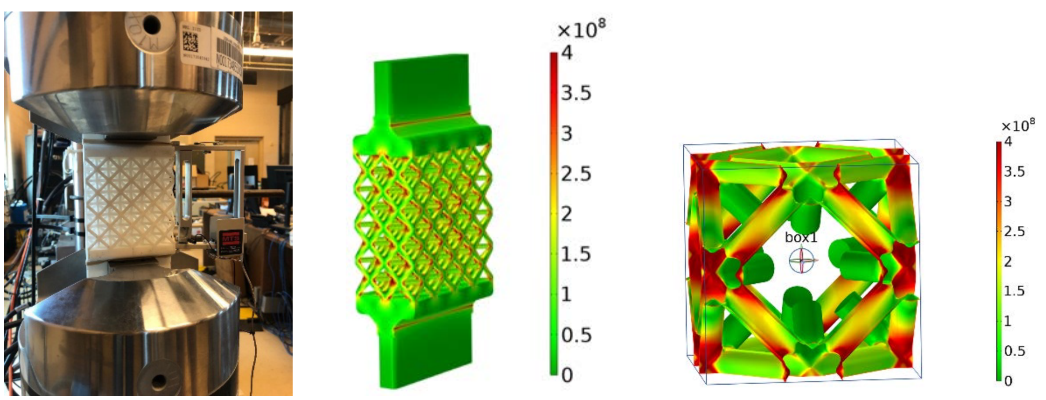

Fig. 1 – Fatigue testing configuration (left). Contours of von Mises stress: coupon scale (center) and detail showing the missing central node (right)

Funding: The authors acknowledge support for this work by the Office of Naval Research through the Naval Research Laboratory’s core funding.

References:

[1] Apetre, N. A., Michopoulos, J. G., Rodriguez, S. N., Iliopoulos, A., Steuben, J. C., Graber, B. D., & Arcari, A. (2024). Toward Fatigue-Tolerant Design of Additively Manufactured Strut-Based Lattice Metamaterials. Journal of Computing and Information Science in Engineering, 24(5).

[2] Arcari, A., Strickland, E. P., Apetre, N. A., & Michopoulos, J. G. (2025). On the assessment of low cycle fatigue performance of octet-based structural metamaterial. International Journal of Fatigue, 108936.

Enhancing Hydrogen Production in Ethanol Reforming via Oxygen Vacancy-Rich Supports and Transition Metal Synergy

Gene Yang*, Jiangtiang Li, and Deryn Chu
DEVCOM Army Research Laboratory, 2800 Powder Mill Rd, Adelphi, MD 20783
**Corresponding Author Email: gene.yang4.ctr@army.mil*
Keywords: Ethanol CPOX, hydrogen production, Ni-based catalysts, non-noble metals, oxygen vacancies, ceria support

Catalytic partial oxidation (CPOX) of ethanol enables efficient hydrogen production with rapid startup and compact system design, offering potential for distributed energy applications [1-3]. This work investigates the design of Ni-based catalysts supported on gadolinium-doped ceria (GDC), focusing on how oxygen vacancy concentration and metal–support interactions govern product selectivity and catalyst stability. GDC is employed as a support to provide high oxygen mobility and redox activity [4]. These properties are critical for oxidizing carbonaceous intermediates and suppressing catalyst deactivation. Preliminary experiments using Ni-GDC catalysts demonstrate high hydrogen yield but also reveal an increasing trend in C_2 hydrocarbon formation over time, indicating gradual catalyst deactivation. Interestingly, incorporating a small amount of Ru into the Ni-GDC system stabilized the C_2 product distribution and improved long-term performance, underscoring the importance of metal synergy in promoting selectivity and resistance to deactivation. Building on these insights, this research aims to replicate the stabilizing effect using entirely non-noble metal combinations—specifically, Ni with Fe, Co, and Cu—supported on oxygen-vacancy-rich GDC. Particular emphasis is placed on achieving uniform metal dispersion, strengthening metal–support interactions, and anchoring active sites in a manner that resists sintering and carbon accumulation. This approach aims to uncover structure–function relationships critical for the design of stable, high-performance catalysts in ethanol reforming systems.

Funding: Research was sponsored by the Army Research Laboratory and was accomplished under Cooperative Agreement Number W911NF-24-2-0079. The views and conclusions contained in this document are those of the authors and should not be interpreted as representing the official policies, either expressed or implied, of the Army Research Laboratory or the U.S. Government. The U.S. Government is authorized to reproduce and distribute reprints for Government purposes notwithstanding any copyright notation herein.

References:

[1] R. Chaubey, S. Sahu, O. O. James, and S. Maity, "A review on development of industrial processes and emerging techniques for production of hydrogen from renewable and sustainable sources," *Renewable and Sustainable Energy Reviews,* vol. 23, pp. 443-462, 2013.
[2] D. Zanchet, J. B. O. Santos, S. Damyanova, J. M. R. Gallo, and J. M. C. Bueno, "Toward understanding metal-catalyzed ethanol reforming," *ACS Catalysis,* vol. 5, no. 6, pp. 3841-3863, 2015.
[3] R. Ma, B. Xu, and X. Zhang, "Catalytic partial oxidation (CPOX) of natural gas and renewable hydrocarbons/oxygenated hydrocarbons—A review," *Catalysis Today,* vol. 338, pp. 18-30, 2019.
[4] O. Tojira, J. G. Lomonaco, T. Sesuk, S. Charojrochkul, and P. Tepamatr, "Enhancement of hydrogen production using Ni catalysts supported by Gd-doped ceria," *Heliyon,* vol. 7, no. 10, p. e08202, 2021.

Impact of Metal Oxide Supports on Low Temperature RWGS Activity over K-Mo_2C Catalysts

Cameron Holder[1,*], Andrew Shabaev, [1] Jeffrey Baldwin,[2] and Heather Willauer[1]

[1]*Materials Science and Technology Division, Naval Research Laboratory, 4555 Overlook Ave. SW, Washington, DC 20375*

[2]*Acoustics Division, Naval Research Laboratory, 4555 Overlook Ave. SW, Washington, DC 20375*

**Corresponding Author Email: cameron.f.holder.civ@us.navy.mil*

Keywords: CO_2 Utilization, RWGS, Supported Catalysis

To promote energy independence, broader energy security, and "Freedom of Action" for the warfighter, our group at the Naval Research Laboratory is developing a process to transform CO_2 that has been captured from seawater into sustainable aviation fuels for the Navy. A pivotal step in this transformation process is the reverse water gas shift reaction (RWGS). Since the RWGS is an endothermic process, this reaction is typically conducted at higher temperature; however, the use of elevated temperatures can result in catalyst deactivation, higher energy requirements, place constraints on design of the reactor. Therefore, it is paramount to develop catalysts that can efficiently convert CO_2 into CO at lower temperatures. Transition metal carbides, particularly Mo and W, have excellent catalytic properties for the RWGS, especially when promoted with alkali transition metals and supported on a metal oxide support [1,2]. The identity of the metal oxide support has been shown to be highly influential in the overall catalytic activity. To this end, the goal of this study was to better understand how various metal oxide supports affected the RWGS activity of potassium promoted Mo_2C to help further optimize future catalyst compositions for the low temperature RWGS reaction.

A variety of different metal oxide supported Mo_2C catalysts were synthesized and evaluated for the low temperature RWGS. While the reaction temperature was maintained at 300 °C throughout all experiments, various space velocities were probed. This enabled accurate comparisons between catalysts based on CO site time yields. Our results indicated that when Mo_2C was supported on non-reducible and Lewis acidic supports such as alumina, the highest CO site time yields were observed. Furthermore, when Mo_2C was supported on reducible metal oxides such as ceria, RWGS activity was significantly hindered due to over-reduction to an inactive Mo phase. This was contrary to our initial hypothesis as reducible oxides have been reported to actively and synergistically participate in the reaction mechanism, leading to increased activity. Finally, the evaluated catalysts were also stable under testing conditions for a minimum of 12 hours on stream [3]. These results indicate that optimal catalysts compositions for the low temperature RWGS reaction may incorporate transition metal carbide materials supported on non-reducible and Lewis acidic supports.

References:

[1] R. B. Levy and M. Boudart, "Platinum-Like Behavior of Tungsten Carbide in Surface Catalysis", SCIENCE, 1973, **181** , 547-549

[2] M. D. Porosoff, J. W. Baldwin, X. Peng, G. Mpourmpakis, and H. D. Willauer, "Potassium-Promoted Molybdenum Carbide as a Highly Active and Selective Catalyst for CO_2 Conversion to CO", *ChemSusChem*, 2017, **10**, 2408 - 2415

[3] C. F. Holder, J. R. Morse, P. M. Barboun, A. R. Shabaev, J. W. Baldwin, and H. D. Willauer, "Evaluating metal oxide support effects on the RWGS activity of Mo_2C catalysts", CATAL. SCI. TECHNOL., 2023, 13, 2685-2695

Experimental and Numerical Fatigue Analysis of Imperfect Octet Lattices

Attilio Arcari[1,*], Nicole A. Apetre[2]
[1]Center for Corrosion Science and Engineering, [2]Materials Science and Technology Division
[1,2]U.S. Naval Research Laboratory, 4555 Overlook Avenue SW, Washington, DC, 20375
**Corresponding Author Email: attilio.arcari.civ@us.navy.mil*
Keywords: metamaterials, fatigue life, durability and reliability of metamaterials, laser bed powder fusion, PA2200 - Polyamide 12.

While metamaterials created by additive manufacturing exhibit enhanced multiphysics properties compared to traditional solid materials, their durability and damage tolerance are critical concerns. This study addresses these concerns by examining the fatigue behavior of octet-cell lattice metamaterials. An initial state of damage is introduced in the coupon by removing one of the nodes of the metamaterial structure located in the center of the sample geometry, therefore severing all connected struts. While sample stiffness remained unaffected, the fatigue life of the samples was reduced by almost one order of magnitude with respect to the sample without the center damage. These structures were 3D-printed using PA2200 nylon via laser powder bed fusion. Experimental measurements of fatigue life are compared with computational simulations to analyze damage progression and ultimate failure mechanisms.

Prior work [1,2] examined the fatigue life of metallic and polymeric metamaterials through numerical and experimental approaches. Numerically, the fatigue life of Ti-6Al-4V octet and Kelvin lattices was predicted as a function of relative density. Experimentally, the completely reversed low-cycle fatigue life of PA2200 octet metamaterials with varying strut thicknesses was measured and correlated with normalized effective stiffness degradation. Analysis of sequential fatigue failures of struts within the metamaterial structure identified nodes in the sample's core volume as the critical connection points for structural integrity. Additionally, the analysis of pre-damaged samples was successful in identifying the critical nodes in the samples where fatigue failures started from. A methodology to assess the fatigue life of imperfect lattices is sought in the current work, to develop an understanding of the effects of stress concentrators caused by deviations from a perfect lattice on fatigue life.

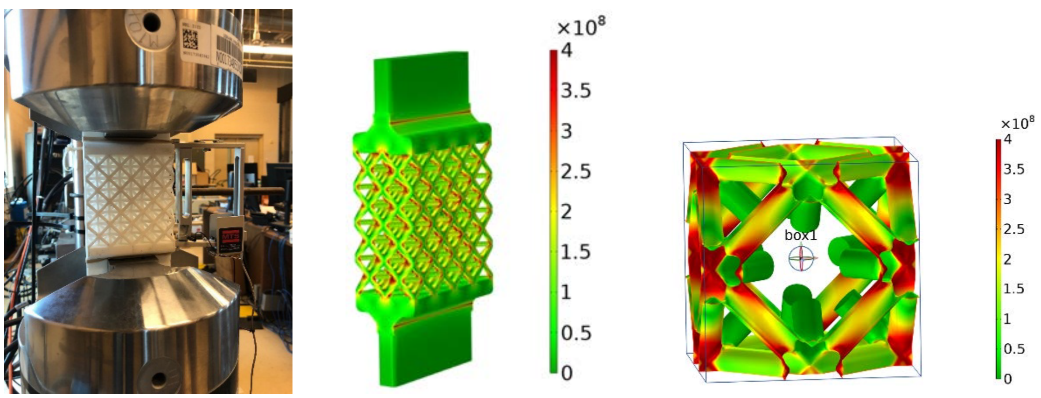

Fig. 1 – Fatigue testing configuration (left). Contours of von Mises stress: coupon scale (center) and detail showing the missing central node (right)

Funding: The authors acknowledge support for this work by the Office of Naval Research through the Naval Research Laboratory's core funding.

References:

[1] Apetre, N. A., Michopoulos, J. G., Rodriguez, S. N., Iliopoulos, A., Steuben, J. C., Graber, B. D., & Arcari, A. (2024). Toward Fatigue-Tolerant Design of Additively Manufactured Strut-Based Lattice Metamaterials. Journal of Computing and Information Science in Engineering, 24(5).

[2] Arcari, A., Strickland, E. P., Apetre, N. A., & Michopoulos, J. G. (2025). On the assessment of low cycle fatigue performance of octet-based structural metamaterial. International Journal of Fatigue, 108936.

Influence of Tetraalkylammonium Additives on Zn-Ni Electrodeposition

Carlos M. Hangarter,[1] Christopher Klug, [1] Andrew Purdy, [1] Chris Breshike, [2] Youngchan Kim,[2] Steve Policastro[1]

[1]Chemistry Division, U.S. Naval Research Laboratory, Washington, DC 20375

[2]Materials Science and Technology Division, U.S. Naval Research Laboratory, Washington, DC 20375

We aim to develop a theoretical framework for the use of organic additives to tailor Zn-Ni coating properties. This presentation reports on the influence of tetraalkylammonium additives in the electrodeposition of ZnNi sacrificial corrosion coatings. Cyclic voltammetry (CV) was utilized with rotating disc electrodes to identify S-shaped negative differential resistance indicative of suppressor behavior**.** Experimental results were used to determine additive isotherms and were compared with molecular dynamics modeling results. Electrochemical quartz crystal microbalance and CV were used to understand additive influence on adsorption behavior and underpotential deposition features. EQCM was also combined with chronoamperometry to understand the influence of additives on Zn, Ni, and ZnNi electrodeposition. Results from the latter were also paired with energy dispersive X-ray spectroscopy to obtain partial currents for Zn, Ni and H reduction. Hydrogen content is critical in the performance of sacrificial corrosion coatings for high strength steels. These coatings were consequently examined with glow discharge optical emission spectroscopy depth profiling to measure through thickness hydrogen content within the deposits.

Next-Generation Electrochemical Desalination for Enhanced Warfighter Autonomy

Zachary G. Neale,[1,*] Ramsay B. Nuwayhid,[2] Meghanne E. Tighe,[3]
Ryan H. DeBlock,[1] Debra R. Rolison,[1] and Jeffrey W. Long[1]

[1] *Surface Chemistry Branch (Code 6170),*
U.S. Naval Research Laboratory, Washington, DC, USA
[2] *National Research Council Postdoctoral Associate,*
U.S. Naval Research Laboratory, Washington, DC, USA
[3] *American Society for Engineering Education Postdoctoral Fellow*
U.S. Naval Research Laboratory, Washington, DC, USA
**Corresponding Author Email: zachary.g.neale.civ@us.navy.mil*
Keywords: electrochemical desalination; redox-mediated electrodialysis; potable water generation

Sustaining warfighter operations requires reliable access to potable water. Present reliance on logistical resupply poses significant cost and risk, especially in contested environments. Leveraging local water sources offers a pathway to enhanced mission endurance and survivability. While reverse osmosis (RO) excels in seawater desalination, its scalability for individual or small unit use and efficiency with brackish water are limited. Our research explores electrochemical desalination methods as a portable, energy-efficient alternative for brackish water purification. We investigate new materials and device designs, including NRL's patented silver sponge electrodes for faradaic chloride removal and redox-mediated flow cells utilizing graphite felt electrodes with controlled surface functionality. We analyze key design parameters and benchmark performance of a small-scale device, targeting the potable water requirements of individual and team-level warfighters operating in remote environments.

Chemistry-Driven Design of Quantum Heterostructure for RF and Power Applications

Mahesh Neupane

DEVCOM Army Research Laboratory Army Research Office (ARO), Durham, NC 27709

Heterointerfaces between ultra-wide bandgap semiconductors offer incredible potential for RF and power application related devices, due to their extreme robustness in high-power, high-frequency and high-temperature operating environment. Polar heterovalent interfaces, such as the (100) diamond/cBN interface, with < 2% lattice mismatch, demonstrate the greatest capability for tuning of various electronic properties, such as band offsets, since different interfacial atomic configurations result in dramatically different interfacial properties. Our work investigates the role of interfacial chemistry in the structural and electronic properties of the (100) diamond/cBN heterostructure by implementing scalable quantum chemistry simulations. The observed binding energy analysis reveals that the interfacial intermixing between B/N and C contributes to enhanced stability of the resultant heterostructure. Analysis of the interfacial potential profiles also uncovers an interesting composition-dependent "Type-II to Type-I" switching of the band alignment between (100) diamond and cBN systems. The heterostructures with the B terminated cBN layer exhibit type-II band alignment with (100) diamond layer, whereas the N terminated interfaces show type-I band alignment, which allows electron conduction across the interface blocking hole conduction, providing a much-needed route for n-type diamond doping. We show that modulation of the interfacial chemistry through mixing carbon into the interface provides a pathway for continuously tunable electronic properties at the interface. This chemistry-driven work expands crucial knowledge of the structural and electronic properties of diamond/cBN heterojunctions, paving the way for future understanding and implementation of high-quality diamond/cBN heterointerfaces in RF and power device applications.

Chromatoscopy: A New Paradigm for Chemical Sensing

Tyler J. Huffman[1]*, Christopher J. Breshike[1]; Daniel Corbin[1]; Robert Furstenberg[1]; R. Andrew McGill[1]

1. Naval Research Laboratory, Washington, DC 20375
*Corresponding Author Email: tyler.j.huffman3.civ@us.navy.mil
Keywords: "Chemical Analysis, Chemical Detection, Infrared, Optics, Automation".

We present a new paradigm for chemical analysis that promises to enable lab-quality chemical analysis in the field, allowing for rapid detection of chemical threats whilst greatly reducing false alarm rate.

Traditionally, chemical analysis of complex mixtures is performed by first separating the mixture into its component parts – typically via some chromatography technique – before the components are identified and quantified – typically via some spectroscopy (or mass spectrometry) technique. This "end-column paradigm" has achieved great success because the separation step addresses the weakness of the spectroscopy techniques in handling complex mixtures. However, the chromatography half of the analysis has its own weaknesses, most notably that it is generally a slow process, particularly without an expert user to optimize the separation parameters. This lack of speed and/or reliance on an expert user are the primary limitations to lab quality chemical analysis in the field. Here we present our work towards a new paradigm of chemical analysis – the in-column paradigm – in order to allow for rapid identification and sensing of chemical components before they elute from the chromatography column.

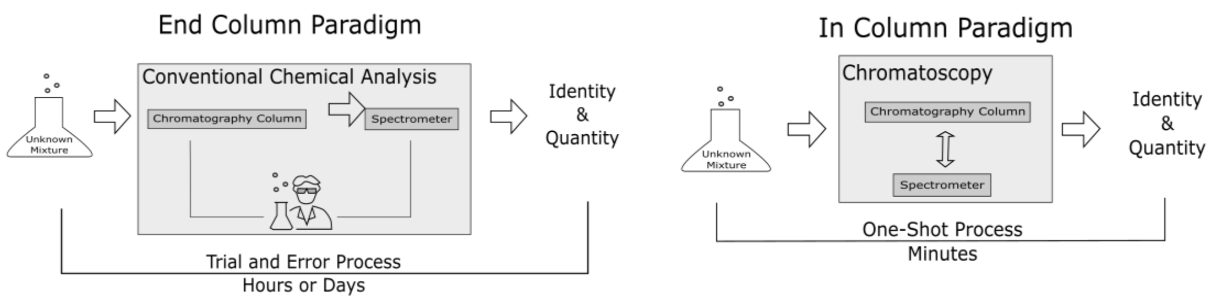

Fig. 1: Flowcharts comparing both end-column and in-column paradigms of chemical analysis.

Synthesis and Characterization of Bio-based Epoxy Resins Derived from Thymol and Carvacrol

Natalie A. Vest[1*], Catherine A. Sarantes[1], K. Randall McClain[1], Elise Tseng[1], Jessica Cash[1], Lawrence C. Baldwin[1], Joshua E. Baca[1], and Benjamin G. Harvey[1]

[1]*Chemistry Division, Naval Air Warfare Center Weapons Division, 1900 N. Knox Rd. Bldg. 02489 RM 1030 MS 6303, China Lake, CA 93555*

**Corresponding Author Email: natalie.a.vest.civ@us.navy.mil*
Keywords: bio-based, epoxy, thermoset, aerospace, oxidative coupling, domestic feedstocks

Many conventional epoxy resins utilized in the aerospace and electronic sectors are based on petroleum-derived bisphenol A (BPA). However, BPA is synthesized from petrochemicals sourced through tenuous supply chains and has been shown to have negative estrogenic effects, which supports the exploration of less-toxic bisphenols that can be produced domestically. In this work, we describe the synthesis of sterically hindered bisphenols derived from naturally occurring plant extracts including thymol (thyme) and carvacrol (oregano), via a catalytic oxidative approach that can be conducted in water. The bisphenols were converted to epoxy resins and cross-linked with commercial 4,4'-methylenebis(2-ethyl-6-methylaniline) (MEMDA) to generate robust networks (Fig. 1). The thermochemical properties of these networks were evaluated by a suite of analytical techniques including differential scanning calorimetry (DSC), thermogravimetric analysis (TGA), thermomechanical analysis (TMA), and microscale combustion calorimetry (MCC). The properties of the networks were then compared to conventional petroleum-based BPA epoxy, to which the carvacrol dimer showed a comparable T_g of 170.5 °C to similar commercial BPA systems (170.9 °C) [1]. Through the development of efficient, high-throughput synthetic routes consistent with the tenets of green chemistry, full-performance bio-based epoxies can be produced that offer similar performance compared to conventional BPA-based epoxies while offering improved sustainability and reduced long-term health effects.

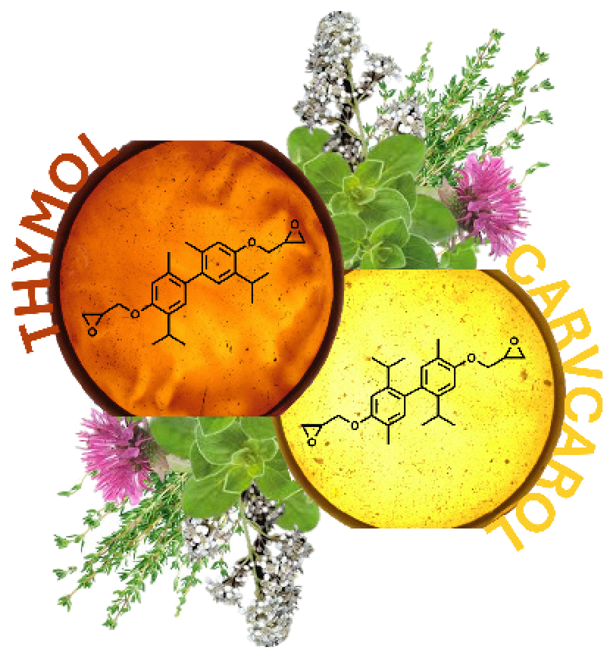

Fig. 1 – Microscope images of two cured pucks made from thymol and carvacrol derived epoxies with MEMDA with the specific chemical structure centered in each puck, surrounded by plant sources for thymol and carvacrol.

Funding: DoD SMART SEED Innovation Award

References:

[1] M. D. Garrison and B. G. Harvey, "Bio-based hydrophobic epoxy-amine networks derived from renewable terpenoids," *Journal of Applied Polymer Science*, vol. 133, no. 45, Mar. 2016, doi: https://doi.org/10.1002/app.43621.

Next-Generation Manufacturing Exploiting Combustion Synthesis And Directed Self-Assembly for Energy Storage and Catalysis

Sarah Bindon, Thomas Colburn and Reinhold H. Dauskardt*,

Department of Materials Science and Engineering, Stanford University, Stanford, CA 94025

**Corresponding Author Email: dauskardt@stanford.edu*

Keywords: manufacturing, nanocomposites, energy storage, catalysis.

We demonstrate next-generation manufacturing using a self-assembling polymer as the fuel source in a combustion reaction to generate highly structured nanoporous transition metal oxide films at low temperature on flexible substrates in a matter of minutes using our patented porogen-integrated rapid oxidation (PiRO) process. DoD target applications include optoelectronics, sensing, energy storage, and catalysis.

Structured mesoporous metal oxide films have important DoD target applications in optoelectronics, sensing, energy storage, and catalysis. Nanolayered capacitors with small form factors (<5 µm thickness) on flexible substrates with much higher energy recovery and density are a pivotal technology to bridge the gap between existing energy storage and next-generation batteries and capacitors. However, current manufacturing via traditional sol-gel approaches requires aging and sintering over hours or days to yield controlled, meso-scale porosity at the cost of manufacturability.

Next-generation manufacturing using a self-assembling polymer as the fuel source in a combustion reaction is demonstrated to generate highly structured nanoporous transition metal oxide films at <200°C in minutes with our patented porogen-integrated rapid oxidation (PiRO) process. The films show an open-cell, face-centered cubic structure of spheroidal pores. Additional ligands can be coordinated with the metal cation to stabilize and control the self-assembly.

We demonstrate manufacturing with PiRO on flexible polymeric substrates. The nanoporous films can be filled with a second phase polymer to produce nano-composite films with desirable mechanical, thermal and dielectric properties. Our method offers a tunable, scalable, low temperature, and hence lower-cost method to generate large area structured nanoporous and nanocomposite metal oxide films.

We demonstrate nanolayered capacitors with exceptional energy storage and Co, Ni, and Cu oxide films with high thermocatalytic selectivity to CO_2 reduction to produce valuable fuels and chemicals.

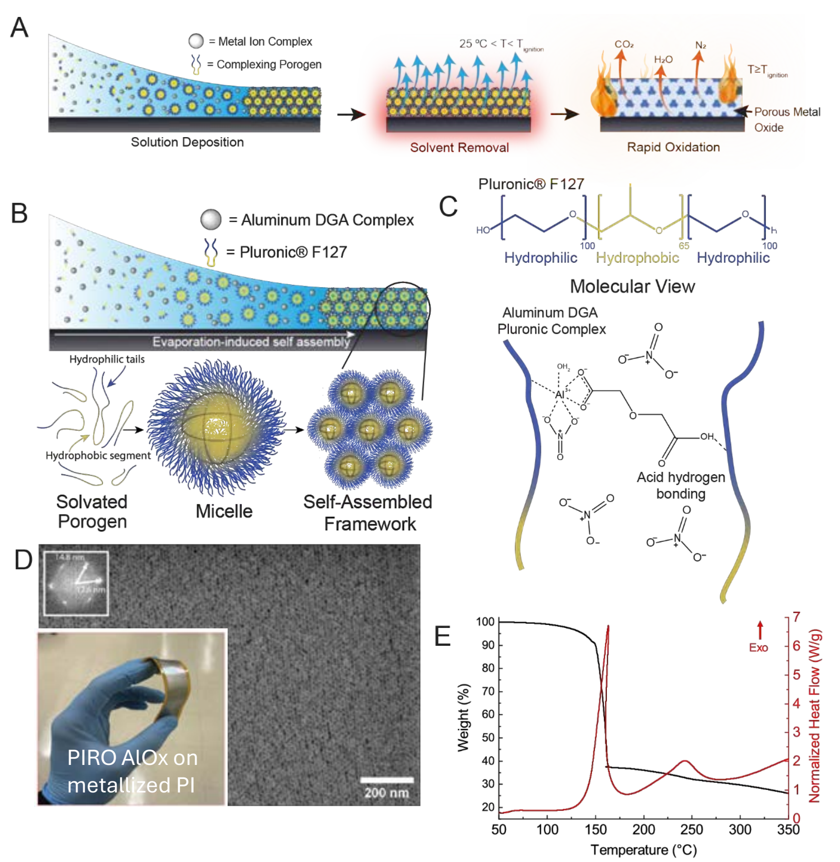

Fig. 1 - **Combining directed self-assembly and solution combustion for next-generation PIRO.** A. Open-air spray film deposition, micelle self-assembly, solvent removal and combustion. B. Self-assembly of the tri-block co-polymer. C. Metal complexation involving nitrate anions, diglycolic acid, and PEO segments. D. SEM of a Al_2O_3 film with inset of FFT highlighting the periodic pore structure and processing on flexible polyimide. E TGA/DSC showing the rapid combustion reaction at low temperature.

4. Topic: Additive Manufacturing

Electron Beam Additive Manufacturing of Tungsten

Frank Kellogg[1*], Kurtis Watanabe[2], Francisco Medina[2], Brandon McWilliams[3]
[1]SURVICE Engineering, 4695 Millennium Dr., Belcamp MD, 21017
[2]University of Texas El Paso, College of Engineering - W.M. Keck Center for 3D Innovation Advanced Manufacturing and Aerospace Center, 1800 Hawthorne St., El Paso, Texas 79968
[3]DEVCOM Army Research Laboratory, Aberdeen Proving Ground, MD 21005
[*]Franklin.R.Kellogg.ctr@army.mil
Keywords: Tungsten, Electron Beam Additive Manufacturing, A2X

Tungsten has the highest melting point and density of any pure metal, making it an attractive material for use in the extreme environments that the U.S. Army increasingly needs to operate in. These properties also make tungsten a difficult metal to form using traditional manufacturing techniques. Additionally, it is a relatively hard material with a very high Ductile-to-Brittle-Transition-Temperature (DBTT), it is above 200 ºC for tungsten, that causes tungsten to behave like a brittle material at room temperature, making the machining of tungsten difficult. A lot of these drawbacks can be mitigated through the production of near-net shaped tungsten parts through additive manufacturing (AM). However, AM of tungsten is a non-trivial proposal. The high melting point leads to the usage of higher energy densities than other materials and the high DBTT means that tungsten parts cannot deform in response to the build up of residual stresses during AM, making it difficult to create tungsten parts without massive cracks. A third hurdle to AM tungsten is that, while tungsten is relatively inert to oxygen in the solid state, oxygen uptake during melting is very detrimental to the final properties of the part. The only AM technique that can readily mitigate all these issues is Electron Beam AM (EBM). In EBM, the build is kept under a high vacuum, preventing oxygen take up, and parts can be built at very high temperatures, mitigating the DBTT issues. In this study, an Arcam A2X EBM system was used to manufacture AM tungsten samples. While initial attempts at building with tungsten led to parts with large levels of porosity, herein we will show how this issue can be mitigated through changes to simple variables like part packing density and support structures. This will be shown through optical microscopy results revealing fully dense tungsten parts, albeit with large, elongated grains.

Interface Evolution During Melt-Infiltration of Ceramic Matrix Composite Preforms Created via Continuous Fiber Additive Manufacturing

David J. Mitchell[1,*]

[1]*Departments of Materials Science and Engineering and Mechanical and Aerospace Engineering, University of Central Florida, 12760 Pegasus Drive, ENG I, Suite 207, Orlando, FL 32816*

**Corresponding Author Email: david.j.mitchell@ucf.edu*

Silicon melt-infiltration of additively manufactured continuous carbon fiber preforms was performed. Automated fiber placement of the carbon fibers in a polyether ether ketone matrix was performed. Pyrolysis converted the polymer matrix to porous carbon, and reactive melt-infiltration converted part of the carbon matrix to silicon carbide. The C/C-SiC composites had 10–20% porosity, flexural strength of 235 MPa, and displayed toughness. This effort investigated how the reactive melt-infiltration process would behave. Future work will investigate the effect of polymer/infiltrant composition on the chemistry and structure of the interfaces created.

Ultra-high temperature ceramic matrix composites (UHTCMCs) are a critical technology in the development of hypersonic vehicles traveling at greater than Mach 5 [1, 2]. Shape stable leading edges are required for controlled flight at such high speeds. Additive manufacturing (AM) and reaction melt-infiltration (RMI) provide the opportunity for rapid, cost-effective manufacturing of UHTCMC components, with printing and densification occurring in days, rather than weeks or months. There are significant chemical processes and interactions involved in the printing and densification processes. A model C/C-SiC system was selected for demonstration, employing continuous carbon fibers (C_f) printed with a polyether ether ketone (PEEK) matrix, which is presently utilized for fabricating polymer matrix composites. Silicon RMI is also currently used in a production environment for the SiC/SiC CMCs in the GE GEnx engines. The baseline processes were combined with the result of creating a composite structure with a C/SiC sheath around the C_f tows and veins of SiC between the tows, (Fig. 1) [3].

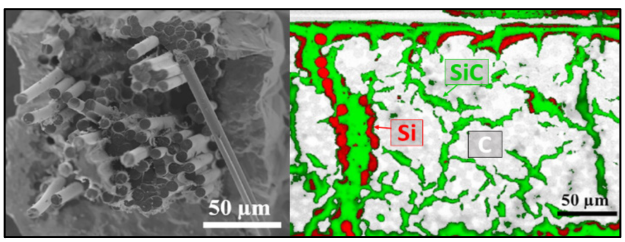

Fig. 1 – SEM and Raman spectroscopy showing the sheath of C/C-SiC surrounding a carbon fiber tow.

The C/C-SiC CMCs exhibited porosity of 10–20%, flexural strength of 235 MPa, and Weibull modulus of 3.21. The composites displayed toughness via a stepwise failure mechanism involving load up, fracture and load drop, followed by repeating the cycle, as shown in (Fig. 2) [3]. Fabrication of this prototypical C/C-SiC CMC via AM and RMI with silicon provided a glimpse into how such UHTCMCs could be fabricated. Continued investigation should focus on developing a basic science understanding of how the interfaces are formed, the effect that polymer composition and metal infiltrant have on the chemistry, level of penetration and temperature capability of the RMI matrix product. Lower melting temperature polymers than PEEK should be investigated, which would provide additional flexibility for the printing process. Oxidation resistance is key to a successful 2200°C leading edge, such as required for a Mach 10 vehicle [4, 5]. For this reason, melt infiltration with a combination of Si and refractory metals in the presence of C and B in the polymer matrix should be investigated, because modified diborides that form a silica rich outer glassy layer that impedes diffusion/permeation of oxygen show the best promise for applications at 2200°C [5].

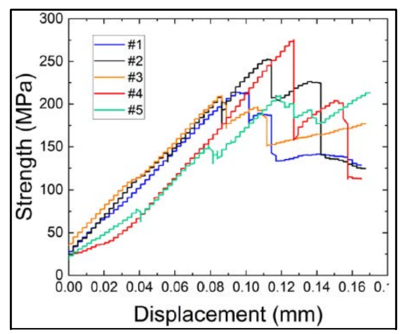

Fig. 2. Flexure test results of C/C-SiC.

References:

[1] C. W. Ohlhorst *et al.*, "Development of X-43A mach 10 leading edges," 2005 2005, Paper IAC-05-D2. 5.06 ed.

[2] C. Peebles, "The X-43A flight research program: lessons learned on the road to Mach 10," AIAA/NASA, 2007.

[3] C. L. Cramer, B. Yoon, M. J. Lance, E. Cakmak, Q. A. Campbell, and D. J. Mitchell, "Additive Manufacturing of C/C-SiC Ceramic Matrix Composites by Automated Fiber Placement of Continuous Fiber Tow in Polymer with Pyrolysis and Reactive Silicon Melt Infiltration," *Journal of Composites Science*, vol. 6, no. 12, 2022, doi: 10.3390/jcs6120359.

[4] A. B. Peters *et al.*, "Materials design for hypersonics," *Nature communications*, vol. 15, no. 1, p. 3328, 2024.

[5] K. A. Kane, B. A. Pint, D. Mitchell, and J. A. Haynes, "Oxidation of ultrahigh temperature ceramics: kinetics, mechanisms, and applications," *Journal of the European Ceramic Society*, vol. 41, no. 13, pp. 6130-6150, 2021, doi: 10.1016/j.jeurceramsoc.2021.05.055.

Micro 3D-Printed In-Situ Packaged Inertial Switch

Regan Kubicek *, Daniel Quinn, Joshua Tyler, and Gabriel Smith
DEVCOM Army Research Laboratory, 2800 Powder Mill Rd, Adelphi, MD 20783
**Corresponding Author Email: regan.d.kubicek.civ@army.mil*
Keywords: 3D printing, MEMS, sensors, additive manufacturing

This work details the development and characterization of a novel, in-situ packaged inertial switch fabricated using a combined two-photon polymerization (TPP) 3D printing and sputter deposition process. The device, constructed on a flexible polyethylene terephthalate (PET) substrate, demonstrates robust and repeatable activation at acceleration levels of 1000 *g*, as validated through rigorous shock table testing. This approach provides a significantly faster and more cost-effective manufacturing route compared to traditional, multi-step Micro-Electro-Mechanical Systems (MEMS) fabrication techniques.

Driven by the Department of Defense (DoD) demand for adaptable and customized inertial sensing solutions, this research explores additive manufacturing beyond conventional microfabrication. We demonstrate a fully integrated 3D printed MEMS inertial switch, utilizing TPP with IP-S photoresist on laser-cut, indium tin oxide (ITO)-coated PET film (using a standard DiLL process [1]). The monolithic design incorporates both the inertial sensing element – comprising a proof mass and electrical contact pads – and its protective packaging into a single unit. Following 3D printing, a 20nm chromium/100nm gold (Cr/Au) layer is deposited via sputter coating, and subsequent laser ablation is employed to define critical electrical isolation features (Fig. 1). Further electrical isolation is integrated directly into the device design [2]. Electrical connectivity is achieved through conductive anisotropic tape (3M 9703) to a breakout board, facilitating streamlined testing and characterization. Shock testing, performed on a shock table, confirmed reliable activation at 1000 *g*.

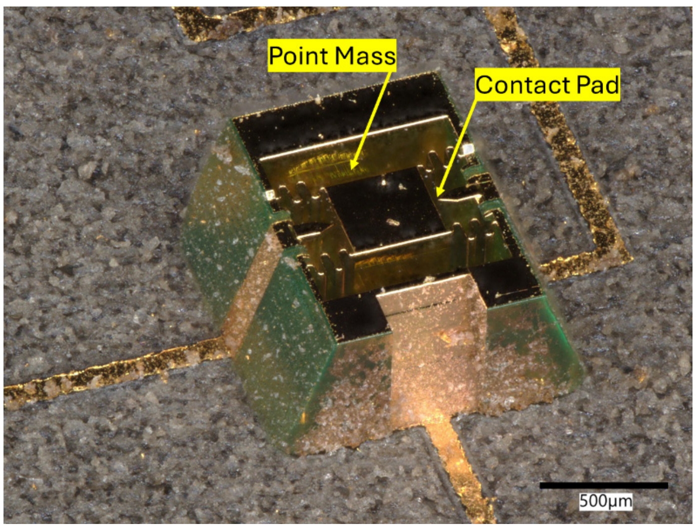

Fig. 1 – 3D-printed packaged inertial switch. The point mass and contact pad is show. Sensor is metallized using sputter deposition. Laser patterning provides electrical isolation.

This 3D printing methodology enables the rapid prototyping and fabrication of complex, functional microdevices with tailored geometries and mechanical properties. The resulting packaged inertial switch offers a simple, low-power, and reliable solution for applications where traditional accelerometer-based systems are impractical or unsuitable. This work establishes a promising pathway for the advancement of MEMS sensor and actuator development, and future research will focus on refining performance characteristics and expanding to high acceleration applications.

References:

[1] R. Kubicek, M. Babaei, A.I. Weber, and S. Bergbreiter, "A New Sensation: Digital Strain Sensing for Disturbance Detection in Flapping Wing Micro Aerial Vehicles," in 2021 IEEE/RSJ International Conference on Intelligent Robots and Systems (IROS), 2021, pp. 7505-7511.
[2] S. Kim, C. Velez, R.S Pierre, G.L. Smith, and S. Bergbreiter, "A two-step fabrication method for 3D printed microactuators: characterization and actuated mechanisms," Journal of Microelectromechanical Systems, vol. 29, no. 4, p. 544-552, 2020.

Developing a Methodology to Determine Minimum Feature Size in Laser Powder Directed Energy Deposition

Joshua Taggart-Scarff[1], Dr. Clara Mock[1]
[1]DEVCOM Army Research Laboratory, 6300 Rodman Rd, Aberdeen Proving Ground, MD 21005
**Corresponding Author Email: Joshua.k.taggart-scarff.civ@army.mil*
Keywords: Directed Energy Deposition, Minimum Feature Size, Additive Manufacturing.

Laser powder directed energy deposition (DED) is an additive manufacturing (AM) process with potential benefits across many industries including but not limited to aerospace, automotive, and repair [1,2]. Benefits include full automation capability, lower residual stresses and higher dimensional stability over welding processes in repair, large build volumes, and multi-material capability [1,2]. Currently there has been little effort in understanding the minimum printable feature size or dimensional accuracy capabilities of laser powder DED. This is likely due to the process being used predominantly for near net shape applications where the parts are post machined to final dimensions. This does not leverage the full potential of the process to produce near net parts and results in unnecessary material waste. To achieve the full potential of the process to achieve near net parts, it is necessary to understand the limitations of the process. This paper describes a methodology for determining the minimum printable feature size and dimensional accuracy. Understanding these limitations will provide valuable information that will allow engineers to more effectively design parts for manufacturing via laser powder DED with tighter tolerances. A high strength steel alloy powder feedstock had a particle size of 45-106 um and spheroidal morphology was used to produce square and cylindrical boss specimens. Two (2) process parameter sets were used on RPM Innovations Inc. model 222 (RPM Innovations, Inc, Rapid City, SD) laser powder Directed Energy Deposition (DED) machine. Three (3) sets of specimens per process parameter set were produced for a total of six (6) sets of specimens. Specimen X, Y, and Z dimensions were measured and compared to designed dimensions to determine the amount of overbuild and dimensional accuracy. Overbuild is the defined as the amount of material that exceeds the designed CAD dimensions of the part, see Fig. 1A. Surface roughness was also measured on the square bore specimens. It was found that the average amounts of XY dimension overbuild are close to the respective laser spot sizes. The amount of stabilized overbuild is approximately 15% and 35% larger than laser spot size 1 for the cylindrical and square boss specimens respectively and approximately 15% and 40% larger than spot size 2 for the cylindrical and square boss specimens respectively as shown in Fig. 1B. Future work will investigate the effect of more processing parameter sets. Work will also be done investigating the relationship between melt pool dimensions and overbuild.

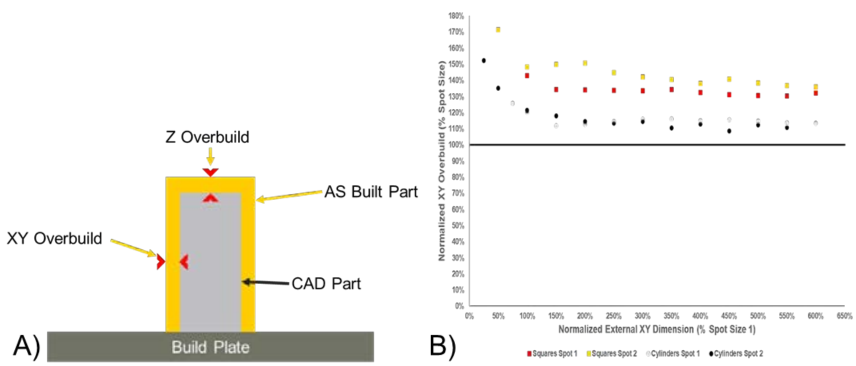

Fig. 1: A) Diagram of CAD part and overbuild, B) Plot of normalized average XY dimension overbuild for square and cylinder boss specimens. XY overbuild normalized by respective laser spot size.

References:

[1] A. Saboori, A. Aversa, G. Marchese, S. Biamino, M. Lombardi, and P. Fino, “Application of Directed Energy Deposition-Based Additive Manufacturing in Repair,” *Applied Sciences*, vol. 9, no. 16, p. 3316, Aug. 2019, doi: https://doi.org/10.3390/app9163316.
[2] G. Piscopo and L. Iuliano, “Current research and industrial application of laser powder directed energy deposition,” *The International Journal of Advanced Manufacturing Technology*, Jan. 2022, doi: https://doi.org/10.1007/s00170-021-08596-w.

5. Topic: AI and Data Science

Open World Embodied Task Planning and Execution

Corban Rivera[1*], David Handelman[1], Daniel Cassenti[2] and Celso De Melo[2]
[1]*Johns Hopkins Applied Physics Lab,* 11100 Johns Hopkins Rd, Laurel, MD *(JHUAPL)* 20723
[2]*DEVCOM Army Research Laboratory, 2800 Powder Mill Road, Adelphi, MD (ARL) 20783*
**Corresponding Author Email: Corban.Rivera@JHUAPL.edu*
Keywords: robotics, planning, large pretrained models, agentic frameworks

This work presents a unified framework for open-world embodied task planning by combining ConceptGraphs—an open-vocabulary 3D scene graph representation—with ConceptAgent, a planning system that uses precondition grounding and LLM-guided tree search to execute natural language tasks reliably in unstructured environments.

Robots operating in open-world environments require scene representations that are both **semantically rich** and **structurally efficient** to support flexible task planning and execution. Traditional fixed-label maps are too rigid to adapt to novel concepts or abstract instructions.

ConceptGraphs[1] is an object-centric 3D mapping system that integrates RGB-D sensor input with vision-language foundation models to build **open-vocabulary 3D scene graphs**. It segments scenes into class-agnostic object candidates, associates them across multiple views, and labels each object with rich caption embeddings (via CLIP, GPT-4, etc.) rather than fixed semantic classes. Inter-object spatial relationships are then inferred and encoded as graph edges, yielding a compact, scalable graph that supports natural-language querying and planning. Demonstrations on wheeled or legged robot platforms show its ability to support abstract-language object grounding, navigation, manipulation, and flexible retrieval tasks.

ConceptAgent[2] builds on ConceptGraphs by adding a robust task planning and execution layer driven by LLMs. It leverages two key innovations: (1) **Predicate Grounding** ensures that preconditions for actions are formally verified (and infeasible actions filtered), reducing execution failures and enabling recovery from hallucinated plans. (2) **LLM-guided Monte Carlo Tree Search (MCTS)** uses LLMs to propose action branches and evaluate plans, combined with self-reflection to dynamically optimize execution paths.

In simulation over 30 simple tasks in three layouts, ConceptAgent achieved a ~19 % task completion rate—nearly doubling performance of baseline LLM planners (~8–10 %)—and added ~20 % absolute gains on moderate and hard variants via the integrated enhancements. In real-world trials using a Spot robot, it successfully completed ~40 % of mobile manipulation tasks in low-clutter randomized settings, underscoring its robustness for embodied tasks.

From Perception to Execution - By combining **ConceptGraphs** for scene representation with **ConceptAgent** for grounded planning, the unified framework enables **open-vocabulary perception**, **language-conditioned planning**, and **reliable execution** in unstructured, dynamic environments. The scene graph provides a structured, natural language-compatible world model; predicate grounding constrains planning to executable sequences; and LLM-guided tree search enables flexible, adaptive decision making. Contributions include:

- Demonstrate how open-vocabulary 3D scene graphs can scale scene understanding beyond fixed taxonomy and support abstract task specifications.
- Introduce a planning architecture (ConceptAgent) that minimizes execution failures via precondition grounding and improves adaptability via LLM-driven tree search.
- Present empirical validation in both simulation and hardware showing substantial improvements over prior LLM-only planning baselines.

Funding: This research was sponsored by the Army Research Laboratory and was accomplished under Cooperative Agreement Number W911NF-21-2-0211.

References:

[1] Gu, Qiao, Ali Kuwajerwala, Sacha Morin, Krishna Murthy Jatavallabhula, Bipasha Sen, Aditya Agarwal, Corban Rivera et al. "Conceptgraphs: Open-vocabulary 3d scene graphs for perception and planning." In *2024 IEEE International Conference on Robotics and Automation (ICRA)*, pp. 5021-5028. IEEE, 2024.

[2] Rivera, Corban, Grayson Byrd, William Paul, Tyler Feldman, Meghan Booker, Emma Holmes, David Handelman et al. "Conceptagent: Llm-driven precondition grounding and tree search for robust task planning and execution." *arXiv preprint arXiv:2410.06108* (2024).

Guaranteeing Stability for Evolutionarily Trained Multiagent Systems

Connor Yates[1,*], Kyle Crandall[1]
[1]*Naval Research Laboratory, 4555 Overlook Ave SW, Washington, DC 20375*
**Corresponding Author Email: connor.l.yates.civ@us.navy.mil*
Keywords: Multiagent System, Lyapunov Stability

We propose using Lyapunov Neural Networks (LNN) to provide stability guarantees for evolutionary learning multiagent systems by solving domains of attraction. Demonstrated on a multiagent switch-puzzle problem, our experiments show LNN's can generate stability certificates for instances of teams trained to solve the switch-puzzle under sparse reward settings amenable to evolutionary multiagent learning. This enables us to leverage gradient-free optimization methods while still ensuring a stable result. Future research will look at how teammate and environmental changes require updates to a trained LNN.

Guaranteeing stable performance of an arbitrary Artificial Intelligence (AI) system is a difficult task, but one that is of increasing importance with the ever-growing use of AI. Drawing from the well-established field of Control Theory, Lyapunov stability analysis provides tools to analyze and create certificates proving correct operation over a region of the state space [1]. Unlike most Safe Reinforcement Learning (Safe-RL) approaches, which focus on training-time validation, Lyapunov functions can solve for domains of attraction on a pre-trained policy. However, Lyapunov functions are typically constructed by hand using expert knowledge and require unique proofs of correctness for each target application. They also are difficult to apply to multiagent learning problems due to unmodeled interactions between agents and the black-box learning structures that prevent introspection.

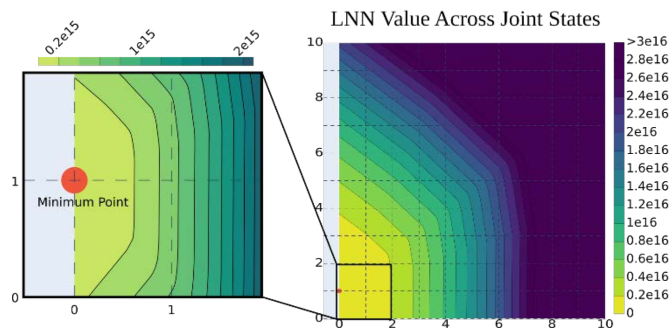

Fig. 1. The learned stability region is everywhere the learned Lyapunov function is monotonically decreasing to the minimum; in this example, the stability region covers the entire state space.

The contribution of this work is to prove the stability of the result of a multiagent evolutionary algorithm through LNN application. We apply Lyapunov Neural Networks (LNN) [2,3], a recent technique to learn the Lyapunov stability function of a black-box policy, to multiagent learning problems. We specifically investigate multiagent evolutionary learning, as it can be leveraged in problems with no differentiable form or long action-feedback delays. Using LNN's, the neural networks generated by the EA have a well-defined domain of attraction.

We train two agents using Covariance Matrix Adaptation Evolution Strategies (CMA-ES) on an increasingly difficult decentralized coordination problem. Two agents in separate hallways must move to the correct space to press a switch. The agents are only rewarded when both switches are depressed at the same time. Sparse reward problems are difficult to learn and are not solvable with other Safe-RL techniques. Agents were trained for 1000 generations using CMA-ES. The resulting policies were used to train the LNN for seven epochs of 100,000 iterations each. The largest level set of the LNN (Fig. 1, darkest region), shows the LNN monotonically decreases as the agents move under the learned policies, converging to the goal point.

Future research will expand the analysis to more complex multiagent interactions, with varying team size and problem spaces, and focus on updating the LNN as teams change. Problems where stochasticity is involved, or reliably working alongside the same teammate is not guaranteed, present a challenge to this current framework.

Funding: NRL Karles Fellowship

References:

[1] Khalil, Hassan. *Nonlinear Systems*. Third. Upper Saddle River, NJ 07458: Prentice Hall, 2002.
[2] Crandall, Kyle, Connor Yates, and Corbin Wilhelmi. "Lyapunov Guarantees for Learned Policies." In *Adaptive and Learning Agents Workshop*. Auckland, NZ, 2024.
[3] Richards, Spencer M., Felix Berkenkamp, and Andreas Krause. "The Lyapunov Neural Network: Adaptive Stability Certification for Safe Learning of Dynamical Systems." In *Proceedings of The 2nd Conference on Robot Learning*, 466–76. PMLR, 2018.

AgOS: Aggregated Opinion Synthesis

Dr. Christopher W. Hays*
Space Control Branch, Air Force Research Laboratory Space Vehicles Directorate, 35005 Aberdeen Dr SE, Kirtland AFB, NM., 87117
**Corresponding Author Email: christopher.hays.5@spaceforce.mil*
Keywords: Information Fusion, Trusted Systems, Sensor Networks, Signal Processing

Fusing probability density functions (pdfs) is a fundamental technique with applications to a broad spectrum of science and mathematics [1]. While a specific form of the more general information fusion, it has several attractive properties that have made it widely applicable e.g. decentralization, privatization, computationally efficient, source agnostic. However, many pdf fusion techniques make broad assumptions about the *reliability* or *trustworthiness* of information sources; specifically, many techniques utilize optimization-based approaches without considering the reliability of the pdfs to be fused. **.** In nominal scenarios, this approach yields an 'optimal' fused pdf, assuming the underlying statistics are known; unfortunately, most practical scenarios are off nominal, e.g., model uncertainty, parameter tuning error, sensor degradation, etc. Each of these cases deteriorates sensor performance and reduces the reliability of information provided by that sensor. Therefore, fusion results may degrade if they are too reliant on unreliable, untrustworthy, or even faulty information. If trust is incorporated, the vast majority make use of what is referred to as a 'reliability coefficient' [2-4] which scales pdfs by the reliability coefficient which have traditionally been computed from historical performance measures. The idea here is 'find the optimal reliability coefficient, find a feasible fusion solution'. This contrasts with many of the nominal approaches which seek to find a fusion coefficient to find some information-theoretic metric extremum. **Fundamentally, this work seeks a balance; it develops a methodology to take the opinions from untrustworthy sources *'with a grain of salt'* while maintaining a solution space for information-theoretic approaches to explore.**

We consider $k \in \{1, \dots, K\}$ information sources each providing an "opinion" on some unknown random vectorized quantity $\boldsymbol{x}$. Each information source opinion is modeled by a pdf $p_k(\boldsymbol{x})$ and is aggregated at a "fusion center" to provide a fused pdf $p_f(\boldsymbol{x})$. We refer to the function employed by the fusion center as the "opinion pooling function." The fusion center also maintains a scalar trust value t_k for each information source* to take into consideration within the opinion pooling function. The full final manuscript will explore techniques on how to consider trust within the opinion pooling function. As such, this paper is in part literature survey, part novel contribution. Specifically, we consider several approaches to take opinions with a grain of salt, most of which center on framing an information-theoretic optimization problem with trust as a constraint or bilinear optimization variable. The full manuscript includes sample scenarios to compare and contrast developed techniques with the current state-of-the-art and demonstrate the efficacy of techniques compared to the reliability coefficient and optimization without trust techniques.

Funding: This work is supported by SMART SEED Innovation Award [Grant #FA9453-21-2-0064].

References:

[1] Koliander, G., El-Laham, Y., Djurić, P. M., & Hlawatsch, F. (2022). Fusion of probability density functions. Proceedings of the IEEE, 110(4), 404-453.

[2] Venanzi, M., Rogers, A., & Jennings, N. R. (2013). Trust-based fusion of untrustworthy information in crowdsourcing applications.

[3] Kaplan, L., Şensoy, M., & de Mel, G. (2014, July). Trust estimation and fusion of uncertain information by exploiting consistency. In *17th International Conference on Information Fusion (FUSION)* (pp. 1-8). IEEE.

[4] Rogova, G. L., & Nimier, V. (2004, June). Reliability in information fusion: literature survey. In *Proceedings of the seventh international conference on information fusion* (Vol. 2, pp. 1158-1165).

*We assume these trust values are defined and fixed. Calculating trust values based on historical performance and adaptively setting trust values for fusion is not consider in the present manuscript. However, it is within the scope of future efforts.

Associativity-Peakiness Metric for Contingency Tables

Naomi E Zirkind[1*], William J Diehl[2]

[1]DEVCOM Army Research Laboratory, 2800 Power Mill Road, Adelphi, MD 20783
[2]DEVCOM Army Research Laboratory; U.S. Army Europe and Africa, Unit 29351 Box 100, APO, Wiesbaden, Germany
**Corresponding Author Email: naomi.e.zirkind.civ@army.mil*
Keywords: contingency tables, clustering algorithms, contingency table metrics, unsupervised learning

A new metric is presented for contingency tables that are outputs of clustering algorithms. The metric's dynamic range exceeds those of similar metrics as shown by evaluation of simulated contingency tables. This metric facilitates research in evaluation of clustering algorithms for a wide variety of applications.

Clustering algorithms reveal connections among unlabeled data samples. To find an algorithm that could effectively form clusters of unlabeled data samples collected in theater, create a data set of labeled samples similar to those that would be collected in theater, and assemble a set of algorithms to cluster this data without awareness of the labels. Tabulate the performance of each algorithm in a contingency table whose rows are the true labels and whose columns are the clusters formed, resulting in a set of contingency tables, one for each algorithm. To select the best-performing contingency table, a numerical metric that summarizes each table is needed, similar to mean per-class accuracy for confusion matrices. Such a metric does not yet exist [1] (scilit-learn developers), but is presented here: the associativity-peakiness (AP) metric, which measures the associativity between clusters and truth classes, as well as the confidence level of the associativity.

Metrics do exist for truth-prediction pair tables [2] (scikit-learn developers), which is a less informative way of tabulating the data produced by a clustering algorithm. This research compares the AP metric with several of these metrics and shows that the AP metric has higher dynamic range (and thus sensitivity) than the existing metrics, and is computationally simpler.

To explore the performance of the various metrics over a wide range of contingency tables, a set of 500 contingency tables with random values (with fixed sum) was generated. Histograms were generated of each metric's score for each contingency table (Fig. 1, left side). These histograms illustrate the dynamic range of the metrics. The AP metric was used to evaluate performance of a clustering algorithm using data at various noise levels. The AP metric gave meaningful results in characterizing signal clustering performance of an algorithm at various noise levels (Fig. 1, right side). The AP metric is a useful tool that enables comparison of various clustering algorithms and/or datasets.

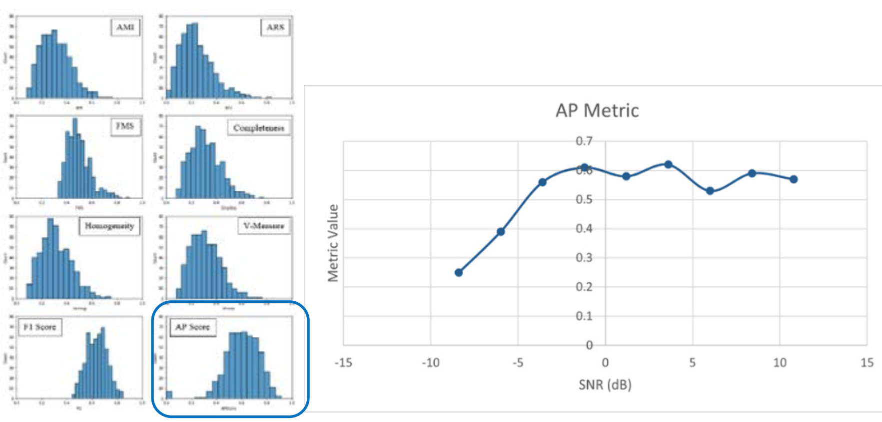

Fig. 1 – Set of histograms of metric values for six metrics, and AP metric in lower right corner (left side); AP metric scores for datasets at various signal-to-noise ratios (right side)

[1] scilit-learn developers, "2.3 Clustering -- scikit-learn 1.6.1 documentation," [Online]. Available: https://scikit-learn.org/stable/modules/clustering.html#contingency-matrix. [Accessed 20 March 2025].

[2] scikit-learn developers, "2.3 Clustering -- scikit-learn 1.6.1 documentation," [Online]. Available: https://scikit-learn.org/stable/modules/clustering.html#clustering-performance-evaluation. [Accessed 20 March 2025].

Predicting Process Completion Time on Heterogeneous Edge Devices in Resource Constrained Environments Using Liquid Neural Networks

Cleon Anderson[1], Matthew Dwyer[2], Scott Brown[1], and David Harman[1]
[1]Parsons Corporation, Aberdeen Proving Ground, MD, USA

[2]DEVCOM Army Research Laboratory, Aberdeen Proving Ground, MD, USA
Corresponding Author Email: cleon.r.anderson.ctr@army.mil
Keywords: "performance prediction, edge computation, neural networks"

With the increasing deployment of edge devices across various industries, optimizing AI/ML models in resource-constrained environments has become a crucial challenge. In such settings, where devices often face limited bandwidth, power, and fluctuating computational resources, ensuring efficient execution of tasks is vital. This is particularly important in contested environments, such as military operations and disaster response, where device heterogeneity and communication protocol variability add further complexity. Recent innovations in quantization and optimization techniques offer solutions for reducing latency and improving task completion rates in these stochastic environments. Distributed workflows, which include both model and data distribution, are key strategies to mitigate resource constraints, but their performance often hinges on the weakest link in the system. To address this challenge, we propose a novel approach for modeling process runtime under varying resource constraints, leveraging state-of-the-art AI/ML techniques. In this study, we explore the use of Liquid Neural Networks (LNNs) to predict the time to completion of inferencing processes running on a cluster of heterogeneous devices with varying resource limitations at a given future timestamp. Through a comparative analysis of models, including LSTM, VARMA, Vector Auto-regressive, and Transformer architectures, we demonstrate that LNNs outperform others in predicting runtime at future time steps. Our findings suggest that LNNs are particularly well-suited for handling the dynamic nature of resource-constrained environments, providing accurate estimates of process completion time in scenarios characterized by device and network variability. This predictive capability offers significant advantages for anticipating system behavior and optimizing resource allocation in environments where future conditions may be uncertain.

Improving Situational Awareness by Automating the Common Operational Picture (COP) for Integration with Unmanned Systems

Indranil Sur[1], Aswin Raghavan[1,*], and James Zachary Hare[2]

[1]Center for Vision Technologies, SRI, 201 Washington Rd, Princeton, NJ 08540, USA

[2]DEVCOM Army Research Laboratory, 2800 Powder Mill Road, Adelphi, MD 20783, USA

**Corresponding Author Email: aswin.raghavan@sri.com*

Keywords: Robustness to Denial/Degradation, Multi-Agent Reinforcement Learning, Distributed State Prediction.

The integration of unmanned systems equipped with advanced sensors promises to improve situational awareness (SA) and mitigate the “fog of war”. However, several challenges must be overcome to automate the COP in Denied, Degraded, Intermittent and Limited (DDIL) environments. We present our recent research to automate the COP using Multi-Agent (Deep) Reinforcement Learning (MARL). The COP learning problem is posed as distributed state prediction under partial observability, where every agent produces a local COP from local observation and communication. The major findings from experiments in the Starcraft-2 simulation environment are: (1) Precise COPs with less than 5% error (vs ground truth) are produced despite denial of GPS and degraded visual range; (2) On coordination tasks, agents that optimized COP error and task reward outperform agents that optimized task reward only, in terms of robustness to DDIL; and (3) COP-based pre-training is a viable path to a foundation model for MARL. This research enables the study of distributed cross-echelon C2 with sparse communications and the impact of large-scale autonomy on warfighter SA.

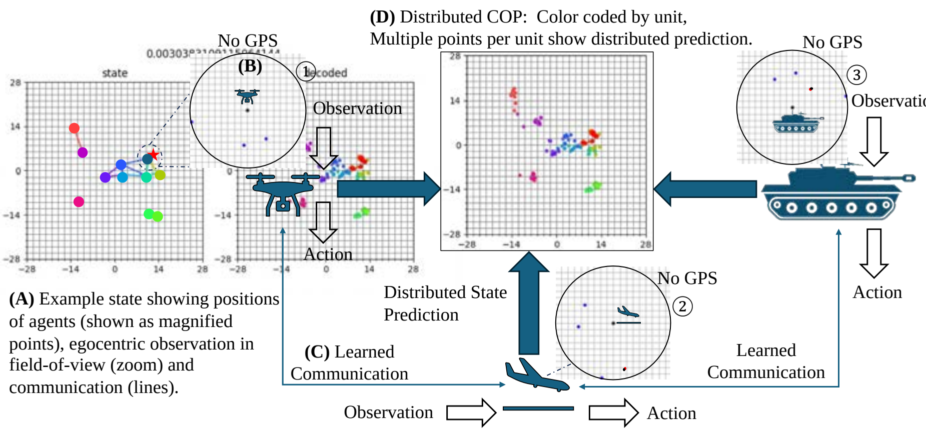

Fig. 1: Illustration of the distributed COP prediction problem via learned inter-agent communication. (**A**) Example scenario with air and ground agents. (**B**) Example (GPS denied) egocentric observation: range and bearing of units in field-of-view. (**C**) Agents encode the (history of) observations, actions and COPs and communicate. (**D**) Messages are integrated and decoded to a COP per agent.

Fig. 1 illustrates the distributed COP prediction problem. Fig. 2 shows the agent architecture for learned C-dimensional inter-agent communication: $\mathcal{C}_{out}, \mathcal{C}_{in}$ are trained end-to-end such that multi-round communication $\mathcal{C}_{in}(\mathcal{C}_{out}(\mathcal{C}_{in}(\dots)$ produces an embedding that can be decoded to a COP [1,2]. These COP-grounded policies are significantly more robust to DDIL [2].

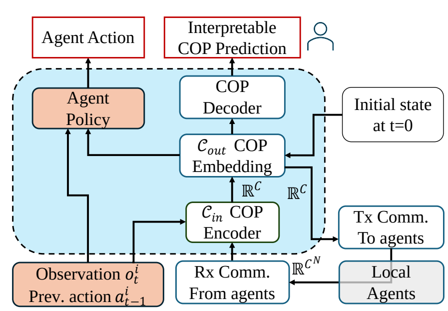

Fig. 2: Anatomy of an Agent and comms.

Funding: This material is based upon work supported by Army Research Laboratory (ARL) under the Army AI Innovation Institute (A2I2) program Contract No. W911NF-22-2-0137.

[1] I. Sur, A. Raghavan, A. Rahman, J. Z. Hare, D. Cassenti, and C. Busart, “Data-Driven Distributed Common Operational Picture from Heterogeneous Platforms using Multi-Agent Reinforcement Learning” in Intl. Command and Control Research and Technology Symposium (ICCRTS) 2024.

[2] P. Yu, B. Lee, A. Raghavan, S. Samarasekera, P. Tokekar, and J. Z. Hare, “Enhancing Multi-Agent Coordination through Common Operating Picture Integration” in First Workshop on Out-of-Distribution Generalization in Robotics at Conference on Robot Learning 2023.

Machine Learning Methods for Processing Real World PIV Data

Talya Stehley[1,*], Jason Geder[1], and Alisha Sharma[1]
[1]*Laboratories for Computational Physics and Fluid Dynamics, Naval Research Laboratory, 4555 Overlook Ave SW, Washington, DC, 20375*
**Corresponding Author Email: talya.h.stehley.civ@us.navy.mill*
Keywords: machine learning, computer vision, AI/ML, flow visualization.

This work intends to evaluate the current state of the art in ML for PIV and its accuracy on the corpus of real-world experimental PIV data available at NRL

Particle image velocimetry (PIV) is a technique in experimental fluid mechanics for visualizing aerodynamic or hydrodynamic flows. In a wind tunnel or water tank test, the flow is seeded with tiny, reflective particles, small enough to not disrupt the flow. These particles are then illuminated by a pulsing laser and photographed in rapid succession. Currently, cross-correlation methods are commonly used to get flow velocity vectors from successive image pairs generated by PIV experiments. However, these methods are computationally expensive, and require significant amounts of tuning and post-processing, demanding significant time and expertise from the practitioner.

Tracking particle motion between PIV image frames is a specific problem within the larger domain of optical flow. In the past few years, several papers have demonstrated that machine learning models designed for general optical flow can be successfully adapted to the domain of PIV. In 2020, Cai et al. demonstrated that their PIV-LiteFlownet-en model was more accurate than existing state-of-the art cross-correlation methods, in addition to being significantly faster [1]. However, the data they tested on was idealized synthetic data, which is more regular and less noisy than real-world experimental data. In 2021, we compared the model from Cai et al. with a model based on the same architecture but trained using an unsupervised method from Zhang and Piggott [2]. While the supervised model from Cai et al. performed better on most flow cases from the JHTDB, its level of accuracy became more highly variable on synthetic data to which gaussian noise had been added to more accurately reflect experimental conditions [3] (Fig. 1).

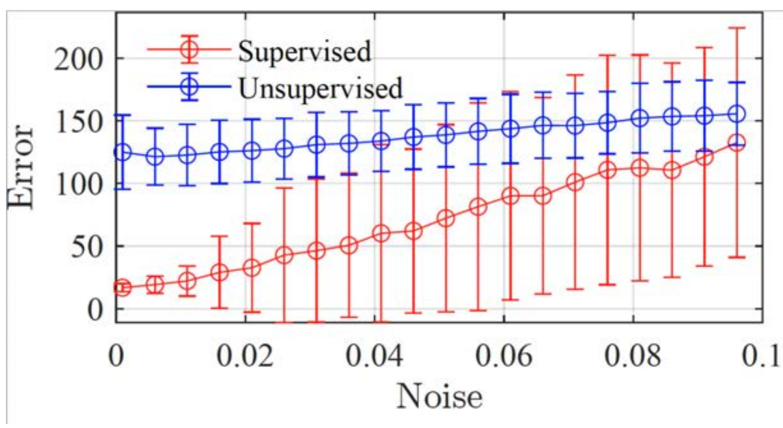

Fig. 1 Though the supervised version of PIV-LiteFlownet-en is on average more accurate, especially, the standard deviation of the accuracy gets significantly higher when noise is introduced. While the unsupervised model is on average less accurate, it is far more robust to noise, which may be more desirable for experimentalists

Our group has access to a large corpus of real world PIV data from experiments performed at NRL, and the state of the art in ML for PIV has continued to advance. This works aims to determine whether a network called RAFT-PIV (introduced by Lagemann et al. [4]) is accurate on NRL experimental data.

References:

[1] Shengze Cai, Jiaming Liang, Q. Gao, C. Xu, and R. Wei, “Particle Image Velocimetry Based on a Deep Learning Motion Estimator,” IEEE Trans. Instrum. Meas., vol. 69, no. 6, pp. 3538–3554, Jun. 2020, doi: 10.1109/TIM.2019.2932649.
[2] M. Zhang and M. D. Piggott, “Unsupervised Learning of Particle Image Velocimetry,” arXiv:2007.14487 [cs, eess], Jul. 2020, Accessed: Aug. 13, 2020. [Online]. Available: http://arxiv.org/abs/2007.
[3] T. Stehley “Machine Learning Approaches for Particle Image Velocimetry” B.A. thesis, CS Dept., YU, New York, NY, USA, April 2021. [Online]. Available: https://hdl.handle.net/20.500.12202/6903
[4] C. Lagemann, K. Lagemann, S. Mukherjee, and W. Schröder, “Deep recurrent optical flow learning for particle image velocimetry data,” Nat Mach Intell, vol. 3, no. 7, pp. 641–651, Jul. 2021, doi: 10.1038/s42256-021-00369-0.

ProcgenOOD: A Benchmark Environment to Study Generalizable Skills in Reinforcement Learning

Song Park[1*] and Kevin Corder[2]
[1]*DEVCOM Army Research Laboratory, 6791 Aberdeen Blvd, APG, MD 21005*
[2]*Parsons, 14291 Park Meadow Dr, Suite 100, Chantilly, VA 20151*
**Corresponding Author Email: song.j.park.civ@army.mil*
Keywords: Generalization, reinforcement learning, artificial intelligence

Reinforcement learning (RL) methods have proven effective in sequential decision-making tasks in well-defined and controlled environments, including abstract strategy board games [1], real-time strategy video games [2], simulated fighter aircraft dogfights [3], and robotic manipulation tasks [4]. However, a persistent challenge in RL research is the lack of generalization where RL agents often overfit to the specific environments or scenarios they are trained on, and subsequently fail to transfer learned skills to new related situations. This limitation raises concerns about the robustness and reliability of RL systems, especially in real-world applications where variability and uncertainty are inherent.

To address this gap, we have developed ProcgenOOD, a benchmark environment for studying the generalization performance of RL algorithms. ProcgenOOD extends Procgen [5], the standard benchmark that leverages procedural generation to create diverse environments, with additional capabilities for evaluating algorithms on out-of-distribution (OOD) experience. Specifically, our enhanced framework allows data to be withheld via customizable holdout variables (e.g., player sprite or level difficulty) from training or evaluation level generation. Each environment holdout variable is sampled with a given holdout fraction independently for training or evaluation, and well-ordered variables may additionally be sampled with interpolation or extrapolation. This highly flexible setup enables detailed experimentation to evaluate the performance of RL policies when exposed to incomplete or biased training distributions.

We reproduced the original results in our ProcgenOOD benchmark without holding out variables, implemented as a single-process training setup without gradient averaging. While it is well-known that PPO is sensitive to hyperparameters [6], we found that altering batch size had a substantial impact on training performance. Furthermore, increasing the number of updates per training batch led to significant degradation in performance. With the verification phase complete, we present preliminary OOD evaluation results obtained using the holdout variable and holdout fraction.

Ultimately, we aim to provide the RL community with a flexible environment for benchmarking generalization capabilities, facilitating more reproducible and interpretable research in the pursuit of RL agents that perform reliably in the face of environmental variability. This work introduces our environment ProcgenOOD, presents compelling results for its need in the RL community, and documents design considerations for the diverse generalization experiments for evaluating learned generalizable skills. Furthermore, we anticipate that ProcgenOOD will contribute to the exploration and advancement of techniques and algorithms that enhance generalization.

References:

[1] D. Silver *et al.*, “Mastering the game of Go with deep neural networks and tree search,” *Nature*, vol. 529, pp. 484–489, 2016.
[2] C. Berner *et al.*, “Dota 2 with large scale deep reinforcement learning,” *arXiv preprint arXiv:1912.06680*, 2019.
[3] A. P. Pope *et al*., "Hierarchical reinforcement learning for air combat at DARPA's AlphaDogfight trials," in *IEEE Transactions on Artificial Intelligence*, vol. 4, no. 6, pp. 1371-1385, Dec. 2023.
[4] D. Kalashnikov *et al*, “MT-Opt: Continuous multi-task robotic reinforcement learning at scale,” *arXiv preprint arXiv:2104.08212*, 2021.
[5] K. Cobbe, C. Hesse, J. Hilton, and J. Schulman, “Leveraging procedural generation to benchmark reinforcement learning,” in *Proc. 37th Int. Conf. Machine Learning (ICML'20)*, vol. 119, 2020.
[6] S. Huang *et al.,* “The 37 Implementation details of proximal policy optimization,” *ICLR Blog Track*, 2022.

A Funder's Perspective on Evaluation within the Research Ecosystem

Melissa C. Day[1*]

[1] Booz Allen Hamilton, Arlington, VA, USA 22203

*Corresponding Author Email: day_melissa@bah.com
Keywords: research evaluation; bibliometric analysis

A funder's role in the research ecosystem is perhaps most often thought of as upstream (by providing an award for an idea), but there is also a notable downstream component (by using publications and other outputs to show return on investment and justify additional awards). The Air Force Office of Scientific Research (AFOSR) manages all 6.1 Basic Research appropriations within the Air Force, and now features a growing science analytics group to assist in evaluating its funded research activity and impact. Effective evaluation requires several elements: knowing what portfolio information is available internally and externally, the ability to track a variety of research outcomes, establishing what impacts are expected and available for different portfolios, and understanding how to speak about these investments to different audiences. The process is further driven by recent demand signals, including government-level implications of the Evidence Act and NSPM-33, and evaluator- and researcher-level calls for responsible metrics and better metadata standards. This talk will discuss how AFOSR is approaching research evaluation, what researchers can do to improve the data quality of their submissions, how the group is promoting bibliometric literacy among staff, and some lessons learned about the workflow thus far.

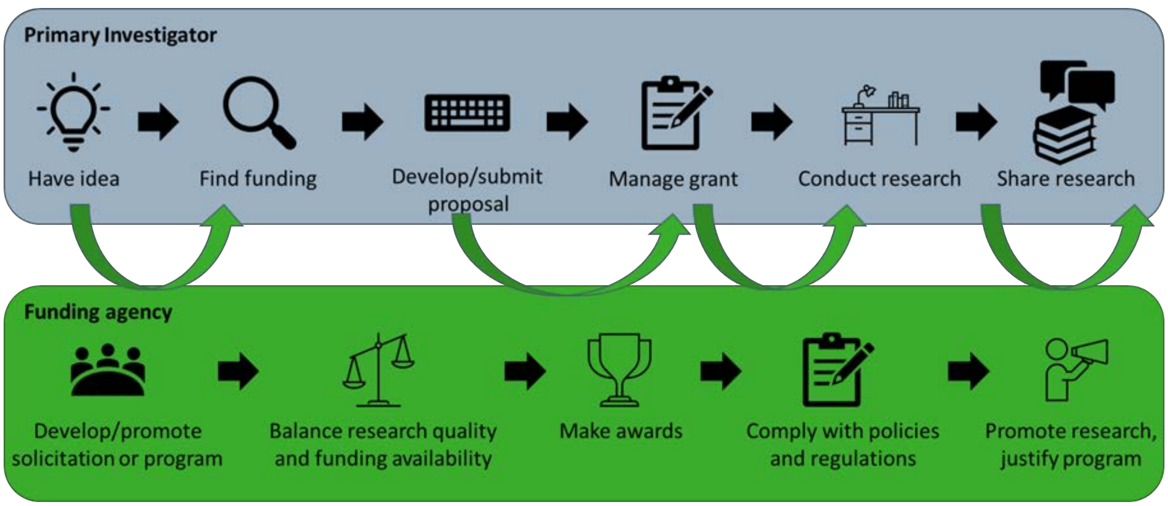

Fig. 1. Depiction of an abridged researcher-funder ecosystem.

Adaptive-Distributed Solutions to Inferencing in Resource Constrained Environments

Scott Brown[1], Matthew Dwyer[2], David Harman[1], and Cleon Anderson[1]
[1]Parsons Corporation, Aberdeen Proving Ground, MD, USA
[2]DEVCOM Army Research Laboratory, Aberdeen Proving Ground, MD, USA
Corresponding Author Email: scott.e.brown96.ctr@army.mil
Keywords: "Machine learning, Edge Computing, classification"

The future of information gathering is fast becoming reliant on low size, weight, and power (SWaP) sensors deployed to the edge. While these devices may have a connection to higher powered or cloud enabled devices, many of them will likely be isolated into smaller clusters of similar devices or simply have limited network resources available for reachback. In these cases, the latency and throughput of analytic tasks is limited by the network and computational capabilities of edge servers. Distributed solutions are available to help solve resource constraints at the edge, including data-distributed inferencing (DDI) and model-distributed inferencing (MDI). These solutions are effective in the presence of specific computational and network constraints; however, due to static workload allocation, they are susceptible to dynamics in network and compute performance. To address performance degradation introduced by dynamic conditions, an adaptive layer has been implemented for each of the algorithms, respectively. In this adaptive logic, the performance of each distributed worker is considered, as well as the availability of the network, when deciding the workload distribution. For DDI the adaptive mechanism will control the distribution of data among workers, while adaptations to the MDI workflow involve adjusting layer distribution among workers. To showcase the potential for each adaptive distributed solution, a testbed will be utilized to allow for tuning of both device computation and network connection capabilities which will enable evaluation of these techniques on a comparable heterogeneous network of devices. Results showcase the performance for each adaptive distributed solution when compared to its non-adaptive base algorithm, as well as compared to one another, in terms of both analytic throughput, compute and network utilization.

5.3 Session: Human-AI Collaboration

Mitigating Hallucination in LLM-Based Task-Team Design with Submodular Optimization: Application to Command and Control at Higher Echelons

Saurabh Farkya[1], Aswin Raghavan[1,*]
[1]*Center for Vision Technologies, SRI, 201 Washington Rd, Princeton, NJ 08540, USA*
**Corresponding Author Email: aswin.raghavan@sri.com*
Keywords: Decision Support AI, Human-Machine Teaming, LLM with Theoretical Guarantees, AI using Doctrine

Many decision-making processes work by planning a set of tasks or goals to be achieved and assigning a team (manned or unmanned) to each task. Recently, Large Language Models (LLMs) have been used to automate task design, team design, or both, however, they suffer from explicit and implicit hallucinations of the LLM. We present a novel method that combines LLM-based task and team design with Submodular Optimization (SO) to derive theoretical optimality guarantees for a class of task structures. We apply the method to a challenging Command and Control (C2) scenario at the Company level. We report that the combination of LLM and SO achieves significantly higher win rates compared to LLM baselines. Second, we demonstrate user interfaces for human-in-the-loop control at the planning and execution levels. These interfaces enable multiple future user studies on large scale human-machine teaming with manned and unmanned teams.

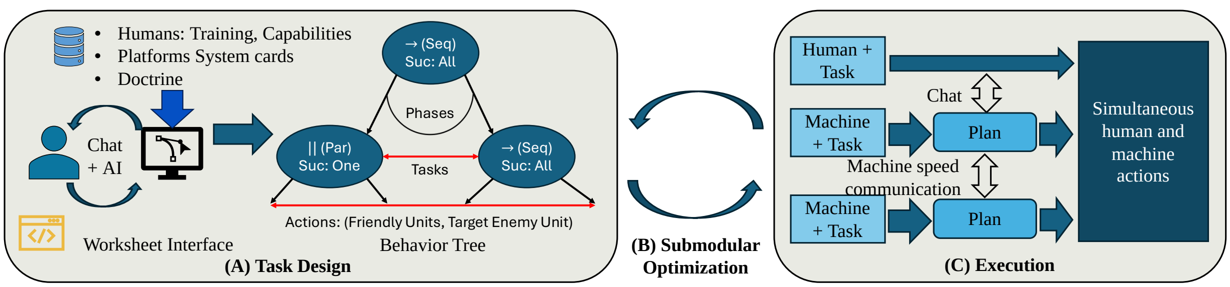

Fig. 1. Overview of the approach. (A) Task Design (or COA) is generated as a behavior tree using an LLM, Doctrine and human-in-the-loop. (B) Efficient Submodular procedure optimizes the team assignments given the COA. (C) The assigned teams execute their tasks simultaneously. They deliberate on the execution of a given task with human-to-machine or machine-to-machine communication.

Fig. 1 shows an overview of the approach. The LLM is prompted (using a template) to generate a behavior tree with three levels of nodes: (1) Top level nodes are the sequential phases of the COA, (2) Next level nodes each have a task, each task can be parallel (||) or sequential (→), (3) Lowest level nodes have an Action, defined as a team of friendly units and a target enemy unit. Each node has a descriptive purpose and a success condition (denoted “suc”) (See [1] for semantics of behavior tree execution). Teams in Action nodes are initialized by the LLM. Submodular optimization (Fig. 1 (B)) finds the best team using the total damage to the enemy as the cost function. We use the greedy algorithm [2] for sequential nodes (approximation guarantee of $1 - 1/e$) and Submodular Welfare Optimization (SWO) for parallel nodes (1/2-approximation) [3]. Fig. 2 shows the empirical performance such as win rate and num. iterations of our method vs LLM directly assigning teams to tasks and randomly initialized SO.

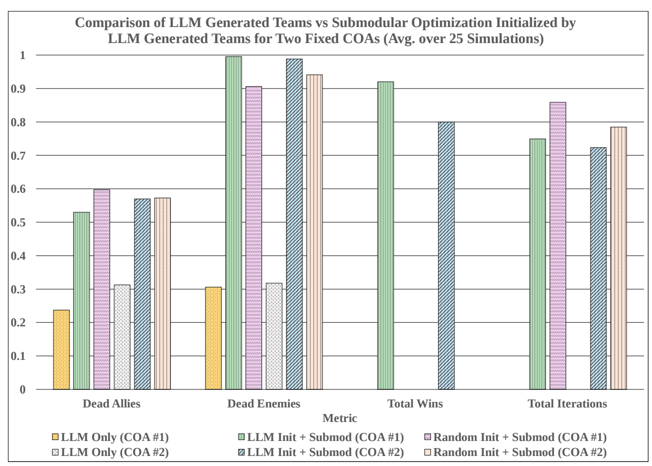

Fig. 2. Given a fixed COA, Submodular Optimization and LLM Generated Initial Teams are both needed for 100% Win Rate.

[1] M. Colledanchise and P. Ögren (2018), Behavior Trees in Robotics and AI: An Introduction, arXiv:1709.00084.
[2] Krause, A., & Golovin, D. (2014). Submodular function maximization. *Tractability*, *3*(71–104), 3.
[3] Buchbinder, N. and Feldman, M. (2018). Submodular functions maximization problems. In Handbook of Approximation Algorithms.

Human Feedback via Sketching to Adapt Intelligent System Behavior

Ellen Novoseller*, William Duong, Anna Madison, Sarah Al-Hussaini, Nicholas R. Waytowich, Vernon J. Lawhern

Humans in Complex Systems, DEVCOM Army Research Laboratory, 7101 Mulberry Point Rd, Aberdeen Proving Ground, MD 21005

**Corresponding Author Email: ellen.r.novoseller.civ@army.mil*

Keywords: Multi-agent systems, reward learning, human feedback, sketch-based feedback.

In complex multi-agent scenarios, reward functions for training Artificial Intelligence (AI) agents to perform desired behaviors are often unknown. Human-guided machine learning approaches enable humans to train AI agents via intuitive interactions, such that humans can convey their preferences to adapt AI behaviors without necessarily having any knowledge about AI [1]. Prior work on human-guided machine learning considers a range of human feedback modalities, for example teleoperated demonstrations, ratings, rankings over behaviors, and language. However, many of these feedback modalities may not extend to systems with many interacting AI agents, where a human might need to tailor their feedback for different agents or give feedback to several agents at once. Meanwhile, human feedback via sketching remains understudied and could enable humans to intuitively interact with multi-agent AI systems to convey information pictorially, e.g. about task goals or suggested strategies. This work demonstrates how human sketches could be leveraged to learn a reward model representing human objectives and to facilitate effective multi-agent planning. Each agent learns a reward model capturing the human's intent by interpreting the sketches as demonstrations and as corrections to the agent's plans; the agent then utilizes this reward model to generate plans in coordination with the other agents. Human-guided machine learning via sketching has the potential to improve the Army's Command and Control (C2) decision-making process, e.g., by reducing the time-consuming burden of developing courses of action (COAs) through enabling AI capabilities that incorporate human guidance [2]. For instance, with sketch-based feedback, personnel could receive a pictorial representation of an AI-generated plan of action and red-ink it to convey feedback to the AI, e.g. demonstrating preferred paths for units to follow, identifying regions to capture and to avoid, and highlighting other features of interest on the map. Sketched feedback may be particularly natural in map-based tasks such as arise in C2, potentially enabling humans to intuitively markup a map depicting a proposed COA or other task information, provide feedback to many agents with just a few markings, and facilitate agent adaptation in novel situations, e.g. under adversarial conditions with opposing forces.

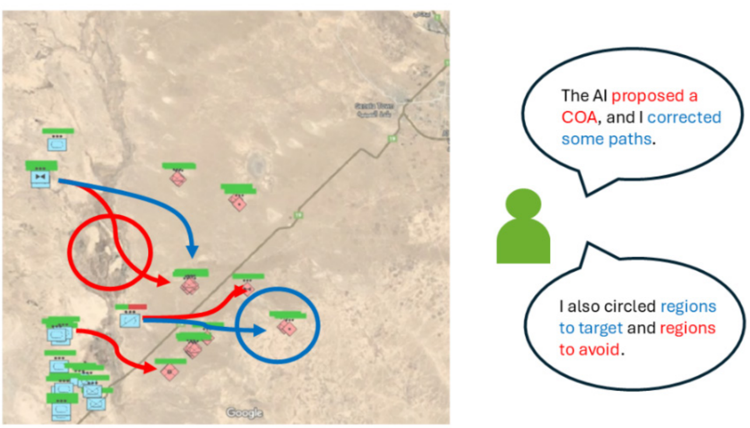

Fig. 1 – Illustration of sketch-based human-AI interaction. The AI proposes a COA (red arrows), and human personnel can then correct some of these paths (blue arrows). The human operator might also circle regions to target (blue circles) and regions to avoid (red circles).

References:

[1] Vinicius Goecks et al. "Integrating Behavior Cloning and Reinforcement Learning for Improved Performance in Dense and Sparse Reward Environments." *Proceedings of the 19th International Conference on Autonomous Agents and MultiAgent Systems*. 2020.

[2] Anna Madison*, Ellen Novoseller*, Vinicius G. Goecks*, Benjamin T. Files, Nicholas Waytowich, Alfred Yu, Vernon J. Lawhern, Steven Thurman, Christopher Kelshaw, and Kaleb McDowell. Scalable Interactive Machine Learning for Future Command and Control. *Proceedings of the International Conference on Military Communication and Information Systems (ICMCIS)*, 2024.

Leveraging Foundation Models to Enhance Mental Model Formation and Communication in Human-AI Collaboration

Mariela M. Perez-Cabarcas[1,*], Alexa Harris[1], Anthony Lattanze[2], Mingyang Mao[3], Anthony Baker[1], Matthew Zomorodi[2], Xiaomin Lin[3], Tinoosh Mohsenin[3], and Kaleb McDowell[1]
[1]Humans in Complex Systems, DEVCOM Army Research Laboratory, Aberdeen Proving Ground, MD 21005
[2]Institute of Applied Engineering, University of South Florida, Tampa, FL 33620
[3]Department of Electrical and Computer Engineering, Johns Hopkins University, Baltimore, MD 21818
**Corresponding Author Email: mariela.m.perez-cabarcas.civ@army.mil*
Keywords: Cognitive Enhancement, Communication, Human-Intelligent System Interaction, Mental Model Formation, Multimodal AI, Retrieval-Augmented Generation (RAG)

Enhancing human cognition in complex, fast-paced operational settings requires intelligent systems that can facilitate collective sensemaking amid vast, unstructured information streams [1]. Inspired by real-time AI-assisted memory support systems [2], this work leverages multi-modal foundation models (e.g., text and vision) and retrieval-augmented generation (RAG) to develop AI-driven tools that support information flow among Soldiers. We designed novel human-intelligent system interactions, such as voice assistants providing real-time, context-aware feedback, to streamline mental model formation, communication, and shared situational awareness. These capabilities are integrated into an agent-based experimental platform (Fig. 1) designed to identify and support human cognitive needs for real-time information processing. The platform incorporates information reframing techniques and multimodal context processing, optimized through pilot studies. System evaluation examines query types, context characteristics, and feedback mechanisms to assess response quality and latency. Insights from these evaluations have guided iterative system development and informed the design of preliminary user studies focused on Army-relevant operational contexts. This research contributes to the development of adaptive AI systems that enhance situational awareness, optimize human-AI collaboration, and improve real-time decision support in high-stakes scenarios.

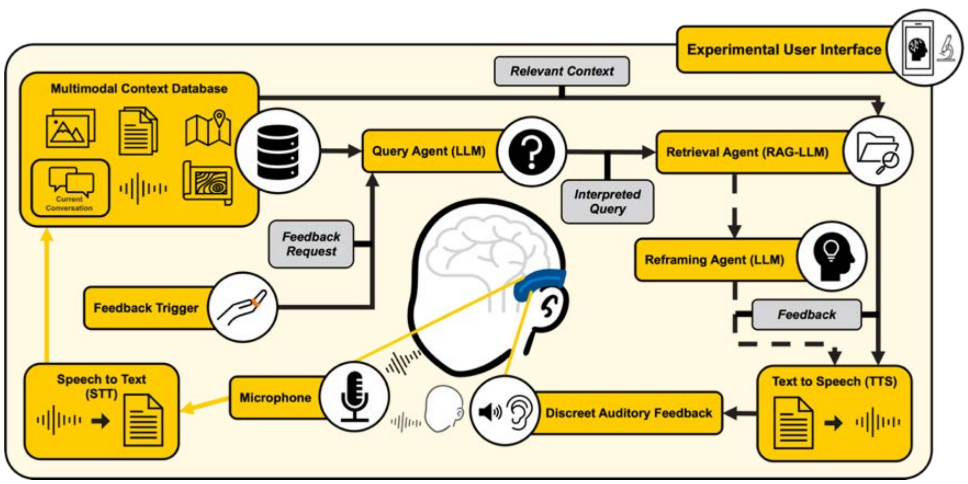

Fig. 1 – Agent-Based Experimental Platform Overview. The system monitors and stores real-time user interactions alongside domain context. When prompted, a query agent interprets the request based on the current context. The retrieval agent retrieves the relevant context and generates language-based feedback. If the user requires information in a different format, the reframing agent adjusts the feedback to match their needs. The final feedback is delivered as discrete auditory feedback.

References:

[1] A. Madison, K. McDowell, V. G. Goecks, J. Hansberger, C. M. Olney, C. Ahern, A. Marathe, N. Waytowich, C. Kenney, and C. Kelshaw, "'New' challenges for future C2: Commanding soldier-machine partnerships," arXiv preprint, arXiv:2503.08844, 2025. [Online]. Available: https://arxiv.org/abs/2503.08844.

[2] W. D. Zulfikar, S. Chan, and P. Maes, "Memoro: Using large language models to realize a concise interface for real-time memory augmentation," in Proc. CHI Conf. Human Factors Comput. Syst., May 2024, pp. 1–18. doi: 10.1145/3613904.3642450.

COA-GPT v2: An AI-Assisted MDMP Platform for Accelerating C2 Planning

Nicholas Waytowich[1,*], Vinicius G. Goecks[1]

[1]*DEVCOM Army Research Laboratory, Aberdeen Proving Ground, Maryland*

**Corresponding Author Email: nicholas.r.waytowich.civ@army.mil*

Keywords: Command and Control, MDMP, LLM, Generative AI.

The Military Decision-Making Process (MDMP) is resource-intensive and time-consuming, posing critical limitations in the fast-paced environment of future multi-domain operations. To address this, we introduce COA-GPT v2**,** a novel system powered by advanced multi-agent reasoning and multimodal Large Language Models (LLMs) to accelerate the MDMP. COA-GPT streamlines and automates routine MDMP tasks, enabling staff planners to shift their focus toward higher-order strategic analysis and decision-making. By combining generative AI with subject matter expertise via human-in-the-loop guidance, COA-GPT represents a transformative step in modernizing command and control processes.

COA-GPT employs a multi-agent architecture orchestrating multiple multimodal LLMs and specialized external tools to collaboratively produce MDMP planning outputs with human staff. It systematically generates doctrinally aligned products for Mission Receipt, Mission Analysis, and COA Development, streamlining traditional resource-intensive tasks and significantly reducing planning timelines. The platform integrates multimodal inputs, including text, images, geospatial data, and audio, ensuring comprehensive data synthesis and enhanced situational awareness.

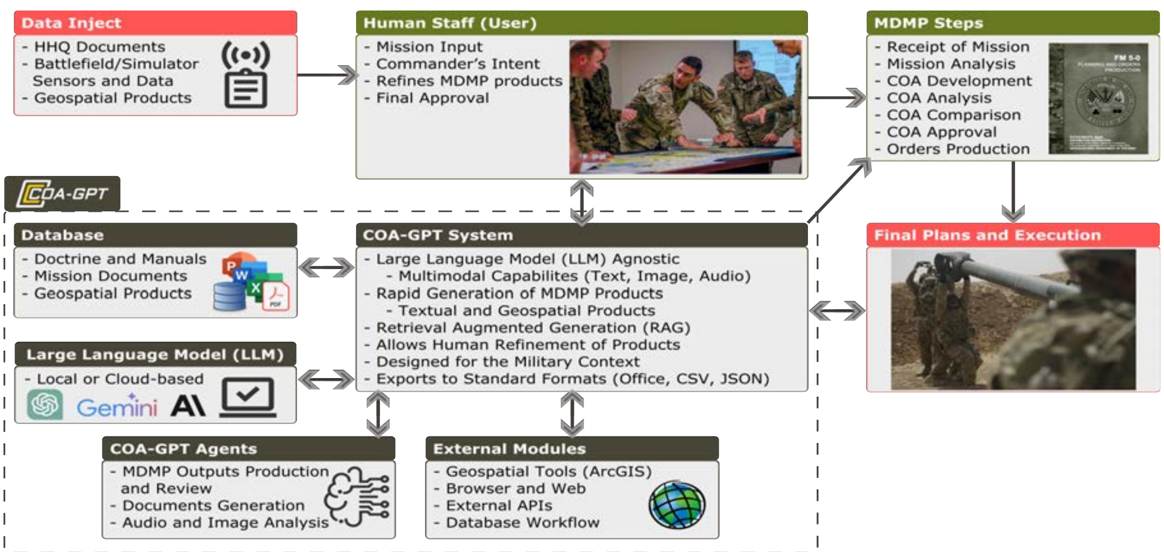

Fig. 1: COA-GPT v2: illustrating the input data, its main components, and how it interacts with the staff to generate the MDMP products.

COA-GPT was evaluated by the Mission Command Battle Lab (MCBL) on a brigade-level training scenario used at the Command and General Staff College (CGSC). Test participants rated the system on doctrinal accuracy, completeness, and effectiveness, indicating high satisfaction levels for Mission Analysis (average rating above 3.5/5) and even higher for COA Development (above 4.0/5). The system was praised for providing "50-70% solutions" and has the potential to significantly reduce initial workloads, although human oversight is still necessary to ensure full accuracy.

COA-GPT's integration could dramatically enhance the agility and effectiveness of military command structures, enabling smaller, distributed planning cells to operate efficiently in contested environments. Its capabilities suggest substantial implications across DOTMLPF-P. Ultimately, COA-GPT offers a transformative approach to military planning, balancing computational efficiency with critical human judgment.

[1] VG Goecks, N Waytowich, "COA-GPT: Generative pre-trained transformers for accelerated course of action development in military operations." 2024 International Conference on Military Communication and Information Systems (ICMCIS).

Forging Capability in an Age of Convergent Transformation

Jason S. Metcalfe
Humans in Complex Systems, DEVCOM Army Research Laboratory, 7101 Mulberry Point Rd., Aberdeen Proving Ground, MD 21005
Author Email: jason.s.metcalfe2.civ@army.mil

Keywords: human–machine integration, hybrid collectives, cyber-physical systems, strategic synthesis, multimodal fusion, collective capability, trust formation, experimental infrastructure, foundational science.

Evolving operations and shrinking decision timelines have exposed a critical vulnerability in traditional acquisitions: *reliance on initial solution certainty and rigid, parallel lines of effort*. These models assume predefined solutions may be cleanly decomposed and independently executed. Yet in practice, coordination often fails at (and between) the seams. We offer a foundational science approach wherein capability is not the fusion of optimized systems, but the emergent expression of potential across interacting agents coordinated under appropriate, objective constraint [1]-[2], and understood as dynamically organized in response to task demands and mission requirements.

Drawing on the principle of *soft assembly* [3], we propose cultivating diverse, and limited, functional action units whose compositional interplay enables task adaptation, not failure, when plans or subsystems falter. Contrasted with traditional methods (Fig. 1), this formation-driven view aligns with Waddington's concept of potentiality [4] and Newell's ecological model of coordination [5], reframing design around the propagation of latent, flexible functional potential through real-time management of formation-based constraints. This perspective implies a decisive move beyond traditional Human–Autonomy Teaming, toward Hybrid Intelligence Units that form the basis of Human–Machine Integrated Formations—where capability is distributed, resilience is shared, and solutions are assembled dynamically rather than imposed prescriptively.

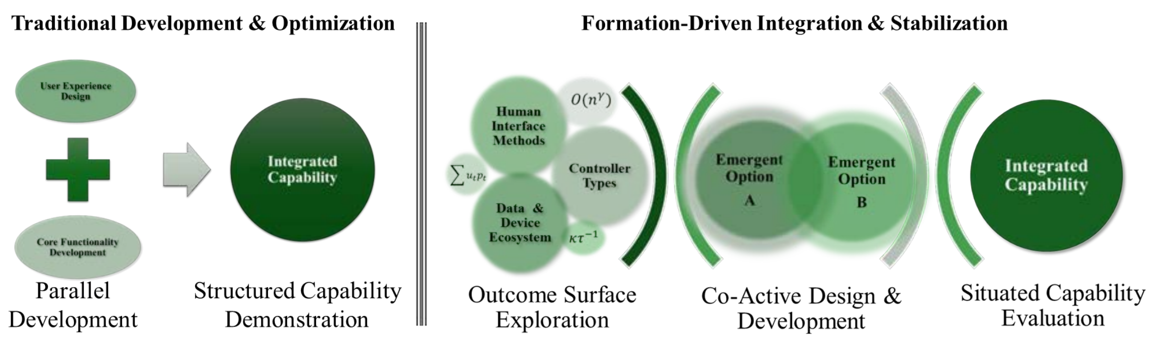

Fig. 1 – **Traditional capability development and optimization versus formation-driven integration and stabilization**. Traditional methods (left) rely on predefined solutions and discrete handoffs, while the formation-driven approach (right) emphasizes exploration and soft-assembly for adaptive composition and distributed robustness.

References:

[1] R. A. Brooks, "Intelligence without representation," *Artificial Intelligence*, vol. 47, no. 1–3, pp. 139–159, Jan. 1991.
[2] N. J. Cooke, J. C. Gorman, C. W. Myers, and J. L. Duran, "Interactive team cognition," *Cognitive Science*, vol. 37, no. 2, pp. 255–285, Mar. 2013.
[3] E. Thelen and L. B. Smith, *A Dynamic Systems Approach to the Development of Cognition and Action*. Cambridge, MA, USA: MIT Press, 1994, ch. 3, pp. 45–69.
[4] C. H. Waddington, *The Strategy of the Genes*. London, UK: Allen & Unwin, 1957, ch. 2, pp. 17–34.
[5] K. M. Newell, "Constraints on the development of coordination," in *Motor Development in Children: Aspects of Coordination and Control*, M. G. Wade and H. T. A. Whiting, Eds. Dordrecht, Netherlands: Martinus Nijhoff, 1986, ch. 12, pp. 341–360.

5.4 Session: Sensing and Multimodal Processing

Advancing Defense AI with Synthetic Data, Closed-Loop Simulation, and Domain Adaptation

Guangkun Li* and Anna Loskiewicz-Buczak

Johns Hopkins University - Applied Physics Lab, 11100 Johns Hopkins Road, Laurel, Maryland 20723
**Corresponding Author Email: homer.li@jhuapl.edu*
Keywords: Domain Adaptation, Synthetic Data Generation, Zero Shot, Closed-Loop Simulation, War Gaming.

This talk presents our recent efforts at the Johns Hopkins University Applied Physics Laboratory to transition cutting-edge AI research into practical defense applications. Our work began with synthetic data generation for Project Maven, leveraging tools such as Blender [1], Unreal Engine [2], and custom game engine pipelines to produce high-fidelity imagery for visible-spectrum and infrared sensor applications. The observed performance degradation when models trained on synthetic data were applied to real-world imagery highlighted the need for domain adaptation (DA) strategies.

In addition to benchmarking widely studied unsupervised domain adaptation (UDA) methods, including adversarial training, VAEs, and GANs, we developed our own DA techniques to better reflect real-world constraints. UDA assumes access to unlabeled data from the target domain, which creates an artificial limitation in many operational contexts. In practice, while fully labeled target datasets may not be available, it is often feasible to label a small number of samples. We found that in such semi-supervised settings—where limited labeling is permitted—simple fine-tuning of models significantly outperformed more complex UDA approaches. This insight led us to explore a more challenging and practical scenario: when no target domain data containing the class of interest is available at all during training. To address this, we developed a novel zero-shot domain adaptation (ZSDA) framework [3] incorporating class-aware feature alignment and latent space projection, and demonstrated strong generalization performance across modalities such as x-ray and sonar.

In a parallel line of work, we are advancing closed-loop simulation capabilities by integrating real-time situational updates into interactive environments such as Arma 3 [4], Virtual Battle Space 4 [5], Blender, and Unreal Engine. These efforts support dynamic AI development for mission-relevant tasks such as missile seeker tracking, UAV and small object detection, anomaly detection, and digital twin site modeling. Building on this simulation expertise, we are also developing AI-driven large-scale simulation and wargaming capabilities using large language models (LLMs). By controlling game SDKs directly, LLMs enable real-time generation, coordination, and variation of complex battle scenarios, supporting scalable experimentation for future command and control decision-making and large-scale operational modeling.

References:

[1] https://www.blender.org/

[2] https://www.unrealengine.com/en-US

[3] Li, Guangkun, et al. "Zero shot domain adaptation for x-ray baggage scanning." Synthetic Data for Artificial Intelligence and Machine Learning: Tools, Techniques, and Applications. Vol. 12529. SPIE, 2023.

[4] https://arma3.com/

[5] https://bisimulations.com/products/vbs4/

Mapper for Out-of-Distribution Data Environments

Dr. Erin Hausmann[1*] and Dr. Katie Rainey[2]
[1] Department of Navy, Naval Information Warfare Center Pacific, 53560 Hull Street, San Diego, CA 92152
[2]Department of Navy, 53560 Hull Street, San Diego, CA 92152
**Corresponding Author Email: erin.m.hausmann.civ@us.navy.mil*
Keywords: topological data analysis, Mapper, Out-of-Distribution, machine learning.

Machine learning (ML) models can perform extraordinarily well in controlled environments. However, out in the "real"-world, performance drops due to the unpredictable nature of the environment. The usual approach to ensure good performance is to obtain a plethora of high-quality labeled data from the relevant environment. However, when working in a Naval setting this is often not practical or even possible. We use tools from Topological Data Analysis (TDA) to help us analyze, understand, and characterize the effects of changes to operating conditions on the performance of Naval ML systems. Specifically, we use the TDA tool, Mapper, to explore the latent space of Naval ML systems. Mapper, in short, takes a possibly high dimensional dataset and reduces it to a low-dimensional graph, while still preserving information from the original dataset—unlike other dimension reducing techniques. After applying Mapper to the latent space of ML models, we see that there is a qualitative difference between the latent space of in-distribution data to out-of-distribution datasets. To quantify this difference, we have begun investigating a generalized version of Optimal Transport applied to these Mapper graphs. Although this metric appears to be promising, it remains to be shown that it is statistically significant.

Funding: SEED Grant, OSD.

References:

[1] E. Purvine, D. Brown, B. Jefferson, C. Joslyn, B. Praggastis, A. Rathore, M. Shapiro, B. Wang, and Y. Zhou. "Experimental Obserbations of the Topology of Convolutional Neural Network Activations". Proceedings of the 37th AAAI Conference on Artificial Intelligence (AAAI), 2023.

EOIR Fusion of Targets Signatures Using Gaussian Splatter

Minas Benyamin and Geoffrey H. Goldman

[1]*DEVCOM Army Research Laboratory, 2800 Powder Mill Road, Adelphi, MD 20783-1197.*
Email:Minas.d.benyamin.civ@army.mil
Keywords: Fusion, EOIR, 3DGS, decoys

The latest technology for generating signatures of targets of interest is affecting the performance of surveillance systems. However, their joint signatures across different modalities are usually not consistent with a real target. We propose using an emerging technique of scene representation and rendering called 3D Gaussian Splatter (3DGS) to generate robust 3D object models using fused electro-optical (EO) and infrared (IR) imagery. We collected data on a small unmanned aerial system with collocated EO and IR cameras for analyzing the approach. Using 3DGS with fused EO-IR imagery, we create detailed 3D target signatures that allow us to view targets of interest from different angles, distances and views. This model produces a more robust representation of the target which can be input into standard ATR algorithms.

Event-Based Sensing and Artificial Intelligence for Improving Directed Energy Control Systems

Joseph Cox

We investigate technology including Event-Based Sensing (EBS) and Artificial Intelligence (AI) and their ability to improve the Laser Directed Energy Weapon (LDEW) control systems. Specifically, the EBS and AI technologies are applied to tasks including automatic target detection and recognition for automated control of the LDEW. As part of the SMART SEED Grant program, this effort attempts to feed a greatly reduced data stream (100x reduction as demonstrated in local experiments [1] and as cited by DARPA [2]) into a high-performing YOLO-like [3] neural network, to achieve high detection performance with the automated system. The effort is partitioned into three years, with the current second year focused on preparation for field testing. This year's outcomes include a publication on constructing a relevant AI dataset, a presentation on building an automated event-based detection system, and a patent submission on the automated detection algorithm. In addition, the work led to the construction of a state-of-the-art baseline LDEW control system that is used in live LDEW demonstrations and compared against an automated control system. Overall, the effort is on schedule, with the EBS work completed in the beginning of the year, and the AI work completed towards the end of the year.

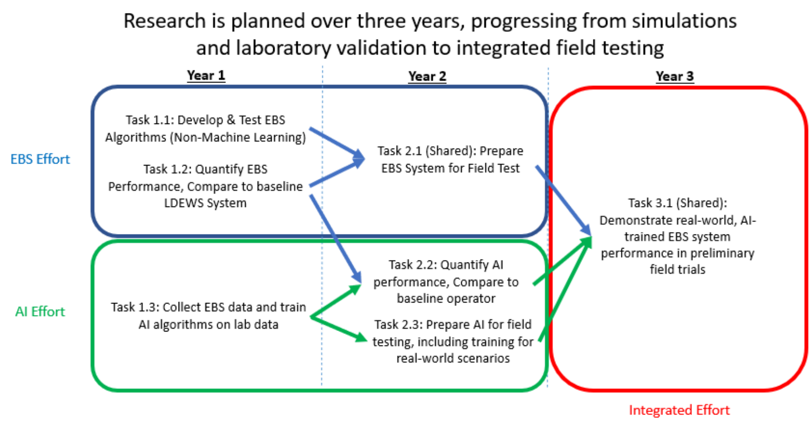

Fig. 1: Diagram demonstrating the breakdown of tasks in the proposed research. The diagram is organized to highlight the year of the task, the relationship of the task to the specific effort, and the relationships between the different tasks.

References:

[1]: Cox, Joseph C., Amit Ashok, and Nicholas Morley. "Reduced spatiotemporal bandwidth of motion stabilized event-based imaging sensors: experimental demonstration." *Applied Optics* 62.23 (2023): G128-G142.

[2]: DARPA 2023 Justification Book, Volume 1, Page 143

[3]: Redmon, Joseph, et al. "You only look once: Unified, real-time object detection." *Proceedings of the IEEE conference on computer vision and pattern recognition*. 2016.

Limitations on Resource Reallocation for Task Execution

Eric Graves[1,*], Robert Davis[2], Olena Tkachenko[2] and Kevin Chan[1]
[1]DEVCOM Army Research Laboratory, 2900 Powder Mill Road, Adelphi, MD. 20783
[2]Parsons Contracting, 6210 Guardian Gateway, Suite 200, City Aberdeen Proving Ground, MD. 21005
**Corresponding Author Email: eric.s.graves9.civ@army.mill*
Keywords: Reallocation, Quickest Change Detection, Fundamental Limits, Information Theory.

In networks where communication and computation resources are allocated to the execution of tasks, monitoring of progress of that execution conceptually enables reallocation when performance is inexplicably slow. There is a potential cost to reallocation though, if resources are reallocated erroneously then holistic system performance can degrade. Determining the fundamental limits and trade-off of reallocation will help ensure that implementation of the reallocation system would maximally improve performance subject for an appropriate error tolerance. To this end we consider the reallocation system in the hypothesis testing framework. Using this framework, we bound how quickly a system may reallocate based upon the level of performance degradation and the expected performance of an alternative allocation. In particular, we show the order of convergence in the law of large number dictates that total task execution time is maximized when the degradation of this execution time is small. That is, the lost by a small increase in task execution time will be greater than the time lost by a large increase in task execution time due to the amount of time it takes to detect that change. Such an observation is important in attacking adversarial networks using resource allocation as well as determining when resources should be reallocated in our networks.

6. Topic: Quantum Science and Technologies

Synchronizing the Washington DC Metropolitan Quantum Network (DC-QNet)

Wayne McKenzie[1*], Anne Marie Richards[1], Ya-Shian Li-Baboud[2], Ivan A. Burenkov[2], Anouar Rahmouni[2], Thomas Gerrits[2], Adam T. Black[3], Daniel E. Jones[4,2*], Alejandro Rodriguez Perez[5], and T. G. Akin[6]

[1]Laboratory for Telecommunication Sciences, College Park, MD 20740, USA
[2]National Institute of Standards and Technology, Gaithersburg, MD 20899, USA
[3]Naval Research Laboratory, Washington DC, 20375, USA
[4]DEVCOM Army Research Laboratory, Adelphi, MD 20783, USA
[5]Goddard Space Flight Center, National Aeronautics and Space Administration, Greenbelt, MD 20771, USA
[6]Clock Development Division, United States Naval Observatory, Washington, DC 20392, USA
**Corresponding Author Email: wmckenzie@ltsnet.net, daniel.e.jones161.civ@army.mil*
Keywords: quantum networks, quantum communication, time synchronization

Quantum networking protocols relying on interference and precise time-of-flight measurements require high precision clock synchronization. Here we describe the design, implementation, and characterization of two optical time transfer methods used in the Washington DC metropolitan quantum network (DC-QNet).

The Washington DC metropolitan quantum network (DC-QNet) comprises seven locations connected by deployed underground and/or aerial optical fibers [Fig. 1(a)]. Performing quantum networking protocols over such a deployed metropolitan network requires high precision clock synchronization. Here we describe two optical two-way time and frequency transfer (OTWTFT) methods used to synchronize the nodes of the DC-QNet [1]. Active electronic stabilization (ELSTAB) was able to achieve sub-picosecond time deviation (TDEV) at integration times from 1 - 10^5 s over multiple different lengths of deployed fiber. In comparison, the White Rabbit-Precision Time Protocol (WR-PTP) was able to achieve 10-picosecond TDEV's over similar fiber lengths at comparable integration times.

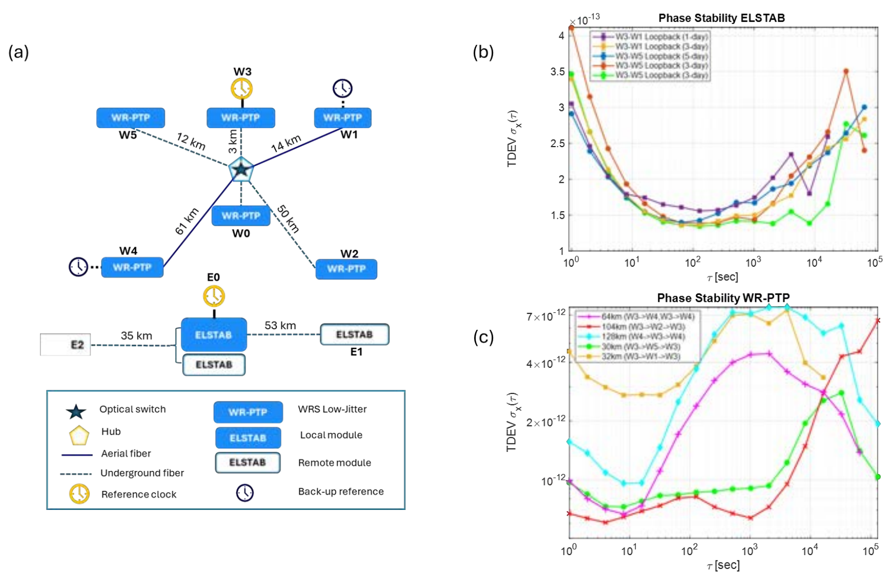

Fig. 1 – (a) Diagram of ELSTAB and WR-PTP time synchronization networks in the DC-QNet. (b) TDEV measurements performed over W3-W1 and W3-W5 loopbacks using ELSTAB. (c) TDEV measurements of various DC-QNet links using WR-PTP.

References: [1] W. McKenzie, et al. "Clock synchronization characterization of the Washington DC metropolitan quantum network (DC-QNet)," Appl. Phys. Lett. **125**, 16 (2024).

Learning Equivariant Maps with Variational Quantum Circuits

Zachary P. Bradshaw[1], Margarite L. LaBorde[1,*], Ethan N. Evans[1], and Matthew Cook[1]
[1]*Naval Surface Warfare Center-Panama City Division, Panama City, FL, 32407*
**Corresponding Author Email: margarite.l.laborde.civ@us.navy.mil*
Keywords: quantum computing, quantum information, symmetry.

Geometric quantum machine learning uses the symmetries inherent in data to design tailored machine learning tasks with reduced search space dimension. Leveraging the strength of this field as motivation, we demonstrate a procedure to learn equivariant maps between representations of symmetry groups on a quantum computer, allowing us to preserve the symmetric properties of encoded data. We illustrate the procedure for several example representations.

Amidst the recent rise in popularity of quantum machine learning (QML), geometric quantum machine learning has proven a particularly promising candidate for near-term implementations. However, many QML algorithms suffer from the barren plateau problem [1,3], where an overly large expressivity leads to vanishingly small gradients in the training space. Geometric quantum machine learning [4] answers this problem by using symmetries inherent in the learning problem to restrict the search space and alleviate the barren plateau problem [2]. In this framework, data is encoded onto the quantum computer via an equivariant map which preserves the symmetry structure of the original data.

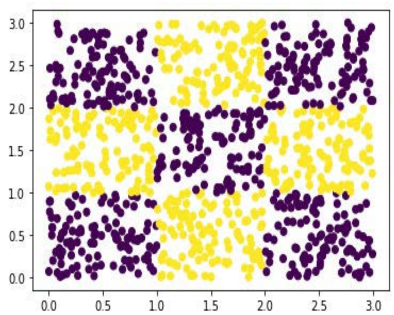

Fig. 1. Classification problem with D_4 symmetry. Points of the same color have the same class.

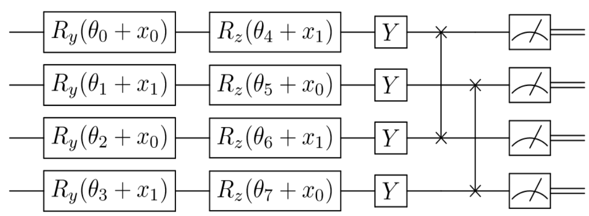

Fig. 2. Circuit for learning equivariance between two representations of D_4 using both R_y and R_z rotation gates. The data is encoded as $x = (x_0, x_1)$.

In this work, we show how a variational quantum circuit can be used to learn this map between unitary representations of finite groups. In Fig. 1, we show an example of a classification problem with inherent symmetry in the data—a 3x3 checkerboard pattern. This data is invariant under flips about the vertical axis as well as rotations by 90°. These transformations generate the group D_4, or the dihedral group of order 4. Fig. 2 shows a quantum circuit which can learn to embed this data in such a way that this symmetry is preserved. Data points are initially encoded according to coordinates (x_0, x_1) using angle embedding. Additional parameters $\{\theta_i\}_{i=0}^{7}$ are then trained until the data respects an equivalent symmetry on the Hilbert space of the quantum computer. After this training process is completed, the embedding map learned from this procedure can be used in any desired QML algorithm on this data and still preserve the symmetry of the original set.

Funding: Funding provided by OUSD through the SMART SEED grant.

References:

[1] A. Arrasmith, Z. Holmes, M. Cerezo, and P. J. Coles. "Equivalence of quantum barren plateaus to cost concentration and narrow gorges." *Quantum Science and Technology*, 7(4):045015, Aug. 2022.

[2] M. Larocca, F. Sauvage, F. M. Sbahi, G. Verdon, P. J. Coles, and M. Cerezo. "Group-invariant quantum machine learning." *PRX Quantum*, 3(3), Sept. 2022.

[3] J. R. McClean, S. Boixo, V. N. Smelyanskiy, R. Babbush, and H. Neven. "Barren plateaus in quantum neural network training landscapes." *Nature Communications*, 9(1), Nov. 2018.

[4] M. Ragone, P. Braccia, Q. T. Nguyen, L. Schatzki, P. J. Coles, F. Sauvage, M. Larocca, and M. Cerezo. "Representation theory for geometric quantum machine learning." *arXiv preprint arXiv:2210.07980*, 2023.

Projected Classical Shadows

Brian T. Kirby[1,2*], Zhen Qin[3], Joseph M. Lukens[4,5,6], and Zhihui Zhu[3]

[1]DEVCOM Army Research Laboratory, Adelphi, MD 20783, USA, [2]Tulane University, New Orleans, LA 70118, USA, [3]Department of Computer Science and Engineering, The Ohio State University, Columbus, Ohio 43210, USA, [4]Elmore Family School of Electrical and Computer Engineering and Purdue Quantum Science and Engineering Institute, Purdue University, West Lafayette, Indiana 47907, USA, [5]Quantum Information Science Section, Oak Ridge National Laboratory, Oak Ridge, Tennessee 37831, USA, [6]Research Technology Office and Quantum Collaborative, Arizona State University, Tempe, Arizona 85287, USA

**Corresponding Author Email: Brian.T.Kirby4.civ@army.mil*

Keywords: quantum networks, quantum communications

Here we introduce the projected classical shadow (PCS) method which adds a projection state onto a target subspace to the original classical shadow (CS) proposal allowing both for the full recovering of a density matrix as well as the incorporation of prior information.

The characterization of quantum systems through quantum state tomography becomes impractical as systems increase in size due to the exponential scaling of Hilbert space – a scaling reflected in the number of copies required and the computational resources needed to process them. In response, the alternative approach of CS was introduced which allows for the prediction of key properties about a quantum state without requiring full state reconstruction [1]. The original CS proposal is based on the repeated execution of single-shot Haar-random projective measurements which are then inverted to create a “shadow” of the underlying quantum state. As compared to the least squares and regularized least squares approaches to performing the same inversion, CS leverages the physics of the measurement process to significantly reduce computational requirements [2].

However, the shadow produced by the CS procedure is not a physical density matrix and there is no natural way for including prior information into the process. Here we show that including a projection step onto a target subspace accomplishes each of these while reaching the information-theoretic bound on the recovering error in terms of the Frobenius norm between the reconstructed and true density matrices [3].

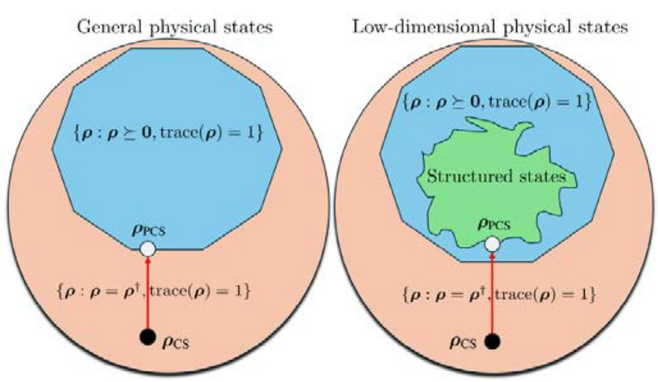

Fig. 1 – Illustration of proposed PCS method. Given an initial CS estimate ρ_{CS} lying in the space of Hermitian and unit-trace matrices (not necessarily PSD), we compute the closest state ρ_{PCS} in the physical space of interest—either the space of all possible states (left) or a subspace possessing a desired structure (right).

Funding: We acknowledge funding support from the National Science Foundation (CCF-2241298, EECS-2409701) and the U.S. Department of Energy (ERKJ432, DE-SC0024257). We thank the Ohio Supercomputer Center for providing computational resources and the Quantum Collaborative led by Arizona State University for providing valuable expertise and resources. A portion of this work was performed at Oak Ridge National Laboratory, operated by UT-Battelle for the U.S. Department of Energy under Contract No. DE-AC05-00OR22725.

References: [1] Huang, Hsin-Yuan, Richard Kueng, and John Preskill. "Predicting many properties of a quantum system from very few measurements." Nature Physics 16.10 (2020): 1050-1057. [2] Zhu, Zhihui, Joseph M. Lukens, and Brian T. Kirby. "On the connection between least squares, regularization, and classical shadows." Quantum 8 (2024): 1455. [3] Qin, Zhen, et al. "Enhancing Quantum State Reconstruction with Structured Classical Shadows." arXiv preprint arXiv:2501.03144 (2025).

Polarization-Preserving Quantum Frequency Conversion for Trapped-ion Quantum Networking

Michael Kwan[1,3,*], Bradley Kerkhof[2,3], Kate S. Collins[3], Q. Sara Quraishi[1,4],and Edo Waks[1,2,3]
[1]Department of Physics, [2]Department of Engineering, [3]Institute for Research in Electronics and Applied Physics, University of Maryland, College Park, MD 20742
[4]Army Research Laboratory, Adelphi, MD 20783
**Corresponding Author Email: mkwan@umd.edu*
Keywords: quantum frequency conversion, trapped ions, quantum networking.

We demonstrate two-stage, polarization-preserving quantum frequency conversion to shift Ba+ single photons at 493 nm to the telecom O-band for quantum networking. We anticipate three orders of magnitude improved SNR over our prior work converting to the telecom C-band.

While trapped ions are well developed technologies for both quantum computation and simulation, incorporating them into nodes of a quantum network typically requires quantum frequency conversion (QFC). QFC extends the network operating range given that most atomic ions emit polarization-entangled photons in the visible or near-infrared wavelengths. We have built two concatenated stages of polarization-preserving QFC to frequency down-convert the $^{138}Ba^+$ ion's 493-nm photons to the telecom O-band at 1287 nm. Both stages are designed in a Sagnac-interferometer-type configuration using a thermally quasi-phase-matched periodically poled lithium niobate (PPLN) waveguide.

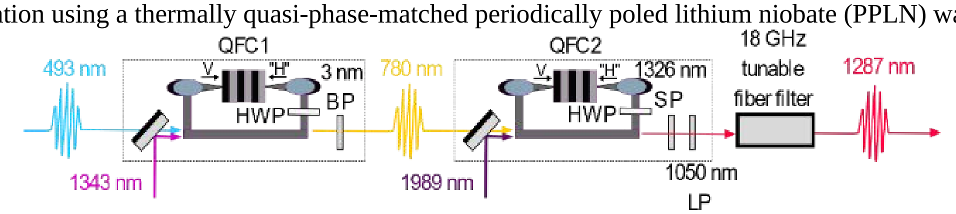

Fig. 1. Schematic of the two-stage, polarization-preserving QFC setup. The first stage QFC converts 493 nm to 780 nm using a 1343-nm pump laser. The second stage QFC then converts from 780 nm to 1286 nm using a 1989-nm pump laser.

The first-stage converter has been well characterized [1], and here we characterize the recently built second-stage O-band converter, shown in Fig. 1. We measure the maximum external conversion efficiencies for each orthogonal polarization converted by waveguide to be 59% and 56%, corresponding respectively to ~40% and ~38% fiber-to-fiber conversion. The conversion efficiency difference can be attributed to asymmetries in coupling to the waveguide as well as imperfect phase matching.

To confirm the conversion of arbitrary input polarizations into the second-stage QFC, quantum process tomography [2] was performed by injecting a CW source at 780 nm. Polarizations corresponding to the H, V, D, L poles of the Ponicaré sphere were sent through the converter and the Stokes parameters at the output were measured. These measurements were used to determine the process matrix representing the operation that transforms arbitrary input polarizations to their respective output polarizations. The overlap between the ideal and measured process matrices defines the process fidelity of the converter [2].

Without frequency-stabilizing the injected light, we measure the process fidelity of the second-stage, polarization-preserving QFC to be around 98%. The limiting factors to the process fidelity include alignment and frequency drifts of the injected 780-nm input and 1989-nm pump lasers, which spawn relative differences in conversion efficiencies between the orthogonal polarizations converted through the waveguide. Waveplate rotation errors limit the purity of the prepared states and the accuracy of the measured output states. Similar to the first-stage QFC [1], we expect 1~3% drop in ion-photon entanglement fidelity through this stage alone.

With this O-band conversion scheme, we anticipate three orders of magnitude improvement in signal-to-noise ratio [3] over our prior work converting to the telecom C-band, where previously [5] the pump laser frequency's proximity to the converted photon frequency resulted in a significant amount of Raman anti-Stokes noise photons.

Funding: Army Research Laboratory Cooperative Agreement

References:

[1] J. Hannegan, J. D. Siverns, and Q. Quraishi, "Entanglement between a trapped-ion qubit and a 780-nm photon via quantum frequency conversion," Phys. Rev. A **106** 02441 (2022).

[2] I. Chuang and M. A. Nielsen, "Prescription for experimental determination of the dynamics of a quantum black box," J. Mod. Opt. **44**, 11-12, 2455-2467 (1997).

[3] U. Saha *et al.*, "Low-Noise Quantum Frequency Conversion of Photons from a Trapped Barium Ion to the Telecom O-band," ACS Photonics **10**, 8, 2861-2865 (2023).

[4] J. Hannegan *et al.*, "C-band single photons from a trapped ion via two-stage frequency conversion," Appl. Phys. Lett. **23**, 119 (8): 084001 (2021).

Scalable integrated quantum dot networks and quantum biological imaging

J. Q. Grim[1,*], A. S. Bracker[1], C. S. Kim[1], M. Kim[2], E. Flagg[3], B. Warr[4], L. P. Swick[4]
A. Terrasson[5], N. P. Mauranyapin[5], W. P. Bowen[5]

[1] U.S. Naval Research Laboratory, 4555 Overlook Avenue SW, Washington, D.C. 20375, USA
[2]Jacobs, Hanover, MD; [3]Department of Physics and Astronomy, West Virginia University, Morgantown, WV, 26506 USA
[4]NREIP student internship at the U.S. Naval Research Laboratory, 4555 Overlook Avenue SW, Washington, D.C. 20375, USA
[5]Australian Research Council Centre of Excellence in Quantum Biotechnology, School of Mathematics and Physics, University of Queensland, Australia
**Corresponding Author Email: joel.q.grim.civ@us.navy.mil*
Keywords: Quantum optics, quantum sensing, solid-state quantum emitters, integrated quantum optics.

We have developed a platform, along with quantum emitter tuning techniques, that enables on-chip quantum dot networks[1], [2]. These networks serve as a test bed for multi-emitter quantum optics demonstrations, motivated by the potential for advancements in photonic quantum computing, simulation, communication, and sensing. Our approach uses semiconductor quantum dots (QDs), which can host electron/hole spin qubits and can be connected with 'flying qubit' single photons. While QDs have become very advanced with numerous demonstrations of high photon indistinguishability, quantum transistors, and spin-spin entanglement, these efforts have been limited to one, and at most, two QDs – a limitation shared by all solid-state single photon sources. Our team has recently achieved a breakthrough with a technique that enables scalable tuning of QDs into resonance. Leveraging this technique, we demonstrated an entangled, superradiant state from three QDs coupled to the same nanophotonic waveguide[1]. We have also used this technique to realize collective scattering of laser light from two QDs, and have observed an enhanced optical nonlinearity at the few-photon level. We are extending this work to quantum emitters in materials such as silicon and diamond. Finally, we will present results of fast quantum-enhanced biological imaging of living cells using squeezed-light Raman microscopy[3], conducted in the Queensland Quantum Optics Lab led by Prof. Warwick Bowen at the University of Queensland, Australia. This work addresses the fundamental constraint of shot noise on the resolution, sensitivity, and speed of light-based microscopes.

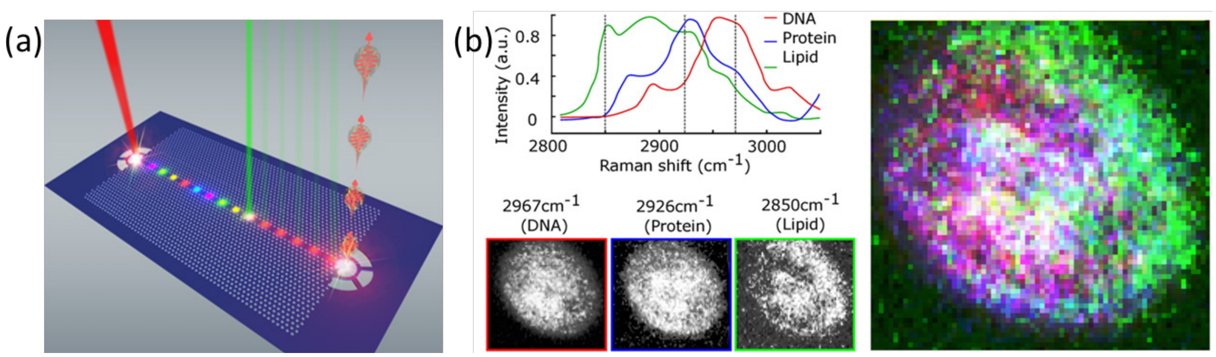

Fig. 1 – (a) Schematic of a photonic crystal waveguide with embedded quantum dots used for integrated quantum optics demonstrations (see refs.[1], [2]. (b) Multi-spectral quantum bio-imaging of a living yeast cell (see ref. [3])

Funding: This work was supported by the U.S. Office of Naval Research; Australian Research Council Centre of Excellence in Quantum Biotechnology (CE230100021); and Centre of Excellence for Engineered Quantum Systems (CE170100009); Air Force Office of Scientific Research (FA9550-20-1-0391, FA9550-22-1-0047).

References:

[1] J. Q. Grim *et al.*, "Scalable in operando strain tuning in nanophotonic waveguides enabling three-quantum-dot superradiance," *Nature Materials*, vol. 18, pp. 963–969, 2019, doi: 10.1038/s41563-019-0418-0.

[2] J. Q. Grim *et al.*, "Scattering laser light from two resonant quantum dots in a photonic crystal waveguide," *Phys. Rev. B*, vol. 106, p. L081403, 2022, doi: 10.1103/PhysRevB.106.L081403.

[3] A. Terrasson *et al.*, "Fast biological imaging with quantum-enhanced Raman microscopy," *Opt. Express*, vol. 32, no. 21, pp. 36193–36206, Oct. 2024, doi: 10.1364/OE.523956.

Error-tolerant Advantages of the CVQE Algorithm by the Probability Distribution Analysis

Yi-Hua Lai[1,*], John P.T. Stenger[1], and Daniel Gunlycke[1]

[1]U.S. Naval Research Laboratory, Washington, DC 20375

**Corresponding Author Email: yi-hua.lai.ctr.tw@nrl.navy.mil*

Keywords: "Quantum Computing", "Quantum Algorithm", "Quantum Chemistry", "Quantum Simulation".

The cascaded variational quantum eigensolver (CVQE) has been developed [1-2] to utilize one-time quantum circuit measurements for later classical optimization. This novel technique not only portrays a significant potential in simulating electronic systems that require exponentially growing classical resources as the system size increases, but also saves iterative communication between the QPU and the CPU that usually happens in conventional VQE [3]. Nevertheless, while CVQE offers complete freedom to choose the guiding state as input, a good choice for the guiding state can lead to efficient energy convergence with minimal resources. In this work, we analyze the wave-function probability distributions from different stages of the CVQE with the guiding state prepared by the discretized adiabatic evolution [4], intending to find the limit and the optimal setting based on the effects of this approach.

We demonstrated an example of the hydrogen complex (i.e., $H_2 + H_2^+ \rightarrow H_3^+ + H$) numerically for an energy curve along the intrinsic reaction coordinates. The reaction coordinate of the lowest-energy point is used for probability distribution analysis. By tuning the adiabatic evolution parameters N_t and dt, we define the three regimes, "Minimal Guiding State", "Ideal Unitary Matrix Multiplied Guiding State", and "Rough Guiding State." We found that the "Minimal Guiding State" and the "Ideal Unitary Matrix Multiplied Guiding State" are too large for the Noisy Intermediate-Scale Quantum (NISQ) computers [5] to properly process, though they may be theoretically preferred. On the other hand, "Rough Guiding State" may neither satisfy the discretized adiabatic condition nor match any close to the ideal ground state; however, the Fock states generated by the immature adiabatic evolution can still support the subspace critical to the effective Hamiltonian for later diagonalization. Specifically, a single-step adiabatic evolution ($N_t = dt = 1$) would save the quantum resources while keeping the CVQE-optimized results as good as other guiding states of longer adiabatic evolution. The CVQE simulations implemented on the real QPU, which displays errors, can be difficult. Still, with proper post-processing of the sampling data, we can reach the correct ground-state values within a smaller subspace through filtering. To efficiently run CVQE simulation with adiabatic state preparation on the noisy QPU, we suggest preparing the guiding state with the single-step evolution ($N_t = dt = 1$), sampling a large number of shots, and choosing a probability threshold for filtering the dominant Fock states.

With this dynamical system as an example, we have exhibited how a chemical reaction can be simulated using the CVQE algorithm with discretized adiabatic state preparation. The protocol and demonstration from this attainable system will contribute to a better choice of the guiding state generically for larger many-body systems simulated by the CVQE algorithm in the future.

Funding: We acknowledge QC resources from IBM through a collaboration with the Air Force Research Laboratory (AFRL). Yi-Hua Lai thanks the National Research Council Research Associateship Programs for support during her post-doctoral tenure at NRL.

References:

[1] D. Gunlycke, C. S. Hellberg, and J. P. T. Stenger, "Cascaded variational quantum eigensolver algorithm," Physical Review Research, vol. 6, no. 1, Mar. 2024.

[2] J. P. T. Stenger, C. S. Hellberg, and D. Gunlycke, "Implementing Jastrow-Gutzwiller operators on a quantum computer using the cascaded variational quantum eigensolver algorithm," Physical Review A, vol. 107, no. 6, Jun. 2023.

[3] A. Peruzzo et al., "A variational eigenvalue solver on a photonic quantum processor," Nature Communications, vol. 5, no. 1, Jul. 2014

[4] Wim van Dam, M. Mosca, and U. Vazirani, "How powerful is adiabatic quantum computation?," Jun. 2002

[5] J. Preskill, "Quantum Computing in the NISQ era and beyond," Quantum, vol. 2, no. 2, p. 79, Aug. 2018

NV-based Quantum Gyroscope with Advanced Control Pulses

Sean Lourette[1,2], Andrey Jarmola[1,2], Jabir Chathanathil[1], Sebastián C. Carrasco[1], Dmitry Budker[2,3,4], Svetlana A. Malinovskaya[5], A. Glen Birdwell[1], Tony G. Ivanov[1], Vladimir S. Malinovsky[1,*]
[1]DEVCOM Army Research Laboratory, Adelphi, MD 20783
[2]Department of Physics, University of California, Berkeley, CA 94720
[3]Helmholtz-Institut Mainz, 55099 Mainz, Germany
[4]Johannes Gutenberg-Universität Mainz, 55128 Mainz, Germany
[5]Department of Physics, Stevens Institute of Technology, Hoboken, NJ 07030
**Corresponding Author Email: vladimir.s.malinovsky.civ@army.mil*
Keywords: Quantum Sensing, Quantum Control, Quantum Gyroscope, NV centers

We use novel control techniques to improve long-term stability of diamond-based sensors, such as gyroscopes and frequency standards.

Nitrogen-vacancy (NV) centers in diamonds are a promising solid-state platform for quantum sensing and metrology due to their resilience to environmental conditions and capability to sustain long coherence times at room temperature. Our previous work has leveraged those characteristics into a practical demonstration employing a novel gyroscopic setup that maps rotation into phase shifts in the nuclear spin manifold of ^{14}N [1]. Those shifts are mapped into populations for direct optical readout (Ramsey interferometry). However, we found that two factors limit the long-term stability of the device. The first is that temperature variations alter the nuclear structure. The second is that it is impossible to address all NV centers in the sample with the same power (pulse area), hindering the system's control. Both factors create additional temperature-dependent phase shifts.

To solve the aforementioned problems, we developed two generalized Ramsey schemes: one—shown in Fig. 1—utilizing stimulated Raman adiabatic passage (STIRAP) for pulse-area resilience [2] and a novel dynamical elimination protocol using modulated zero-pulse-area fields to directly suppress the sensitivity to temperature variations [3].

Our results pave the way for enhanced long-term stability in diamond-based sensors (clocks, gyroscopes, magnetometers), advancing quantum metrology and spectroscopy. We anticipate that the newly developed techniques will find widespread application across atomic and molecular systems, enabling robust control methods for quantum technology.

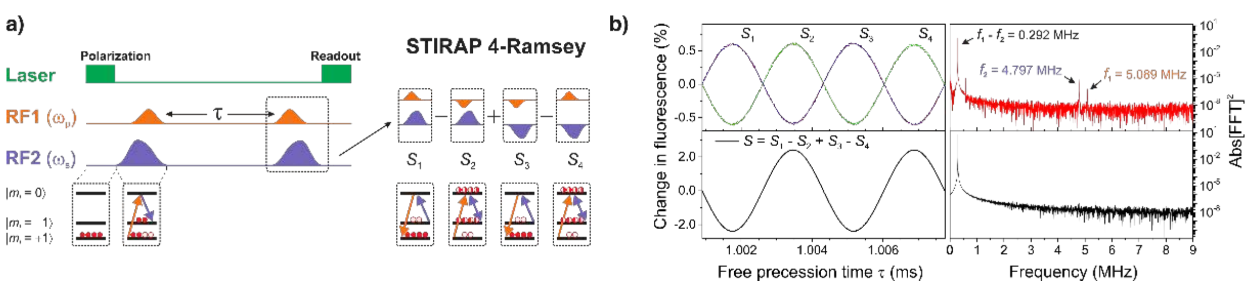

Fig. 1 – STIRAP 4-Ramsey pulse sequence. a) illustrates the experimental sequence. b) shows experimental results exhibiting cancellation of unwanted frequencies (and sensitivities).

References:

[1] A. Jarmola *et al.*, "Demonstration of diamond nuclear spin gyroscope," Sci. Adv. **7**, eabl3840 (2021).
[2] S. Lourette *et al.*, "Ramsey interferometry of nuclear spins in diamond using Stimulated Raman adiabatic passage," Quantum Sci. Technol. **10**, 015032 (2025).
[3] S. C. Carrasco *et al.*, "Dynamically Enhanced Two-Photon Spectroscopy", arXiv:2411.05670 (2024); *Phys. Rev. Lett. in press.*

Spin-Spin Interactions and Coherence Limits in Isotopically-Purified 4H-SiC

S. T. White[1,*], I. Lekavicius[2], A. P. Purdy[2], S. G. Carter[3+], D. J. Pennachio[2], J. R.Hajzus[2], A. L. Yeats[2], R. L. Myers-Ward[2]

[1]NRC Research Associate at the U.S. Naval Research Laboratory, Washington, DC, 20001, USA

[2]U.S. Naval Research Laboratory, Washington, DC, 20375, USA

[3] Previously: U.S. Naval Research Laboratory, Washington, DC, 20375, USA

[+]Current affiliation: Laboratory for Physical Sciences, College Park, MD, 20740, USA

**Corresponding Author Email: samuel.t.white26.ctr@us.navy.mil*

Keywords: quantum sensing, spin coherence, magnetometry, point defects

Isotopic purification improves the coherence time and magnetic field sensitivity of V2 ensembles in 4H-SiC, but the remaining limits on coherence are unclear. We examine spin-spin interactions with residual isotopes and other V_{Si}, estimating that the former limits coherence at low doses, but the latter at high doses.

The *k*-site silicon vacancy (V2) in 4H silicon carbide (SiC) is an appealing quantum magnetometer: an intrinsic defect, addressable optically or electrically at ambient conditions, in a material more tractable than diamond [1]. Previously, we showed that coherence times (which limit magnetometer sensitivity [2]) are ~10X longer in isotopically-purified SiC, but decrease with electron irradiation dose—showing that isotope spins limit coherence in natural SiC, but irradiation-produced defects limit coherence in isopure SiC [3]. Coherence times are extended further in the {|-1/2⟩, |+1/2⟩} basis, which is insensitive to variation in the zero-field splitting (ZFS) [3]. In this basis, we have achieved sub-nT/√Hz sensitivity, yet it remains to be shown what now limits the coherence times and whether further improvements can be achieved.

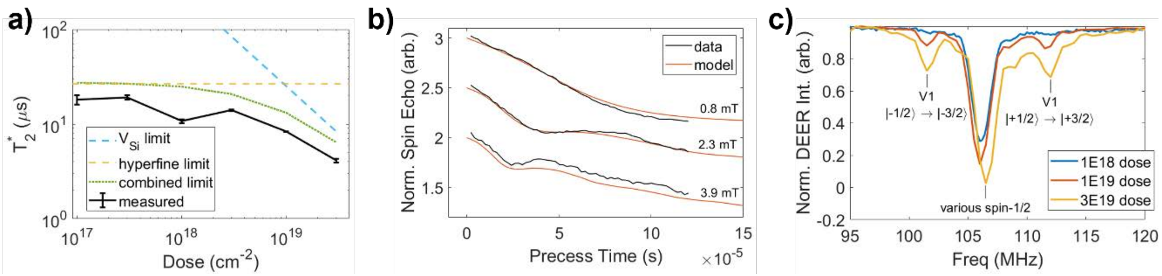

Fig. 1 – Based on our models, T_2^* (a) is limited by hyperfine interactions at low dose and by other V_{Si} at high dose. Echo decay curves (b) exhibit oscillations typical of ESEEM, evincing hyperfine interactions. DEER spectroscopy (c) shows interaction with V1 spins at high dose.

In this work, we investigate the spin-spin interactions between V2 centers and other species in the SiC lattice to determine what limits the coherence times (Fig. 1a). Even in isopure samples, we observe electron spin echo envelope modulation (ESEEM) arising from ^{13}C and ^{29}Si (Fig. 1b). Using the known density of ^{13}C and ^{29}Si, we model the observed ESEEM and show that hyperfine-induced dephasing limits the inhomogeneous lifetime (T_2^*) at the lowest irradiation dose. We also use double electron-electron resonance (DEER) spectroscopy to demonstrate interaction with other V2 and V1 (*h*-site silicon vacancy) centers at high dose (Fig. 1c). Using a reasonable estimate of the V1/V2 density as a function of dose, we show that they are likely to be the limiting dephasing source at high doses.

Funding: This work was supported in part by the U.S. Office of Naval Research, the Defense Threat Reduction Agency, and an appointment to the NRC Research Associateship Program at the U.S. Naval Research Laboratory administered by the Fellowships Office of the National Academies of Sciences, Engineering, and Medicine.

References:

[1] A. Lohrmann, B. C. Johnson, J. C. McCallum, S. Castelletto, "A review on single photon sources in silicon carbide," Rep. Prog. Phys., vol. 80, no. 3, Jan. 2017, Art. no. 034502

[2] J. F. Barry, J. M. Schloss, E. Bauch, M. J. Turner, C. A. Hart, L. M. Pham, R. L. Walsworth, "Sensitivity optimization for NV-diamond magnetometry", Rev. Mod. Phys., vol. 92, no. 1, Mar. 2020, Art. no. 015004

[3] I. Lekavicius, R. L. Myers-Ward, D. J. Pennachio, J. R. Hajzus, D. K. Gaskill, A. P. Purdy, A. L. Yeats, P. G. Brereton, E. R. Glaser, T. L. Reinecke, S. G. Carter, "Orders of magnitude improvement in coherence of silicon-vacancy ensembles in isotopically-purified 4H-SiC", PRX Quantum, vol. 3, no. 1, Mar. 2022, Art. no. 010343

Coherence and Sensing using Dressed States with Silicon Vacancies in 4H-SiC

Ignas Lekavicius[1*], Samuel White[2], Andrew Yeats[1], Daniel Pennachio[1], Jenifer Hajzus[1], Andrew Purdy[1] and Rachael Myers-Ward[1]
[1]*U.S. Naval Research Laboratory, 4555 Overlook Ave SW, Washington, DC 20375*
[2] *NRC Postdoctoral Scholar at U.S. Naval Research Laboratory*
**Corresponding Author Email: ignas.lekavicius.civ@us.navy.mil*
Keywords: point defects, quantum optics, sensing, magnetometry.

Defects in solid state systems possessing room temperature spin coherence are promising platforms allowing for quantum sensing of various fields at ambient conditions. In this work we use dressed states to create a Λ-system in the S=3/2 ground state of the silicon vacancy center in isotopically pure 4H-SiC. The dark-state based readout of this system allows us to characterize a previously inaccessible coherence within the V2 ground state, as well as utilize a more sensitive Δm_s =3 superposition for Ramsey magnetometry.

The sensitivity of point-defect based sensors increases with their concentration but the spin coherence properties generally deteriorate due to numerous factors, such as strain inhomogeneity and spin-spin interactions[1]. We investigate defects in silicon carbide due to the industrial maturity of the host crystal as compared to diamond. Previous results performed isotopic purification of the host crystal to suppress the defect interactions with the nuclear spins in the lattice, resulting in a drastic improvement in the spin coherence times. These improvements revealed a defect density dependence of the coherence times, the source of which was investigated by using a different basis from (1) or (2) shown in Fig. 1a [2]. Using this isotopically pure V2 ensemble, we demonstrated a DC magnetic sensitivity of 4 nT/√Hz with a calculated shot noise limit of 200 pT/√Hz[3].

In this work, we exploit the full capabilities of the S=3/2 ground state of the V2 silicon vacancy center in isotopically pure 4H-SiC, using dressed states to access coherence within the "triple quantum" basis of the {|+ 3/2⟩, |-3/2⟩} in V2 ensembles. This basis maintains the strain and electric field insensitivity of the previously used basis while also offering a superposition state with Δm_s =3 for greater response to magnetic field measurements, which we use to demonstrate magnetic sensitivity improvements. We also characterize the inhomogeneous coherence time (T2*) across a series of ensemble densities and compare with the coherence times in previously used bases. The differing effects of dephasing from magnetic, strain and electric field noise across the three sets of measurements allow us to further attribute sources of coherence limits within our defect ensemble.

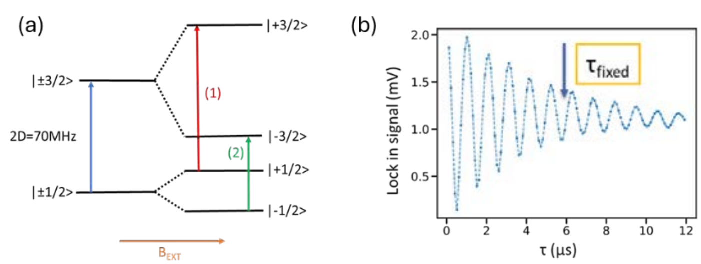

Fig. 1: (a) Energy level structure of V2 silicon vacancy. Shown in red and green are the Δm=1 transitions with an intrinsic ODMR contrast. (b) A Ramsey interference signal for a V2 ensemble. The frequency of the signal is set by the detuning of RF drive of the spin transitions. Fixing the free evolution time (τ) allows for real-time detection of changes in the spin-drive detuning (i.e. Zeeman shifts induced by external magnetic fields)

References:

[1] J. F. Barry *et al.*, "Sensitivity optimization for NV-diamond magnetometry," *Rev. Mod. Phys.*, vol. 92, no. 1, p. 015004, Mar. 2020, doi: 10.1103/RevModPhys.92.015004.

[2] I. Lekavicius *et al.*, "Orders of Magnitude Improvement in Coherence of Silicon-Vacancy Ensembles in Isotopically Purified 4H-SiC," *PRX Quantum*, vol. 3, no. 1, p. 010343, Mar. 2022, doi: 10.1103/PRXQuantum.3.010343.

[3] I. Lekavicius *et al.*, "Magnetometry Based on Silicon-Vacancy Centers in Isotopically Purified 4H-SiC," *Phys. Rev. Appl.*, vol. 19, no. 4, p. 044086, Apr. 2023, doi: 10.1103/PhysRevApplied.19.044086.

Enhanced Readout Contrast of V2 Ensembles in 4H-SiC through Resonant Optical Excitation

Infiter Tathfif [1, 2, *], Charity Burgess [3], Brenda VanMil [3], and Samuel G. Carter [1]

[1] *Laboratory for Physical Sciences, College Park, MD 20740*

[2] *Department of Electrical and Computer Engineering, University of Maryland, College Park, MD 20742*

[3] *DEVCOM Army Research Laboratory, Adelphi, MD 20783*

**Corresponding Author Email: infiter@umd.edu*

Keywords: Quantum sensing, defects, SiC

Using resonant optical excitation at low temperature (~4 K), we demonstrate two orders-of-magnitude improvement in contrast for optically-detected magnetic resonance (ODMR) of V2 silicon vacancies in SiC. This approach can be used for magnetic imaging of quantum materials and devices at low temperatures.

Favorable optical and spin properties of the V2 silicon vacancy defect in 4H-SiC have made it a promising candidate for quantum technologies [1]. For quantum sensing with defect spins, the contrast in optically-detected magnetic resonance (ODMR) is an important metric, which tends to be rather low (<1%) for V2 ensembles using off-resonant laser excitation [2]. To improve contrast, we resonantly excite the V2 ensembles at low temperatures and compare our findings with off-resonant excitation. Our measurements show a ~90 times improvement for ODMR contrast over the off-resonant case for fairly low resonant excitation (Fig. 1). We hypothesize that for a particular wavelength, the resonant laser excites a subset of defects within the ensemble and drives only one of the spin-selective optical transitions for each defect. This leads to a strong spin polarization, contributing to the high readout contrast. To test our hypothesis and further characterize the behavior, we examine the dependence of the contrast on the laser linewidth and the sample temperature. Modulating the resonant laser linewidth up to 1 GHz, corresponding to the splitting of the two optical transitions, results in the contrast decreasing by 50%. As the temperature is increased to 60 K, the contrast decreases and reaches the off-resonant value, presumably due to linewidth broadening. Although the PL signal is 50 times weaker than the off-resonant excitation due to the reduced number of defects in the sub-ensemble, the sensing figure of merit (FoM) is 10 times higher, making the resonant approach still the best choice for sensing at low temperatures. Due to the high readout contrast and reduced laser power requirements, we plan to utilize this resonant technique for wide-field magnetic imaging of quantum materials and devices at low temperatures.

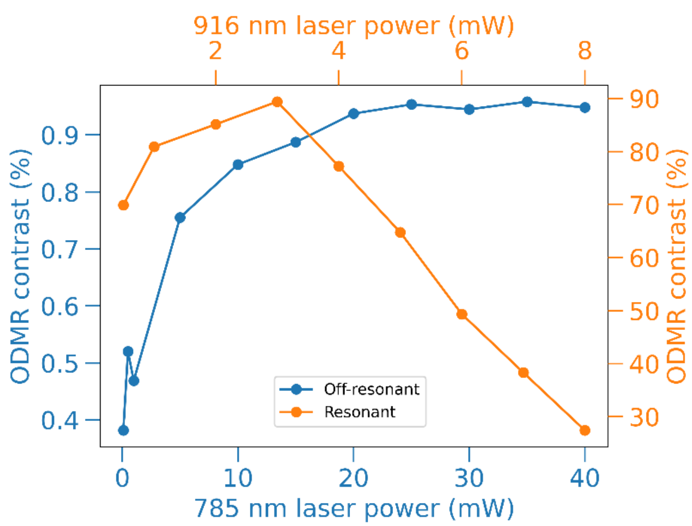

Fig. 1: ODMR contrast (%) as a function of laser power.

References:

[1] S. Castelletto *et al.*, "Silicon Carbide Photonics Bridging Quantum Technology," *ACS Photonics*, vol. 9, no. 5, pp. 1434–1457, May 2022, doi: 10.1021/acsphotonics.1c01775.

[2] I. Lekavicius *et al.*, "Orders of Magnitude Improvement in Coherence of Silicon-Vacancy Ensembles in Isotopically Purified 4 H - SiC," *PRX Quantum*, vol. 3, no. 1, p. 010343, Mar. 2022, doi: 10.1103/PRXQuantum.3.010343.

6.3 Session: Quantum Optics

High-Dimensional Entanglement in Optical Fibers

Siddharth Ramachandran
Boston University, 8 Saint Mary's Street, Boston, MA 02215
Corresponding Author Email: sidr@bu.edu
Keywords: Orbital Angular Momentum, Quantum Entanglement, Optical Fiber Networks, High Dimensionality

Entangling photons in higher-dimensional Hilbert spaces offers greater security for quantum encryption and access to more efficient schematics for quantum computing. We show that four-wave mixing of topologically confined modes in fibers offers a robust, scalable pathway for increasing dimensionality with low noise.

Entangling photons in the orbital angular momentum (OAM) degree of freedom, demonstrated over 20 years ago, yields a promising pathway for increasing the dimensionality of quantum sources, of utility in high-dimensional communications as well as in efficient quantum computing algorithms in higher-dimensional Hilbert spaces. One of the primary means of generating entangled-photon sources with diversity in OAM has been the use of spontaneous parametric down-conversion in bulk $\chi^{(2)}$ nonlinear crystals, but this approach suffers from the need for lossy procrustean filtering [1]. An efficient single-aperture source that could emit photons in tailorable, on-demand OAM superpositions would help transition the field to more deployable scenarios much as integrated optics has helped in the development of quantum sources operating in the conventional, fundamental, ground state, Gaussian-shaped mode.

Here, we show that the use of ring-core optical fibers that enable the transport of a large ensemble of OAM carrying modes, yields a versatile platform for engineering quantum sources by exploiting spontaneous four-wave mixing (SFWM) between fiber modes [2] along with precise control of the pump OAM spectrum [3]. Fibers stably transmitting OAM modes were developed roughly a decade ago, and with the recent discovery of a topological means of robust light guidance [4], have now yielded a multimode platform with as many as 100 stable modes with diversity in OAM as well as spin angular momentum (SAM) [5]. This provides for a plethora of SFWM phase matching possibilities enabling unprecedented control over several important attributes: (1) this allows shaping the joint spectral densities (JSD) [6], ranging from correlated, uncorrelated, to anti-correlated, as needed for applications ranging from entanglement to heralding, simply by switching the angular momentum content of the pump; (2) it allows achieving wavelength indistinguishability across a range of SFWM pairs in different OAM orders [7], thereby directly yielding a high-dimensional photon source; and (3) it enables entangling across dimensions, such as between OAM and SAM [8], enabling the generation of hyper-entangled states.

This talk will describe recent experiments aimed at the development of compact, single-aperture devices whose biphoton emissions can be engineered to exploit the spatial dimension of light.

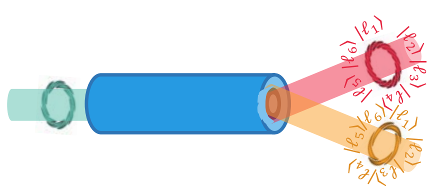

Fig. 1 – Schematic representation of a pump in an OAM comb resulting in bi-photon pairs that are entangled in the OAM degree of freedom, enabling high-dimensional quantum state generation.

Funding: Vannevar Bush Faculty Fellowship (N00014-19-1-2632); ONR MURI (N00014-20-1-2450)

References:

[1] A.C. Dada et al., "Experimental high-D 2-photon entanglement and violations of generalized Bell inequalities," *Nature Phys.* **7**, 677 (2011).
[2] X. Liu et al., "Nonlinear FWM with enhanced diversity and selectivity via spin and OAM conservation." *APL Photonics* **5**, 010802 (2020).
[3] D.I. Shahar et al., "Generation of spatial combs digitized by orbital angular momentum." *APL Photonics* **9**, 016113 (2024).
[4] Z. Ma et al., "Scaling information pathways in optical fibers by topological confinement." *Science* **380**, 278 (2023).
[5] V. Ashok at al., "Scaling to 100 modes by exploiting topological confinement." In *OFC* M2A.1 (2024).
[6] X. Liu et al., "Generation and engineering of orbital angular momentum biphotons in optical fibers," Optica Quantum **3**, 280 (2025)
[7] D.I. Shahar et al., "Low Noise, 9-Dimensional Fiber-Based Biphoton Source." *CLEO* FF107.7 (2025).
[8] S. Wanare et al., "Toward Generation of Hyperentanglement in Optical-Fibers." *CLEO* PS200.49 (2025).

Cavity-Enhanced Light Control in Thin-Film Lithium Niobate Photonic Integrated Circuits

Dashiell L. P. Vitullo[1,] , Mikkel Heuck[2], Dirk R. Englund[3]*
[1]*DEVCOM Army Research Laboratory, 2800 Powder Mill Rd, Adelphi, MD 20783, USA*
[2]*Dept. of Electrical and Photonics Engineering, Technical University of Denmark, 2800 Kgs. Lyngby, DK*
[3]*Research Laboratory of Electronics, Massachusetts Institute of Technology, Cambridge, MA 02139, USA*
**Corresponding Author Email: Dashiell.L.Vitullo.civ@army.mil*
Keywords: thin film lithium niobate, photonic integrated circuits, quantum optics, photonic crystal cavities.

The ability to control light underlies tasks in sensing, networking, and the processing of both classical and quantum information. The emerging thin-film lithium niobate integrated photonic platform boasts a strong intrinsic optical nonlinearity that can be further enhanced with optical cavities for low-SWaP light control. I report progress in on-chip light control enhanced using photonic crystal cavities on this platform, including coherent optical modulation and controllable intercavity coupling towards pulse reshaping and photon storage.

Photonic integrated circuits (PICs) offer SWaP and scalability benefits that make them an enabling technology for both classical and quantum networks. Integrated nonlinear-optical materials in particular offer a path towards quantum logic operations not otherwise achievable with optical qubits. Thin-film lithium niobate (TFLN) is a PIC platform that exhibits a strong intrinsic nonlinear-optical response, making it a promising platform for efficient light control [1]. We review our progress in using photonic crystal cavities (PhCC) to enhance the nonlinear-optical response in light control operations on TFLN PICs. Specifically, we investigate (a) cavity-enhanced electro-optically (EO) actuated coherent modulation with an ultra-small footprint [Fig. 1(a)], and (b) coupled photonic crystal cavities with EO tunable cavity-waveguide coupling [Fig. 1(b)].

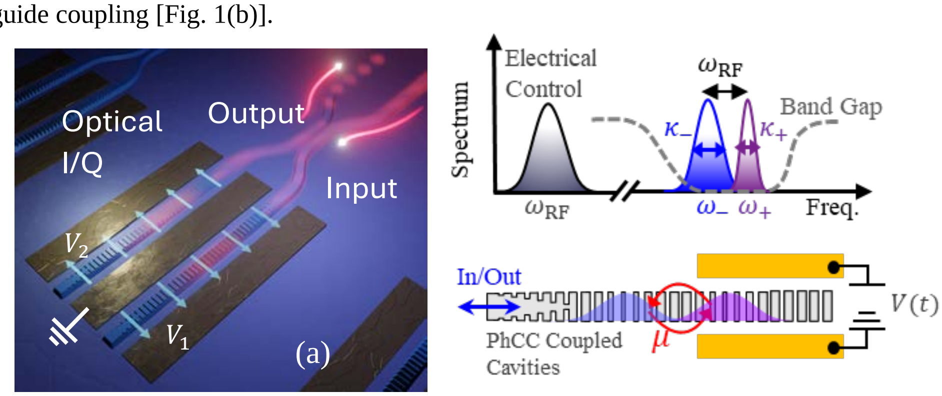

(b)

Fig. 1 – (a) Schematic illustration of our TFLN coherent optical modulator design, where modulated voltages encode information into optical field quadratures. (b) Bottom: schematic illustration of coupled and eletro-optically tunable photonic crystal cavities. Top: Illustration of the spectrum of the three-wave mixing process between the electrical control field and two optical fields occupying optical cavity supermodes.

Modern networks rely on coherent modulation to densely encode information in both the amplitude and phase of optical signals. We report a PhCC-enhanced TFLN in-phase/in-quadrature (I/Q) modulator capable of GHz scale operation of 4-symbol quadrature amplitude modulation with a footprint of 40 μm × 200 μm [2].

We report demonstration of two coupled TFLN PhCC where the coupling between hybridized supermodes of the coupled cavities can be controlled electro-optically via the amplitude and phase of an applied radio frequency signal with $\omega_{RF} = \omega_+ - \omega_-$ [3]. The quality factor is tunable with dynamic range > 20 and an intrinsic value $Q_i = 2.6 \times 10^5$.

Funding: Made possible by FY21 LUCI Fellowship from DoD Basic Research Office in OUSD (R&E) and accomplished under Cooperative Agreement Number W911NF-22-2-0127.

References:

[1] D. Zhu et al., "Integrated photonics on thin-film lithium niobate," Adv. Opt. Photon., vol. 13, p. 242, 2021.
[2] H. Larocque et al, "Photonic Crystal Cavity IQ Modulators in Thin-Film Lithium Niobate," ACS Photonics, vol. 11, no. 9, p. 3860, 2024.
[3] M. Rasmussen et al., "Photonic Crystal Cavities in Lithium Niobate with Controllable Coupling," Quantum 2.0 conference 2025 (submitted).

Instantiation of 1D Topological Lattices with the Surface Nanoscale Axial Photonics Platform

Nathaniel Fried[1,2], Avik Dutt[1], and Dashiell L. P. Vitullo[2,*]
[1]Institute for Physical Science and Technology, University of Maryland, College Park, MD 20742
[2]DEVCOM Army Research Laboratory, 2800 Powder Mill Rd, Adelphi, MD 20783
**Corresponding Author Email: Dashiell.L.Vitullo.civ@army.mil*
Keywords: Topological Photonics, Nanotechnology, Optical Microresonators, Analog Hamiltonian Simulation

We experimentally demonstrate the first instantiation of a topologically nontrivial Hamiltonian with the Surface Nanoscale Axial Photonics (SNAP) platform. We observe the transition of topological zero edge modes between highly localized and delocalized regimes.

Here we provide the first demonstration of topologically nontrivial phenomena on the Surface Nanoscale Axial Photonics (SNAP) platform [1], whereby whispering gallery modes (WGM) are formed by nanoscale effective radius variations (ERV) on optical fiber surfaces. Several topological phenomena have been reported using other optical platforms – on-chip photonic microring arrays and synthetic dimensions – but has been constrained by loss and non-uniformity [2]. The SNAP bottle microresonators (SBMRs) are well suited to topological photonics as they exhibit extremely low-loss propagation, high quality factors, and can be precisely coupled into long chains.

SNAP devices can be characterized by collecting transmission spectra through a perpendicularly-aligned tapered optical fiber across the length of the device. The resulting spectrogram's transmission dips correspond to the excitation of longitudinal modes, and can be fit to simulations to determine the ERV profiles [3].

We experimentally realize multiple copies of a prototypical lattice that exhibits nontrivial topology: the Su-Schrieffer-Heeger (SSH) model [2], with different coupling ratios within a single SBMR array by leveraging the multiple longitudinal mode families (Fig. 1a). In the SSH model, the staggered coupling strengths separate the modes into positive and negative energy bands, and induce topological zero-energy modes around a monomer edge truncation. We observe localized edge states within the bandgaps of the two mode families (Fig. 1b). The mode near 1554.55 nm is more strongly localized than the one near 1554.4 nm. This indicates that the latter is near the topological-trivial phase transition. Using this as a starting point, we anticipate our SNAP platform's post-fabrication tunability and low-loss nature enabling analog Hamiltonian simulation of a wide variety of lattices, including more generalizable models than the one described here.

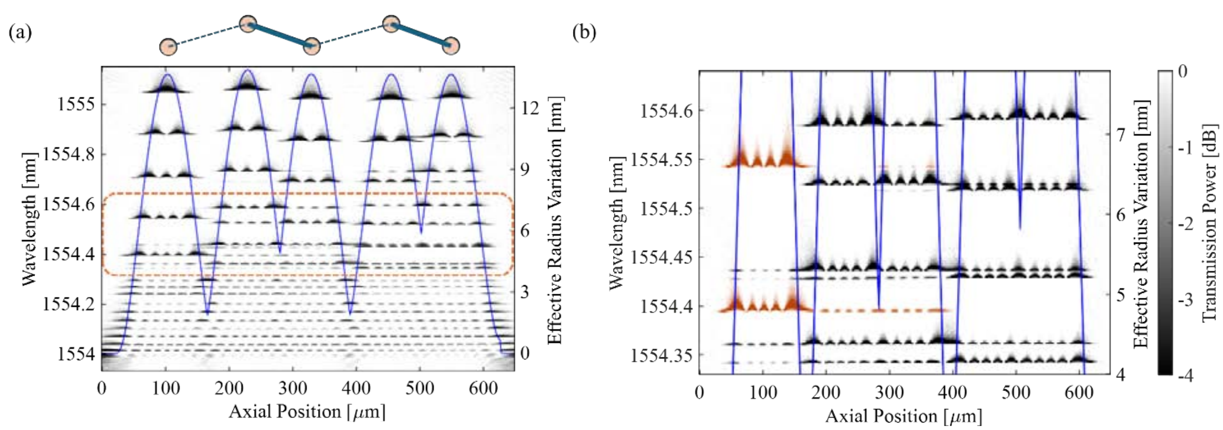

Fig. 1: (a) Spectrogram of a SNAP device with overlayed ERV curve (blue), and a diagram on top indicating each site in the model. (b) Zoomed-in view of orange square in (a), indicating the weakly localized edge modes (orange) from two mode families.

Funding: NSF-DEVCOM INTERN program.

References:

[1] Sumetsky and Y. Dulashko, "SNAP: Fabrication of long coupled microresonator chains with sub-angstrom precision," Opt. Express 20, 27896 (2012).
[2] H. Price et al., "Roadmap on topological photonics," J. Physics: Photonics 4, 032501 (2022).
[3] D. Vitullo et al., "Coupling between waveguides and microresonators: the local approach," Opt. Express 28, 25908 (2020).

Transfer of Hexagonal Boron Nitride Quantum Emitters onto Arbitrary Substrates with Zero Thermal Budget

Dante J. O'Hara[1,*], Hsun-Jen Chuang[1], Kathleen M. McCreary[1], Mehmet A. Noyan[1], Sung-Joon Lee[1,2], Enrique D. Cobas[1] and Berend T. Jonker[1]

[1]*Materials Science and Technology Division, U.S. Naval Research Laboratory, Washington, D.C. 20375, USA*

[2]*Postdoctoral Associate with the American Society for Engineering Education*

**Corresponding Author Email: dante.j.ohara.civ@us.navy.mil*

Keywords: atomic force microscopy, nanoindentation, quantum information, single-photon sources, 2D materials

The van der Waals material hexagonal boron nitride (hBN) has emerged as a promising candidate for hosting room temperature single-photon emitters (SPEs) for next-generation quantum technologies. However, the requirement of a high temperature anneal (850 °C or higher) to activate the SPEs in hBN makes it difficult to integrate into hybrid structures that cannot tolerate such temperatures, including all silicon-based circuits. In this work, we present a method to deterministically activate quantum emitters in multilayered hBN on a process substrate, followed by a zero thermal budget transfer to a target substrate. This technique does not lead to any degradation or loss of photon purity in the hBN emitters and provides a procedure for combining high-purity emitters with other exciting photonic, magnetic, or electrical properties to explore new physical phenomena. The ability to transfer hBN emitters onto arbitrary substrates creates new technological possibilities to incorporate these quantum photonic properties into photonic integrated circuits and plasmonic devices.

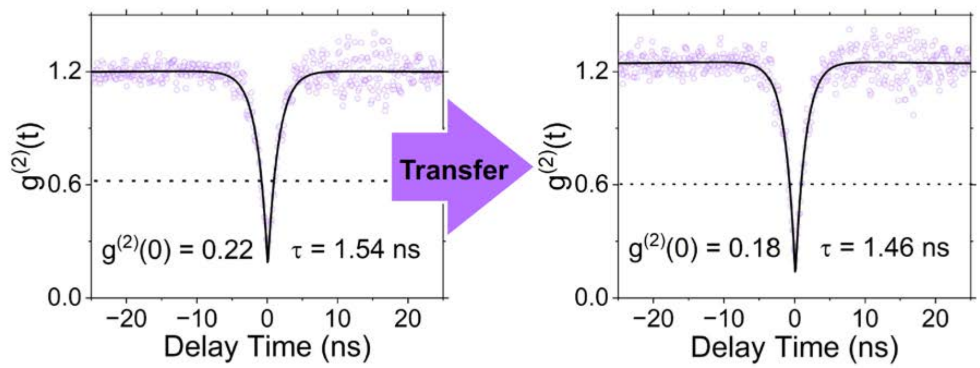

Fig. 1 – Second-order time correlation measurements of hBN emitters before (left) and after (right) transfer to SiO_2/Si substrate.

References:

[1] D. J. O'Hara, H-J. Chuang, K. M. McCreary, M. A. Noyan, S-J. Lee, E. D. Cobas, and B. T. Jonker, "Transfer of hexagonal boron nitride quantum emitters onto arbitrary substrates with zero thermal budget," APL Mater., **12**, 071104, July 2024 xxx.

Squeezed Quantum Frequency Combs in Nanophotonics for Quantum Sensing

Avik Dutt[1,*], Yichen Shen[2], and Ping-Yen Hsieh[1,2]
[1]University of Maryland, College Park, MD,20742
**Corresponding Author Email: avikdutt@umd.edu*
Keywords: Squeezed light; frequency combs; nanophotonics; silicon nitride.

We report strong, frequency-tunable squeezing of 5.6 dB (directly detected) using an on-chip Si_3N_4 microresonator, surpassing previous nanophotonic demonstrations. We also show quantum advantage in spectroscopy using a quantum frequency comb generated from the same microresonator.

Nanophotonic generation of squeezed light promises scalable quantum advantage in sensing and information processing, yet demonstrations of strong, broadband, and tunable squeezing on-chip remain limited. We report two complementary advances in silicon nitride (Si_3N_4) microring resonators operating respectively in above- and below-threshold regimes, achieving state-of-the-art quantum noise reduction and mode agility. In the first advance, we realize 3.7 ± 0.2 dB of directly detected squeezing [1], corresponding to >10 dB inferred on-chip, from a strongly overcoupled microring operating as an above-threshold optical parametric oscillator (OPO). The device, fabricated in a CMOS-compatible foundry, features a 450 GHz free spectral range (FSR), enabling moderate OPO threshold. The squeezing is robust across pump detunings and multiple devices, and matches theoretical predictions based on overcoupling and detection loss, without degradation from classical excess noise.

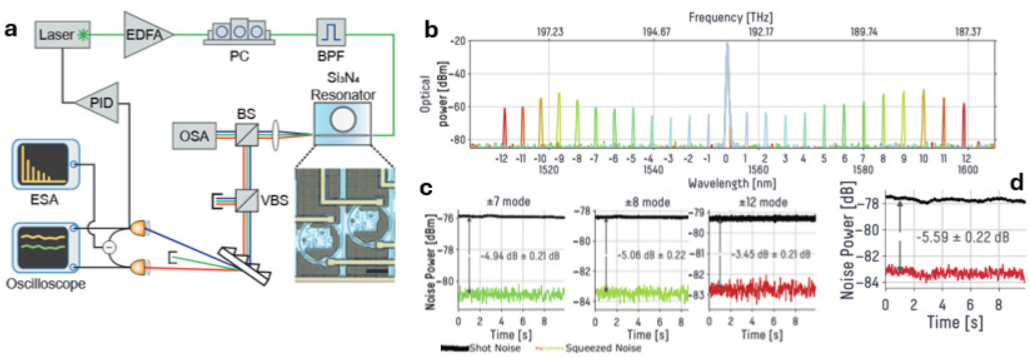

Fig. 1. **a.** Schematic setup of the silicon nitride nanophotonic ring resonator acting either as a parametric oscillator above threshold (OPO) or an amplifier below threshold (OPA). **b.** Seeded OPA showing comb-like structure of pairwise signal-idler gain. Corresponding two-mode squeezing for a few representative modes is shown in **c,** for pump at 1554 nm. **d.** Highest squeezing of 5.6 dB measured with pump at 1587 nm.

In the second advance, we implement a seed-assisted optical parametric amplifier (OPA) that enables direct detection of 5.6 ± 0.2 dB squeezing in the below-threshold regime [2]. To the best of our knowledge, this is the largest squeezing level measured from a nanophotonic source, surpassing previous nanophotonic demonstrations in both the continuous-wave and pulsed regimes. The approach reveals a quantum frequency comb (QFC) comprising 16 qumode (quantum mode) pairs spanning 11 THz. We also show coarse and fine spectral tunability across a full FSR using a 210-GHz device [2]. This architecture enables practical access to multimode squeezed vacua via bright seed-stimulated beams, bridging the detection simplicity of bright squeezing with the scalability of vacuum-based continuous-variable quantum platforms. As a practical application of this frequency-tunable quantum frequency comb source, we show a quantum-enhanced absorption spectroscopy measurement of hydrogen cyanide near 1528 nm. Our work demonstrates the potential of low-loss silicon nitride nonlinear nanophotonics [3] as a platform for fully integrated, scalable quantum sensing and computing technologies.

Funding: NSF QuSeC-TAQS # 2326792, NSF CAREER # 2340835, and NAWCAD # N004212310002.

References:

[1] Y. Shen*, P.-Y. Hsieh*, D. Srinivasan, A. Henry, G. Moille, S. K. Sridhar, A. Restelli, Y.-C. Chang, K. Srinivasan, T. A. Smith, and A. Dutt, arXiv:2505.03734 (2025).
[2] Y. Shen, P.-Y. Hsieh, S. K. Sridhar, S. Feldman, Y.-C. Chang, T. A. Smith, and A. Dutt, Optica 12, 302 (2025).
[3] A. Dutt*, A. Mohanty*, A. L. Gaeta, and M. Lipson, Nat. Rev. Mater. 9, 321 (2024)

7. Topic: Robotics and Manufacturing

Graph-based Topology Optimization of Musculoskeletal Networks in Adaptive Structures

Trent White[1,*] and Todd Henry[2]
[1]*DEVCOM Army Research Laboratory South, College Station, 77843, Texas, USA*
[2]*DEVCOM Army Research Laboratory, Aberdeen Proving Ground, 21005, Maryland, USA*
**Corresponding Author Email: trent.d.white.civ@army.mil*
Keywords: adaptive structures, graph-based topology optimization, multidisciplinary design

Flying organisms exhibit impressive responses to complex environments through geometric reconfigurations that are both learned experientially via repetitive perception-control action sequences and mediated innately by the morphology of the body (i.e., its form and relations between its structures) [1]. In designing small uncrewed aerial systems (sUAS) capable of similar reconfigurations and feats, it is essential to consider that learned and embodied responses of a reconfigurable mechanical system are constrained to the coupled structural, motor, and sensory networks composing the body. This presents a major difficulty as the system must be considered as a whole using multidisciplinary approaches during early design stages while limiting assumptions imposed on the body to elucidate high-level design principles. Thus, there exists a need for a topology-based design framework to study the couplings between networks constituting the morphology of optimal adaptive structures that perform various disparate functions.

The objective of the work completed to date is to advance the state-of-the-art in graph-based topology optimization of adaptive structures by combining global and local optimization techniques. The computational framework developed consists of three nested optimization layers and determines the *distribution* and *sizing* of passive (i.e., skeletal) and active (i.e., muscular) material representative of tensile linear actuators. As shown in Fig. 1, the first layer is driven by the SPIDRS method [2] that heuristically evolves the "material" topology (i.e., graph). The second layer consists of a nonlinear constrained optimization that computes locally optimal "musculoskeletal" topologies (i.e., W_2) and member sizing (i.e., W_1). For control-based objectives, a third layer is required that consists of a bounded-variable least-squares problem that optimizes the control actions (i.e., actuation strains).

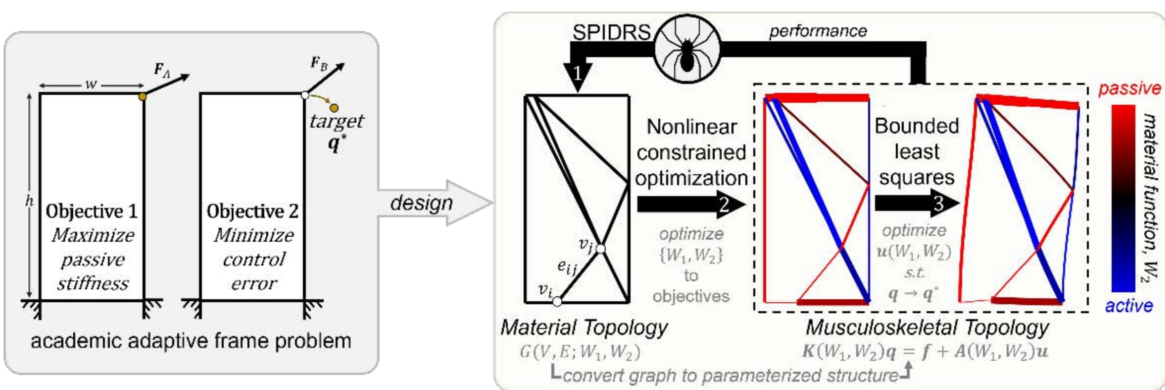

Fig. 1 – A schematic outlining the proposed 3-layer optimization framework for adaptive structures.

Following an exposition on the mathematical formulation and implementation, case studies will be presented that demonstrate utility in identifying key design principles with multiple competing design objectives. The primary objective of interest is limited to static reconfiguration to prescribed target shapes or positions. To date, the key finding is that the proposed formulation accelerates convergence of the outer evolutionary layer relative to the current state-of-the-art because performance of every material topology (i.e., graph) is measured with respect to a locally optimal musculoskeletal topology. This work will conclude with an outlook on including sensory networks for identifying underlying relations between optimal structural, motor, and sensory networks in reconfigurable mechanical systems.

Funding: This work is supported through the SMART SEED Grant.

References:

[1] A. Cangelosi, J. Bongard, M. H. Fischer, and S. Nolfi, "Embodied intelligence," Springer handbook of computational intelligence, pp. 697–714, 2015.

[2] R. Brent, H. Bielefeldt, J. K. Darren, and H. Marcelo, Topology Optimization via L-System and Genetic Algorithms: Bioinspired Encoding for Generative... Design. Cambridge University Press, 2025.

Toward Adaptive Robotic Inspection

LoriAnne Groo[1,*], Liam Murray[1,2], Tyler Lesthaeghe[1,2], Matthew Cherry[1], Sean Donegan[1], Andrew Gillman[1]

[1]Materials and Manufacturing Directorate, Air Force Research Lab, WPAFB, OH 45431
[2]University of Dayton Research Institute, Dayton, OH 45469
**Corresponding Author Email: lorianne.groo.1@us.af.mil*
Keywords: non-destructive inspection, robotics, automation

Traditional nondestructive evaluation/inspection (NDE/I) across the aerospace sector is reliant on a combination of skilled human inspectors and high-precision automated systems. As a result, an inherent tradeoff exists between the process versatility available through human decision making and the efficiency achieved using automated robotic systems. With ongoing developments related to manufacturing complexity such as topology optimization and additive manufacturing, the ability to rapidly inspect complex, variable components before and during service in a low-volume, high-mix scenario is of increasing interest. In order for robotic systems to meet these demands, versatility in sensing modality, operational environment, and path planning will be required. To this end, this work presents advancements and challenges related to the goal of adaptive, autonomous, robotic NDE/I.

Ultimately, the desired robotic NDE/I workflow would be compatible with a wide variety of NDE/I techniques, part geometries, and materials and would require little to no human input, instead implementing autonomy and decision-making capabilities. As an initial step towards this vision, ongoing efforts are employing a baseline automated robotic eddy current testing process that relies on limited user input and has been tested on a subset of geometries and materials. Current efforts use a 6-axis collaborative robot with an integrated eddy current sensor and additional vision and laser-based sensors for surface reconstruction and path planning for the part under test. Note that although the initial setup uses a single NDE/I approach, the hardware and software design and integration are deliberately modular, allowing for versatility in both the robotic platform and NDE/I modality. In particular, Robot Operating System, or ROS, is implemented for software development in an effort to establish a robot-agnostic workflow for rapid adaptation and implementation in various inspection environments. Spatial registration of the relevant NDE/I data to the part of interest is achieved through the integration of additional open-source software, Dataguzzler, with the ROS environment to maintain modularity and flexibility of the software. Results and findings will be presented to address the question of whether collaborative robotic systems can be used for reliable NDE/I measurements while maintaining versatility in part geometry. Additional considerations, open research questions, and future directions will also be discussed.

Funding: This material is based in part upon work supported by the U.S. Air Force under Contract FA8650-19-D-5230.

Solving the Euler Angle Singularity Problem (without Quaternions)

Mark Bundy*
DEVCOM Army Research Laboratory, Aberdeen Proving Ground, MD 21005-5069
**Email: mark.l.bundy2.civ@army.mil*
Keywords: frame rotations, Euler angles, quaternions, robotics, motion tracking

Planning, tracking, and control of rotating objects is common in engineering and computer graphic applications. For example, describing/tracking/planning the time-dependent attitude of an air platform or a robotic arm relative to a fixed frame of reference is of engineering interest. However, the traditional mathematical solution of this nonlinear problem, often caveats the range of its trusted solution to avoid what appears to be a mathematical singularity, where the angular rates used to track the attitude of a rotating body would become infinite, and therefore undefined at a particular body orientation. Mathematicians such as Leonhard Euler (vector algebra and Euler angles), Arthur Caylee (matrix algebra), and William Rowan Hamilton (quaternion algebra) are prominent in the literature describing coordinate frame transformations. A brief review will be given of how the motion of a rotating frame/body can be referenced to a fixed frame, using both vector and quaternion algebra and how/why/where an angular singularity in the solution can arise. Fig. 1 shows one frame of a Matlab- coded video simulation of identical vector and quaternion solutions to an example frame-rotation problem. It is often claimed in literature that quaternion algebra can be used to avoid the problem, but contrary to such claims, it will be shown that quaternions provide no added value in solving the problem. Moreover, it will be shown how the singularity problem can be avoided/solved using either vector or quaternion algebra by a reasoned adjustment of the numerical integration step needed to iteratively solve the non-linear problem. Fig. 2 shows an example-solution to the Euler angle singularity problem, using the appropriately prescribed and adjusted downward integration step size as the pitch angle reaches its maximum value near, but never equal to the singularity condition at 90 degrees. Several solution approximation methods are presented based on a user-defined level of angular precision (acceptable number of decimal places).

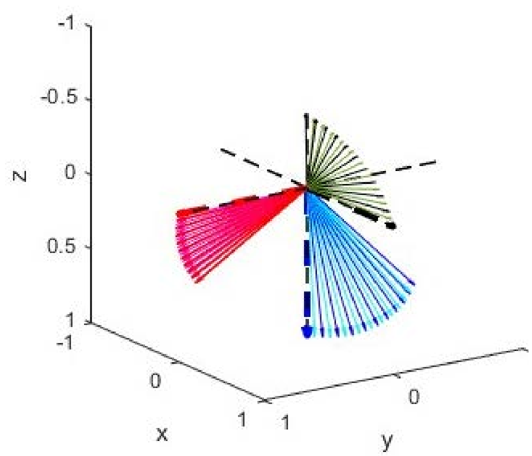

Fig. 1 – Example: Identical quaternion-(olive, magenta, cyan) and Euler-(black, red, blue) based solution for body frame x-y-z basis vectors for a gyroscope-based yaw-pitch-role angular-rate of 0.5:2:1.

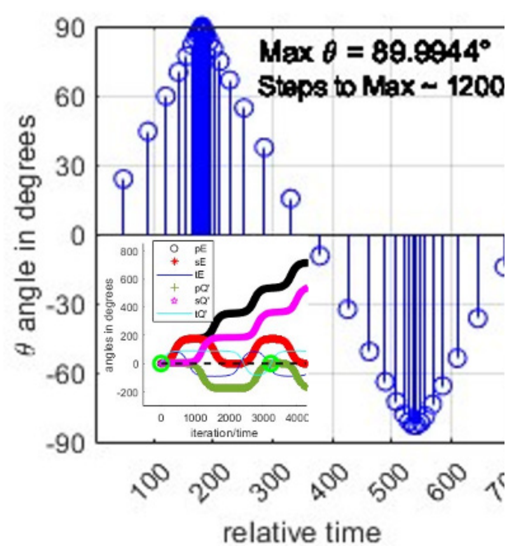

Fig. 2 – Non-singular Euler pitch angle solution, θ, based on pitch-angle adjusted iterative time step.

Computationally Efficient Navigation and Social Cohesion are a Feature of this Bug

Kevin R. Pilkiewicz[1,*], Michael L. Mayo[1], Audrey B. Harrison[1], Anne M. Mayo[1], Craig Carrigee[1], and Katherine Daftari[2]

[1]*Environmental Laboratory, U.S. Army Engineer Research and Development Center, 3909 Halls Ferry Rd, Vicksburg, MS 39180*

[2]*Northrop Grumman Mission Systems, 1550 W Nursery Rd, Linthicum Heights, MD 21090*

**Corresponding Author Email: Kevin.R.Pilkiewicz@erdc.dren.mil*

Keywords: Collective motion, adaptive navigation, information theory, swarm robotics

Current Army solutions for autonomous navigation typically require high-resolution cameras to visualize relevant environmental features and high-performance computing to interpret those images and calculate an optimized route. Simple organisms like insects lack both sophisticated visual sensing and high-level cognitive processing capabilities, yet they are capable both individually and collectively of navigating complex environments with relative ease. To better understand this phenomenon, we captured video of American cockroaches, *Periplaneta americana* (Insecta: Blattidae), traversing a sequence of cylindrical obstacles within a narrow, plexiglass enclosure (Fig. 1A). As a kind of control experiment, we also recorded simple bristlebots (Hexbug Nano®) crossing the same enclosure, since bristlebots navigate solely through physical collisions and are definitively asocial. While the roaches also principally navigated their environment via a collisional mechanism, they additionally exhibited a queue-forming social tendency that discouraged high-density jamming and enabled large groups of organisms to traverse the obstacle-induced bottleneck of the experimental enclosure more efficiently. We found that we could largely reproduce the phenomenology of the collective roach behavior with a simple agent-based model wherein all movement decisions were determined by the contact states of the agent antennae (Fig 1B). We demonstrate how modifying the interaction rules of this model can dramatically erode the social cohesion of the agents, making their motion more closely resemble that of the bristlebots, and we conclude by speculating how the rules of the agent-based model could by implemented in low-cost, autonomous robots that could replicate the collective navigational capabilities of a roach swarm.

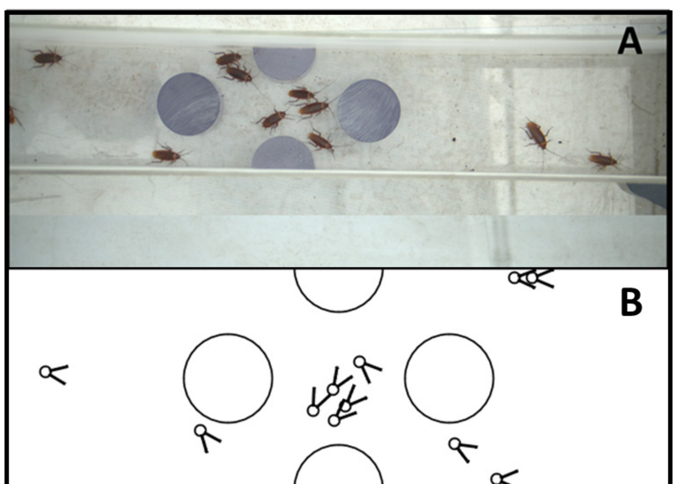

Fig. 1 – (A) Snapshot from a video recording of a swarm of roaches (P. americana) navigating a sequence of obstacles. (B) A configuration from an agent-based simulation designed to mimic the collective navigational behavior of the roaches with a simple, informationally efficient set of movement rules.

Funding: Funding was provided by the U.S. Army Engineer Research and Development Center (ERDC) through the Installations and Operational Environment (IOE) 6.1 basic research program. Opinions, interpretations, conclusions, and recommendations are those of the author and are not necessarily endorsed by the U.S. Army.

An Anti-Windup Dynamic Inversion Control Architecture for Autonomous Underwater Vehicles with Actuator Constraints

J. Kyle Zelina[1]
[1] *Naval Surface Warfare Center, Panama City Division, 110 Vernon Ave, Panama City, FL 32407*
**Corresponding Author Email: john.k.zelina.civ@us.navy.mil*
Keywords: "Autonomy, Dynamic Inversion, Anti-Windup".

It is known that failing to account for actuator saturation when developing control laws can often lead to undesirable system performance or instability. This paper investigates the use of a Nonlinear Dynamic Inversion (NDI) controller complete with a nested actuator inversion to prevent windup for use on an autonomous underwater vehicle (AUV). The nested loop inverts the desired vehicle dynamics using knowledge of actuator limits to ensure the requested response does not exceed actuator constraints. A 6-DOF AUV model is presented, and tasked with navigating through predefined waypoints. Development of the dynamic inversion controller is discussed, including the addition of a nested inversion scheme for anti-windup compensation. Test results are provided to demonstrate overall controller performance as well as demonstrate anti-windup properties.

When developing control architectures for nonlinear systems, it is sometimes necessary to consider nonlinear control methodologies to achieve desired system performance. One method of achieving this is to leverage knowledge of undesirable system dynamics, and provide control input that negates these dynamics. This framing of the control problem can then enable the user to prescribe desirable system dynamics, and inject these dynamics as an input to the system. This process is known as Nonlinear Dynamic Inversion Control (NDI). NDI controllers are widely utilized in literature [1] as it provides a simplistic formulation and robustness [2]. Moreover, NDI allows the user to precisely define the system response and does not require scheduling. One drawback to dynamic inversion control is that while the system response can be set by the user, it is not always obvious whether the desired response will violate actuator limitations. Saturating the actuator can result in damage to the actuator and can also induce performance degradation and instability. To avoid this, a multitude of anti-windup techniques have been developed [3]. In this paper, a nested inversion anti-windup scheme is offered where the desired system response shifts with the available control effort.

This work investigates the application of an anti-windup NDI controller for an AUV seen in Fig. 1. This vehicle was produced in-house at NSWC PCD facilitated through internal funding, but has been made available as a test platform for this work. The AUV dynamics are modeled, complete with empirically-obtained hydrodynamic parameters. Detailed formulation of the proposed NDI controller is provided and tasked with controlling the AUV through an environment via waypoint navigation. The controller is tested both in sim and on the vehicle to evaluate controller performance.

Fig. 1 – AUV ISO Illustration

Funding: This work was made possible by the DoD SMART SEED Grant.

References:

[1] Griffith, T., Zelina, J. K., Gruenwald, B. C., and Bryson, J.,"Dynamic Inversion with Adaptive Augmentation for a High-Speed Guided Projectile," AIAA SCITECH 2023 Forum (p.2647), 2023. https://doi.org/10.2514/6.2023-2647.

[2] Menon, P., Iragavarapu, V., and (n.d.), E. O., "Nonlinear missile autopilot design using time-scale separation," In Guidance, Navigation, and Control Conference, 1997. https://doi.org/10.2514/6.1997-3765.

[3] Herrmann, G., Menon, P., Turner, M., Bates, D., and Postlethwaite, I., "Anti-windup synthesis for nonlinear dynamic inversion control schemes," Int. J. Robust Nonlinear Control 2010; 20:1465–1482, 2009. https://doi.org/10.1002/rnc.1523.

8. Topic: Ultra-Wide Band Gap

Electrical and Microstructural Analysis of Heteroepitaxial p-GaN/n-Ga_2O_3 Junctions Formed by MOCVD

Emma G. Rocco[1], Alan G. Jacobs[1], Daniel J. Pennachio[1], Hannah N. Masten[2], Tolen Nelson[2], Michael A. Mastro[1]

[1] U.S. Naval Research Laboratory, 4555 Overlook Ave. SW, Washington, D.C. 20375
[2] NRC Postdoctoral Associate Residing at the U.S. Naval Research Laboratory, 4555 Overlook Ave. SW, Washington, D.C. 20375
**Corresponding Author Email: emma.g.rocco.civ@us.navy.mil*
Keywords: Gallium Nitride, GaN, Gallium Oxide, β-Ga_2O_3, Metal organic chemical vapor deposition, MOCVD, 4D-STEM, P-N Diode, High-Power Electronics, Wide Bandgap Materials, Ultra-Wide Bandgap Materials

Wide and ultra-wide bandgap semiconductors are essential in favor of the continued advancement of high-power electronics for efficient power handling, conversion and amplification systems. β-Ga_2O_3 is an attractive candidate for these applications with an ultra-wide bandgap energy of 4.8 eV and a maximum critical electric field estimated to be 8 MV/cm. However, no reliable p-type conductivity has been achieved for β-Ga_2O_3 due in part to a predicted polaronic state and large effective mass for holes. While p-type oxides including NiO and $LiGa_5O_8$, have been reported in heterojunctions with n-Ga_2O_3 for the formation of p-n diodes [1, 2], p-type III-nitrides are of particular interest for heterojunctions with n-Ga_2O_3 due to mature processing and integration with current power electronics, ability for alloying to achieve a wide range of bandgap energies, attainable p-type conductivity, and high thermal conductivity. Initial studies of Ga_2O_3/GaN heterojunctions formed via metal organic chemical vapor deposition (MOCVD) exhibit a six-fold in-plane grain rotation measured by x-ray diffraction (XRD), with grain structure also observed in atomic force microscopy (AFM).

In the present study, we investigate the microstructural and electrical properties of GaN/Ga_2O_3 heterostructures. Ga- and N-polar GaN:Mg were deposited via MOCVD on c-plane sapphire substrates, and the Mg-dopants activated with a post-growth anneal. Following GaN deposition, the wafers were exposed to air ambient and transferred to a dedicated III-oxide MOCVD chamber for the growth of n-Ga_2O_3 utilizing SiH_4 as the n-type dopant precursor. Here, we will discuss the fabrication of quasi-vertical n-Ga_2O_3/p-GaN heterojunctions and test structures. Data presented include sheet and contact resistivity of the heteroepitaxial n-Ga_2O_3, I-V characteristics of the Ga_2O_3/GaN heterojunction, and properties of the underlaying GaN structure after deposition of the Ga_2O_3 film. Scanning Transmission Electron Microscopy (STEM) was utilized to further probe the heterointerface and microstructure of the epitaxial Ga_2O_3. An abrupt heterointerface is observed between the GaN:Mg and Ga_2O_3:Si layers with a single atomic layer of disorder and 4D-STEM imaging highlights the six-fold in-plane rotation of {-201} Ga_2O_3 grains. This work lays the foundation for high performance heteroepitaxial devices leveraging both the high breakdown field of Ga_2O_3 and mature processing and large area fabrication methods of p-type III-Nitrides.

Funding: This research was funded by the Office of Naval Research, through NRL 6.1 Base Program.

References:

[1] H. Wan, *et al.*, "NiO/ β-$(Al_xGa_{1-x})_2O_3$ /Ga_2O_3 heterojunction lateral rectifiers with reverse breakdown voltage > 7 kV," *J. Vac. Sci. Technol. A*, vol. 41, 032701 (2023).
[2] K. Zhang, *et al.*, "Discovery of a Robust P-Type Ultrawide Bandgap Oxide Semiconductor : $LiGa_5O_8$," *Adv. Electron. Mater.*, vol. 11, no. 1, (2025).

Diamond Surface Preparation for CVD Growth of Quantum and High Power Electronics Materials

Jonathan B. Levine-Miles,[1*], Michael A. Mathews Jr.[1], Daniel J. Pennachio[2], Tatyana I. Feygelson[1], and Bradford B. Pate[1]

[1]Chemistry Division, U.S. Naval Research Laboratory, 4555 Overlook Ave SW, Washington D.C. 20375

[2]Electronics Science and Technology Division, U.S. Naval Research Laboratory, 4555 Overlook Ave SW, Washington D.C. 20375

**Corresponding Author Email: jonathan.b.levine-miles.civ@us.navy.mil*

Keywords: "diamond, ultrawide bandgap materials, quantum".

There is renewed interest in single crystal diamond as an advanced material with applications in high power electronics and quantum systems due to its ultrawide bandgap, extreme thermal conductivity, high breakdown voltage and high carrier mobility. For example, diamond's high thermal conductivity is becoming a critical factor for improved SWaP as increasingly high current densities in next generation devices necessitate a material capable of dissipating generated heat. A key challenge that remains is standardization and growth of high quality, low defect density diamond epi layers. Here we report on surface preparation and growth for enhanced crystalline quality via a removal of subsurface damage through a novel reactive ion etch process. Process parameters, AFM, XPS, and X-ray diffraction data will be presented contrasting the standard Scaife polishing with the etch process. Additionally, the current capabilities of the Naval Research Lab's diamond deposition facility will be presented with an emphasis on single crystal diamond growth and incorporation of impurities, including n- and p-type doping as well as novel color center candidates.

References:

[1] M.A. Matthews, Jr., J.B. Levine-Miles, B.B. Pate, "Fluorine Plasma Assisted Remediation of Single Crystal Diamond Surfaces" *Submitted JVSTA*, April 2025.

Rapid Semiconductor Defect Mapping with a U-Net Deep Learning Model

James C. Gallagher[1], Nadeemullah A. Mahadik[1], Robert E. Stahlbush[1], Karl D. Hobart[1], and Michael A. Mastro[1]

[1] U.S. Naval Research Laboratory, 4555 Overlook Ave SW, Washington D.C. 20375
Corresponding Author Email: james.c.gallagher26.civ@us.navy.mil
Keywords: Convolutional Neural Network, U-Net, SiC, Wide Bandgap Semiconductor

Accurate assessment of the defect density, defect types, and preferably the specific location and type of each defect is necessary for the development and manufacture of long-lifetime high-power semiconductor devices. Such defects can cause electrical carrier traps, unintentional dopants, and variable optical properties. This can lead to semiconductor devices having lower efficiency, decreased breakdown voltages, and reduced survivability in extreme environments. In order to eliminate or mitigate these defects, methods for screening the quality of semiconductor wafers have been developed. However, even in higher quality semiconductors the defect concentration is often over 1000 cm^{-3}, which precludes wafer-scale manual assignment of individual defects. Traditional computational algorithms applied to the assignment of defects from wafer-scale measurement techniques are overly sensitive to measurement parameters that cause image variation and to sample specific variation in defect size, shape, density, and location particularly relative to a sample edge. This presentation discusses the development and application of machine learning based algorithms for the wafer-scale assignment of multiple defect types with a particular focus on defects in large-area SiC.

Multiple machine learning architectures were constructed to assess the defectivity in images from profilometry, x-ray topography, and photoluminescence imaging. Input data to train and validate the model was created by manually marking the pixels containing the defects. The trained models were capable of distinguishing multiple types of defects including threading dislocations and screw dislocations. The most successful model was a U-Net based convolutional neural network. A U-Net-based convolutional neural network has two paths in the neural network: a contracting path for extracting global features in the image, and an expansive path for precise localization of the defects. Connections between the two paths allows the model to distinguish regions of the image with and without defects. The U-Net achieved rapid, wafer-scale defect mapping within minutes, often exceeding the accuracy of manual mapping even with imperfect training data.

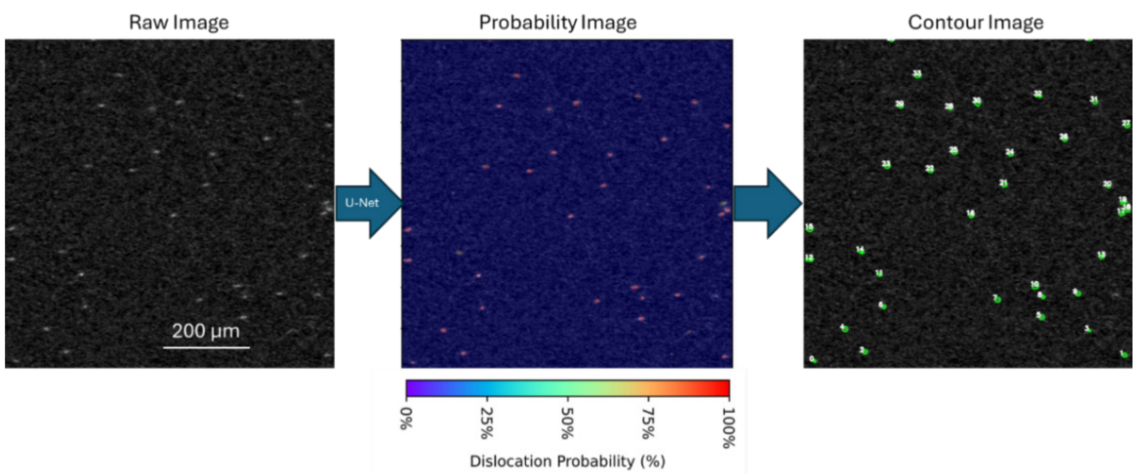

Fig. 1. (Left) Example image x-ray topography image where the dislocation defects appear as white dots in the raw image. (Center) The U-net extracts the probability of each pixel belonging to the defect in less than a few seconds. (Right) Contouring can be used to circle and calculate the size and shape of the defects.

This research was funded by the Office of Naval Research.

Computational Spectroscopy for Point Defects in AlN and AlGaN

Darshana Wickramaratne[1,*], John L. Lyons[1], Mackenzie Siford[2], Md Shafiqul Islam Mollik[2], Jason Forbus[2], and Mary E. Zvanut[2]

[1] *Center for Computational Materials Science, U.S. Naval Research Laboratory, Washington, DC 20375,*
[2] *Department of Physics, University of Alabama at Birmingham, Birmingham, Alabama 35233, USA*

**Corresponding Author Email: darshana.k.wickramaratne.civ@us.navy.mil*
Keywords: AlN, AlGaN, doping, defects,

Aluminum nitride (AlN) and high-Al content AlGaN alloys are promising materials for the future of high-power electronics and optoelectronics that operate in the ultraviolet. The successful application of these materials is predicated on achieving thorough knowledge of the underlying defect physics. In this talk I will discuss two examples of how first-principles calculations played a crucial role in the identification of defects in AlN and AlGaN.

Electron-paramagnetic resonance (EPR) measurements of AlN have frequently observed a hyperfine signal that is commonly assigned to a donor-like defect. Often referred to as the *D5* hyperfine signal, the microscopic origin of this putative donor defect has been debated since first being observed more than two decades ago. Using a combination of first-principles calculations and photo-EPR measurements of AlN we show this *D5* defect is in fact due to a deep acceptor, carbon substituting on the nitrogen site, and is not due to a deep donor [1]. These results also allow us to comment on the possible role of carbon on the optical absorption and luminescence spectra observed in as-grown AlN.

Recent studies have proposed germanium as a viable *n*-type dopant for high-Al content AlGaN and AlN. However, combining experimental results with theoretical analysis, we demonstrate that beyond a critical Al composition of 50%, germanium behaves as a *DX*-center in AlGaN, suppressing its ability to lead to *n*-type conductivity [2]. These findings provide important guidance for doping strategies aimed at achieving efficient *n*-type conductivity in high Al-content AlGaN and AlN.

Funding: D.W and J.L.L were supported by the Office of Naval Research through the Naval Research Laboratory's Basic Research Program.

References:

[1] D. Wickramaratne, M. Siford, M. S. I. Mollik, J. L. Lyons, and M. E. Zvanut, "Direct evidence for carbon incorporation on the nitrogen site in AlN," Physical Review Materials, vol. 8, no. 9. American Physical Society (APS), Sep. 11, 2024. doi: 10.1103/physrevmaterials.8.094602.

[2] J. Forbus, D. Wickramaratne, J. L. Lyons, and M. E. Zvanut, "Nonradiative quenching of EPR signals in germanium-doped AlGaN: Evidence for DX-center formation," Applied Physics Letters, vol. 126, no. 4. AIP Publishing, Jan. 27, 2025. doi: 10.1063/5.0249701

Correlation between Highly Red-Shifted Photoluminescence and Growth Temperature Dependent Electron Mobility in Plasma-Assisted MBE-Grown High-Al Content *N*-Type Algan

L.S. Larkin[1, *], M. Ji[1], Y. Chen[1], D.F. Storm, G.A. Garrett[1], A.V. Sampath[1], and M. Wraback[1]
[1]DEVCOM Army Research Laboratory, 2800 Powder Mill Road, Adelphi, MD 20783
**Corresponding Author Email: leighann.s.larkin.civ@army.mil*
Keywords: AlGaN, ultrawide bandgap, MBE

Ultrawide bandgap (UWBG) materials, such as high-Al fraction AlGaN, are attractive for high-power and high-frequency electronic devices. However, the electron mobility, μ_e, a critical factor in the performance of electronic devices, is reported to be significantly lower in AlGaN grown with plasma-assisted molecular beam epitaxial (PA-MBE) relative to metal-organic chemical vapor deposition (MOCVD) grown AlGaN [1]. One potential cause for this behavior may involve the appearance of nanoscale compositional inhomogeneities (NCIs) [2-4], associated with the III-rich growth environment of PA-MBE. These NCIs can generate sub-bandgap states which both generate red-shifted UV emission [2-4] and create a large density of shallow bandtail states that can impact μ_e.

In this work, we investigated the correlation between red-shifted UV emission and the electron mobility in *n*-type $Al_xGa_{1-x}N$ ($x > 0.79$, $n_0 \sim 10^{19}$ cm^{-3}) as a function of growth temperature, T_{growth}. The photoluminescence (PL) showed emission at ~4.7 eV for direct pumping of the localized states, which is red-shifted by ~870 meV, with respect to the anticipated near-band-edge emission. The integrated intensity of the 4.7 eV PL peak, attributed to emission from NCIs associated with the capture of photoexcited holes and their recombination with electrons filling the localized states, increases with increasing T_{growth}, while μ_e decreases from 8.5 to 4 $cm^2V^{-1}s^{-1}$, more than expected for the change in μ_e in this Al content range. These results suggest that the density of localized states responsible for the NCI emission increases with T_{growth}, leading to more effective filling of the deep localized states by conduction electrons, which is consistent with a measured drop in Hall measured n_e with increasing T_{growth} by more than two times. This may open more availability of unoccupied shallow traps just below the band edge, and enhanced interaction of the conduction electrons with these shallow localized states via trapping/release would reduce their mobility. Further results examining the dependence of μ_e on additional growth parameters and doping densities will be discussed.

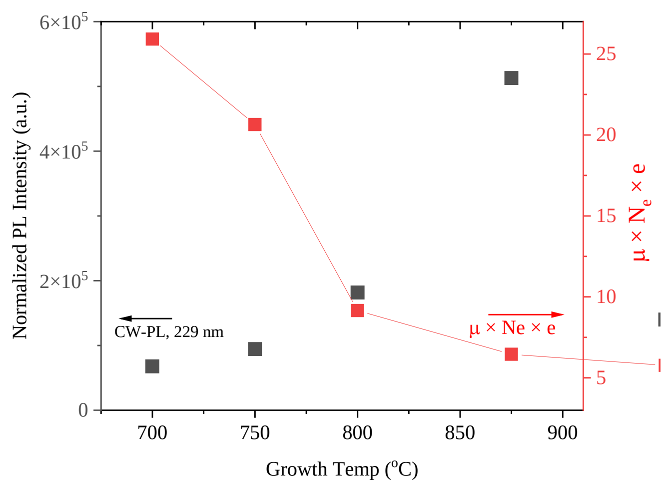

Fig. 1 –The integrated intensity of the red-shifted peak (left-hand-side) and the product of μ_e, the carrier concentration, N_e, and electric charge, e, (right-hand-side) as a function of growth temperature.

References:

[1] S. Li, et al., *Appl. Phys. Lett.* **125**, 112102 (2024).
[2] C.J. Collins, et al., *Appl. Phys. Lett.* **86**, 031916 (2005)
[3] W.L. Sarney, et al., *J. Elect. Mater.* **53**, 2789 (2024).
[4] L.S. Larkin, et al., accepted for publication *PSSB* (2025).

Defect Quantification in Diamond using High Resolution X-ray Diffraction

Elias Garratt[1,*], Tia Gray[2], Michael A. Mathews[3], Jonathan B. Levine-Miles[3], and Bradford B. Pate[3], Glen Birdwell[1], and Tony Ivanov[1]

[1]Electromagnetic Spectrum Sciences Division, Army Research Laboratory, Adephi MD 20783
[2]Department of Materials Science and NanoEngineering Rice University, Houston, TX 77005
[3]Chemistry Division, Naval Research Laboratory, Washington, DC 20375
**Corresponding Author Email: elias.j.garratt.civ@army.mil*
Keywords: diamond, XRD, defect

Recent investment in large area diamond substrate research and development has renewed interest in non-destructive ways to characterize and quantify defects in diamond. In this work we demonstrate the how edge- and screw-type defects in heteroepitaxial, homoepitaxial, and high pressure high temperature diamonds are quantified using high resolution x-ray diffraction techniques. Additionally, we introduce full-width at ten-thousandth maximum as a measure of sub-surface damage characterization in diamond samples subject to various processing techniques.

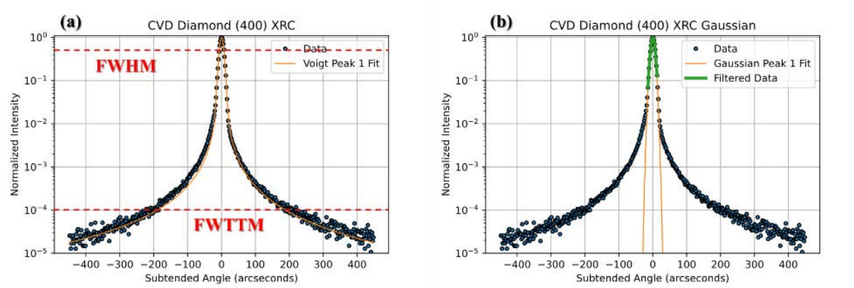

Fig. 1. (a) Voigt and (b) Gaussian fittings of CVD diamond (400) x-ray rocking curve. (a) Full-width at half maximum (FWHM) and full-width at ten-thousandth maximum (FWTTM) are shown. (b) Filtered Data (green line) is used to calculate dislocation density.

Recent commercial and government investment in diamond, including large area diamond wafers (≥25 mm diameter), has renewed interest in non-destructive defect characterization techniques to support these on-going efforts. Past research into dislocation density quantification on III-nitride materials has proved that high-resolution x-ray diffraction reliably obtains accurate measurements of dislocation density compared with transmission electron microscopy and x-ray topography [Metzger 1998, Kaganer 2005, Moram 2009, Romanitan 2017, Dolabella 2022]. However, it has yet to gain widespread traction in the diamond community as a tool for dislocation density characterization. Here we present work in high-resolution x-ray diffraction as a model technique to obtain a statistically significant measure of dislocation density. Diffuse scatter analysis formalism developed by [Warren and Averbach 1950, 1952, Wilkins 1970, Krivoglaz 1996, Kaganer 2005, and Kopp 2014] established the canonical equations for dislocation density, and work by Romanitan 2017 demonstrated that dislocation density can be determined solely from an analysis of a Gaussian fitting to the XRC peak. Combining these two approaches and adapting the geometric and crystallographic contributions to x-ray scattering from lattice strain, screw- and edge-type dislocation densities have been quantitatively determined for homoepitaxially, heteroepitaxially, and high pressure high temperature grown samples. Additionally, characterization of the subsurface damage region in diamond due to processing is presented and key diffraction peak parameters of full-width at thousandth and ten-thousandth maximum are introduced and semi-quantitative measures of the amount of damage in the processed diamond.

References:

1. Warren and Averbach 1950, doi: 10.1063/1.1699713
2. Warren and Averbach 1952, doi: 10.1063/1.1702234
3. Wilkins 1970, doi: 10.1002/pssa.19700020224
4. M.A. Krivoglaz 1996, doi: 10.1007/978-3-642-74291-0
5. Metzger 1998, doi: 10.1080/01418619808221225
6. Kaganer 2005, doi: 10.1103/PhysRevB.72.045423
7. Moram 2009, doi: 10.1088/0034-4885/72/3/036502
8. Kopp 2014, doi: 10.1063/1.4865502
9. Romanitan 2017, doi: 10.1016/j.ssc.2017.09.018
10. Dolabella 2022, doi: 10.1002/smtd.202100932

Quantum Relaxation Times and Charge Transport in Diamond Conduction Channels

S. Rudin*, G. Rupper, M. Neupane, L. De La Cruz, A. G. Birdwell
DEVCOM Army Research Laboratory, Adelphi, Maryland 20783, USA
**Corresponding Author Email: sergey.i.rudin.civ@army.mil*
Keywords: diamond FET,charge transport.

The physical characteristics of diamond, such as high thermal conductivity of 23 W/cmK and high breakdown field of 13 MV/cm suggest that diamond is a promising semiconductor material for high power operation. A high carrier concentration of up to 10^{14} cm^{-2} in two-dimensional hole gas formed at a hydrogenated diamond surface by the mechanism of transfer doping is achievable [1]. Large optical phonon energy in bulk diamond results in a very large momentum relaxation time limited by optical phonon scattering, opening a possibility of high-quality plasma resonance. We explored the transport properties of diamond based quasi-two-dimensional conduction channels formed at the hydrogenated diamond surfaces and at the interfaces of diamond/gate dielectric heterostructures. The band parameters and valence band alignments used in our work were found from performing DFT calculations. The 2D density of mobile holes and capacitance were calculated as a function of the gate voltage with the given acceptor density for a gated diamond/$Al_2O_3$and diamond/Al_2O_3/HfO_2 heterostructures, fig. 1.

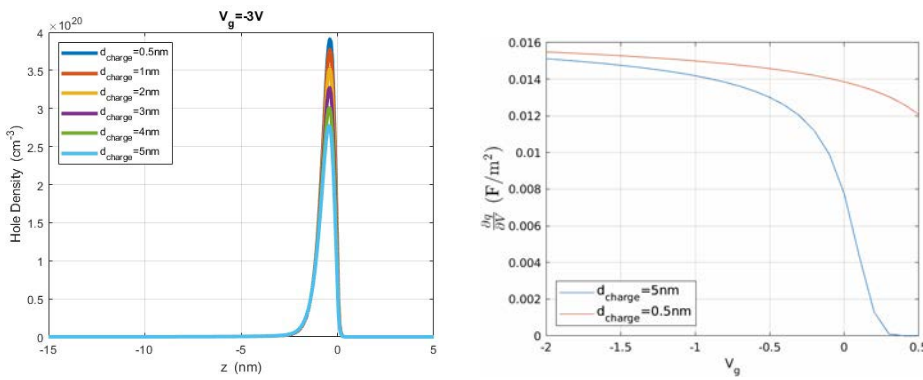

Fig. 1. (a) 3D density distribution of mobile holes as a function of the vertical distance from the diamond/oxide interface, d_{charge} is the distance from the fixed negative charges in the oxide from the interface; (b) capacitance as a function of the gate voltage for two different positions of the fixed negative charges.

In higher mobility channels subject to electric fields a hydrodynamic model allows a convenient scheme for analysis of charge transport under both constant and high frequency electric fields. To apply hydrodynamic model, we evaluated relevant carrier relaxation times. In the carrier-carrier collision dominated regime the hydrodynamic model can be used to study carrier transport in conduction channels of diamond-based Field Effect Transistors (FETs). In the hydrodynamic regime the parameters are quasi-particle quantum lifetime determined by hole-hole scattering, momentum relaxation time due to hole-phonon and hole-impurity scatterings, and momentum diffusion time that characterizes the spread of the carrier distribution in the **k**-space due to the hole-hole scattering. When the carrier quantum lifetime τ_0 is smaller than momentum relaxation (transport) time τ_{tr}, hydrodynamic transport regime applies. In high mobility FETs the shear viscosity and the in-channel thermal conductivity are important transport coefficients for the input to the TCAD modeling of FETs. We find that shear viscosity is the dominant parameter to determine the high-frequency plasmonic response of high mobility FETs. In the high-density regime we obtained an analytical approximation for the viscosity and heat conductivity that can be conveniently used in the numerical solutions of hydrodynamic model equations to study the current and voltage response of the gated diamond channel to the high frequency electric field.

References:

[1] D. Ruzmetov, J. Weil et al. "RF Performance of Diamond Transistors", Proceedings of Government Microcircuit Applications and Critical Technology Conference GOMAC 2023.

9. Topic: Power and Energy

9.1 Session: Nuclides for Defense I

Nuclide Power Research – Nuclear Isomers for Extreme Mission Durations

James J. Carroll
DEVCOM Army Research Laboratory,
2800 Powder Mill Road, Adelphi, MD 20783
Keywords: Nuclear isomers, isomer depletion, induced energy release, extreme mission durations, aerial ISR

Nuclear metastables (isomers) may provide a way to tap into nuclear-scale energies at sufficient power density to support the Army of 2040+, but success will depend sensitively on physical processes that are only beginning to be fully understood. Principal among these are processes by which radioactive decay rates can be effectively enhanced on demand. This presentation will survey the results of ARL research into such “isomer depletion” or “isomer switching” processes, as well as the status and next steps in the ARL program.

Energy storage in chemicals, whether fuels or batteries, forms the basis for the U. S. Army’s many energy- and power-hungry applications. However, these materials are restricted in energy density as they are ultimately based on the binding energy of atoms to each other, on the order of an eV and leading to macroscopic intrinsic energy densities of less than the “chemical limit” of about 5×10^4 J/g. Conversely, binding energies of particles within most atomic nuclei are on the order of 8 MeV, leading to macroscopic intrinsic energy densities greater than 10^9 J/g. Nuclear fission and fusion reactions can tap into even higher energy densities, but even “moveable” reactors like that in Project Pele are too large for use in applications like UAS (and fission creates significant hazards for by-products). On the other hand, radioisotopes provide a way to tap into nuclear-scale energies at smaller physical sizes and in generally less hazardous manners.

The power density available from the decay of any radioisotope is proportional to the inverse of the characteristic lifetime of the radioisotope. Reaching a higher power density would seem easily achievable by selecting a radioisotope with a short lifetime. However, once created any radioisotope material will begin to release its energy immediately: no “ignition” is required. Thus, a short lifetime may mean all the energy is released before needed. For “standard” radioisotopes, their application space is, therefore, limited to low power density and long lifetimes, perhaps useful for unattended sensors at the < 1 W_e level. Propulsion, on the other hand, requires much higher power of more than several hundred W_e. Nuclear isomers are radioisotopes that possess two (or more) macroscopic lifetimes, so that a long-lived state (the isomer state itself) can serve for energy storage while a shorter-lived state can provide the larger power density needed for propulsion. The process for “switching” one of these materials from isomer to higher power has been demonstrated in several cases, including among the 12 known isomers with lifetimes greater than 1 year (attractive for production and storage). Reviews of the relevant physics and earlier experimental results may be found in Refs. [1, 2]; of particular note was the first demonstration led by ARL scientists of a new physical effect, nuclear excitation by electron capture (NEEC) [3].

While in the basic research phase, projections for future capabilities are striking: The Figure shows a comparison between what is currently possible for a modest-sized UAS and what could be possible beyond the chemical limit using nuclear isomers.

This presentation will review recent results and progress of ARL basic research into energy release from isomers. The particular focus will be on efforts to characterize the new effect of NEEC for isomer switching.

Fig. 1: Current chemical-powered capabilities (lower) compared with anticipated isomer capabilities (upper) for a Stalker-sized UAS.

References:

[1] J. J. Carroll, "Nuclear metastables for energy and power: Status and challenges," in *Innovations in Army Energy and Power Materials Technologies*, E. C. Shaffer and T. S. Zheleva Eds. Millersville, PA: Materials Research Forum, 2018.
[2] J. J. Carroll and C. J. Chiara, "Isomer Depletion," *Eur. Phys. J. Spec. Top.*, vol. 233, p. 1151, 2024.
[3] C. J. Chiara *et al.*, "Isomer depletion as experimental evidence of nuclear excitation by electron capture," *Nature,* vol. 554, pp. 216-218, 2018.

Lifetimes of Excited States in ^{127}Cs

Connor Gautam[1,2,3*], C.J. Chiara[2], G. J. Lane[4], A. J. Mitchell[4], J. W. McClory[1], J. J. Carroll[2]
[1]*Department of Nuclear Engineering, Air Force Institute of Technology, WPAFB, OH, 45433*
[2]*DEVCOM Army Research Laboratory, 2800 Powder Mill Rd, Adelphi, MD 20783*
[3]*Fibertek, 13605 Dulles Technology Dr, Herndon, VA 20171*
[4]*The Australian National University, Australia, Canberra, ACT 2600*
**Corresponding Author Email: connor.m.gautam.ctr@army.mil*
Keywords: Isomer Power, Nuclear Structure Physics, NEEC

The nuclide ^{127}Cs has been proposed for the study of nuclear excitation by electron capture (NEEC), a potential mechanism by which to induce the release of energy from nuclear isomers for Army applications. ^{127}Cs exists in an intermediate mass region between quadrupole deformed nuclei and spherical nuclei near the "magic" proton number 50. The viability of measuring NEEC in ^{127}Cs depends, among other factors, on the lifetimes of the states feeding and depopulating the isomer. Experiments were conducted at the Australian National University (ANU) to measure the lifetimes of these states. Lifetimes of seven excited states were measured through a combination of methods. These new measurements indicate that observation of NEEC through an implantation experiment is feasible. Reduced transition probability measurements indicate a possible change in nuclear shape above the $\pi h_{11/2}$ bandhead.

Long-lived isomers with lifetimes on the order of years could be a source of controlled nuclear power capable of being set to a low-activity isomeric state or a high activity depletion state [1]. As part of a fundamental-science initiative to explore the dynamics of isomeric and other excited states, a series of experiments was conducted using the Compton Suppressed Array (CAESAR) at the ANU. The CAESAR array is comprised of three different detector types: high-purity germanium (HPGe) detectors for high-resolution spectroscopy of the γ-ray energies, lanthanum bromide ($LaBr_3$) detectors for timing resolution, and low-energy photon spectrometers (LEPS) for energy resolution in the sub-100-keV domain.

These experiments used the 5n-fusion evaporation channel of ^{9}Be on ^{123}Sb to produce an excitation function that informed related experiments at Argonne National Laboratory's Gammasphere facility as well as the 4n fusion-evaporation channel of ^{11}B on ^{120}Sn. Both reactions provide coincidence and lifetime data on ^{127}Cs. Isomeric states such as $\pi h_{11/2}$ bandhead level in ^{127}Cs are a test case for the physics of isomer depletion. The current data on ^{127}Cs compiled in the Evaluated Nuclear Structure Data File (ENSDF) indicates that the states surrounding ^{127}Cs's 55-μs isomer have poorly defined half-lives, with a simple upper limit of $t_{1/2} < 8$ ns. The $\pi h_{11/2}$ and $\pi d_{5/2}$ bands are, respectively, potential feeding and depletion pathways for the isomer and are of particular interest. The viability of an implantation experiment such as in ^{93}Mo [2] depends on the isomer being populated prior to reaching a "degrader" foil. Long lifetimes, on the order of nanoseconds, above the $\pi h_{11/2}$ bandhead would prevent this method from being successful.

Three methods were used to assess the lifetimes of the excited states of ^{127}Cs. The generalized mirror symmetric centroid difference method (GMCD) [3] uses the difference between the centroids of forward (feed→decay) and reverse (decay→feed) time-difference spectra along with an energy dependent correction term to measure lifetimes on the order of tens to hundreds of picoseconds. For levels with lifetimes on the order of nanoseconds a fit with a gaussian-convolved-exponential was employed. For the longest-lived isomer in the level scheme, a pulsed-beam measurement was used, and the lifetime was extracted from the exponential decay of the isomer.

The measured lifetimes for the relevant bands indicate that observation of NEEC in an experiment similar to that reported in [2] is feasible. Reduced transition probabilities were calculated for the gamma-ray transitions observed in this work and compared to quasiparticle-triaxial-rotor calculations performed by Aydin et al. [4]. The measured transition probabilities show an abrupt change in behavior for the $15/2^-$ to $11/2^-$ transition in the $\pi h_{11/2}$ band. This change in transition rate is a potential indicator of a change in the nuclear shape and merits further study.

References:

[1] Carroll, J.J., Chiara, C.J. Isomer depletion. *Eur. Phys. J. Spec. Top.* **233**, 1151–1160 (2024).
[2] C. Chiara et al., "Isomer depletion as experimental evidence of nuclear excitation by electron capture", Nature **554**, 216 (2018).
[3] J.-M. Règis, et al, "The Generalized Centroid Difference method for lifetime measurements via γ-γ coincidences using fast timing arrays, EPJ Web of Conferences **93**, 01013 (2015).
[4] S. Aydin, et al, "Lifetime measurements and evidence for triaxial nuclear shapes in ^{127}Cs", Phys. Rev. C **104**, 054309 (2021).

Response of a Diamond Radiovoltaic Device to MeV Ion Beams

Norina Kwanmongkholpong [1,*], Nusrat H. Sarwahrdy[1], John D. Demaree [1], Vijay Parameshwaran[1], Marc S. Litz[1]

[1]Army Research Lab, 2800 Powder Mill Rd, Adelphi, MD 20783

**Corresponding Author Email: marc.s.litz.civ@army.mil*

Keywords: Power & Energy, Radioisotopes, Energy Conversion, Schottky Diode, Degradation.

This study documents the modeling and experimental evaluation of a diamond Schottky barrier diode (DSBD) exposed to an alpha particle beam, to determine its potential as a radiovoltaic energy conversion device. Nuclear scattering models using alpha particles were used to estimate the secondary electrons and vacancies generated in diamond exposed to fluxes of these particles, and the energy deposited from alpha and secondary electrons was numerically calculated as a function of depth in the diamond. Drift and diffusion equation modelling of electron transport in diamond was then performed to calculate the current and voltage (IV) expected from the DSBD. These IV numerical results were then compared to measured current and voltage scans during exposure of a prototype device to a flux of energetic He+ ions from a positive ion accelerator.

To simulate alpha particles from a typical radionuclide source such as ^{241}Am, 3.72 MeV helium ions were directed onto a DSBD device consisting of a 5 μm thick Gd foil metal on top of 400 μm diamond. Helium ions of this energy will fully penetrate the 5um Gd foil, and deposit energy directly in the topmost 5 μm of the diamond, with ion-generated secondary electrons filling the first 2 μm into the diamond. In this experiment, 100 pA of current was measured from the DSBD from a 200 pA alpha beam. This measured current is consistent with a generated electron density (within the first 2 μm of diamond) of 10^{13} electrons per cc. While the DSBD described in this paper was designed for use as a neutron detector, with a thick Gd layer and very thick diamond layer for neutron interception, a more optimized device design could provide much greater energy conversion efficiency from radionuclide sources, while retaining the excellent radiation damage resistance of a diamond-based device.

Scintillator Materials Characterization for Alpha Photovoltaic Energy Converters

Nusrat H. Sarwahrdy[1,*], G. Amalthea Trobare [1], John D. Demaree [1], Nicholas P. Barbieri[1], Jeremy L. Smith[1], LeighAnn S. Larkin[1], Vijay Parameshwaran[1], Michael Wraback[1], Marc S. Litz[1]

[1]Army Research Lab, 2800 Powder Mill Rd, Adelphi, MD 20783

**Corresponding Author Email: nusrat.h.sarwahrdy.ctr@army.mil*

Keywords: Power & Energy, Radioisotopes, Energy Conversion, Scintillators, Degradation, Light Yield.

Radio-Photovoltaics (RPV) can be used as mW-level power sources. These devices make use of scintillators to convert energy from radioisotopes, such as alpha or beta particles, to light, which is absorbed in photovoltaic to generate electrical power (Fig 1). Absolute light yield and radiation damage resilience were calculated and measured in ten scintillators suitable for use in alpha-photovoltaic (APV) energy conversion devices. The scintillators were exposed to alpha fluences 10^{10} - 10^{15} ions/cm^2 to experimentally measure long-term damage to these materials. Scintillator light yield was calculated from IV curves in a calibrated InGaP photovoltaic diode. CsI:Tl had the largest initial light yield (4.8 kph/MeV) of all scintillators evaluated. An alpha fluence of 8.6×10^{14} ions/cm^2 reduced the light yield by 90% in CsI:Tl. The initial system efficiency of CsI:Tl on InGaP was measured to be 0.23%. Alpha-photovoltaic energy conversion devices with this initial system efficiency comprised of 1mCi (3.7×10^7 alphas/s) of ^{241}Am on CsI:Tl scintillators mounted on 1 cm^2 active region InGaP PIN photovoltaic diodes will produce 747.9 nW/cm^2 of electrical power. The power output from alpha stimulated CsI:Tl is 30 times better than the conventional ZnS:Ag scintillator when used with an InGaP energy converter.

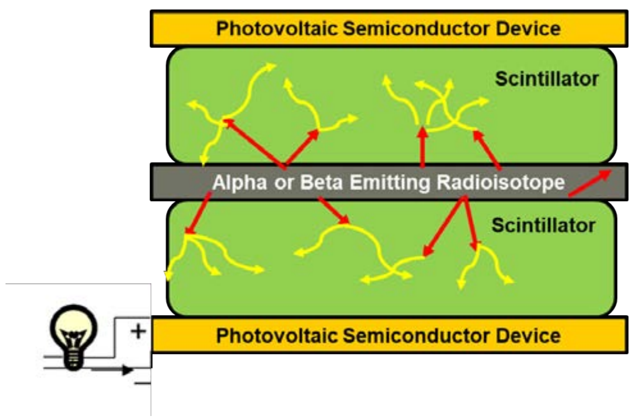

Fig. 1 – Geometry of sandwiched RPV. Radiation is captured by the scintillator and converted to light. The light is then converted to electricity by the PV.

Overview of AFIT Nuclear Program

John W. McClory
Air Force Institute of Technology, Department of Engineering Physics, 2950 Hobson Way, Wright-Patterson AFB. OH 45433
**Corresponding Author Email: john.mcclory@us.af.mil*
Keywords: Nuclear engineering; nuclear physics; nuclear weapons effects.

The Air Force Institute of Technology (AFIT) provides graduate educational programs in nuclear engineering, nuclear physics, and nuclear weapons effects, policy, and proliferation. AFIT's nuclear graduate programs are nationally unique as they educate military members, DOD civilian employees, and DOD contractors in the employment and consequences of use of nuclear weapons. The programs include an ABET accredited Master of Science degree, Doctor of Philosophy degree, and graduate certificate. The educational programs provide a broad foundation in nuclear technology and engineering focused on the needs of the DOD and broader U.S. government. The unique combination of coursework, research, and laboratory practice provides the student with experience working in the fields of nuclear weapon effects, proliferation of nuclear weapons, nuclear physics, nuclear detection, nuclear forensics, the nuclear fuel cycle, and nuclear power. Along with coursework, the degree programs require the completion of theses and dissertations that address technical nuclear problems related to national defense needs. These research efforts are in the broad categories of Nuclear Environments and Effects, System Response and Survivability, and Signatures Characterization and Exploitation. These research and educational efforts are sponsored and coordinated by the AFIT Nuclear Expertise for Advancing Technology (NEAT) Center of Specialized Research. The NEAT Center develops intellectual capital and knowledge through research, education and publication, and addresses technical nuclear acquisition and war fighting challenges. Current research in nuclear reaction cross-sections, nuclear structure and lifetimes, radiation source development, and actinide characterization address Nuclides for Defense research needs.

Adelphi Pelletron Experimental Facility Status Update

J. C. Marsh[1,*], J. J. Carroll[1], W. D. Kulp[2], and J. R. Vanhoy[1,3]

[1]DEVCOM Army Research Laboratory, 2800 Powder Mill Rd., Adelphi, MD 20783
[2]Defense Threat Reduction Agency, Fort Belvoir, VA 22060
[3]General Technical Services, LLC., 1451 Route 34 South, Suite 301, Wall Township, NJ 07727
**Corresponding Author Email: jarrod.c.marsh.civ@army.mil*
Keywords: Pelletron, Neutron, Cross Section, Ion, Accelerator

The Adelphi Pelletron Experimental (APEX) facility relies on a tandem Van de Graaff ion accelerator manufactured by the National Electrostatics Corporation capable of producing high-current proton beams with up to 6 MeV kinetic energy. An Army capability, the Defense Threat Reduction Agency (DTRA) has supported APEX for a multi-year program to produce well-characterized neutron fields enabling the study of reaction cross sections for various materials. APEX is now near operational status, and its capabilities will be reviewed.

Fig. 1: The APEX facility showing the ion sources (grey) to the far right, accelerating tank (blue) center, and the target chamber (grey) to the left.

Tandem Van de Graaff accelerators use electrostatic potentials to accelerate ions. Negative ions are created in the ion sources then injected into the low-energy end of the accelerating tank with kinetic energies around 50 keV and are drawn towards the positive terminal in the center of the tank. The terminal in APEX can create tunable electric potentials up to 3 MV. When the ions pass through the terminal region, they are stripped of electrons; the exact number removed is determined by the ion species and the stripping conditions. The now-positive ions are then repelled from the terminal towards the high-energy end of the accelerating tank. This acceleration process within the tank provides a kinetic energy boost to reach a total accelerated energy of $T = (n + 1)qV$, where n is the final charge state of the accelerated ion, q is the elemental charge unit, and V is the accelerating potential. The total kinetic energy is the sum of the injector energy and the accelerating energy from the tank. The maximum possible beam current depends on the ion source and beam species; however, proton beams up to 100 μA are possible.

The primary mission of APEX is to study neutron-reaction cross sections. These cross sections govern many aspects of nuclear reactions, specifically fission reaction rates, and are therefore extremely important to know precisely. Unfortunately, neutron-reaction cross sections have been thoroughly studied over a wide range of neutron energies only for a handful of isotopes. In most cases, the available data are an extrapolation from a few widely scattered data points using the most up-to-date theoretical models available. Most of these data have not been experimentally verified. Cross-section studies at APEX will begin using a 3-in×3-in CLYC-7 scintillator capable of resolving both neutron and gamma-ray energies. Future upgrades will include a chopper-buncher for a time-of-flight station on one of the alternate beamlines.

Secondary missions for APEX include assisting the study of nuclear isomers in support of Army persistent intelligence, surveillance, and reconnaissance (ISR) unmanned aerial systems (UAS) objectives. Future capabilities could include the development of novel, intense radiation fields and radiation effects on materials.

Enhancement of Beta Decay Via Photon Interaction: Third Order Diagrammatic Contributions

Steven McNamara
Department of Engineering Physics, Air Force Institute of Technology, 2950 Hobson Way, Wright-Patterson AFB, OH 45433
steven.mcnamara.3@us.af.mil

Keywords: Beta decay, QFT, photo-beta decay, forbiddenness, enhanced decay rates, radio-isotope propulsion, direct URCA.

Throughout nuclear physics and engineering, constant transition probabilities are a good approximation for many commonly considered decay processes. However, for beta and beta plus decay, changes in the environment of a nuclear system have been shown to enhance the decay rate by various means: chemical environment [1] [2], pressure [3], and ionization state [4]. In this talk, we explore modifying beta-decay rates through interactions with the electromagnetic (EM) field. We will first provide a review the modes of enhancing beta-decay rates through EM interactions; introducing a photon enhanced free neutron decay rate and a forbiddenness lifting excited state decay. These two processes would be in competition and relevant in different environments and applications. The modified free neutron decay rate is of key interest to the URCA process of neutron stars, where it dominates the decay rate of a free neutron, while the forbiddenness lifting process is relevant for engineering applications such as thrust control radio-isotope propulsion for space systems.

Funding: [Optional] Funding acknowledgement.

References:

[1] T. Ohtsuki, H. Yuki, M. Muto, J. Kasagi, and K. Ohno, "Enhanced electron-capture decay rate of7Be encapsulated in C60 cages," Physical Review Letters, vol. 93, no. 11, 2004.
[2] A. Ray, P. Das, S. Saha, et al., "Observation of large change of 7Be decay rate in Au and Al2O3 and its implications," Physics Letters B, vol. 455, no. 1-4, pp. 69–76, 1999.
[3] L.-G. Liu and C.-A. Huh, "E¡ect of pressure on the decay rate of 7 Be," Tech. Rep. [Online]. Available: www.elsevier.com/locate/epsl.
[4] F. Bosch, T. Faestermann, J. Friese, et al., "Observation of Bound-State b 2 Decay of Fully Ionized 187 Re: 187 Re-187 Os Cosmochronometry," Tech. Rep., 1996.

Investigating Lithium-Mediated Ammonia Electrochemical Synthesis in Non-Aqueous Media for Enhanced Army Operations

Ana I. Alvarez[1,*], Michael A. Yusov[2], Ryan J.R. Jones[2], David R. Baker[1], and Karthish Manthiram[2]

[1]*DEVCOM Army Research Laboratory, 2800 Powder Mill Rd, Adelphi, MD 20783*

[2] *California Institute of Technology, 1200 East California Blvd., Pasadena, CA 91125*

**Corresponding Author Email: ana.i.alvarez4.civ@army.mil*

Keywords: lithium-mediated electrochemical ammonia synthesis, fuel, nitrogen reduction

As the U.S. Army seeks to increase its capability in distributed operations and its resiliency against disruptions in resupply, there is a need for a liquid fuel produced at, or near, the point-of-need. Electrochemical nitrogen reduction to ammonia offers a compelling solution due to its distributed operation capabilities, high energy density, and ease of storage. This work focuses on lithium-mediated electrochemical ammonia synthesis (LiMEAS) in a non-aqueous medium as a promising avenue for decentralized ammonia production. Leveraging lithium's efficacy in breaking the strong nitrogen triple bond at ambient conditions to form Li_3N, which subsequently reacts with a proton source to generate ammonia, this work employs a high-throughput platform to enable rapid screening with reliable statistical basis for analysis of key performance parameters. We delve into the impact of various electrolyte additives on ammonia faradaic efficiency and yield, with a particular emphasis on understanding the mechanistic influence of the solid electrolyte interphase (SEI) on the reaction pathway. Furthermore, recognizing the practical constraints of distributed operation, we explore the effects of air and water as direct inputs to the electrochemical reactor. This analysis provides crucial insights into the system's robustness and feasibility for on-site ammonia generation in challenging environments, ultimately contributing to the development of a resilient and transformative energy solution for the U.S. Army.

a)

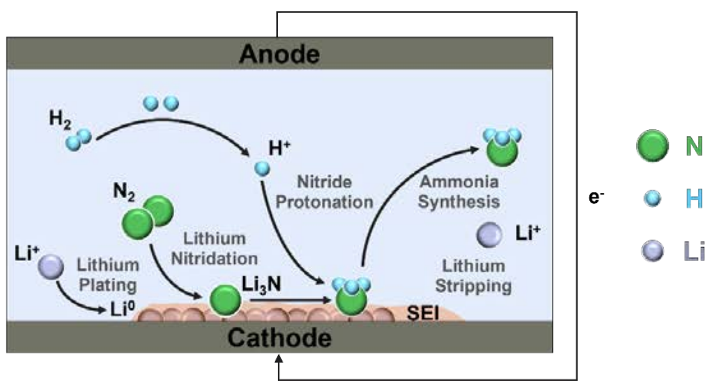

b) **Electrochemical Reactions:**

Anode: $H_2 \rightarrow 2H^+ + 2e^-$

Cathode: $Li^+ + e^- \rightarrow Li^0$

(Electro)Chemical Reactions:

$$Li^0 + N_2 + BH + e^- \rightarrow LiN_xH_y + B^-$$

$$LiN_xH_y + BH + e^- \rightarrow B^- + Li^0 + NH_3$$

Fig. 1 (a) Schematic of lithium-mediated electrochemical ammonia synthesis. (b) List of (electro)chemical reactions taking place on the electrodes and in the electrolyte.

Funding: Cooperative agreement between DEVCOM Army Research Laboratory and California Institute of Technology (W911NF-24-2-0154).

Operational Energy from Seawater

Heather D. Willauer[1*], Cameron F. Holder[1], Jeffrey W. Baldwin[2], Andrew R. Shabaev[1]
[1]*Materials Science & Technology Division, U.S. Naval Research Laboratory, 4555 Overlook Avenue SW, Washington, DC 20375*
[2]*Acoustics Division, U.S. Naval Research Laboratory, 4555 Overlook Avenue SW, Washington, DC 20375*
** Corresponding Author Email:* heather.d.willauer.civ@us.navy.mil

Keywords: seawater, carbon dioxide, hydrogen, fuel

The world's oceans are the largest carbon reservoirs containing approximately 38,000 gigatons of carbon. Carbon along with hydrogen are the principle building blocks needed to produce hydrocarbon fuel. The big question that NRL research is seeking to answer is "How to recover inorganic carbon (CO_2) from seawater along with hydrogen in quantities needed to synthesize operational fuel at or near the point of use for the U.S. Navy?" This brief will discuss the technology developmental progress of the NRL electrolytic cation exchange module (E-CEM) along with the synthesis of CO_2 and H_2 to hydrocarbons. The integration of these technologies has the potential to offer a novel way to convert electricity into a portable, storable, versatile, high-energy density synthetic operational fuel in theater.

Enhancing Ethanol Reforming for Efficient Hydrogen-Rich Fuel Production

Jiangtian Li* and Deryn Chu

DEVCOM Army Research Laboratory, 2800 Powder Mill Rd, Adelphi, MD 20783

** Corresponding Author Email: jiangtian.li.ctr@army.mil;*

Key words: Ethanol Reforming; Hydrogen Fuel; Catalysts; Reaction Pathway Control; Carbon Deposition.

Hydrogen is one of the most promising energy carriers and a crucial fuel for fuel cell systems. However, its generation, storage, and transportation present significant challenges. On-site hydrogen production using transportable fuels offers a flexible strategy for practical applications. Among potential fuel options, ethanol stands out as a viable alternative due to its relatively high hydrogen content, wide availability, low production costs, ease of handling, transportation, and storage, non-toxicity, and compatibility with existing logistics networks. Given these advantages, hydrogen production through ethanol reforming is considered a promising approach. However, during the reforming process, as shown in Fig. 1, ethanol undergoes multiple reaction pathways, leading to the formation of undesirable byproducts that adversely affect catalyst performance and reduce overall efficiency. Therefore, developing active, selective, and robust catalysts capable of minimizing the detrimental effects of side reactions is essential for advancing practical applications of ethanol reforming fuel cell systems. Rh is the state-of-the-art catalyst, demonstrating superior activity and stability for ethanol reforming. However, its high cost limits its industrial application. Reducing the concentration of noble metals and developing non-noble metal-based catalysts are essential for scaling up industrial applications. Ni is highly effective in breaking C-C bonds; however, Ni catalysts are prone to deactivation due to carbon deposition, which blocks access to active sites, and sintering of active sites, which decreases active surface area.

This presentation will discuss our recent research efforts to control reaction pathways and carbon deposition behavior in ethanol reforming. Our results indicate that reducing surface acidic sites significantly suppresses the dehydration of ethanol to produce C_2H_4, the major source of carbon deposition. Additionally, alloying Ni with other metals alters the coordination environment of intermediates, guiding the reaction towards desired products. By controlling reaction pathways and carbon deposition at the atomic scale, we aim to enhance ethanol reforming for more efficient hydrogen generation and improved carbon deposition resistance.

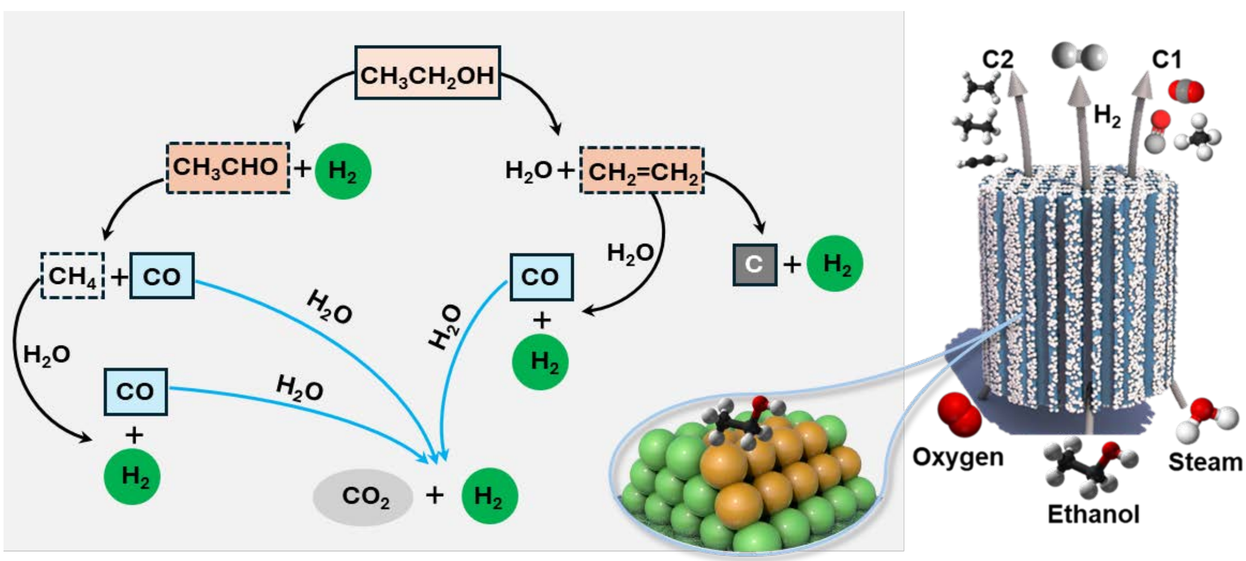

Fig. 1. Potential reaction pathways in the ethanol reforming process that lead to both hydrogen production and the formation of undesirable byproducts. By controlling these reaction pathways, it is possible to mitigate undesired reactions and selectively target the production of desired products.

Effect of Electrolyte Anion Adsorption on the Performance of Solid Polymer Electrolyte Membrane Fuel Cells (SPEMFCs)

Deryn Chu

DEVCOM Army Research Laboratory, Adelphi, MD 20783, United States

Email: Deryn.d.chu.civ@army.mil

Keywords: Platinum; Acid Electrolyte; Solid Polymer Electrolyte Membrane Fuel Cells (SPEMFCs); Hydrogen; Methanol

Solid Polymer Electrolyte Membrane Fuel Cells (SPEMFCs) are a key enabling technology for potential portable power sources due to their high specific energy, high power density, and lightweight nature compared to conventional batteries. Currently, the most effective electrode catalysts for SPEMFCs are platinum (Pt). When performing cyclic voltammetry on a Pt electrode in various acidic electrolytes, the primary feature observed is a distinct pair of peaks related to the adsorption and desorption of hydrogen on the Pt surface. The exact peak potential and shape vary depending on the specific acid used and its concentration, primarily due to differences in the anion adsorption behavior on the Pt surface. This paper will present and discuss H_2-Nafion (H_2/-SO_3^-), direct methanol (CH_3OH-Nafion, SO_3^-) and reformed methanol (H_3PO_4 doped PBI and Ion Pair Electrolyte). It will examine the effect of anion adsorption on the Pt surface and its impact on surface activity. A thorough investigation and understanding of the electrochemical performance characteristics associated with anion adsorption on the Pt surface are essential for advancing SPEMFC systems toward practical applications.

Scalable 3D Architectures for High-Performance Rechargeable Alkaline Zn-MnO_2 Batteries

Ryan H. DeBlock[1], Andrew B. Geltmacher[2], Hunter O. Ford[1], Zachary G. Neale[1], Debra R. Rolison[1], and Jeffrey W. Long[1*]

[1]*Code 6170, Surface Chemistry Branch, U.S. Naval Research Laboratory, Washington, DC USA*
[2]*Code 6350, Multifunctional Materials Branch, U.S. Naval Research Laboratory, Washington, DC USA*
**Corresponding Author Email: jeffrey.w.long26.civ@us.navy.mil*
Keywords: "zinc battery, aqueous energy storage, batteries".

Rechargeable alkaline Zn-MnO_2 batteries offer a compelling combination of safety, sustainability, and cost-effectiveness. However, their widespread adoption has been hindered by limitations in cycle life, primarily due to Zn dendrite formation and MnO_2 cathode degradation. Building on our successful development of high-performance 3D Zn sponge anodes [1,2], we present recent advancements in engineering scalable, monolithic MnO_2 cathode architectures tailored for cylindrical cell formats. These architectures, synthesized using sol-gel and microwave techniques, surpass the energy and power capabilities of conventional MnO_2/carbon composite cathodes. Furthermore, we utilize X-ray computed microtomography (XCMT) to provide in-depth visualization and analysis of the 3D structure of our novel Zn sponges, including in situ imaging during cycling in prototype alkaline cells. This study highlights a promising pathway towards realizing the full potential of rechargeable alkaline Zn-MnO_2 batteries as a safe and sustainable energy-storage solution.

[1]. Parker, Joseph F., Christopher N. Chervin, Irina R. Pala, Meinrad Machler, Michael F. Burz, Jeffrey W. Long, and Debra R. Rolison. "Rechargeable nickel–3D zinc batteries: An energy-dense, safer alternative to lithium-ion." *Science* 356, no. 6336 (2017): 415-418.

[2]. Ko, Jesse S., Andrew B. Geltmacher, Brandon J. Hopkins, Debra R. Rolison, Jeffrey W. Long, and Joseph F. Parker. "Robust 3D Zn sponges enable high-power, energy-dense alkaline batteries." *ACS Appl. Energy Mater.* 2, no. 1 (2018): 212-216.

Controlling Voltage and Capacity through Selective Doping in Fe-Based Energy Storage Materials

Michelle D. Johannes[1], Ryan H. DeBlock[2], Hunter O. Ford[2], Jeffrey W. Long[2], Michael Swift[1] and Debra R. Rolison[2]

[1]Code 6390, Center for Materials Physics and Technology, U.S. Naval Research Laboratory, Washington, DC 20375

[2]Code 6170, Surface Chemistry Branch, U.S. Naval Research Laboratory, Washington, DC 20375

**Corresponding Author Email: michelle..d.johannes.civ@us.navy.mil*

. batteries,computation,novel materials

There is an ever-growing need for electrochemical energy storage devices that circumvent the safety and critical materials pitfalls of current Li-ion technologies. This work details analysis of a class of earth abundant vanadium ferrite materials, developed at NRL, that can operate in both standard non-aqueous- and in aqueous-based electrolyte environments [1]. We conduct a density functional theory investigation of the intercalation mechanisms, comparing Li+ to Na+ and evaluating the effect of V concentration. We find that strong V-Fe bonding is behind an unexpected upward shift in the $Fe^{2+/3+}$ redox potential (compared to standard Fe oxide materials. Concurrent experimental XAS evaluation of the K-edge of V and Fe as a function of state-of-charge find the same redox sequence and shift in voltage [2]. We then proceed to investigate the effect of various redox inactive dopants (Al, Zn) on both voltage profile and capacity to find optimal chemical composition for safer, aqueous-based operation. We conclude that defect states, still of the same V-Fe character, form just below the conduction band, and have a strong effect on the voltage. The number and energy position of these states depends strongly on the site preference of the dopant which may be controlled by temperature/oxygen partial pressure, resulting in an experimental knob by which these materials may be synthesized according to need.

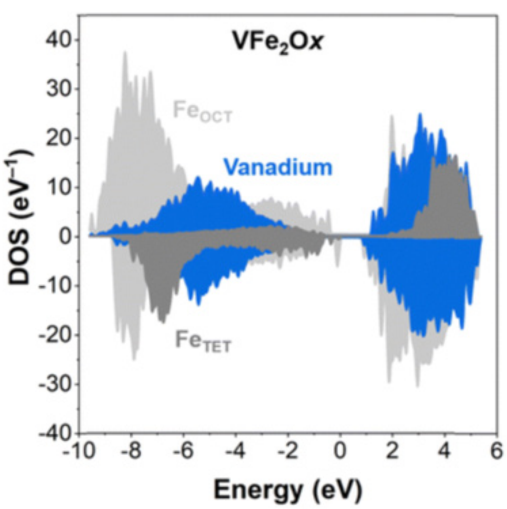

Fig. 1 – Density of states showing the strong hybrization between Fe and V that drives the voltage upward and shifts the redox sequence in comparison to un-doped Fe_2O_3 (maghemite). Strong exchange coupling anti-aligns the Fe at the tetrahedral site vs. those at the octahedral site.

Funding: This work was supported by the Office of Naval Research (N0001423WX00604). H. O. F. was an NRL–National Research Council Postdoctoral Associate (2021–2024).

References:

[1] C. N. Chervin, J. S. Ko, B. W. Miller, L. Dudek, A. N. Mansour, M. D. Donakowski, T. H. Brintlinger, P. Gogotski, S. Chattopadhyay, T. Shibata, J. F. Parker, B. P. Hahn, D. R. Rolison, J. W. Long, "Defective by design: vanadium-substituted iron oxide nanoarchitectures as cation insertion hosts for electrochemical charge storage." J. Mater. Chem. A, 3.22 (2015): 12059–12068.

[2] R. H. DeBlock, M. D. Johannes, H. O. Ford, M. W. Swift, D. R. Rolison, J. W. Long, “Deconvolving lithium-ion redox in vanadium-iron oxide aerogels using X-ray absorption spectroscopy and density functional theory.” PhysChemChemPhys., 2025,**27**, 6146-6153

NMR Insight into Electrochemical Charge Storage in Metal Oxides

Mark O. Bovee[1,*], Christopher A. Klug[1], Jeffrey W. Long[1], Ryan H. DeBlock[1], Debra R. Rolison[1], Zachary G. Neale[1], Hunter O. Ford[1], Michelle D. Johannes[2], Ramsay B. Nuwayhid[1], & Zoey A. Warecki[2]

[1]Chemistry Division, U.S. Naval Research Laboratory, 4555 Overlook Ave SW, Washington, DC 20375
[2]Materials Science and Technology Division, U.S. Naval Research Laboratory, 4555 Overlook Ave SW, Washington, DC 20375
**Corresponding Author Email: mark.o.bovee.civ@us.navy.mil*
Keywords: Energy Storage Systems, NMR

Significant line broadening in ^1H NMR spectra and short ^1H spin-lattice relaxation times provide insight on the interaction between protons and Mn^{4+} in manganese (IV) oxide-based battery materials.

Although lithium-ion batteries have significantly increased in popularity as energy storage systems since the first commercial design was introduced in 1991 [1], there are growing concerns over the future supply chain availability of Li-ion battery component materials as well as warfighter safety regarding the flammability of these devices' organic electrolyte [2]. These concerns incentivize the search for alternative energy-storage systems that harness more Earth-abundant materials and operate with safe water-based electrolytes. Various transition metal oxides (MO_x, M = Mn, Ti, Fe) comprising abundant metals may be used for such purposes in aqueous-based batteries and supercapacitors [3]. Despite their inherent advantages, there remain fundamental questions regarding redox mechanisms, for example the complex interplay between protons (from H_2O) and supporting electrolyte cations (e.g., Li+, Na+, K+) for charge insertion into the MO_x structure as related to efficient charge storage and minimizing degradation and parasitic reactions.

In this presentation, we report on our current research efforts to better understand the underlying chemistry behind an aqueous-based MnO_2 battery system. These measurements span a variety of different techniques with an emphasis on Nuclear Magnetic Resonance (NMR) spectroscopy. By utilizing NMR to study the local environment surrounding protons in these systems, we're able to learn about their interaction with manganese metal centers in an effort to unravel the chemical processes of this system.

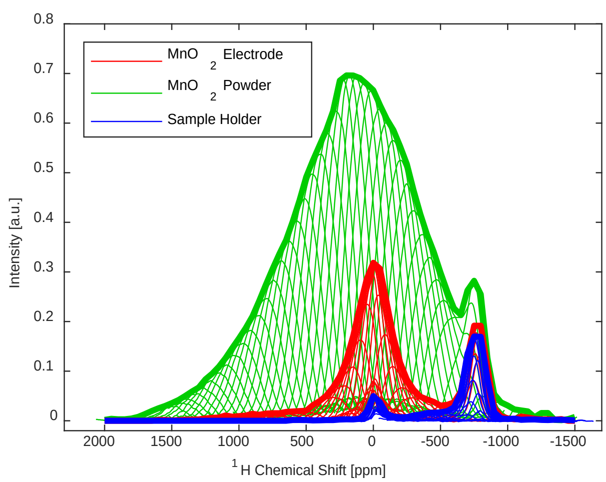

Fig. 1: ^1H spectra of commercial MnO_2 powder (green) and fabricated MnO_2 electrode (red) as well as the background signal (blue) of the sample holder. Spectra require multiple NMR measurements to be collected. Individual measurements are represented by thin lines, and the overall ^1H lineshapes of each sample are represented by thick lines.

Fig. 1 contains proton NMR spectra collected at 11.7 T of commercial MnO_2 powder and a MnO_2 electrode fabricated by depositing the material onto carbon cloth. Here, ^1H NMR signal represents water molecules adsorbed onto the samples' surfaces. Inspection of these spectra reveal significant line broadening caused by short distances between protons and paramagnetic Mn ions (Mn^{4+}). This line broadening scales as $1/r^3$, where r represents the internuclear distance between these species; thus, the broader ^1H lineshape of the MnO_2 powder indicates its protons are closer in proximity to Mn^{4+} than protons in the MnO_2 electrode. This conclusion is further corroborated by ^1H spin-lattice relaxation measurements of these materials which illustrate an overall faster recovery of proton magnetization in the MnO_2 powder relative to the MnO_2 electrode. Measurements of this kind illustrate the insight NMR provides on these systems, and this information will be important when we start performing *in situ* measurements on device-like configurations.

References:

[1] Nishi et al. Non Aqueous Electrolyte Cell. Patent 4,959,281, 08/29/1989, 09/25/1990
[2] Wang et al. "Thermal runaway caused fire and explosion of lithium ion battery." *Journal of Power Sources* 2012, 208, 210-224
[3] Ko et al. "Deciphering charge-storage mechanisms in 3D MnOx@carbon electrode nanoarchitectures for rechargeable zinc-ion cells." *MRS Communications* 2019, 9, 1, 99-106

Self-Powered PVDF-Based Vibrometers for CNC Milling Monitoring

Katie L. Ruland[1,*], Kathleen Coleman[2]
[1]DEVCOM Army Research Laboratory, 2800 Powder Mill Rd, Adelphi, MD 20783
**Corresponding Author Email: katie.l.ruland.ctr@army.mil*
Keywords: piezoelectric, PVDF, vibrometer, self-powered sensors

Computer Numerical Control (CNC) machines are highly versatile, with new capabilities continually being developed. Numerous sensors [1] and machine learning algorithms [2] have been proposed to enhance autonomy and improve human-machine interaction (HMI) while evolving operating procedures to meet demands for high throughput. These solutions typically involve low size, weight, and power (SWaP) IoT sensors that monitor tool wear and cutting forces. This work alternatively proposes self-powered sensors based on a polyvinyl difluoride (PVDF) piezoelectric transducer for these applications for further advancement of autonomy and size reduction [3,4]. This study demonstrates a new class of self-powered piezoelectric-based sensor in a highly CMOS compatible form-factor that may be used in various CNC and milling machines to improve human machine interactions (HMI). The rectified output of the milling event was used to flip the state of a ferroelectric capacitor (FeCap), demonstrating the potential for long term storage of data indicating excessive wear on the milling tool. The rectified output was additionally used to charge a 100nF capacitor to .24V, demonstrating potential for a self-powered sense and response such as wireless transmission of milling event data.

To develop the self-powered piezoelectric sensor, Cr/Au electrodes (100nm, Ø = 4mm) were sputtered on each side of 120µm poled PVDF film (PolyK Technologies, d33>28pC/N), forming a metal-insulator-metal (MIM) capacitor (12pC). Since Au wire bonding directly to the soft PVDF film, had a low yield, Cr/Au wire bond pads (100nm) were sputtered onto a Si wafer and the PVDF was adhered to the Si using a pressure sensitive adhesive and a 2 mm well for silver epoxy to electrically connect the bottom PVDF electrode to the bottom wire bond pad. The top electrode was then electrically connected to the top wire bond pad using silver paint. Finally, the sensor was wire bonded into a DIP package and sealed with EPO-TEK 930-4. Fig. 1a shows an image of the fabricated device. The DIP package was soldered onto a PCB to connect the sensor to a full bridge rectifier (Diodes Inc., SDM02M30LP3).

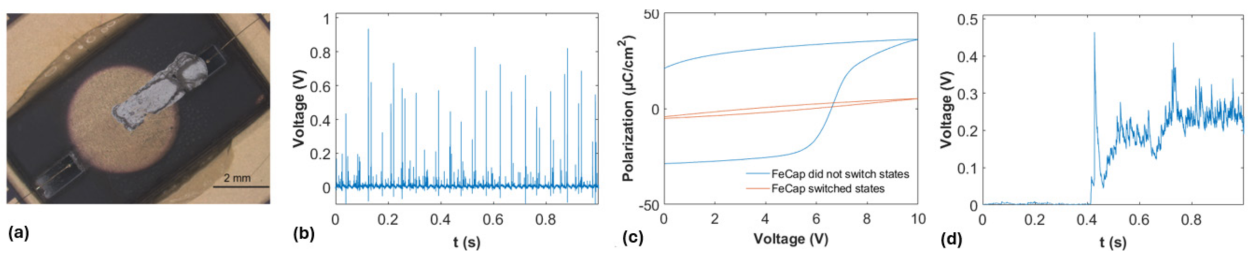

Fig. 1. (a) Device before sealing with epoxy (b) Rectified sensor output during milling (c) Hysteresis loop measuring the FeCap state before the sensor generated sufficient charge to switch the FeCap (blue) and after (orange)(Radiant Technologies, Precision PiezoMEMS Analyzer) (d) Load capacitor output during milling

Experimental Results: To test the sensor's piezoelectric response, a trench was milled into the sensor package using a tabletop CNC (Genmitsu 3018-PRO) and a nano blue coat CNC router bit (Ø=1.8mm) operating at 10,000 RPM. **Fig. 1b** shows the rectified voltage output from this event (R_L=1.2MΩ). The PVDF transducer produced a peak voltage of 935mV and rms current of 19.7nA after rectification. A 50pC FeCap (52/48 standard ARL PZT line) was then connected at the load of the rectifier and trench was again milled into the sensor package. Fig. 1C shows the result from both the initial milling pass which did not flip the state of the FeCap and the pass in which the FeCap state was flipped, indicating that the sensor can be used to store data that a vibration threshold was reached during milling. The sensor package was then milled into vertically, stopping before the sensor, and the rectified output was used to charge a 100nC ceramic capacitor to .24V (Fig. 1D). This demonstrates a new class of self-powered piezoelectric vibrometers in a highly CMOS compatible form-factor.

References:

[1] S. Choudhari, B. Sujay, S. Singh K. Desai. "Utilizing Vision-Based Object Detection Algorithms in Recognizing Uncommon Operating Conditions for CNC Milling Machine" in ASME 2023 18th International Manufacturing Science and Engineering Conference, New Brunswick, NJ USA, June 12–16, 2023.
[2] E. Traini, G. Bruno, G. D'Antonio, F. Lombardi, "Machine Learning Framework for Predictive Maintenance in Milling", in 9th IFAC Conf. on Manuf. Model., Manage. and ContrI, Berlin, Germany, August 28–30, vol. 52, pp 177-182, 2019.
[3] P. Ueberschlag. "PVDF Piezoelectric Polymer", Sens. Rev., vol 21, pp 118-126, 2001.
[4] G. Sessier. "Piezoelectricity in Polyvinylidene Fluoride". J. Acoustic Soc Amer., vol. 70 pp. 1596-1608, 1981.

10. Topic: Electromagnetic Sciences

Electromagnetic Emissions Mechanisms via Fluid Mechanical Phenomena in Graphene

Jordan Planillo
(NAWCWD –Point Mugu) jordanrudolph.p.planillo.civ@us.navy.mil

Graphene has been extensively researched for its use in next generation microelectronic devices in part due to its exceptional material properties such as high carrier mobility. These properties are of particular interest as graphene provides a platform to study phenomena from classical fluid mechanics in a two-dimensional solid-state form.

In high field, non-equilibrium conditions, the electrons in graphene behave as a compressible gas such that the electrons traverse as a shockwave through the graphene. In the far field, this gives the appearance of a point charge. When constrained to a semicircular shaped channel, the electrons appear to be a rotating electric dipole — a solid-state cyclotron radiation source. The emitted frequency is a function of the saturation velocity and the channel radius. Micron scale arrays of these devices were designed, fabricated, and characterized for operation at microwave frequencies (a). Measurements indicate that emissions due to cyclotron radiation were observed (b) and were independent of the driving stimulus [1]. With further refinements in scale, it is possible to achieve emissions at terahertz frequencies.

At cryogenic temperatures, electrons in graphene behave like a viscous fluid. At low Reynolds number flow conditions (Re 20-50); stable eddy currents can be produced as current flows through a constriction [2]. From an electromagnetic perspective, these eddy currents have a corresponding magnetic dipole moment, which is affected by the current flow rate or by the presence of an external magnetic field (c). Subsequent changes in the flow rate or external magnetic field will result in changes to the magnetic dipoles resulting in electromagnetic radiation. At higher Reynolds number, flow past circular obstructions produce in a periodic vortex shedding (d) at a rate that is proportional to the flow velocity and the obstruction diameter [3] — von Karman vortex street formation. This periodic shedding resembles a radiating oscillating magnetic dipole, which emits at a frequency identical to the vortex shedding rate (e). This presents a means of converting direct current (DC) electrical stimulus to RF emissions.

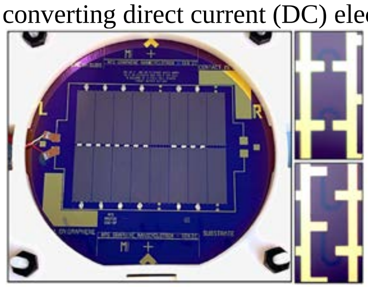

(a)

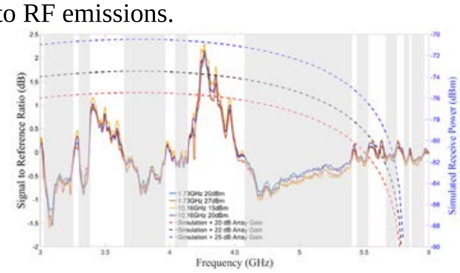

(b)

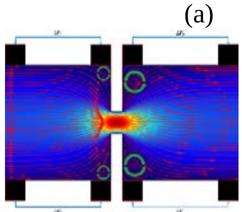

(c)

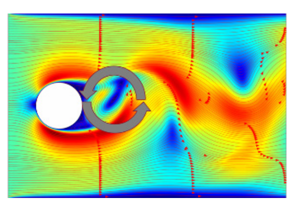

(d)

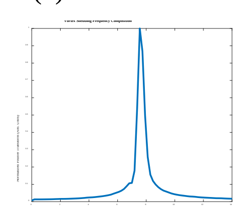

(e)

References:

[1] Planillo, J. et al. Experimental demonstration of cyclotron emissions in micro-scale graphene structures. Sci Rep 14, 13879 (2024)

[2] A. I. Berdyugin et al. Measuring Hall viscosity of graphene's electron fluid. Science. Vol. 364, Issue 6436, pp. 162-165. (2019)

[3] Abernathy, F. H. & Kronauer, R. E. The formation of vortex streets. J. Fluid Mech. 13, 1–20 (1962)

Funding Acknowledgement:

This research is supported by the DoD SMART SEED Grant, ONR ILIR funding, and NAWCWD NISE funding.

Multiband Polarimetric Analysis of Measurements of Man-Made Materials

Sarah J. Becker[1,*], Heather S. Sussman[1], Johanna R. Arredondo[1], Jorge A. Ochoa Gonzalez[1], John S. Furey[2], Kyle L. Klaus[3]

[1]*U.S. Army Engineer Research and Development Center – Geospatial Research Laboratory, 7701 Telegraph Rd, Alexandria, VA 22315*

**Corresponding Author Email: Sarah.J.Becker@usace.army.mil*

[2]*U.S. Army Engineer Research and Development Center – Environmental Laboratory, 3909 Halls Ferry Road, Vicksburg, MS 39180*

[3]*U.S. Army Engineer Research and Development Center – Geotechnical & Structures Laboratory, 3909 Halls Ferry Road, Vicksburg, MS 39180*

Keywords: Multiband, polarimetric, Stokes Vectors, materials, collection geometry

Light interacting with materials can be reflected in varied polarization states. The S_0 Stokes parameter represents the amount of unpolarized light, S_1 represents the amount of horizontally and vertically polarized light, S_2 represents the amount of diagonally polarized light, while the Degree of Linear Polarization (DoLP) calculates the fraction of light that is linearly polarized. Spectral analyses often fail to distinguish between materials that may be spectrally similar, while polarimetric classification of man-made materials is relatively under studied and may be able to enhance man-made material identification. In this research project, sensors measure unpolarized and polarized reflectance responses from materials in the visible (VIS), shortwave infrared (SWIR), and longwave infrared (LWIR) in laboratory and aerial field imagery at varying collection geometries. First, the separability of DoLP responses by man-made material and collection geometry was quantified, and then the relationship between the laboratory and aerial measurements was analyzed. Results show statistically significant separability by material and collection geometry in the VIS, SWIR, and LWIR. Post-hoc pairwise comparisons showed which materials were separable from each other along with which collection geometries were separable from each other; however, the amount of separability differs between the laboratory and field measurements.

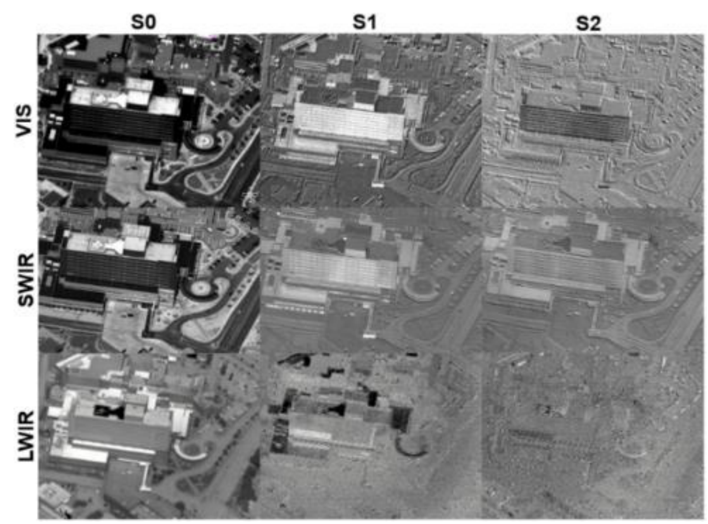

Fig. 1 – S_0, S_1, and S_2 polarimetric imagery in the VIS, SWIR, and LWIR in Grand Junction, CO.

Funding: This research was supported by the DoD Basic Research program.

Qualitative Inverse Scattering for RF Imaging through Unknown Media

Matthew Burfeindt*

U.S. Naval Research Laboratory, 4555 Overlook Ave. SW, Washington, DC 20375

**matthew.j.burfeindt.civ@us.navy.mil*

Keywords: electromagnetics, radar, imaging, inverse problems, ground penetrating radar

We develop an inverse scattering algorithm for reconstructing the shape of targets obscured by media with uncertain electrical and spatial properties. We improve robustness by using an autofocus strategy to overcome unknown propagation effects in the medium and demonstrate performance with experimental data.

Radiofrequency (RF) technology is promising for imaging through obscuring media. Electromagnetic fields at RF wavelengths are able to penetrate a wide variety of materials, which in principle allows for sensing objects that are hidden under the ground, under foliage, or behind walls.

Traditional RF focusing algorithms based on radar signal processing typically operate by backprojecting the received fields to every pixel location in the imaging domain. This does not fully capture the behavior of the electromagnetic wave as it propagates in the domain, which potentially leads to suboptimal leveraging of signal information. In contrast, so-called inverse scattering algorithms extract target properties from the electric fields by inverting a higher-fidelity propagation model. However, achieving robustness is challenging, as the inverse problem is ill-posed.

Qualitative inverse scattering shows promise for overcoming this challenge by limiting the target reconstruction to only its shape, and not its electrical properties [1]. This reduces the complexity of the inverse problem, which potentially allows for more robust results. We have previously developed a qualitative technique that we refer to as the phase-encoded linear sampling method (PE-LSM) [2,3], which further mitigates the ill-posedness of the problem by disciplining the solution using principles based from radar signal processing.

Challenges remain for PE-LSM imaging through unknown obscuration, as the technique requires knowledge of the electrical and spatial properties of the embedding medium. In this study, we evaluate an optimization scheme for mitigating these uncertainties. We iteratively perturb the assumed medium properties and then evaluate the fitness of the assumptions by applying an intensity metric [4] to the resulting imagery. Results for a conducting sphere buried under sand using data from [5] are shown in Fig. 1. The optimized PE-LSM image improves upon the non-optimized PE-LSM image in sharpness and contrast and also evinces finer resolution in the "down" direction compared to backprojection. In our presentation, we will further evaluate the technique across a wider variety of scenarios.

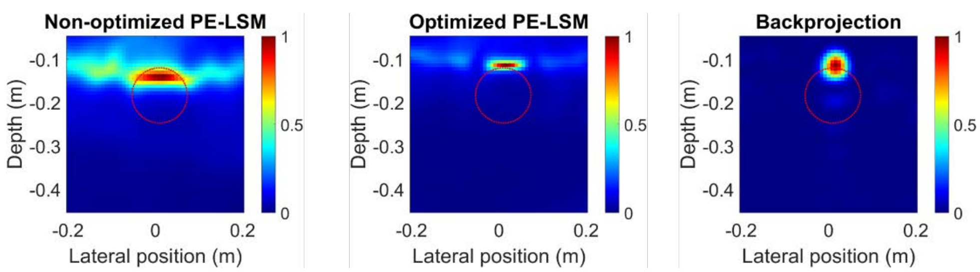

Fig. 1 – Images of a conducting sphere under a sand medium.

Funding: This work was funded by the Office of Naval Research via the NRL Base Program.

References:

[1] M. J. Burfeindt, H. F. Alqadah, and S. Ziegler, "Experimental phase-encoded linear sampling method imaging with a single transmitter and receiver," *IEEE Open J. Ant. Prop.*, vol. 5, no. 4, pp. 942–957, 2024.
[2] M. J. Burfeindt and H. F. Alqadah, "Experimental ground penetrating radar imaging via phase-encoded qualitative inverse scattering," *Proc. IEEE RAPID Conf.*, 2023.
[3] D. Colton, H. Haddar, and M. Piana, "The linear sampling method in inverse electromagnetic scattering theory," *Inverse Problems*, vol. 19, pp. S105-S137, 2003.
[4] H. Jung and K. Kim, "Autofocus Technique Based on Generalized Multilayer Stolt Migration," *IEEE Trans. Geosci. Rem. Sens.,* vol. 56, no. 3, pp. 1386-1393, 2018.
[5] T. Counts, A. Gurbuz, W. Scott, Jr., J. McClellan, and K. Kim, "Multistatic Ground Penetrating Radar Experiments," *IEEE Trans. Geosci. Rem. Sens.,* vol. 45, no. 8, pp. 2544-2553, 2007.

Spatiotemporal Analysis of a Submerged Water Plasma Driven with Nanosecond Long Voltage Pulses

Michael J. Johnson[1*], David R. Boris[1], Tzvetelina B. Petrova[1], Mackenzie E. Meyer[2] and Scott G. Walton[1]

[1] Plasma Physics Division at the U.S. Naval Research Laboratory, Washington, DC 20375
[2] NRC Postdoctoral Research Associate, U.S. Naval Research Laboratory, Washington, DC 20375
**Corresponding Author Email: michael.j.johnson895.civ@us.navy.mil*
Keywords: plasma, water, spectroscopy, pulsed power, nonthermal

Atmospheric pressure plasmas generate a distinct chemical and electrical environment ideal for treating water, making them attractive for applications in wound healing, chemical synthesis, nanomaterial fabrication, and water remediation. These plasmas can operate in a nonequilibrium regime when driven by short pulses of power, lasting tens to hundreds of nanoseconds, that energize electrons but are too short to significantly heat the surrounding gas. This study investigates the impact of pulse width on plasma-water interactions by applying 70–350 ns pulses to an argon plasma submerged in water (Fig. 1a). Plasma properties are analyzed using optical emission spectroscopy and electrical measurements. Results indicate that within the first 15 ns of the pulse, the plasma fully fills the gap between the electrodes (Fig. 1b). After this initial stage, the plasma expands to occupy the entire inter-electrode space for the remainder of the pulse, forming an arc-like plasma where current flow is regulated by the power supply. Essentially, pulse width determines how long the plasma remains in this high-current state. Optical emission spectroscopy revealed that argon dominates the emission immediately after plasma formation, but over time, hydrogen emission becomes more prominent as the plasma dissociates water molecules. This results in higher power consumption at longer pulse widths due to increased energy transfer to the water. Spatial emission profiles show uniform hydrogen emission across the reactor, whereas argon emission weakens near the positive electrode. Significant broadening of emission lines was observed during the pulse, with Stark broadening of hydrogen lines used to estimate electron density. Measurements indicate that a substantial electron density persists for several microseconds after the pulse, likely due to residual voltage on the electrodes during power supply neutralization. At the longest tested pulse width (350 ns), the post-pulse current lasted nearly 10 µs, highlighting not only the influence of pulse width on plasma dynamics but also the importance of other system parameters in determining plasma lifetime.

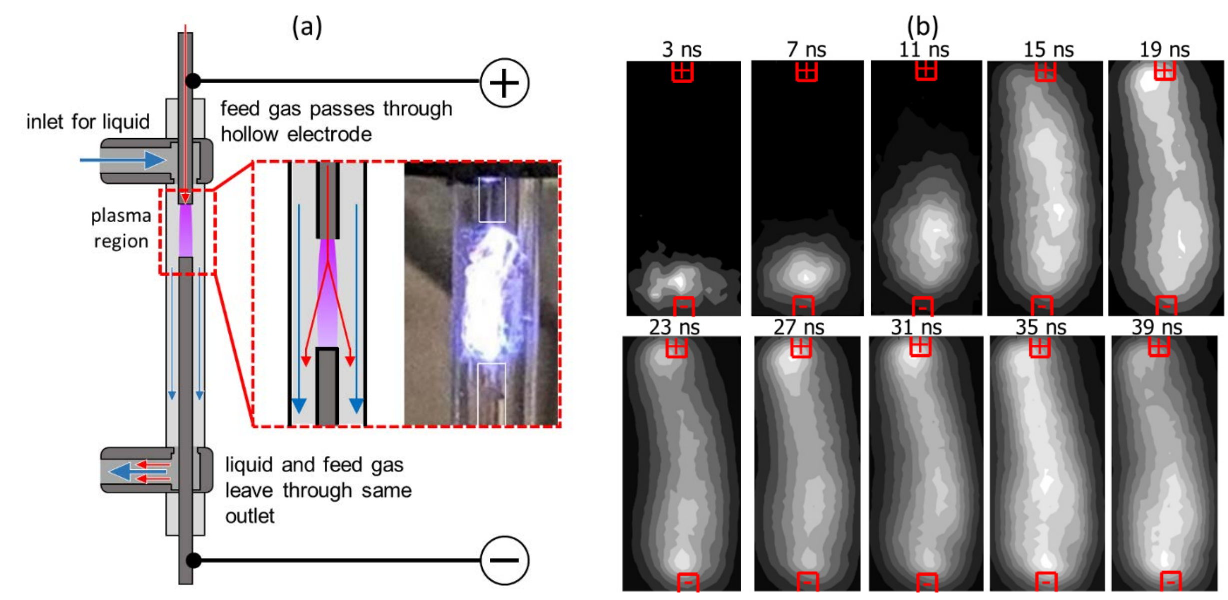

Fig. 1 – (a) Schematic of plasma-water reactor and (b) high speed images of plasma formation.

Funding: This work was partially supported by the U.S. Naval Research Laboratory Base Program.

Novel Circulator Design Using a Rat Race Coupler for High Isolation in Simultaneous Transmit and Receive (STAR) Systems

Sanghoon Shin*
Tactical Electronic Warfare Division, U.S. Naval Research Laboratory, Washington, DC 20375, USA

**Corresponding Author Email: sanghoon.shin.civ@us.navy.mil*
Keywords: Coupler, Circulator, Isolator, STAR system, Full Duplex communication.

Full-duplex communication systems, particularly Simultaneous Transmit and Receive (STAR) system for electronic warfare applications, require high isolation between transmitter (Tx) and receiver (Rx) channels to minimize self-interference. A circulator is a crucial passive component to realize a full-duplex system with a single antenna. Typical isolation using a ferrite-based circulator achieves a maximum of 20–25 dB between the Tx and Rx channels. In this project, we aim to significantly improve the isolation between the Tx and Rx channels to over 60 dB by using a unique composite topology combining a rat-race 180-degree coupler terminated with a variable reactive load. Fig. 1 shows the estimated simulation results for the achievable isolation between two channels. The red curve represents the projected isolation, while the black curve shows the typical isolation from a ferrite-based commercial off-the-shelf (COTS) circulator in the UHF band. The proposed design can outperform the existing circulator by a factor of three. The key component of this composite structure is the rat-race 180-degree coupler with a tunable filter. The conventional 180-degree coupler has a 50-ohm termination with a single deep null in the isolation curve due to the 180-degree phase difference between the 3-dB coupled ports. By replacing the 50-ohm termination in the difference port of the coupler with a reactive load and incorporating a tunable filter, the bandwidth of the isolation can be broadened, resulting in deeper isolation between the two channels. Additionally, by utilizing this response in conjunction with additional cascaded quadrature couplers, a significantly higher level of isolation can be achieved at least three times higher than what is possible with current non-reciprocal circulators, as shown in Fig. 1. This compact, high-isolation design is applicable across a wide range of frequencies (L through Ku bands) and can be implemented in both low-power, chip-scale platforms for UAVs and high-power waveguide systems for electronic warfare. This patent-pending technology addresses critical needs in several DoD S&T areas.

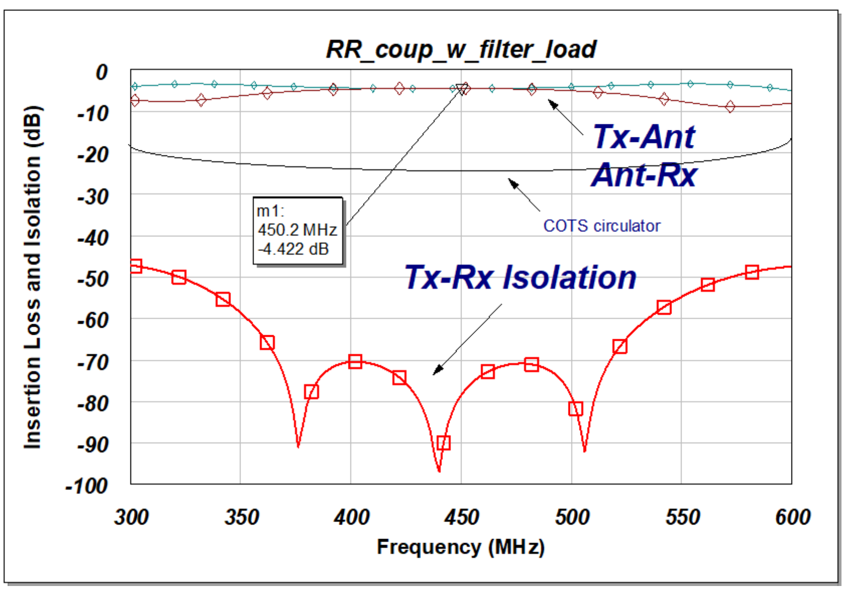

Fig. 1 – **Estimated simulation result for obtainable Isolation between Tx and Rx channel over about 20% fractional bandwidth.** Red-curve shows the projected isolation. The black curve shows the typical isolation from a ferrite-based COTS (commercial off-the-shelf).

References:

[1] Mohamed. H. A. Elsawaf; Amr M. E. Safwat, “Single-Ended-to-Balanced Rat-Race Coupler With Wideband Common-Mode Suppression”, IEEE Transactions on Circuits and Systems II: Express Briefs (Volume: 69, Issue: 4, April 2022)

11. Topic: Emerging Electronics

11.1 Session: Emerging Electronics with Novel Materials

Advanced Electronics at Low Dimensions

Owen A. Vail[1,*] and Ibrahim Boulares[1], Stefan Heiserer[2], Paul B. Seifert[2], Georg S. Duesberg[2], Blair Connelly[1], George de Coster[1]

[1]DEVCOM Army Research Laboratory, Adelphi, Maryland 20783, USA

[2] Institute of Physics, University of the Bundeswehr Munich, Neubiberg 85577, Germany

**Corresponding Author Email: owen.a.vail.civ@army.mil*

Keywords: Nonlinear Hall, Quantum Materials, Harmonic Electronics, Optoelectronics

Quantum Materials encompasses many novel classifications, but we will focus on 2D and Topological Materials. The shared nature of atomically defined carrier channels provides a unifying base by which we study bosonic physics and nonlinear conductivity. With precise control over geometry, in both real-space and in the nontrivial band structure, we can enable devices that fundamentally alter how we approach electronics and optoelectronics. Using quantum materials as thin-film and stackable measurement platforms, we pursue effects such as excitonic condensation and the nonlinear Hall effect. We peer into the harmonics of our measurements, both electronic and spectroscopic, to explore higher order effects that deviate from traditional semiconductor responses. With fine control over the atomic structure, we can craft the electrodynamic environment of our transport channels to rationally design novel low SWaP devices and detectors.

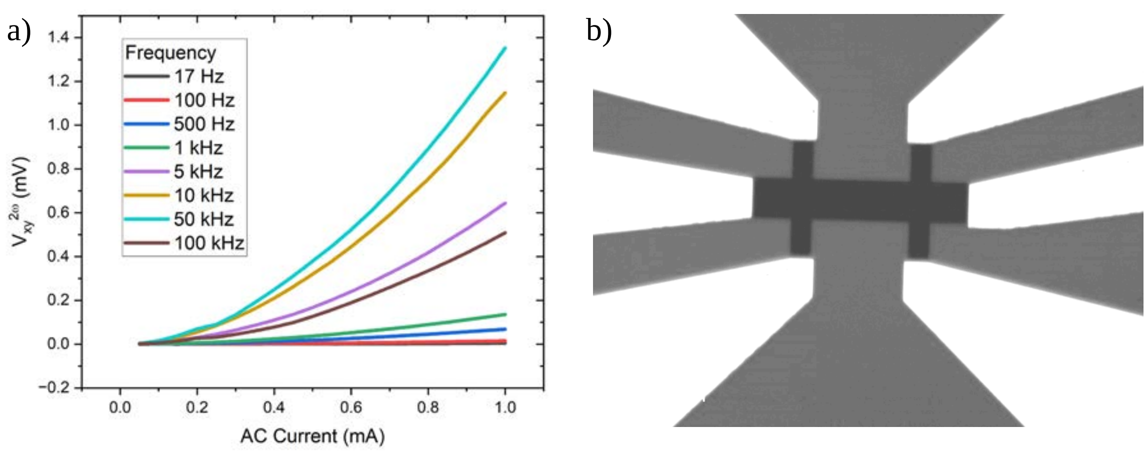

Fig. 1 – (a) Nonlinear Hall effect at various input frequencies and applied currents showing a quadratic response at room temperature. (b) Optical image of 10x30 micron Hall Bar.

Funding: Research was accomplished under Cooperative Agreement Number W911NF-25-2-0010. The views and conclusions contained in this document are those of the authors and should not be interpreted as representing the official policies, either expressed or implied, of the Army Research Office or the U.S. Government. The U.S. Government is authorized to reproduce and distribute reprints for Government purposes notwithstanding any copyright notation herein.

Tailored Geometric Responses and Polarization Sensitivity in $PtSe_2$ Detectors

Eunice Y. Paik[1,*], Owen A. Vail[1], William A. Beck[1], Nikolas Dominik[2], Stefan Heiserer[2], Paul B. Seifert[2], Georg S. Duesberg[2], Blair C. Connelly[1], and George J. de Coster[1,2]
[1]DEVCOM Army Research Laboratory, Adelphi, Maryland 20783, USA
[2]Institute of Physics, University of the Bundeswehr Munich, Neubiberg 85577, Germany
**Corresponding Author Email: eunice.y.paik.civ@army.mil*
Keywords: Polarization, nonlinear optical, detection, transition metal dichalcogenides (TMDs), $PtSe_2$

We investigate polarization sensitivity on the scalable spin-orbit material $PtSe_2$ and show induced photocurrents depend on the input polarization of light and can be tailored by the device's physical geometry.

Non-linear optical (NLO) responses in quantum materials offer a promising route for measuring polarized infrared (IR) light. In materials such as topological insulators, semimetals and transition metal dichalcogenides (TMDs), the strength and temperature dependence of the NLO response to light is predominantly dictated by the strength of spin-orbit coupling, rather than the electronic bandgap. Second order NLO responses yield DC currents and second harmonic generation through frequency difference and sum processes. The former process can be understood as an unbiased photocurrent upon illumination of polarized light, where the current strength and direction depend on the polarization state (i.e., Stokes parameters). This alternative modality for polarized IR detection paves the way for uncooled, high framerate IR polarimeters provided materials of sufficient scalability and NLO strength are identified.

In this work, we report on polarization sensitive photodetectors fabricated on thin films of the TMD $PtSe_2$ whose band structure and spectral sensitivity vary for thicknesses from 1 to 50 nm. Polycrystalline $PtSe_2$ is grown using a thermal assisted annealing process that has been shown to be silicon and back-end-of-the-line compatible [1]. We show that the polycrystallinity of the material enforces an idealized polarization dependent photocurrent response, where unlike single crystal materials, the response strength is not tied to in-plane crystal axes [2,3]. The idealized response allows us to simulate photocurrent profiles in device geometries as a function of incoming light's spot size, spot location, and polarization. In Fig. 1, we show excellent agreement between simulation and experimental measurement of the helicity dependent photocurrent profile.

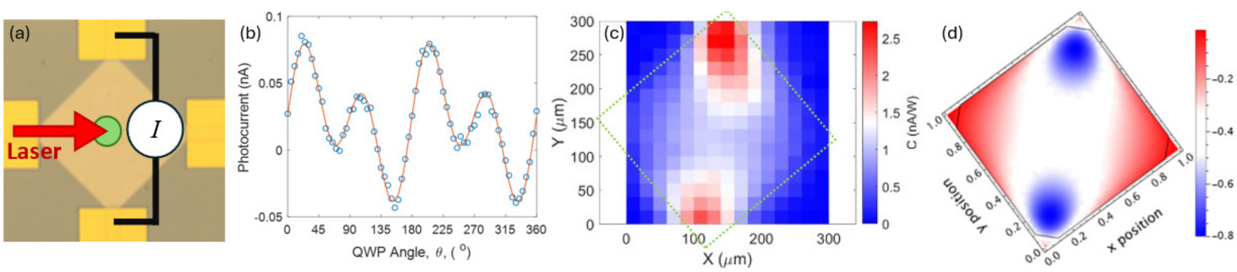

Fig. 1 – Polarization-sensitive photodetection with wafer-scale $PtSe_2$. (a) Image of a square mesa. Arrow and circle indicate laser direction and spot; current is probed perpendicularly. (b) Representative plot of photo-current dependence on incident polarization, where the coefficient, C, represents the magnitude of the response to circularly polarized light, which varies with $sin\,(2\theta)$. (c) Experimental and (d) theoretical results showing the spatial dependence of C, which is maximized near the contacts in the vertical direction.

To optimize the responsivity and polarization sensitivity of our $PtSe_2$ detectors, we experimentally studied a variety of device geometries informed by simulation. Photocurrent measurements are conducted from visible through IR wavelengths to determine spectral dependence of the NLO response for different thicknesses of $PtSe_2$ and demonstrate its viability. Our results show existing scalable materials can be leveraged for new polarimetric-based applications.

References:

[1] M. Prechtl, et al., "Two-dimensional platinum diselenide waveguide-integrated infrared photodetectors," ACS Photonics 9 (3), 859–867 (2022).
[2] B.C. Connelly, P.J. Taylor, G.J. de Coster, "Emergence of threefold symmetric helical photocurrents in epitaxial low twinned Bi_2Se_3," Proc. Nat. Acad. Sci. 121 (5) e2307425121 (2024).
[3] E.Y. Paik et al., "Topological Insulator Based Polarization Sensitive Detection," 2024 IEEE Research and Applications of Photonics in Defense Conference (RAPID), p. 1-2.

Investigating PbSe/PbS Core/Shell Colloidal Quantum Dots for Mid-Wave Infrared Detection

A.E. Colbert[1,*], D. Placencia[1], M.J. Fort, and J.E. Boercker[1]

[1]*Electronics Science and Technology Division, Naval Research Laboratory, 4555 Overlook Ave SW, Washington, DC 20375*

**Corresponding Author Email: adam.e.colbert.civ@us.navy.mil*

Keywords: Lead selenide, nanocrystals, colloidal quantum dots, infrared photodetector.

Photodetection in the mid-wave infrared (MWIR, 3-5 μm) region plays a critical role for sensing and surveillance applications in maritime conditions. Colloidal quantum dots (CQDs) offer a promising route to achieve low-cost infrared photodetectors, enabling direct deposition onto silicon-based image sensors and the potential for wafer-scale manufacturing. However, a key limitation of CQD detector performance with sensitivity in the MWIR region is their low photoluminescence quantum yield (PLQY), or the ratio of photons emitted-to-photons absorbed, which is inversely proportional to the dark current of CQD films. This leads to high dark currents in in CQD-based infrared photodiodes, which in turn increases the noise floor and limits detector sensitivity and dynamic range, therefore restricting the ability to detect dim signatures. State of the art MWIR materials based on mercury telluride (HgTe) CQDs demonstrate PLQY ~0.03% [1], which currently stands as the most importation limitation for thermal infrared applications of these materials [2]. Lead selenide (PbSe) offers an alternative material system with the capability for MWIR detection, having a bulk band gap of 0.27 eV (~4.5 μm) and a large Bohr exciton radius of 46 nm that enables widely tunable absorption via particle size (Fig. 1a). However, use of PbSe for detector applications has been limited due to synthetic challenges associated with the growth of nanocrystals large enough to access the MWIR region, as well as their photochemical stability [3]. In this contribution, we investigate the use of PbSe/PbS core/shell nanostructures as a route to improve the surface passivation and subsequent stability of this material system, demonstrating a ~4X increase of PLQY compared to conventional PbSe cores (Fig. 1b, c). We further tune the synthetic parameters to maximize the CQD size for MWIR absorption, aided by the improved colloidal solubility of the core/shell system, to achieve band gaps exceeding 3.5 μm. Finally, we determine viable processing conditions and ligand exchange approaches necessary to fabricate photodiode devices using the PbSe/PbS CQDs.

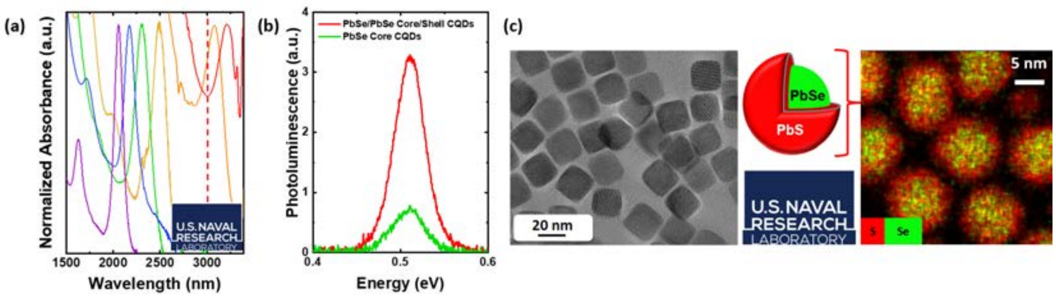

Fig. 1 – (a) Absorbance spectra of PbSe CQDs with band gaps tuned via particle size from the extended short-wave infrared (eSWIR, 2-2.5 μm) through the MWIR. (b) PLQY comparison of PbSe cores (green) vs PbSe/PbS core/shell CQDs (red). (c) Representative electron micrographs of MWIR PbSe (left) and PbSe/PbS core/shell nanocrystals (right) produced by the PIs.

Funding: ONR Code 31 and NRL 6.2 Base Funding.

References:

[1] S. Keuleyan, J. Kohler, P. Guyot-Sionnest, “Photoluminescence of mid-infrared HgTe colloidal quantum dots,” *J. Phys. Chem. C*, vol. 118, pp. 2749-2753, Jan. 2014.
[2] P. Guyot-Sionnest, Ackerman, M. M., X. Tang, “Colloidal quantum dots for infrared detection beyond silicon” *J. Chem. Phys.* vol. 151, no. 060901, Aug. 2019.
[3] T. M. Abeywickrama, A. Hassan, P. T. Snee, “Colloidal synthesis of bulk-bandgap lead selenide,” *Front. Chem.* vol. 6, no. 562, Nov. 2018.

12. Topic: Optics and Photonics

Electrically Controlled Metasurfaces

Charles Pelzman[1], Jason Sun[1], and Sang-Yeon Cho[1]*
[1]*DEVCOM Army Research Laboratory 2800 Power Mill RD, Adelphi MD, USA, 20783*
** Corresponding author Email: sang.y.cho.civ@army.mil*
Keywords: Metasurfaces, Nanophotonics, Electro-refraction, Franz-Keldysh effect.

In this presentation, we report an experimental demonstration of electrically controlled III-V active metalenses. By modulating the electronic band structure of a GaAs-based metalens, the intensity and the curvature of the transmitted wavefront were externally controlled.

Metasurfaces have attracted significant attention due to their ability to control the fundamental wave properties of light, leading to various interesting wave phenomena, such as spin-dependent beam steering and engineering of quality factors through quasi-bound states in the continuum [1,2]. A metalens can be created from a single layer of either periodic or aperiodic subwavelength-scale structures with spatially varying phase responses. Recently, dynamic control of the phase response of metalenses has been reported through mechanical deformation, or liquid-crystal-based index modulation [3,4]. Drawbacks of these approaches include a slow operation speed and limited operational range.

In this presentation, we report the experimental demonstration of an active GaAs based metalens. As shown in Fig. 1-(a), the absorption band edge of the SI-GaAs will shift to longer wavelengths through the Franz-Keldysh effect [5]. By engineering the metalens to work near the band edge of GaAs, strong electro-refraction is expected from the material as predicted by the Kramer-Krönig relation [6]. When applying an electric filed across the metalens, the resulting curvature of the generated wavefront changes which results in a shift in the focal length. To demonstrate this concept, a metalens with a hyperbolic phase profile was designed, fabricated, and experimentally characterized. Fig. 1-(b) shows the measured shift in the location of the focal plane of the fabricated metalens when the applied electric field across the metalens changed from 0 to 2 kV/cm. The measured focal plane was shifted approximately 8 μm closer to the surface of the metalens from its initial location.

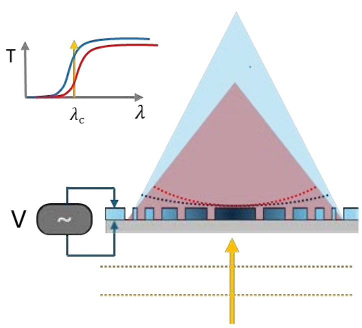

(a)

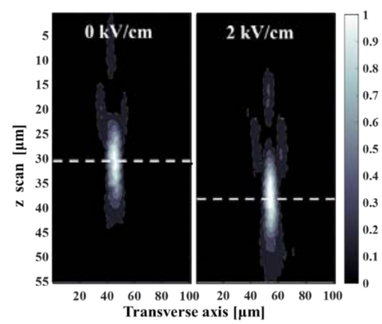

(b)

Fig. 1 (a) Schematic diagram of the active metalens showing the changes in the curvature of the wavefront when an electric field is applied across the device. (b) Captured NIR images showing the focal spot displacement along the optical axis.

In conclusion, we have presented an experimental demonstration of an active metalens. The shift of the focal plane from the metalens was measured using a customized confocal measurement setup. This demonstrated approach holds great potential for developing all-electrically controlled meta-optic devices.

References:

[1] Cho, S.-Y., et al., Control of Quasibound Waves in Spiral Metasurfaces. ACS Photonics, 2022. 9(11): p. 3592-3599.
[2] Khorasaninejad, M., et al., Multispectral chiral imaging with a metalens. Nano letters, 2016. 16(7): p. 4595-4600.
[3] Afridi, A., et al., Ultrathin Tunable Optomechanical Metalens. Nano Letters, 2023. 23(7): p. 2496-2501.
[4] Shalaginov, et al., Reconfigurable all-dielectric metalens with diffraction-limited performance. Nature communications, 2021. 12(1): p. 1225.
[5] Tayebati, P., High contrast, high reflectivity, optical modulator using the Franz-Keldysh effect in a thin film of GaAs. Applied physics letters, 1993. 63(21): p. 2878-2880.
[6] Lucarini, V., et al., Kramers-Kronig relations in optical materials research (Vol.110). 2005: Springer Science & Business Media.

Infrared Nanophotonics in Twisted Naturally-Hyperbolic Calcite Metamaterials

Chase Ellis[1,*], Eric Seabron[2,3], Eric Jackson[1], Xitlali Juarez[2] , Michael Meeker[2], Andrew Lang[2], Brandon Durant[2], Daniel Ratchford[1] ,Rhonda Stroud[1], and Joseph Tischler[1,4]

[1] U.S. Naval Research Laboratory, 4555 Overlook Ave. SW, Washington, DC, USA

[2] NRC Postdoc residing at U.S. Naval Research Laboratory, 4555 Overlook Ave. SW, Washington, DC, USA

[3] Department of Electrical and Computer Engineering, Howard University, 2300 Sixth Street NW, Washington, DC 20059, USA

[4] Department of Physics, University of Oklahoma, 440 W. Brooks St, Norman, OK, USA

**Corresponding Author Email: chase.t.ellis.civ@us.navy.mil*

Keywords: Hyperbolic materials, infrared nanophotonics, phonon polartions, plasmonics

Hyperbolic materials allow light to be confined and controlled at nanoscale dimensions – well-below the diffraction limit. Here, we investigate a new avenue of controlling these unique states of light by controlling the relative orientation between the nanostructured surfaces and the crystal axes of calcite.

Calcite is the quintessential birefringent material **–** possessing different optical properties along its crystal axes. While small differences in the optical permittivity of calcite lead to interesting effects like double refraction in the visible spectral regime – in the infrared, this anisotropy becomes extreme, resulting in simultaneous dielectric and metallic optical behavior along different crystal axes. This extreme anisotropy occurs within the reststrahlen regions of calcite (w=870-888 cm-1 and 1400-1551 cm-1), which is the fundamental property required to support hyperbolic optical modes that are highly directional (depending only on the permittivity) and confined well-beyond the diffraction limit.

While hyperbolic modes have been well-studied in nanostructured materials with high degrees of symmetry – e.g., h-BN and [001]-oriented calcite with cylindrically-symmetric nanostructures and permittivities (isotropic in the sample plane) [1,2] – within this work, we investigate how such modes behave within a low-symmetry calcite system. To accomplish this, we fabricate a series of gratings on [100]-oriented calcite substrates that possess anisotropic optical behavior that lies within the sample plane. We find that these gratings support high quality factor hyperbolic modes ($Q > 200$) that can be tuned throughout the entire reststrahlen region by only changing the relative orientation between the grating and the crystal axes – keeping the grating profile fixed. In addition to experimentally demonstrating this behavior, we have developed a semi-analytical model that predicts how the mode frequency and wave-directionality evolve with grating orientation, eliminating the need to perform full-wave electromagnetic simulations for each grating orientation.

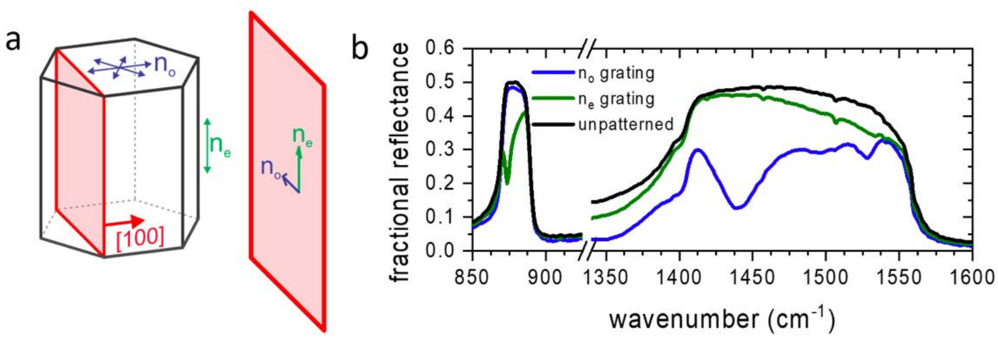

Fig. 1 (a) [100] calcite crystal with anisotropic optical properties along the extraordinary (n_e) and ordinary (n_o) crystal axes and (b) reflectance spectra from gratings aligned ne (green curve) and no (blue curve) crystal axes.

References:

[1] J.D. Caldwell et al. Nature Communications 5, 5221 (2015).
[2] V. Breslin et al. Optica 29, 11760 (2021).

Enhanced Absorption Asymmetry in Symmetry-Broken Metasurfaces

Stephen K. Sanders[1,*], Charles Pelzman[2], Christopher T. Kuhs[3], Henry O. Everitt[3], and Sang-Yeon Cho[2,†]

[1]Oak Ridge Associated Universities, DEVCOM Army Research Laboratory, Rice University, Houston, TX 77030

[2]DEVCOM Army Research Laboratory, Adelphi, MD 20783

[3]DEVCOM Army Research Laboratory South, Rice University, Houston, TX 77030

*Corresponding Authors Emails: *stephen.k.sanders4.ctr@army.mil and †sang.y.cho.civ@army.mil*

Keywords: Metasurface, Quasi-bound states in the continuum, asymmetric absorption, exceptional point.

In this presentation, we report on different symmetry-breaking methods and their impact on the enhancement of asymmetric optical absorption in resonant metasurfaces.

Asymmetric light control is a cornerstone of emerging nonreciprocal photonic technologies, enabling functionalities such as optical diodes, directional sensors, and one-way screens without requiring external biasing. One intriguing way to achieve forward-backward asymmetry is through the presence of exceptional points, which occur in non-Hermitian systems where two or more eigenstates coalesce [1]. Here, we explore two distinct mechanisms for realizing exceptional points and asymmetric optical absorption in passive metasurfaces composed of coupled subwavelength-scale dielectric resonators: (1) structural asymmetry, where the constituent resonators differ in size or shape, and (2) coupling asymmetry, where geometrically identical resonators are asymmetrically coupled.

We analyze model systems of coupled resonators embedded in a metasurface platform. In the structurally asymmetric case, shown in Fig. 1(a), each unit cell consists of two Si resonators of different widths, w_1 & w_2, resulting in detuned individual resonances and broken spatial symmetry. These resonators are separated from an unpatterned 10 nm titanium (Ti) layer by a silica spacer with thickness 200 nm. The Ti layer introduces a non-radiative loss channel to the coupled metasurface system. The interaction between the Ti layer and Si resonators leads to asymmetric coupling between an incident plane wave and the internal resonant modes, depending on the illumination direction. This results in unbalanced absorption and reflection from the metasurface. Panel (b) presents the absorption asymmetry $\eta = A_\mathrm{f}/A_\mathrm{b}$ where A_f and A_b are the absorbance under forward and backward illumination, respectively (see the blue and green arrows in the scheme). For the coupling-asymmetric case, we maintain identical resonator geometries ($w_1 = w_2$) but engineer their spatial arrangement and environment to achieve asymmetric coupling strength between them. Despite the structural symmetry of the resonators, this asymmetric interaction enables different optical absorption, depending on the excitation direction. An example is shown in Fig. 1 (c,d) where (c) shows the absorption asymmetry and (d) depicts the geometry under study. In both cases, as the symmetry breaking (*i.e.*, the ratio of the widths w_1/w_2 or gap separations g_1/g_2) increases, the degree of absorption asymmetry through the metasurface does as well.

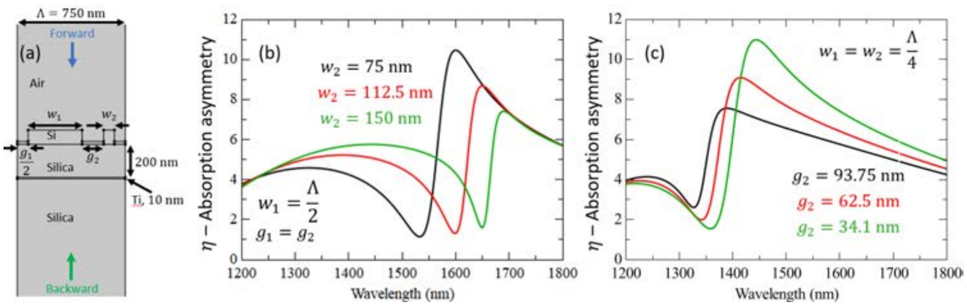

Fig. 1 – (a) Sketch of metasurface geometry under study. (b,c) Absorption asymmetry η of a symmetry-broken array with broken resonator symmetry (b) and broken coupling symmetry (c).

Both schemes lead to significant forward-backward absorption asymmetry, but with different sensitivities and tunability. Structural asymmetry offers broader control over resonance detuning but at the expense of fabrication complexity and potentially scalability. Coupling asymmetry, on the other hand, enables finer and potentially more reconfigurable control, while preserving fabrication simplicity. Our findings highlight the importance of distinguishing between these two routes to non-Hermitian and directionally dependent behavior in metasurfaces.

Funding: This research was sponsored by the Office of the Under Secretary of Defense for Research & Engineering and by DEVCOM Army Research Laboratory under Cooperative Agreement Number W911NF-24-2-0060.

References: [1] S. K. Sanders, C. Pelzman, C. T. Kuhs, H. O. Everitt, and S. Y. Cho, “Control of Asymmetric Absorption using a non-Hermitian meta-membrane,” SPIE Phtonics West, Jan, 2025.

Quasi-bound Band in Photonic Crystal Slabs

Stanislav Tsoi, Nicholas Proscia, Marc Christophersen, Joseph Christodoulides, Hsun-Jen Chuang, Kathleen McCreary, Paul Cunningham, Igor Vurgaftman

[1]*U.S. Naval Research Laboratory, Washington, DC 22375*
**Corresponding Author Email: stanislav.d.tsoi.civ@us.navy.mil*
Keywords: photonic crystals, bound state in the continuum

The bound state in the continuum (BIC) arises at the high symmetry points in the Brillouin zone of photonic crystals due to interference of counter-propagating modes. Its standing-wave field profile has a symmetry that prevents its coupling to far-field radiation and thus leads to a long lifetime. Prior experimental reports have only focused on these localized BIC modes thus limiting potential studies to wavevector-independent applications. In the present work, we measure wavevector-resolved transmission and photoluminescence of monolayer WSe_2 incorporated into a square-lattice photonic crystal slab made of Al disks and show that it supports a quasi-bound band along the Γ-X direction. Furthermore, we find that this band maintains a spectral width similar to that of a typical localized BIC through at least half of the Brillouin zone and terminates in a true symmetry-protected BIC at the Γ point. Our results demonstrate that states in the band arise from interference of partially counter-propagating modes, resulting in a partially standing and partially propagating field. Similar to BIC, the symmetry of the standing component suppresses the coupling to the radiating continuum and results in the extended lifetime. The spectrally narrow dispersing band merging into the BIC at its minimum can potentially facilitate the condensation of exciton-polaritons in the strong coupling regime.

A Study on the Effective Thermal Properties of Graded TPMS and Their Application in Heat Exchangers

Nicole A. Apetre[1,*], John G. Michopoulos[1], John C. Steuben[1], Athanasios P. Iliopoulos[1]
[1]*Science and Technology Division, U.S. Naval Research Laboratory,*
4555 Overlook Avenue SW, Washington, DC, 20375
**Corresponding Author Email: nicoleta.a.apetre.civ@us.navy.mil*
Keywords: metamaterials design, triply periodic minimal surface, multiphysics, heat transfer

The present work investigates the thermal properties of various triply periodic minimal surface (TPMS) architectures through a comprehensive parametric study. Eight representative volume elements (RVEs) will be analyzed: gyroid, diamond, Schwarz primitive, Schwarz diamond, Neovius, Fischer-Koch S, Isotropic Wood Pile (I-WP), and Förstner Random Dots (FRD). The study will determine the effective properties of thermal conductivity, heat capacity at constant pressure, and density of each unit cell as a function of its relative density. These findings provide valuable insights into the thermal behavior of TPMS structures for applications such as heat exchangers.

TPMS's unique geometric properties make them attractive for various applications, from materials science to biomedical engineering and photonics. Their high surface-area-to-volume ratios are particularly beneficial in fields like catalysis, filtration, separation, energy storage, and heat dissipation. However, effectively deploying these complex geometries necessitates a thorough understanding and characterization of their multiphysics behavior. A comprehensive library of equivalent material properties is essential for comparing different TPMS architectures and selecting the optimal structure for a specific application. This present effort focuses on designing and deploying graded TPMS architectures for heat exchanger applications. Building upon previously mentioned RVEs, this study introduces variable wall thicknesses to create graded TPMS structures. A parametric study based on the finite element method (FEM) enables the determination of the equivalent thermal material properties of these graded architectures. The findings contribute to the development of high-performance heat exchangers by enabling the selection of tailored TPMS structures with optimized thermal characteristics.

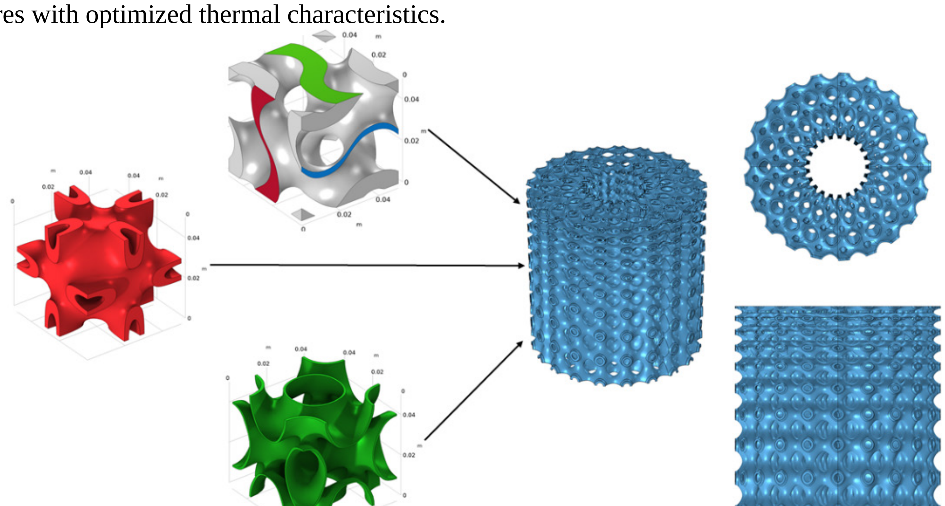

Fig. 1 – RVEs of three TPMS architectures: Gyroid (top), Neovius (middle), and FRD (bottom). These structures are being considered for the design of a generic cylindrical component (right). This study aims to provide a rigorous framework for selecting the optimal TPMS architecture for this application.

Funding: The authors acknowledge support for this work by the Office of Naval Research through the Naval Research Laboratory's core funding.

References:

[1] Apetre, N. A., Michopoulos, J. G., Iliopoulos, A. P., Steuben, J. C., Rodriguez, S. N., Graber, B. D., & Kittur, M. (2024, August). Graded Minimal Surface Periodic Structures for Multiphysics Metamaterial Applications. In International Design Engineering Technical Conferences and Computers and Information in Engineering Conference (Vol. 88346, p. V02AT02A012). American Society of Mechanical Engineers.

The Concept of Engineered Anisotropic Material for RF and Microwave Applications

Quang Nguyen[1*], Theodore Anthony[1], and Amir Zaghloul[1]
[1]DEVCOM Army Research Laboratory, 2800 Power Mill Rd, Adelphi, MD 20783
** quang.m.nguyen7.civ@army.mil*
Keywords: Anisotropic material, cylinder, inclusions

We propose a concept for customizing engineered anisotropic materials for the next generation of antennas and radio frequency (RF) devices. By suspending cylindrical metallic inclusions within a host dielectric substrate, controlling aspect ratio, and aligning to the internal electric field, we generate controlled values of anisotropic permittivity. Simulations and measured data confirm that aligning the inclusions with the electric field yields the highest permittivity and vice versa. Thus, one tunes the permittivity by either rotating the inclusion with respect to the electric field and/or adjusting the aspect ratio.

Typical electromagnetic materials used in the design of RF devices are isotropic dielectric materials. The permittivity is the same in all Cartesian directions and remains independent of any electric field. The characteristics of the subsequent RF device will mainly depend on the design of resonant and bandwidth limited metallic elements. Isotropic dielectric materials provide limited degrees of freedom in optimizing the performance of such a device and mainly act as structural support whose value of permittivity has a limited effect on the device impedance. The value of permittivity is usually restricted to those provided by a small number of available COTS materials. We introduce the concept of engineered anisotropic dielectrics with custom permittivity values that differ based on alignment with an internal E-field. In an anisotropic dielectric material, we define the permittivity by a second order tensor of x, y and z vectors that depend on the orientation of the electric field through the material. The ability to create a custom permittivity profile with respect to direction and frequency enables a new class of engineered materials that provide more degrees of freedom in designing RF and microwave components.

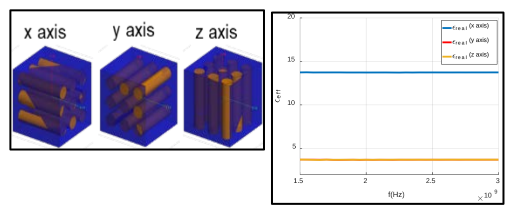

Fig. 1 – Unit cell of the proposal anisotropic materials and their simulation results.

In our past work, we demonstrated there is a considerable difference in dielectric constant with respect to orthogonal axes when anisotropy is present in the medium [1]. However, conventional effective medium theory doesn't accurately account for this anisotropic effect and yields diminished results. Therefore, we need to enforce the anisotropy in the medium and utilize full wave simulations to accurately predict the behavior of the material. We achieve the anisotropic effect by embedding cylindrical metallic inclusions with a certain aspect ratio and aligning their length in certain directions. The inclusion size determines the cutoff frequency of the anisotropic effect. The aspect ratio of the inclusion determines the range of the permittivity values when the electric field is parallel or perpendicular to the material.

We validate our designs via a full-wave numerical simulation. We enforce 2D periodic boundary conditions (PBC) to model the material. The PBC feature enables us to simulate a single unit cell element which greatly reduces the computational resources needed to run the simulations. Typically, the periodic boundary approximation yields accurate predictions as long as the unit cell is less than 0.1 wavelengths in size. To model the anisotropic material, we use the unit cells arranged in 2D cylindrical lattices depicted in Fig. 1. The host material has a dielectric constant of 2.2. The individual cylinders are assumed to be perfect electric conductors (PEC) with a diameter and a length of 0.2 mm and 0.9 mm, respectively. The center spacing between cylinders is 0.3 mm. We impinge the unit cell with a transverse electric field (TE-field) oriented to the x-axis of the substrate propagating along the z-axis. As depicted in Fig. 1, when he E-field is parallel to the length of the cylinders oriented along the x-axis, we achieve the maximum effective permittivity (ε_{eff}). In contrast, when the TE-field is oriented perpendicular to the cylinders along the y or z axes, we achieve the minimum effective permittivity (ε_{eff}). In other words, we tune the dielectric constant by rotating the inclusion with respect to the electric field. We detail more aspects of this work in reference [2].

References:

[1] Mitchell, G., Nguyen, Q.M. and Anthony, T.K., 2020, March. Simulation of effective medium theory for additive manufacturing of dielectric media. In 2020 14th European Conference on Antennas and Propagation (EuCAP) (pp. 1-2). IEEE.

[2] Nguyen, Q.M, Zaghloul, A.I. and Adler, E.D., 2024. Design of Inhomogeneous Surface using Engineered Anisotropic Material for Army Platforms, In 2024 MSS Tri-Service Radar Symposium (TSRS).

Resonant Cavity Interband Cascade Light Emitting Devices with High Spectral Intensity and High Radiance

J. A. Massengale[1,*], C. Iversen[2], C. S. Kim[3], M. Kim[4], C. L. Canedy[3], I. Vurgaftman[3], V. Jayaraman[2], and J. R. Meyer[3]

[1]*NRC post-doctoral research associate residing at NRL*

[2]*Praevium Research, 601 Pine Avenue, Suite C, Goleta CA 93117*

[3]*Naval Research Laboratory, Washington, DC 20375*

[4]*Amentum, 7740 Milestone Parkway, Suite 150, Hanover MD 21076*

**Corresponding Author Email:* jeremy.a.massengale.ctr@us.navy.mil

Keywords: Midwave infrared, light emitting device, resonant cavity

Interband cascade light emitting devices (ICLEDs) [1,2] employ the same active stages stacked in series as interband cascade lasers (ICLs) [3], but without an optical cavity that could provide sufficiently strong feedback for lasing. Although the spectral bandwidth of an ICLED emitting in the midwave infrared (MWIR) is $\delta\lambda \approx 0.5$-$1.5$ μm (70-100 meV), the spectral intensity can be narrowed substantially by placing the emission region within a resonant cavity [4]. Here we report resonant cavity LEDs (RCLEDs) that produce the highest spectral intensities ever reported for LEDs emitting at $\lambda > 3$ μm. These sources are well suited for applications in chemical sensing.

The ICLED wafer was grown at NRL with 10 active stages designed for peak emission near 4.5 μm. Praevium collaborators bonded the chip to a 33-period GaAs/AlGaAs distributed Bragg reflector (DBR), and then deposited a single period Ge/SiO_2 DBR on top. Although the yield was limited, with some device variability, multiple RCLEDs displayed extremely high performance. Fig. 1 shows the light-current-voltage characteristics (a) and emission spectrum (b) for Device A (measured at Praevium) with mesa diameter D = 200 μm. For example, at 300 K the continuous wave output from Device A with was 0.67 mW, while that for Device B (D = 140 μm, measured at NRL) was 1.3 mW. Assuming Lambertian angular distributions of the emission, these correspond to radiances of 0.68 and 2.7 W/cm^{2}sr, respectively, as compared to the highest value of 1.2 W/cm^{2}sr reported elsewhere from an MWIR LED with unprocessed output surface [5]. The spectral linewidths for Devices A and B were only 30 nm and 41 nm, respectively. These are the narrowest reported for MWIR RCLEDs, and correspond to spectral intensities of 39 and 72 mW/cm^{2}nm, respectively. The highest previous value was 7 mW/cm^{2}nm [6].

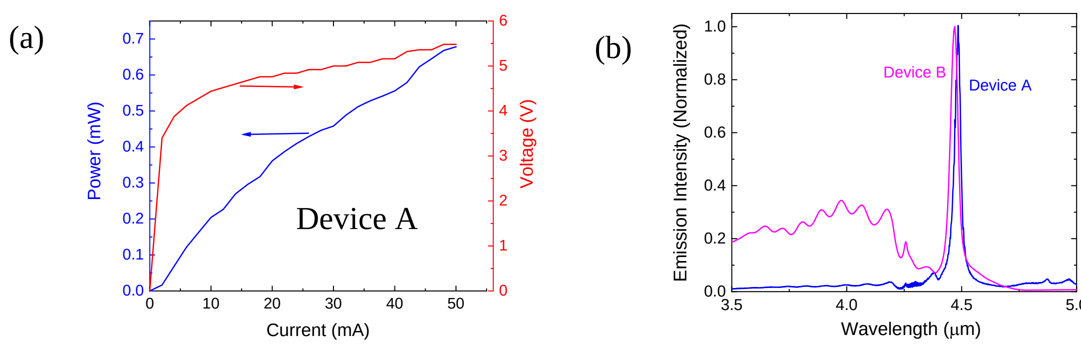

Fig. 1(a) – Light-Current-Voltage properties of Device A; (b) Emission spectra of both devices.

Funding: This work was supported by Navy SBIR Contract No. N6833524C0298

References:

[1] C. S. Kim, W. W. Bewley, C. D. Merritt, C. L. Canedy, M. V. Warren, I. Vurgaftman, J. R. Meyer, and M. Kim, "Improved Mid-Infrared Interband Cascade Light Emitting Devices," *Opt. Engr.* **57**, 011002 (2018).

[2] N. Schäfer, J. Scheuermann, R. Weih, J. Koeth, and S. Höfling, "High efficiency mid-infrared interband cascade LEDs grown on low absorbing substrates emitting >5 mW of output power," *Opt. Engr.* **58**, 117106 (2019).

[3] J. R. Meyer, W. W. Bewley, C. L. Canedy, C. S. Kim, M. Kim, C. D. Merritt, and I. Vurgaftman, "The Interband Cascade Laser,"*Photonics* **7**, 75 (2020).

[4] A Krier, V V Sherstnev and H H Gao, "A novel LED module for the detection of H2S at 3.8 μm," *J. Phys. D.* **33** (2000).

[5] K. N. Schrock, D. A. Montealegre, W. Dai, M. Z. Bellus, L. M. Nichols, and J. P. Prineas, "Microcavity enhancement vs Auger recombination in variable thickness type-II superlattices in resonant cavity mid-infrared light emitting diodes, *J. Appl. Phys.* **135**, 183101 (2024).

[6] N. Schäfer, R. Weih, J. Scheuermann, F. Rothmayr, J. Koeth, and S. Höfling, "Wavelength tuning in resonant cavity interband cascade light emitting diodes (RCICLEDs) via post growth cavity length adjustment," *Sensors* **24**, 3843 (2024).

Spatial Uniformity of Geiger and Linear Mode Response in SiC Ultraviolet Avalanche Photodetectors

Daniel B. Habersat[1], David Liu[2], Franklin Nouketcha[1], Joshua C. Bienfang[3], Gregory A. Garrett[1], Jonathan Schuster[1], Michael A. Derenge[1], Brenda VanMil[1], Michael Wraback[1], Enrico Bellotti[2], Reza Ghandi[4], Mehrnegar Aghayan[4], and Anand V. Sampath[1]

[1]*DEVCOM Army Research Laboratory Adelphi, MD 20783*

[2]*Boston University, Boston, MA 02215, USA*

[3]*National Institute for Standards and Technology, Gaithersburg, MD 20899, USA*

[4]*GE Aerospace Research, Niskayuna, NY 12309, US*

**Corresponding Author Email: daniel.b.habersat.civ@army.mil*

Keywords: avalanche, photodiode, spatial uniformity, single photon, UV detector

A range of Department of Defense applications require ultraviolet single-photon avalanche detectors (UV SPAD) that are low cost, size, weight, and power as well as resilient to shock, high temperatures, and stray magnetic fields. SiC is attractive for UV SPADs as it is inherently blind to visible light, and both high-gain linear-mode and Geiger mode devices have been demonstrated. In this paper, we examine the spatial uniformity of the linear and Geiger mode response of 4H-SiC UV SPADs as a function of crystal axes orientation and the impact of device size and design. The measured responsivity in circular p-i-n diodes is observed to be uniform at unity-gain and degrades as the gain is increased to above 1000 where the response is dominated by localized hot-spots. However, rectangular mesas elucidate how the spatial non-uniformity of the response in rectangular diodes is highly directional, with significantly less variation observed along the [1-100] as compared to the [11-20] direction. In contrast to linear-mode, the spatial uniformity of the Geiger mode response of similar devices is observed to be initially narrowly localized to one side at low excess bias while spreading out with increased bias. The origins of this spatial non-uniformity are explored using TCAD modelling to understand the role of epitaxial growth variation and using full-band, three-dimensional Monte-Carlo modelling[1] (FBMC3D) to examine the effects of anisotropic impact ionization and substrate miscut. Initial FBMC3D results indicate that miscut angle in the substrate alters the average gain value, suggesting a role for these effects in causing spatially non-uniform responsivity across devices.

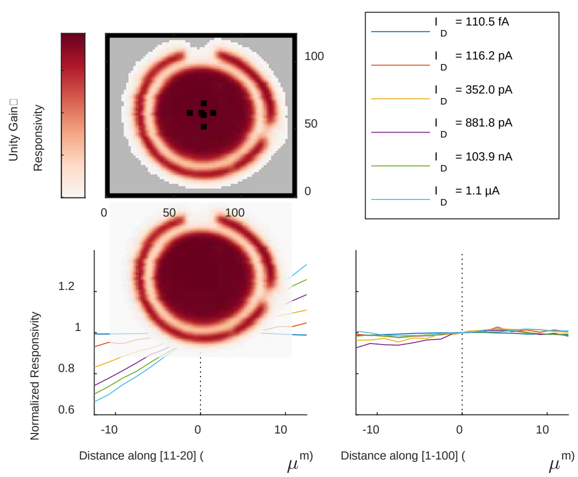

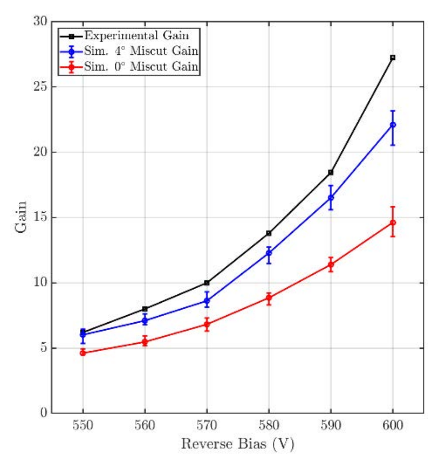

Fig. 1(left) – Spatial map of responsivity for a circular device at unity gain (top left), along with line scans through the center of the device in both the [11-20] and the [11-00] directions at increasing dark current levels (below). By the time dark current has multiplied by at least 10^6, a large linear gradient develops along [11-20] but not along [1-100]. Fig. 2(right) – Comparison of simulated and experimental gain versus bias characteristics showing how substrate miscut changes the average gain produced for a given bias. Data taken from [2].

References:

[1] Prigozhin, Ilya, Stefano Dominici, and Enrico Bellotti. "Fbmc3d—a large-scale 3-d monte carlo simulation tool for modern electronic devices." *IEEE Transactions on Electron Devices* 68.1 (2020): 279-287.

[2] W. S. Loh et al., "Impact Ionization Coefficients in 4H-SiC." *IEEE Transactions on Electron Devices* 55.8 (2008): 1984-1990.

Power Scaling and Nonlinear Suppression in Pulsed 2 µm Fiber Lasers

Joel M. Solomon[1,*], Adrian Nordstrom[2], Meint Agena[1], Colin C. Baker[3], Brian Anderson[1], and Angel Flores[1]

[1]Air Force Research Laboratory, Directed Energy Directorate, 3550 Aberdeen Ave, Kirtland AFB, NM 87117

[2]Texas A&M University, 400 Bizzell St, College Station, TX 77843

[3]Naval Research Laboratory, 4550 Overlook Ave SW, Washington DC 20375

**Corresponding Author Email: joel.solomon.2@us.af.mil*

Keywords: pulsed fiber lasers, nanosecond pulses, thulium, phase modulation

A 1.95 µm high-energy nanosecond thulium-doped all-fiber amplifier is demonstrated producing multi-mJ pulses. Phase modulation, pulse shaping, and novel extra-large mode area fibers were explored to mitigate nonlinear effects.

High power lasers operating between 1.9 to 2.1 µm evolved rapidly over the past decade and are expected to have a vast impact for future industrial, medical, and Directed Energy applications. Notably, recent advancements in high power and high energy 2 µm fiber lasers [1,2] have expanded interest within the remote sensing community. These fiber lasers offer several advantages over conventional solid-state lasers including improved size, weight, and power (SWaP), beam quality, and efficiencies. Moreover, 2 µm fiber lasers demonstrate improved nonlinear performance, eye-safety, and atmospheric transmission compared to their 1 µm counterparts. Pulsed fiber lasers also enable unprecedented temporal agility with variable pulse shapes, pulse widths, and repetition rates that span several orders of magnitude.

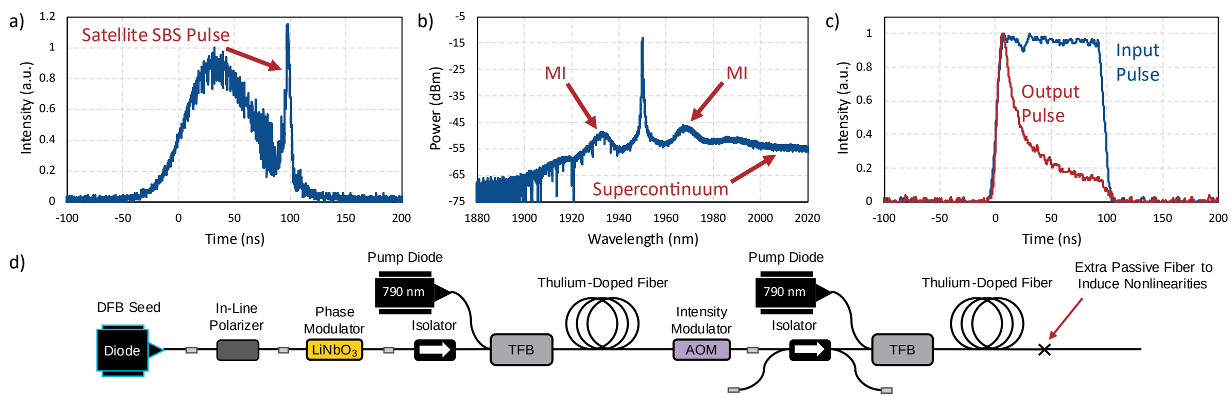

Fig. 1 – (a) Satellite pulse due to stimulated Brillouin scattering. (b) Spectral degradation due to modulation instability. (c) Amplified output pulse distortion due to gain saturation. (d) Schematic of the nanosecond thulium-doped all-fiber amplifier incorporating phase modulation and arbitrary pulse shaping.

Although 2 µm fiber lasers offer improved nonlinear performance compared to prevalent 1 µm systems, the high peak intensities of pulsed fiber lasers can trigger nonlinearities such as stimulated Brillouin scattering (SBS) and modulation instability (MI) as shown in Fig. 1a and 1b, respectively. Moreover, the inherent small core diameters of commercial off-the-shelf (COTS) fibers lead to modest saturation energies and pulse distortion (Fig. 1c). Scaling to high peak powers and energies requires balancing the optical spectrum to attain broader linewidths that can mitigate SBS, maintain coherence, and limit MI. Simultaneously, pulse distortion must be managed to limit both SBS and MI. Towards that end, this work explores phase modulation techniques, predictive pulse shaping, and novel extra-large mode area fibers to mitigate nonlinear effects and scale to multi-mJ energies from a single fiber at 1.95 µm.

Funding: SMART SEED Grant, Chief Scientist Office Innovation Award

References:

[1] J. M. Solomon, B. Anderson, C. C. Baker, D. Rhonehouse, J. Sanghera, and A. Flores. "High-Energy, Narrow-Linewidth Thulium-Doped All-Fiber Amplifier With Active Pulse Shaping." Laser Congress 2023 (ASSL, LAC). Optica Publishing Group, ATh4A.3, 2023.

[2] B. Anderson, J. Solomon, and A. Flores. "1.1 kW, beam-combinable thulium doped all-fiber amplifier." Proc. SPIE 11665, Fiber Lasers XVIII: Technology and Systems. 2021. 116650B.

Plasmonic Semiconductor Nanocrystal Enhanced Random Lasing

Jason E. Kuszynski[1,*]
[1]U.S. Army Space and Missile Defense Command, Redstone Arsenal, Huntsville, AL 35898
**Corresponding Author Email: jason.e.kuszynski.civ@army.mil*
Keywords: "quantum dots, plasmonic, semiconductor, nanocrystals, materials, random lasing".

Plasmonic semiconductor nanocrystals (PSNCs) are explored for their capability to enhance the random lasing performance of quantum dots in solution. While noble metal plasmonic enhancement of organic dyes for random lasing have been long explored,[1] there are limited studies on the feasibility of PSNC enhancement of random lasing for organic dyes and quantum dots (QDs). This work hypothesizes that PSNCs are able to successfully reduce lasing threshold and improve the power slope efficiency of random lasing in solution, especially at longer, NIR wavelengths difficult to access with traditional noble metal plasmonic materials. Careful considerations are made towards the size regime of QDs and PSNCs to ensure that PSNCs are large enough to have a high scattering cross-section to initiate random lasing. $CuInSe_2$ and $Cu_{2-x}Se$ are selected as initial QD and PSNC candidates respectively due to their low toxicity, good Herfindahl-Hirschman index, and high spectral overlap of their emission and plasmon absorption.[2,3] Optical absorption, emission, fluence dependence, and lifetime measurements are performed on the individual QD and PSNC batches along with the QD-PSNC mixture. Measurements of the QD-PSNC solution mixtures are experimentally varied as a function of QD and PSNC concentrations to determine the optimal ratio needed to minimize lasing threshold and maximize the power slope efficiency of the random laser system. (USASMDC Release #5042 26MAR2025; Distribution A: Approved for public release; distribution is unlimited.)

Funding: The author wishes to thank and acknowledge funding received by OUSD(R&E) through the DoD SMART SEED Grant in support of this work.

References:

[1] A. S. L. Gomes, A. L. Moura, C. B. de Araújo, and E. P. Raposo, "Recent advances and applications of random lasers and random fiber lasers," *Prog. Quantum Electron.*, vol. 78, pp. 100343, 2021.

[2] D. Dorfs, T. Hartling, K. Miszta, N. C. Bigall, M. R. Kim, A. Genovese, A. Falqui, M. Povia, and L. Manna, "Reversible tunability of the near-infrared valence band plasmon resonance in $Cu_{2-x}Se$ nanocrystals," *J. Am. Chem. Soc.*, vol. 133, no. 29, pp. 11175-11180, 2011.

[3] W. Lian, T. Datao, P. Hu, X. Song, Z. Gong, T. Chen, J. Song, Z. Chen, and X. Chen, "Broadband excitable NIR-II luminescent nano-bioprobes based on $CuInSe_2$ quantum dots for the detection of circulating tumor cells." *Nano today*, vol. 35, pp. 100943, 2020.

Inversion and Non-inversion Symmetry in Graphene and Tungsten Diselenide

Latha Nataraj[1, *], Trenton R. Ensley[2], Shashi P. Karna[1]

[1] *DEVCOM Army Research Laboratory, Aberdeen Proving Ground, MD 21005*
[2] *DEVCOM Army Research Laboratory, Adelphi, MD 20783*
**latha.nataraj.civ@army.mil*

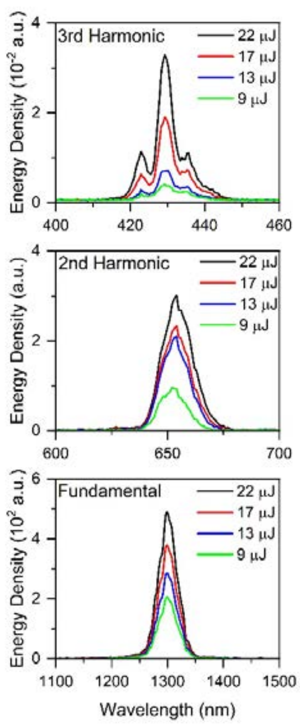

Fig. 1: Second and third order harmonic spectra of monolayer graphene at an excitation wavelength of 1300 nm for varying input energies.

Two dimensional (2D) materials have garnered significant attention over recent decades for photonic applications as they exhibit extraordinary electronic and optical properties vastly different from their bulk counterparts due to the atomic layer thickness and high compatibility with other photonic structures. The carrier density in 2D materials can be tuned using electrical or optical means, which results in the modification of physical properties and optical responses allowing responses over a wide spectral range (UV – mid-wave IR) [1, 2], strong light-matter interaction, and optical nonlinearity [3,4]. These materials hold great promise for several photonic applications such as optical modulation, sensing, photodetection, frequency conversion, ultrafast pulse generation, terahertz wave generation, and optical switching.

Fig. 1 shows the energy-dependence of the 2nd and 3rd harmonics of a 1300 nm input beam in monolayer graphene deposited on a fused silica substrate. Graphene and transition-metal dichalcogenides, such as MoX_2 (X=S, Se) and WX_2 (X=S, Se) are among 2D materials which have been extensively studied for their linear and NLO responses and optical modulation that controls the intensity, phase, or polarization of a light beam passing through these ultrathin materials [5-8]. In this work, we expand upon previous findings and report our experimental results of inversion symmetry and non-inversion symmetry in monolayer graphene and WSe_2. The even- and odd-order harmonics of WSe_2 and monolayer graphene are studied with varied excitation wavelengths spanning the short-wave and mid-wave IR for different input energies and polarization angles. Details of the experiments including metrology, spectroscopy, and NLO properties and the results for graphene and WSe_2 will be presented.

Acknowledgements

This work was performed in support of the Classical-Quantum Hybrid Constructs Applied Research for Science and Technology Priorities.

References

[1] Wang, G. et al. Colloquium: Excitons in atomically thin transition metal dichalcogenides. Rev. Mod. Phys. **90**, 21001 (2018)
[2] Wang, R. et al. Third-harmonic generation in ultrathin films of MoS2. ACS Appl. Mater. Interfaces **6**, 314–318 (2014)
[3] Mak, K. F. & Shan, J. Photonics and optoelectronics of 2D semiconductor transition metal dichalcogenides. Nat. Photonics **10**, 216–226 (2016)
[4] Autere, A. et al. Nonlinear Optics with 2D Layered Materials. Adv. Mater. 1705963 (2018)
[5] Li, D. et al. Multimodal Nonlinear Optical Imaging of MoS2 and MoS2-Based van der Waals Heterostructures. ACS Nano **10**, 3766–3775 (2016)
[6] Rosa, H. G. et al. Second-Harmonic Spectroscopy for Defects Engineering Monitoring in Transition Metal Dichalcogenides. Adv. Opt. Mater. (2018)
[7] Liu, H. et al. Fluorescence Concentric Triangles: A Case of Chemical Heterogeneity in WS2 Atomic Monolayer. Nano Lett. **16**, 5559–5567 (2016)
[8] Yu, H., Talukdar, D., Xu, W., Khurgin, J. B. & Xiong, Q. Charge-Induced Second-Harmonic Generation in Bilayer WSe2. Nano Lett. **15**, 5653–5657 (2015)
[9] Rosa, H.G., Ho, Y.W., Verzhbitskiy, I. *et al.* Characterization of the second- and third-harmonic optical susceptibilities of atomically thin tungsten diselenide. *Sci Rep* **8**, 10035 (2018)

Optimization of Vertical Hole Mobility in LWIR Type II Superlattices Through High-Fidelity Semiconductor Modeling

Jonathan Schuster[1,2], John Glennon[3], Jagmohan Bajaj[2], Enrico Bellotti[1,3]

1- DEVCOM Army Research Laboratory (ARL), 2800 Powder Mill Road, Adelphi, MD 20783
2 - Boston University, Dept. of Electrical & Computer Eng., 8 St. Mary's Street, Boston, MA 02215
3 - Boston University, Division of Material Science & Eng., 15 St. Mary's Street, Boston, MA 02215

Keywords: infrared detectors, type II superlattice (T2SL), LWIR quantum efficiency, hole mobility, Center for Semiconductor Modeling (CSM), numerical simulations, non-equilibrium Green's function (NEGF).

We have identified T2SL structures with high mobility in the presence of disorder and found several promising structures with diffusion lengths much greater than typical absorber thicknesses.

Despite significant success in InAs/InAsSb mid-wave infrared (MWIR) type II superlattice (T2SL) infrared (IR) focal plane arrays (FPAs), long-wave infrared (LWIR) T2SL IR FPAs continue to suffer from low quantum efficiency (QE) due to short minority carrier diffusion length that limits holes collection efficiency. Conventional simulation approaches used to analyze T2SL devices are semi-classical models and consequently do not include the relevant transport physics. The Center for Semiconductor Modeling of Materials and Devices (CSM), established by DEVCOM ARL to understand fundamental and technological limitations of semiconductor material synthesis, device operation and design controllable parameters, has developed a fully quantum mechanical non-equilibrium Green's function (NEGF) model that is able to accurately replicate the transport in real T2SL devices. The CSM used the NEGF model to predict the temperature dependence of the hole mobility in InAs/InAsSb T2SLs and validated the model against measured data. Through modeling, it was confirmed that the hole transport is due to hopping and sequential tunneling, and that hole mobility decreases with decreasing temperature[1]. This effort fulfills the CSM goals to focus on areas with known knowledge gaps and develop physics-based models that predict material and device performance. To overcome the holes transport limitations, and to predict structures with optimized performance, the CSM has utilized superlattice electronic structure analysis, NEGF transport models, and machine learning algorithms to explore alternative T2SL configurations more efficiently. Leveraging the machine-learning predictive capability, the CSM searched for new LWIR T2SL structures optimized for enhanced hole transport in the vertical direction based on the conductivity hole effective mass calculated from the band structure. Enhanced hole transport was then confirmed via subsequent NEGF calculations. Specifically, we performed an extensive investigation over various substrate lattice constants ranging from GaSb to InSb, searching for superlattice structures with high mobility in the presence of T2SL disorder and found several promising structures with diffusion lengths much greater than typical absorber thicknesses (*i.e.* high LWIR QE) that warrant further investigation.

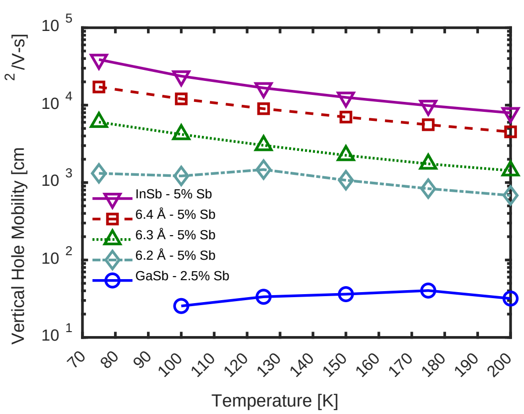

Fig. 1 – Predicted vertical hole mobility as a function of temperature and substrate lattice constant.

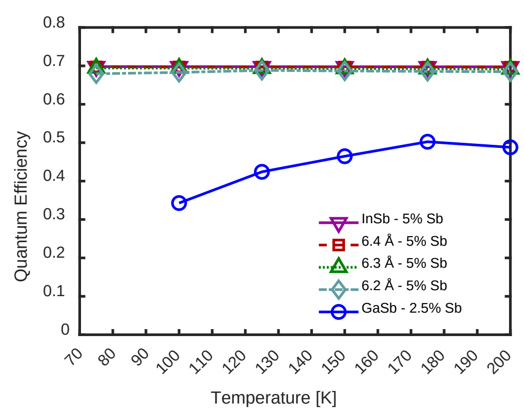

Fig. 2 – Calculated quantum efficiency for the new T2SL structures.

Funding: Boston University was funded through grant W911NF-23-2-0090.

References:

[1] Bellotti, E., Bertazzi, F., Tibaldi, A., Schuster, J., Bajaj, J., and Reed, M., "Disorder-induced degradation of vertical carrier transport in strain-balanced antimony-based superlattices," Phys. Rev. Appl. 16, 054028 (Nov 2021)

Tunable Optical Filtering Using Porous Silicon

Mari-Therese Burton[1,*], David Lunking[1], Ofure Osunbor[1,2], and Aaron Henson[1]
[1]DEVCOM Army Research Laboratory, 2800 Powder Mill Road, Adelphi, MD 20783
[2]University of Maryland, College Park, MD 20742
**Corresponding Author Email: Mari-Therese.S.Burton.civ@army.mil*
Keywords: porous silicon, optics, photonics, electrochemistry, photovoltaics

Etched porous silicon structures have attracted research interest for their unique properties, including the ability to alter the way in which silicon interacts with incident light using common cleanroom and laboratory processes. The resulting porosity, and therefore properties such as refractive index, are highly dependent on the etch conditions, so the experimental conditions can be tuned to produce a set of desired optical properties. This can be used for a variety of optical applications, such as filters on photovoltaic cells for temperature control and mid-infrared range gas sensors [1, 2].

In this work, porous structures are etched into bulk single crystal silicon to investigate the tunability of optical bandpass filters using two etching techniques: metal assisted chemical etching (MACE) and anodic etching of chirped gratings. The pore size created by MACE is directly related to the feature size of metal patterned onto the surface of the silicon, as this metal pattern acts as a catalyst in the oxidation and local dissolution of silicon. Fig. 1 shows the resulting surface structure of a sample etched using MACE, where the square pores were etched underneath an array of Pt squares that was deposited on the surface. The pore sizes can easily be varied to absorb a specific set of wavelengths; those shown in Fig. 1 were designed to block near infrared transmission. Fig. 2 displays the transmitted intensity as a function of wavelength through unetched silicon, the etched silicon from Fig. 1, and an opaque metal reference, demonstrating the efficacy of the MACE-etched pores at blocking the desired wavelength range. Similarly, anodically etching with a sinusoidal variation in current density creates layers of different porosity to produce a chirped grating. This essentially acts as a band-pass filter due to destructive interference between reflections at the interfaces between layers.

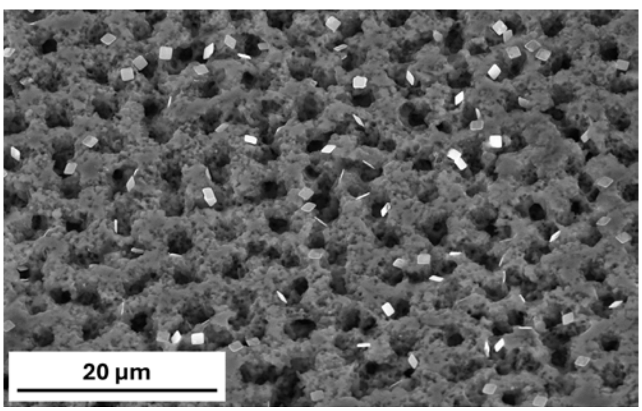

Fig. 1 - Secondary electron SEM image of micron-scale pores in Si created using MACE

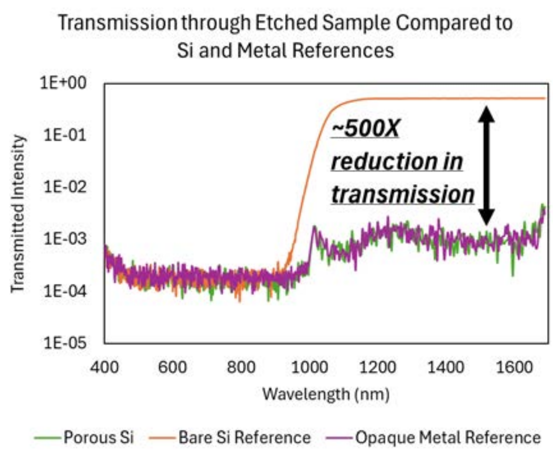

Fig. 2 - Transmission spectra through the porous Si from Fig. 1 compared to unetched, bare Si and opaque metal references

References:

[1] Almarzooqi, N. K, et al. "Experimental investigation of the effect of optical filters on the performance of the solar photovoltaic system," Energy Rep, vol 9, no. 3, May 2023, pp. 336-344

[2] Meziani, S, et al. "Volume detection based on porous silicon waveguide for CO_2 mid-infrared spectroscopy," Opt. Express, vol. 32, no. 8, 2024, pp. 13628-13639.

13. Topic: Social Sciences

13.1 Session: Developing Leadership for Warrior Ethos: Greater Readiness and Lethality

Understanding Identities and their Impact on Learning and Performance

Kimberly M. Wingert[1,*], Madison Romero[2]
[1]*Foundational Science Research Unit, Army Research Institute, 6000 6th St., Fort Belvoir, VA 22060*
[2]*Consortium of Universities of the Washington Metropolitan Area, 1020 19th St., NW, Ste 500, Washington, DC 20036*
**Corresponding Author Email: kimberly.m.wingert.civ@army.mil*
Keywords: leader identities, impostorism, identity-based motivation, learning

The Army develops its personnel throughout the course of their career. These personnel need to be prepared for, adapt to, and maintain readiness and lethality in a complex and uncertain future operating environment. Soldiers must be developed in ways that prepare them for varied scenarios and trained in ways that enable transfer and adaptability in responding to future needs. The goal of the formal and informal learning and development focal area in the U.S. Army Research Institute's Basic Research Program is to understand, support, and optimize learning and development of Soldiers and leaders. By understanding the identities that Soldiers and leaders endorse, it may be possible to leverage that information to develop Soldiers and leaders who are efficient, lifelong, motivated learners who are capable of meeting challenges in the face of uncertainty. Across four projects within this focal area, we aim to understand the identities that Soldiers and leaders endorse and evaluate the impact that these identities have on learning and performance. Project 1 moves beyond asking whether Army leaders identify as a leader and instead asks how they identify as a leader. Shaughnessy and Coats [1] found that Army leaders may endorse a number of different leader identities and these identities vary in terms of the underlying motivations that drive leader behavior. Project 2 aims to understand the development of leader identities with a focus on management of identity threats and leader impostorism. Initial findings have indicated that leader experiences predict both the cognitive and affective components of leader impostorism and that these different components of leader impostorism uniquely predict leader identity threat, which may impact the value that people attribute to their leader identity [2]. Project 3 seeks to understand how future-focused possible identities, the strategies that Soldiers establish to achieve those identities, the sense of connection that they feel to their future self, and their metacognitive experience of difficulty (collectively, identity-based motivation) [3] contribute to individual and team processes and outcomes. This project further aims to evaluate how identity-based motivation is disseminated from leaders to members of their team and whether there are differences as a function of the leader identity their leader endorses. Project 4 focuses on why one component of identity-based motivation, the metacognitive experience of difficulty, is related to the capacity to learn. Results indicated that interpretations of cognitive experience underlie the difficulty mindsets that people endorse, and this has an impact on the capacity to learn. Collectively, these projects highlight several ways that identities and experiences might be leveraged to create ready, motivated, and resilient learners capable of responding and adapting to future needs in ways that maintain lethality in the future operating environment.

Disclaimer: The research described herein was sponsored by the U.S. Army Research Institute for the Behavioral and Social Sciences, Department of the Army (Grant No. W911NF-23-1-0023; Cooperative Agreement No. W911NF-16-2-0092). The views expressed in this presentation are those of the author and do not reflect the official policy or position of the Department of the Army, DOD, or the U.S. Government.

References:

[1] S. P. Shaughnessy & M. R. Coats, "Leaders are complex: Expanding our understanding of leader identity," in *What's Wrong with Leadership?*, 1st ed. Routledge, 2018, pp. 173-188.

[2] S. Braun, grant # W911NF-23-1-0023

[3] D. Oyserman & L. James, "Possible Identities," in *Handbook of identity theory and research*. New York, U.S.: Springer, 2011, ch. 6, pp. 117-145.

Expanding the Theoretical Reach of Honor: An Interdisciplinary Approach

Peter Wang[1,*]

[1]*U.S. Army Research Institute for the Behavioral and Social Sciences, 6000 6th Street, BLDG 1464, Fort Belvoir, VA 22026-5610*

**Corresponding Author Email: peter.p.wang.civ@army.mil*

Keywords: Values, morality, culture, competition, respect

Existing psychological theories of honor focus on reputational threat and cannot account for behaviors in known honor-based groups, including military communities. Reports across disciplines, including sociology, anthropology, and philosophy, reveal a wide array of values that are seen as honorable, as well as common principles that explain heterogeneity in honor values [1,2,3]. We synthesize current knowledge from these fields and psychology to produce a working theory of honor that explains cross-cultural variation in honor values while maintaining a consistent underlying logic. Honor operates by attributing action to character qualities, imbuing them with implications for personal worth based on group values, narratives, and contextual factors that frame the interpretation of behavior (Fig. 1). As such, honor is tied to identity and authenticity concerns. Honor systems rely on this logic to incentivize adherence to group values. Even within a group, there may be substantial heterogeneity in perceptions of honor, as people interpret social situations differently and use different strategies to maintain honor. By defining personal worth in terms of group standards, honor regulates the balance between autonomy and adherence to values, inspiring individuals to meet group expectations while providing space for them to acquire distinction, adapt to context, and flexibly interpret courses of action. Our model may help guide empirical attempts to understand military culture and identity, creating an organizing framework to support efforts to boost unit motivation, decision-making, and overall unit readiness. By inspiring individuals to demonstrate adherence to moral principles, honor may become increasingly important as difficulty, danger, and the consequences of failure increase. The views expressed in this presentation are those of the author and do not reflect the official policy or position of the Department of the Army, DOD, or the U.S. Government.

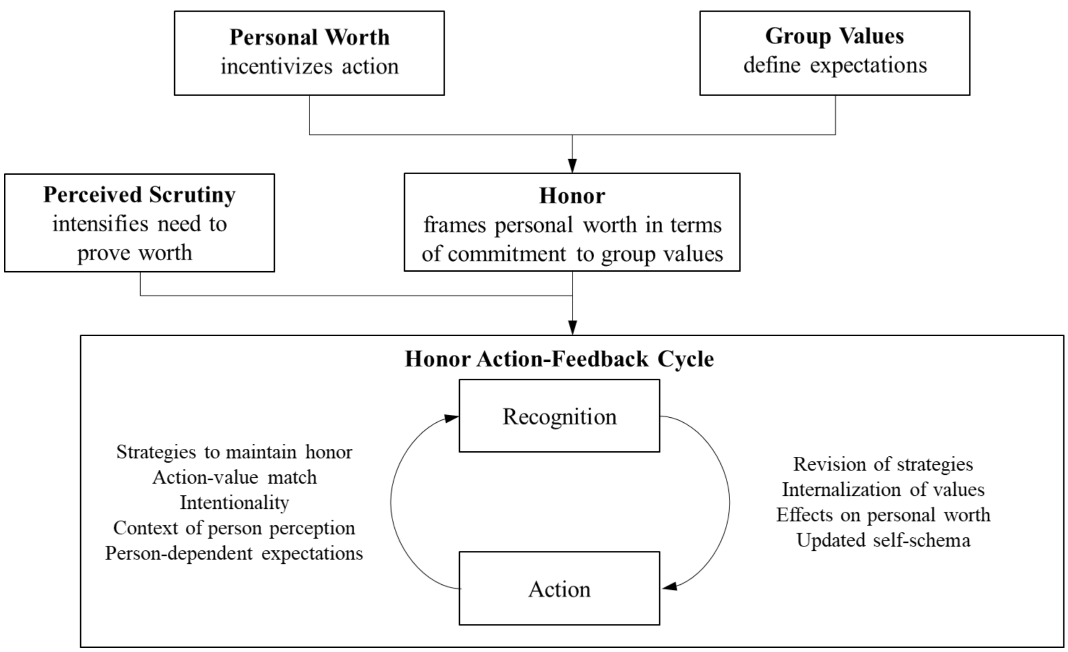

Fig. 1. Honor frames personal worth in terms of commitment to group values, but behavioral effects depend on personal, contextual, and sociocultural factors that determine the meaning of honor at a given moment. Competition amplifies honor behavior by driving up the standards for proof of character and distinction.

References:

[1] J. C. Del Ama, "Honor and public opinion," Hum. Stud., vol. 32, Dec., 2009, pp. 441-460.
[2] E. Ikegami, The Taming of the Samurai: Honorific Individualism and the Making of Modern Japan, 1st ed. Cambridge, MA: Harv. Univ. Press, 1997.
[3] W. Kaufman, "Understanding honor: Beyond the shame/guilt dichotomy," Soc. Theory Pract., vol. 37, no. 4, Oct. 2011, pp. 557-573.

How Teams Experience Leadership Change

Heidi Davis[1*], Stephen Reicher[2], & Alexander P. Wind[3]
[1] *The Consortium of Universities of the Washington Metropolitan Area, 1020 19th Street, NW, Washington, DC*
[2]*University of Saint Andrews, St Mary's Quad, South Street, St Andrews, Fife, Scotland*
[3]*U.S. Army Research Institute for the Behavioral and Social Sciences, 6000 6th Street, BLDG 1464, Fort Belvoir, VA 22060*
**Corresponding Author Email:* heidi.a.davis6.ctr@army.mil
Keywords: Social Identity, Leadership, Teams

Leadership change is a common occurrence in the Army, and if this transition phase does not go well, it can affect unit readiness. Advancing basic research in this area, then, can better ensure units maintain lethality, readiness, and warfighting capabilities during transitionary periods. This project looks at how teams experience leadership change through the lens of social identity theory [1]. Using the Social Identity Model of Leadership [2] and engaged followership [3, 4] we look at how teams adapt when leaders are assigned to a new group. Social identity, a descriptive theory, applies to how all groups behave from those that are novel and brief to complex organizations with a long history. It is the process by which we make choices when in the context of "we" rather than "me".

Social identity theory says that all groups seek positive distinction and will behave in a manner that is relevant to the group concern when the social identity is salient. We will look to other members for social proof when making decisions about what is in the best interest of the group. Conflict if it does arise between groups will occur when members perceive the other group's boundaries as impermeable, unstable, or illegitimate. Put more simply, we feel good about being a part of a group and look to see what aspects of our group make us special. We work toward the wellbeing and prestige of our group. We signal group membership by observing the norms. If a conflict does arise, we will act on behalf of our group's interest. People are more than just one thing, and we all belong to multiple groups and groups within groups. What matters to us in the moment is in part an influence of which group identity is the most salient at the time.

Every member of the U.S. Army is trained extensively on leadership – what it means, how to embody it, and how to make choices that honor that status. We look at the concept of leadership through social identity which says that leaders of groups will often adjust their behaviors based on which group is salient. In this model, leaders are prototypical members of the group, champions of the group, entrepreneurs of that group's identity, and impresarios of that group. Leaders, then, are the best version of the group, are invested in that group's stature, guide the members on what it means to be part of the group, and give structure and organization to the group. Leaders are often assigned to a smaller group within the overall complex organization. This can come with friction as the new leader needs to show that they are *one of us*.

This research project looks at how leaders engage in this process of social identity signaling to gain the trust of group members and utilize their power through the group rather than simply over the group. The U.S. Army engages in social identity signaling in many ways through their values, uniforms, insignia, traditions, rituals, and more. Leaders may ameliorate tension from a new group by signaling their prototypicality, championship, entrepreneurship, and impresarionism of that group's identity. We hope to show how this process of signaling can enhance unit cohesion and group morale allowing units to maintain readiness during critical transitionary periods.

Disclaimer: The research described herein was sponsored by the U.S. Army Research Institute for the Behavioral and Social Sciences, Department of the Army (Cooperative Agreement No. W911NF-16-2-0092). The views expressed in this presentation are those of the author and do not reflect the official policy or position of the Department of the Army, DOD, or the U.S. Government.

References:

[1] H. Tajfel, "Social identity and intergroup behaviour," Social science information, vol. 13, no. 2, pp. 65-93, 1974.
[2] S. A. Haslam and S. Reicher, "Rethinking the psychology of leadership: From personal identity to social identity," Daedalus, vol. 145, no. 3, pp. 21-34, 2016.
[3] S. Reicher and S. A. Haslam, "Engaged leadership and engaged fellowship: Toward a unified analysis if harm-doing and helping," in Doing and helping: Confronting humanity at its worst: Social psychological perspective on genocide, L. Newman Ed. Oxford, GB: Oxford University Press, 2020.
[4] M. E. Birney, S. D. Reicher, and S. A. Haslam, Obedience as Engaged Followership: A Review and Research Agenda. 2024, p. 91.

Potential for Use-inspired Basic Research in the Personnel Sciences to Support Lethality, Readiness, and Warfighting Capabilities

Alexander P. Wind [1,*]

[1]*U.S. Army Research Institute for the Behavioral and Social Sciences, 6000 6th Street, BLDG 1464, Fort Belvoir, VA 22060*

**Corresponding Author Email: alexander.p.wind.civ@army.mil*

Keywords: Pasteur's Quadrant, learning and development, teams science, measurement

The U.S. Army Research Institute for the Behavioral and Social Sciences (ARI) is the Army's lead agency responsible for addressing personnel, organizational, training, and leader development issues by conducting research and development in the behavioral and social sciences. Within ARI, the Basic Research Program serves as a critical link between the military and scientific communities. The mission of the Basic Research Program is to execute foundational research to develop state-of-the-art theory, methods, and models to create the innovative concepts required to support the Army's capabilities and needs related to personnel readiness. The program has impact on contemporary applications by identifying relevant connections and disseminating extant work while also proactively projecting and addressing future needs and gaps in the science. The purpose of this session is to provide an overview the program's conceptualization of use-inspired basic research and to highlight how that model has and will continue to advance the science in support of lethality, readiness, and warfighting capabilities

Historically, 6.1 funds supported basic research on the assumption that applications would be identified at a later point. Stokes upended the model of basic research to argue that foundational scientific gains and potential for application are not sequential endeavors, but rather two important early considerations [1]. Stokes designated this dual-objective approach as Pasteur's Quadrant named for Louis Pasteur whose foundational work in chemistry and microbiology was in response to specific societal needs and facilitated rapid breakthroughs in broad areas in public health and well-being. The ARI Basic Research Program has utilized a use-inspired framework (Fig. 1) to execute foundational research in the personnel sciences directed toward future applications. This session will first highlight examples of prior ARI basic research efforts in areas such as learning and development, teams science, and measurement which are impacting current practice.

Fig. 1 – The Army Procurement Process is designed to transition programs from foundational knowledge (6.1) to a tangible capability with specific value to the Army.

For the second part of this session, we will look at the process of developing and updating strategies for basic research. We will discuss resources for projecting the future operational environment, key capabilities the next generation of warfighters could need, and technological and scientific trends with potential impact. We will then discuss how those projections guide identification of tools and processes which, in turn and with knowledge of the relevant scientific areas, leads to development of basic research objectives and strategies in the personnel sciences.

Disclaimer: The views expressed in this presentation are those of the author and do not reflect the official policy or position of the Department of the Army, DOD, or the U.S. Government.

References:

[1] D. E. Stokes, Pasteur's Quadrant, Washington, D.C., United States: Brookings Institution Press, 1997.

Effects of AI Utilization on Unit Workflow Dynamics

Sean M. Fitzhugh[1,*]
[1] DEVCOM Army Research Laboratory, 7101 Mulberry Point Rd., Aberdeen Proving Ground, MD 21005
*Corresponding Author Email: sean.m.fitzhugh2.civ@army.mil
Keywords: human-AI integration, network analysis, group dynamics, big data

Workflows represent the interactions between unit members and the tasks, tools, and resources they utilize. These interactions reflect the structural configurations between unit members and tasks, and form the basis for several emergent properties (e.g., coordination, shared mental models). Autonomous unit members remain sufficiently novel that it is unclear *how* real-world groups tend to incorporate such autonomous agents into their workflows. While prior research has demonstrated *what* autonomous agents do differently from humans, this research examines *how* human-AI units differ from their human-human counterparts.

This research examines 135,081 groups on GitHub, an online platform facilitating collaboration across multiple spatially and temporally separated users. Users perform a variety of actions falling into three categories: productivity, communication, and project management. Each group's workflow is represented as a dynamic network capturing individuals' timestamped interactions with specific actions. As workflow captures interactions between unit members and the tasks they undertake, this relational perspective is ideal for capturing high resolution behavioral dynamics underlying group workflows. In sum, this research captures 12.6 million actions from 978,840 unique users across 135,081 groups, where each group focuses its efforts on a single repository.

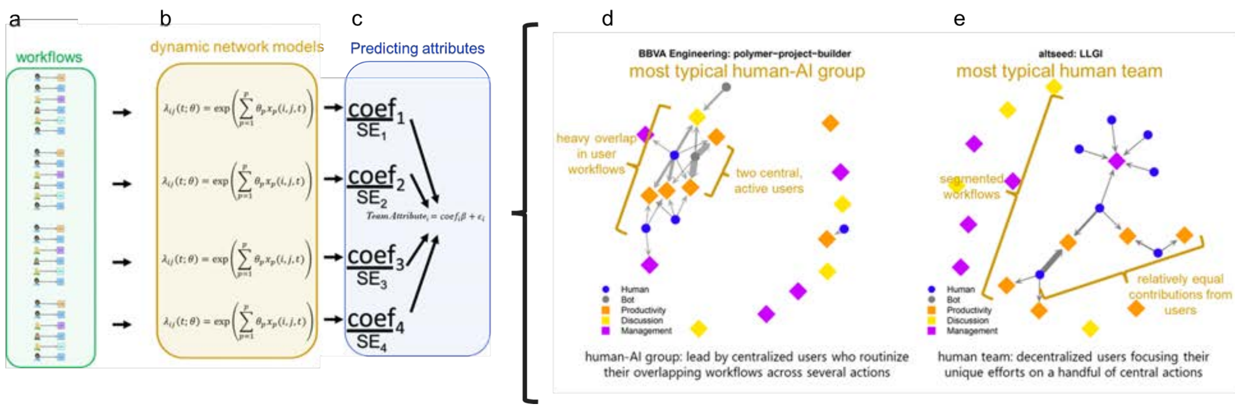

Fig. 1 – a) Each group's workflow is represented as a network of discrete interactions. b)statistical models of these dynamic networks uncover biases in the structure and timing of interactions. c) coefficients from these models are used to predict the presence of AI unit members and the extent of AI utilization. d) the most typical workflow network among human-AI units shows routinized tasking, overlapping workflows, and centralized contributors. e) the most typical human-human unit workflow illustrates a more decentralized, segmented, and equally distributed workflow structure.

A dynamic network model was fit to each workflow network to quantify how individual attributes, network structure, and the timing of prior actions shape the observed workflow. Fitting an identical dynamic network model to each workflow network and comparing standardized coefficients across each model reveals clear differences between human-human units and human-AI units. Results show notable contrasts in how human-human and human-AI units structure their activities. Human-AI unit members routinize their individual workflows but also tend to engage in task switching, together suggesting that individuals focus their workflows on a rotation through a small, core set of activities. Their workflows are also more imbalanced at the individual level, as a small number of users engage in a disproportionate amount of activity. By contrast, human-human units tend to spread their workflows evenly across team members, although they are more narrowly focused on a smaller set of actions. Additionally, their efforts are less driven by prior actions, such as routinization and task-switching. These differences are magnified among units where AI performs a greater proportion of team activity. Beyond workflow structure, human-AI units tended to be larger, more active, and more communicative. This research demonstrates that units utilizing AI adopt fundamentally distinct workflow structures, with critical implications for team properties such as coordination, planning, and trust.

When All-Stars Aren't All That: Changes in Team Member Performance Following Membership Changes

Jordan Epistola[1,3*], Neil G. MacLaren[2] & Changyoon Byun[3]
[1] The Consortium of Universities of the Washington Metropolitan Area, 1020 19th Street, NW, Washington, DC
[2] U.S. Army Research Institute for the Behavioral and Social Sciences, 6000 6th St, Fort Belvoir, VA 22060
[3] Department of Psychology, University of Maryland, 3841 Campus Dr, College Park, MD 20742
**Corresponding Author Email: jordan.j.epistola.ctr@army.mil*
Keywords: Performance Gain, Performance Loss, Effort, Team Dynamics, Basketball, All-Star

Teams are foundational to Army operations, where membership is fluid and personnel frequently transition between roles and team contexts. Understanding how individuals adapt to these changes is essential to maintaining mission readiness and lethality. A key question emerging from the literature is how shifts in team composition affect individual effort and performance. Research suggests that these responses are shaped by two core perceptions: indispensability, or the belief that one's contribution is critical to team success, and social comparison, or the evaluation of one's performance relative to teammates [1, 2]. Changes in team composition can significantly reshape the performance context by influencing perceptions of indispensability and social comparison. These shifts may determine whether individual behaviors comprise effort loss or logical adaptations to new performance contexts [3].

Professional basketball provides a naturalistic environment to explore these dynamics as player roles and performance are visible. All-Star players are both recognized as indispensable to their team's performance and evaluated through social comparison. Changes in teammate composition- such as adding or removing an All-Star player- alters the performance context, potentially shifting perceived indispensability and comparison standards. These shifts offer a natural lens to examine how individual effort and performance adapt in response to team structure. This study examines whether NBA All-Star players adjusted their individual performance in a given season based on changes in team composition from the previous season—specifically, the addition or removal of another All-Star teammate to their team context. NBA regular season game data from 2006–2024 were web scraped from StatHead.com, a comprehensive sports database used for player and team statistics, and then analyzed.

A two-level hierarchical linear model examined how All-Stars adjust their individual performance following changes in All-Star teammate composition. Game observations (Level 1) were nested within Players (Level 2), with teams modeled as a fixed effect. All-Star Gain and Loss were modeled as separate binary predictors. Minutes played were included as a standardized covariate. Two separate performance metrics were examined: Box Plus Minus (BPM), reflecting player efficiency per 100 possessions, and Game Score (GmSc), reflecting cumulative box score totals. All-Star players improved their performance following the removal of an All-Star teammate (BPM: $\beta = 0.06$, $p = .03$; GmSc: $\beta = 0.08$, $p = .00$), while no effects were observed when an All-Star teammate was added.

These findings suggest that shifts in team composition can meaningfully influence the individual performance of high-status athletes. Although mechanisms such as perceived indispensability and social comparison were not directly measured, the observed patterns- including controls for minutes played- align with theoretical expectations. Practically, these results may inform strategies for managing talent and maintaining readiness and lethality. Future work will examine changes in dynamics that occur in response to shifts in team contexts using embedded methods.

Disclaimer: The research described herein was sponsored by the U.S. Army Research Institute for the Behavioral and Social Sciences, Department of the Army (Cooperative Agreement No. W911NF-16-2-0092). The views expressed in this presentation are those of the authors and do not reflect the official policy or position of the Department of the Army, DOD, or the U.S. Government.

References:

[1] C. H. Van Iddekinge, J. D. Arnold, H. Aguinis, J. W. Lang, & F. Lievens. Work effort: A conceptual and meta-analytic review. J. Management, vol. 49, no. 1, pp. 125-157. 2023
[2] A. K. Torka, J. Mazei, & J. Hüffmeier. Together, everyone achieves more—or, less? An interdisciplinary meta-analysis on effort gains and losses in teams. Psychological Bulletin, vol 147, no. 5, p. 504. 2021
[3] D. H. Cymek. Effects of blinded and nonblinded sequential human redundancy on inspection effort and inspection outcome in low prevalence visual search. Scientific Reports, vol. 14, no. 1, 23003. 2024

A Geospatial Data Integration Toolkit for Rapid Resilience Assessment and Resource Planning

Andrew S. Jin[1,*] and Igor Linkov[1]

[1]*Environmental Laboratory, U.S. Army Engineer Research and Development Center, 696 Virginia Road, Concord, MA 01742*

**Corresponding Author Email: Andrew.S.Jin@usace.army.mil*

Keywords: Network science, Resilience, Resource Allocation, Data Management, Decision Science

Resilient infrastructure is crucial for mission assurance. Current resilience assessment methods, however, are often slow, resource-intensive, and retrospective. This project develops a geospatial toolkit for rapid infrastructure resilience assessment and optimized resource distribution during adverse events. The toolkit integrates OpenStreetMap transportation network data with dasymetric weighting and multi-criteria decision analysis (MCDA) to evaluate access to critical infrastructure. This presentation showcases two applications of the toolkit. First, we analyze extreme heat resilience in Southern California by assessing the adequacy of existing cooling centers. Integrating demographic vulnerability data with air conditioning usage derived from smart meter data, we demonstrate how access metrics are affected by air conditioning availability and vulnerability prioritization. Second, we demonstrate the toolkit's ability to track how an installation may be impacted and recover after adverse events like floods. We show that the tool can identify critical bottlenecks access to essential services and identify affected populations. This information informs resource allocation decisions for efficient planning by identifying personnel who may be most impacted by adverse events and prioritizing recovery of key network components.

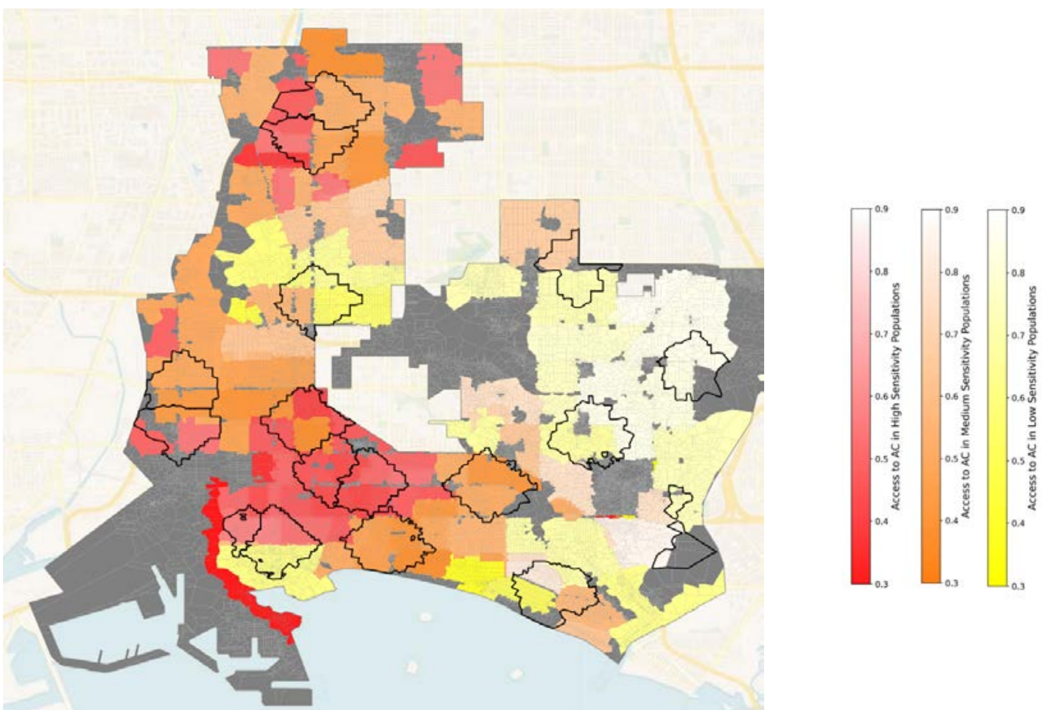

Fig. 1. Map of Long Beach, California with populations specified to the street-intersection level. The catchment areas of cooling centers is highlighted in black circles. Long Beach performs relatively well in Southern California with many cooling centers catching high vulnerability populations with low in-home air-conditioning access.

Funding: This research was funded in part by the United States Department of Defense SMART Scholarship SEED Grant.

Understanding High-dimensional Stochastic Dynamics on Realistic Networks

Kavita Ramanan[1,*]

[1]Division of Applied Mathematics, Brown University
[2], 182 George St, Box F, Boston, MA 02118
**Corresponding Author Email: Kavita_Ramanan@brown.edu*

Keywords: stochastic dynamics, sparse networks, interacting particle systems, mean-field limits

Large collections of randomly evolving particles that interact locally with respect to an underlying network model a variety of phenomena arising in engineering, operations research and the sciences. Due to their high-dimensional nature, these systems are typically intractable to analyze exactly. Classical work, falling under the rubric of mean—field approximations, has mostly focused on the case when this interaction graph is dense. However, most real-world networks are sparse and often random. We describe a new approach, which we refer to as local-field theory, to developing principled approximations for dynamics on realistic networks that beats the curse of dimensionality, and illustrate its efficacy on specific models.

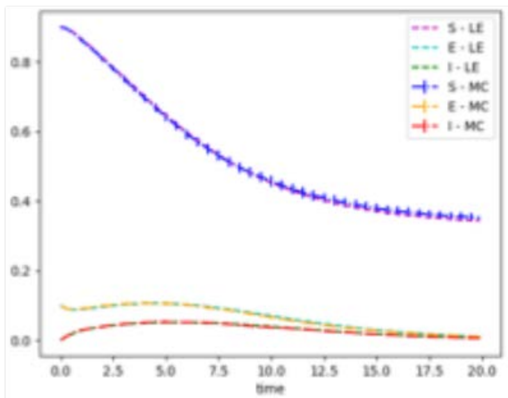

(A) $n = 200,\ \lambda_t \equiv 0.5$

Fig. 1. Comparison of simulations versus local-field theory predictions of evolution of SEIR dynamics of a on a 200-node network, which illustrates efficacy of the approximations.

Funding: The research was supported by the Office of Naval Research under the Vannevar Bush Faculty Fellowship N0014-21-1-2887 and the National Science Foundation under grants

References:

[1] J. Cocomello and K. Ramanan, "Exact description of limiting SIR and SEIR dynamics on locally tree-like graphs," ArXiv:2309.08829v1, Preprint, 2023.

[2] A. Ganguly and K. Ramanan, "Hydrodynamic Limits of non-Markovian Interacting Particle Systems", EJP, vol. 29 , Jan 2024.

[3] D. Lacker, K. Ramanan and R. Wu, "Marginal dynamics of interacting diffusions on. Unimodular Galton-Watson trees," Probab. Theor. Relat. Fields, vol. 187, pp. 817-884, 2023.

[4] D. Lacker, K. Ramanan and R. Wu, "Local weak convergence for sparse networks of interacting processes," Ann. Appl. Probab, vol. 33, no. 2, pp. 643-688, 2023.

[5] D. Lacker, K. Ramanan and R. Wu, "Locally interacting diffusions as Markov random fields on path space," Stoch. Processes and their Appl., vol 140, pp. 817-884, 221.

[6] K. Ramanan, "Interacting stochastic processes on sparse random graphs," Invited paper, Proceedings of the 2022 International Congress of Mathematicians (ICM), vol. 6, pp. 4394-4425, 2022.

[7] K. Ramanan, "Beyond mean-field limits for the analysis of large-scale networks," Queueing Systems, vol. 100, Special issue on "100 views on queues"
2022.

14. Topic: Weapons Sciences and Directed Energy

State-of-the-Art, Time-Resolved Shock Tube/Laser Experiments to Study Pyrolysis and Burning of Energetic Materials and Propellants

Subith Vasu[1,*], Justin Urso[1], and Ramees Rahman[1]
[1]*Department of Mechanical and Aerospace Engineering, University of Central Florida, Orlando, FL 32816*
**Corresponding Author Email: subith@ucf.edu*
Keywords: shock tubes, combustion, energetics, laser spectroscopy, hypersonics

Shock tubes and advanced laser measurements are utilized to measure the products and reactions of propellants and energetic materials and high temperatures relevant to practical applications. In this work, we will present novel experiments to study EM's pyrolysis and oxidation, covering a range of temperatures up to 4000 K, using multiple experimental facilities, including UCF's high-purity shock tube. The results are utilized to improve the predictive accuracy of chemical kinetics models for use in CFD codes.

Energetic materials and propellants (EMs) are used in the DOD's warheads, hypersonic systems, rockets/missiles, and other propulsive systems. EMs must be adaptable in size to fit a family of delivery systems, contain sufficient energy to defeat the target, and have the capability to fly further and faster while being insensitive, munition compliant and affordable. Researchers at DoD and industry are developing detailed chemical kinetics mechanisms that can be used for simulations of reacting flows in solid-fuel ramjet (SFRJ) combustors for hypersonics and the performance of characterization of other energetic materials (EMs). The fuel of interest for the SFRJ application is hydroxyl-terminated polybutadiene (HTPB), which also has uses in energetic devices along with 1,3,5-trinitro-1,3,5-triazinane (RDX), and 1,3,5,7-tetranitro-1,3,5,7-tetrazoctane (HMX). The developed mechanisms are coupled with physics-based computational fluid dynamics (CFD) models to simulate engine performance, warhead lethality, and combustion efficiency. The usefulness of these CFD models is limited by how reliably the actual reaction dynamics are captured in each set of conditions for fuel combustion. Unfortunately, the fidelity of current HTPB/RDX/HMX combustion kinetic models have not been assessed at the combustion conditions of interest to the Navy - mainly due to lack of reliable and relevant data. Measurements are needed to understand the products and their timescales of formation during detonations and combustion of EMs. Such data will provide valuable insights into the chemistry controlling the reaction properties of energetic materials, provide data for validation and refinement of existing EM models, and serve as characterization of newly developed EM formulations' performance and effectiveness.

Solid EMs following initiation, undergo a fast reaction process in which compression waves within the solid enable the formation of a detonation front or a deflagration event. The energy release from RDX, HMX, and HTPB combustion is understood by breaking it into two phases. First, the parent molecule decomposes down via "a few" elementary decomposition reactions reactants, and products. The resultant molecular fragments then undergo combustion at high temperatures (600-4000K). HTPB fragments into 1,3-butadiene and other smaller hydrocarbon species. Such gas phase reactions are difficult to quantify due to the fast timescales and short-lived nature of intermediates experimentally. It would be highly advantageous to analyze the gas phase products and intermediates from the combustion of HTPB/RDX/HMX using ultra-fast time-resolved absorption spectroscopy to determine the concentration and temperature time-histories at the timescales of burning (~µs to ms). Hence, the objective of this effort is to enhance the understanding of EMs reaction kinetics through time-resolved, laser absorption measurements (LAS) across the mid-infrared (MIR) "fingerprint" where quantifiable measurements of species will be obtained as functions of temperature and pressure.

Using a shock tube, EM compounds, products, and their mixtures can be heated to well-defined (T, P, mixture), field-relevant conditions utilizing shock heating. The entire heating process happens within µs timescales; therefore, there is negligible heat loss from the system (compared to slow heating experiments where reactions can occur during the heating). The process can be repeated for different test conditions with excellent reproducibility. Absorption-based diagnostics measure the change in laser intensity when light passes through the medium. They are non-intrusive, in-situ, and can be used to measure high-concentration intermediates, trace species (ppm), and temperature time-histories. Thus, the combination of shock-heating and non-intrusive laser detection provides a state-of-the-art test platform for high-temperature kinetics of EMs. The hydrocarbon species data obtained using non-intrusive, time-resolved laser absorption spectroscopy at MHz rates from these experiments will be utilized to create and refine chemical kinetic models for these compounds. The results are utilized to improve the predictive accuracy of chemical kinetics models for use in CFD codes. (**Funding:** Office of Naval Research).

Microscale Performance Evaluation and Sensitivity Characterization of Energetic Materials

Catherine A.M. Dillier[1,*], Jennifer L. Gottfried[1], and Elliot R. Wainwright[1]
[1]DEVCOM Army Research Laboratory, Aberdeen Proving Ground, MD 21005
**Corresponding author email: catherine.a.dillier.civ@army.mil*
Keywords: energetics; microscale testing; sensitivity; performance; explosives; propellants

Developing and fielding new energetic and reactive materials is expensive and time-consuming, often taking years and millions of dollars to scale up and evaluate. Therefore, relatively inexpensive, high-throughput microscale methods for evaluating the properties of these novel materials are desirable. In our laboratory, we have developed just these. This talk will provide an overview of our microscale techniques for evaluating the performance and sensitivity of new explosive and propellant ingredients and formulations, which require only milligrams and minutes per test rather than the grams and hours conventional testing necessitates, as well as the quantitative diagnostics we have incorporated to better understand the reactions taking place.

Exploring Reaction Kinetics Critical to Predicting Energetic Material Performance and Vulnerability

Rodger E. Cornell[1,*], Michael P. Burke[2], and Michael J. McQuaid[1]
[1]*DEVCOM Army Research Laboratory, Weapon Propulsion Sciences, Aberdeen Proving Ground, MD*
[2]*Department of Mechanical Engineering, Columbia University, 1006 Northwest Corner Bldg., New York, NY*
**Corresponding Author Email: rodger.e.cornell.civ@army.mil*
Keywords: energetic materials; combustion; chemical kinetics; hypersonics; propulsion

Most conventional gun propellants, min-smoke rocket propellants, and explosives comprise organic compounds with nitro (-NO_2), nitroxy (-ONO_2) and/or nitramine (-NNO_2) functional groups. Reacting these functional groups with the organic backbones in the system, they create NOx-rich environments that typically devolve to a set of small molecules that is common to almost all energetic materials (EMs). As a result, it is critical that the DEVCOM ARL chemical kinetics model of this small molecule chemistry is both comprehensive and accurate as it provides valuable insights and quantitative conclusions that can be exploited to increase weapon system performance and decrease vulnerability. That said, recent research has indicated that the current ARL model is likely incomplete due to missing reaction pathways [1,2], a lack of high-pressure validation data, and significant uncertainties in prior rate parameter determinations [3]. To address these shortcomings, emerging capabilities in data science and experimental design are employed to develop a state-of-the-art chemical kinetics model that will serve as the foundation of all ARL models designed to predict the decomposition and combustion of EMs. The work presented here focuses on recent technical progress resultant of a DoD SMART SEED Grant program, including the world's first *ab initio*-based master equation calculations for a large set of H/N/O non-equilibrium kinetic sequences. The impact these newly discovered reaction sequences have on kinetics predictions important to EM combustion is explored. Progress towards the design and construction of a novel high-pressure jet-stirred reactor (HP-JSF) system (Fig. 1) is also discussed. Future work will aim to validate the HP-JSR system and explore novel reactant mixtures that will provide chemical kinetic insights important to solid fuels used for hypersonic propulsion applications.

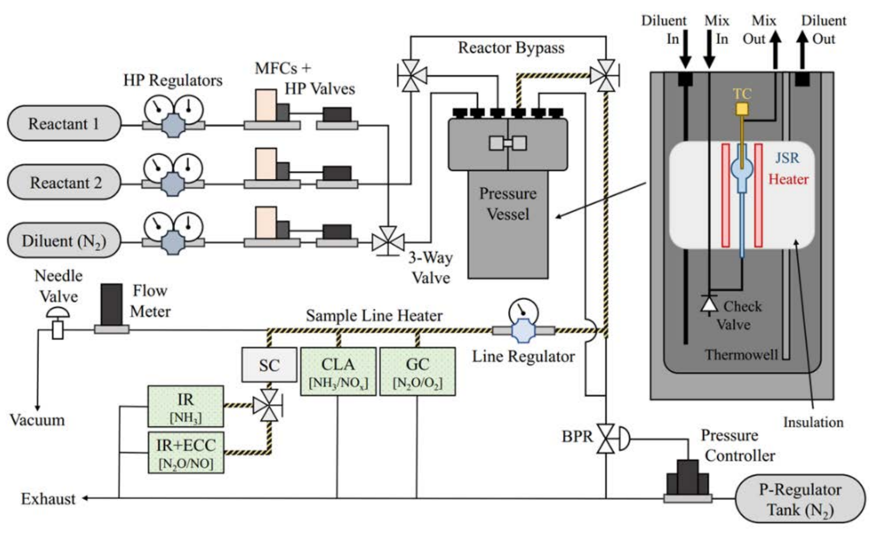

Fig. 1 – A simplified schematic of the high-pressure jet-stirred reactor (HP-JSR) system.

Funding: The authors thank the DoD SMART Scholarship SEED Grant program for continued support.

References:
[1] R.E. Cornell and M.P. Burke, "The discovery of non-equilibrium kinetic sequences important to ammonia/co-fuel and propellant flames," *Proceedings of the Combustion Institute*, vol. 40, no. 1-4, 2024, 105265.
[2] R.E. Cornell and M.P. Burke, "*Ab initio*-based master equation calculations of a large set of non-equilibrium kinetic sequences involving H/N/O species," *Proceedings of the 14th US National Combustion Meeting*, 2025.
[3] J.M. Pankauski, C.E. LaGrotta, J. Lee, R.E. Cornell, and M.P. Burke, "Towards a high-accuracy kinetic database informed by theoretical and experimental data: Anchoring a core reaction set," *Proceedings of the 14th US National Combustion Meeting*, 2025.

Topological Correlation Tracking to Inform the Design of Reactive Materials

Kelsea K. Miller[1,*], Olga Wodo[2], Manny Gonzales[3], and Mike Velez[1,4]
[1]*Materials and Manufacturing Directorate, Air Force Research Laboratory, WPAFB, OH 45433*
[2]*University at Buffalo, Dept. of Materials Design and Innovation, Buffalo, NY 14260*
[3]*Applied Research Associates, Inc., Albuquerque, NM 87110*
[4]*BlueHalo, Materials Characterization Facility, Dayton, OH 45432*
[*]*Corresponding Author Email: Kelsea.Miller@us.af.mil*
Keywords: reactive materials, n-point statistics, heterogenous materials, shock-induced reactions

Reactive materials (RM) are heterogeneous multifunctional materials that exploit the complexity of extreme dynamic environments to enhance effects from the interplay of the RM with existing explosive formulations. This has downstream effects on dynamic phenomena such as fragmentation and shock-induced reactivity – all of which originate within the microstructure of the RM. However, current processing technologies make limited attempt at microstructural optimization of RM formulations. An organized, structured approach to designing smart, optimized RM for use in next generation munitions is needed rather than exhaustively attempting new RM formulations by trial alone.

The heterogeneity that exists within multiphase materials, specifically RM, generates unique topological features that can affect downstream shock wave propagation in extreme environments. These topological features can modify the shock wave and therefore modify the inherent bulk thermodynamic state achieved by the processing of the RM. Thermomechanical processing (e.g. isostatic pressing, swaging, extrusion, ball milling) allows a degree of control to tailor topological and morphological features during RM consolidation. These consolidation methods generate unique microstructures specific to the respective processing route, and we seek to understand how the microstructures evolve during processing and how topology/morphology can influence energetic performance.

Compacted materials generated by thermomechanical processing and synthetically generated microstructures serve as inputs to hydrocode simulations, and by using microstructural characterization functions such as two-point statistics, we can assess the evolution of topology during shock compression and infer correlation to phenomenological events (i.e. hot spot density, high-pressure zones, shock wave percolation). We aim to establish linkages between topology, material properties, and energetic performance and define the relationships between metrics in a multidimensional design space. We seek to define what key microstructural features drive desired response, and use those features to optimize the design and selection of RM.

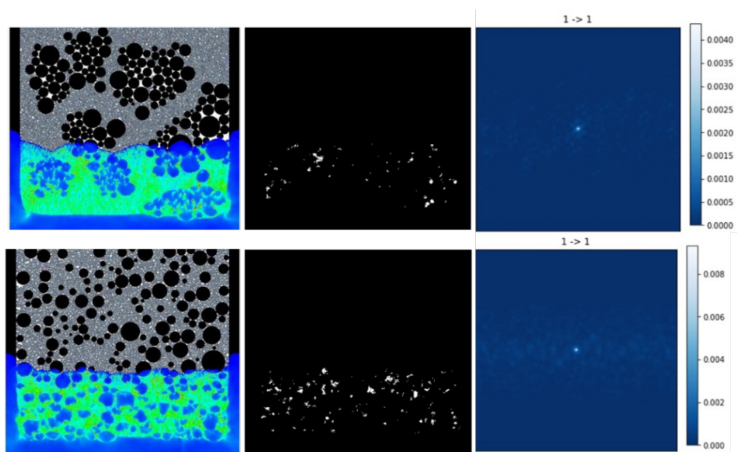

Fig. 1. Clustered (top row) versus randomized (bottom row) solid particle distribution in shock compacted powder beds demonstrating hot spot correlation to microstructure using two-point correlation.

Designing Composite and Metastable Energetic Nanomaterials with Tunable Interfacial Activities via Laser Ablation Synthesis in Solution (LASiS)

Amanda Knopps[1,2], Elijah Davis[3], and Dibyendu Mukherjee[1,2*]

[1]*Department of Chemical, Environmental & Materials Engineering, University of Miami, 1251 Memorial Dr, Coral Gables, FL 33146.*

[2]*Nano-BioMaterials Laboratory for Energy, Energetics & Environment (nbml-E[3]), University of Miami, 4600 Rickenbacker Causeway, Miami, FL 33149*

[3]*Department of Nuclear Engineering, University of Tennessee, 1401 White Avenue, Knoxville, TN 37996*

**Corresponding Author Email: dxm1936@miami.edu*

Keywords: metastable, energetic materials, hyperoxidized Al-oxide, amorphous AlO_x, surface stabilization, LASiS.

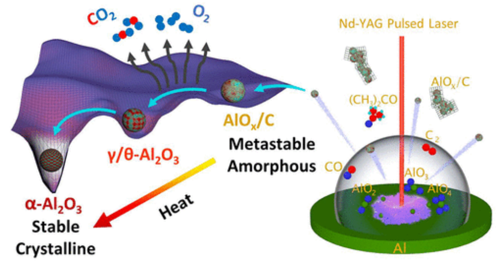

Fig. 1 Metastable a-AlO_x/C NCs trapped via LASiS

Metallized energetic nanomaterials (ENMs) can exhibit kinetically controlled ignition due to large surface areas, metastable structures and small fuel-oxidizer diffusion lengths. Yet, Aluminum (Al) nanoparticles (NPs) in the past have indicated slow detonation rates due to diffusion limitations from oxide formations on Al surfaces. Herein lies the unique yet diverse possibilities of tuning the stability and reactivity of composite ENMs by tailoring their molecular-level metastable structures and interfacial properties. We present results using our patented Laser Ablation Synthesis in Solution (LASiS) technique to synthesize graphitic shell coated Al NPs (C@Al) and amorphous Al-oxides stabilized by interfacial Carbon monolayer (a-AlOx/C NCs) as metastable ENMs that bypass the diffusion limitations of Al NP oxidation and display superior energetic behaviors with fast energy release while showing remarkable stability over long periods of storage. Synthesis of kinetically "frozen" metastable nanostructures has largely remained elusive till date. To that effect, we have employed LASiS as a one-pot non-equilibrium technique to phase-stabilize unusually hyper-oxidized and metastable a-AlO_x/C NCs ($2.5<x\leq3.5$). Structure-composition characterizations across different length-scales reveal highly disordered a-AlO_x (x~3.0) NPs of sizes <10 nm that are remarkably stabilized by ordered interfacial C-monolayer atoms. Only at temperatures >750ºC, the a-AlO_3 structures undergo solid-solid phase transition that culminates in the formation of stable α-Al_2O_3 while releasing excess trapped gases (Fig. 1). Detailed chemical kinetics analyses reveal a relatively large activation energy barrier of ~270±11 kJ/mol for the phase transition of a-AlO_3 NPs into semi-stable equilibrium θ/γ-Al_2O_3 crystallites via disproportionation reactions, while undergoing distinct volume shrinkages with oxidative (O_2, CO_2, CO) gas releases. The observed barrier - being comparable to the oxidation of micron-sized Al particles - further corroborates the unusual stability of the a-AlO_x/C NCs. Atomic Pair Distribution Function (PDF) analyses from high-temperature isothermal X-ray scattering data reveal bond pair re-arrangements during the structural evolution of a-AlO_x NPs transitioning from highly disordered to low-order polycrystalline states. Finally, we demonstrate the versatility of LASiS at tailoring the O/Al ratios in the a-AlO_x/C NCs by tuning the laser flux (Energy density per unit pulse width), thereby allowing us to control the structural re-arrangement and solid-state oxidative gas generation behaviors during their disorder-to-order transitions. Gas chromatography results corroborate the tunability of O/Al ratios by indicating commensurate concentrations of O_2, CO_2, CO release from isothermal heating (T~300-800ºC) of a-AlO_x/C samples with x~1.5-3.0 synthesized via LASiS by using laser fluxes ranging over ~0.11-0.15 J/cm^2/ns.

Funding: We acknowledge grant support from AFOSR (FA9550-19-1-0366) and ONR (N00014-21-1-2507).

References:

[1] E. M. Davis, C. Rawn, D. Mukherjee, et al., "Kinetic analyses for solid-state phase transition of metastable amorphous-AlOx ($2.5 < x \leq 3.0$) nanostructures into crystalline alumina polymorphs." Sci Rep 15, 7854 (2025)

[2] E. M. Davis, J. Johnson, B. Khomami, D. Mukherjee, et al., "Fe-carbide/Fe-oxide-based nanocomposites synthesized as magnetic nanomaterials via laser ablation synthesis in solution (LASiS)," Appl. Surf. Sci., 658, 159682. (2024)

[3] E. M. Davis, G. Duscher, J. Wen, D. Mukherjee, "Laser-induced trapping of metastable amorphous-AlOx/C ($2.5< x \leq3.5$) nanocomposites." ACS Applied Nanomaterials, 6 (13), 10977 (2023)

[4] E. M. Davis, J. L. Gottfried, G. Duscher, D. Mukherjee, "Laser-induced trapping of metastable nanocomposites as high-performance energetic additives." Journal of DoD Research & Engineering, 5(4), 67 (2022) [LIMITED DISTRIBUTION MATERIAL]

[5] S. A. Davari, J. L. Gottfried, D. Mukherjee, et al., "Graphitic coated Al nanoparticles manufactured as superior energetic materials via laser ablation synthesis in organic solvents," Appl. Surf. Sci., 473, 156 (2019)

15. Topic: Acoustics

A Modified Bispectrum Methodology for Harmonic Cluster-like Frequency Grouping, A Signal Processing Implementation

Vijay Kumar Peddinti [1, *]

[1]*Naval Undersea Warfare Center, 1176 Howell Street, Newport, RI 02841*
**Corresponding Author Email: vijaykumar.peddinti.civ@us.navy.mil*
Keywords: Bio-inspired; Auditory system; Frequency tracking; Harmonic grouping; Clustering

This work focuses on the problem of identifying multiple sound sources (with harmonics) in an acoustic signal, specifically in data limited areas. The proposed signal processing implementation generated cluster-like frequency groups (with synthetic time domain data), associated with these different sound sources.

The proposed implementation leverages an auditory inspired peripheral signal processing model (introduced in an earlier paper [1] and later improved in [2] respectively) as the first stage to analyze the input acoustic signal. This auditory inspired adaptive synchrony capture filterbank (SCFB) signal processing architecture acts more like a bank of frequency modulation (FM) receivers rather than a traditional filterbank. These FM receivers lock on to a strong (frequency) signal even in the presence of nearby interfering signals close in frequency, which are slightly weaker in amplitude. The SCFB exhibits many cochlea-like characteristics which are desirable while analyzing speech, music, and other complex sounds.

In the latest work, biomimicry of auditory system was further extended in the auditory inspired peripheral signal processing model, and the estimated output frequency tracks are harmonically grouped (or clustered) by applying a modified bispectrum methodology [3]. Preliminary analysis with multiple (distinct) harmonic sets of synthetic time domain data, where these different harmonic sets are associated with different sound sources, showed promising results. The proposed signal processing implementation generated cluster-like frequency groups, associated with these different sound sources. This harmonic grouping of frequency tracks from the SCFB is a first step in determining the number of speakers (or sound sources) in the (time domain) acoustic signal. Subsequent steps include sound source (or signal) separation.

Funding: This research was funded by the Naval Undersea Warfare Center's In-house Laboratory Independent Research (ILIR) program from the Office of Naval Research (ONR) under N0001423WX00090.

References:

1. Kumaresan R, Peddinti Vijay, Cariani P., “Synchrony capture filterbank: auditory-inspired signal processing for tracking individual frequency components in speech.” Journal of the Acoustical Society of America, 2013; 133(6):4290–310.
2. Peddinti Vijay, Kumaresan R, Cariani P., “Improved Auditory-Inspired Signal Processing Algorithm Design for Tracking Multiple Frequency Components.” SN Computer Science, 1, 62 (2020).
3. Kevin W. Baugh, "On parametrically phase-coupled random harmonic processes," [1993 Proceedings] IEEE Signal Processing Workshop on Higher-Order Statistics, CA, USA, 1993, pp. 346-350

Node-level Signal Processing for Unattended Ground Sensors

Geoffrey H. Goldman, Joydeep Bhattacharyya, Monte Lewis

[1]*DEVCOM Army Research Laboratory, 2800 Powder Mill Road, Adelphi, MD 20783-1197.*
Email: Geoffrey.h.goldman.civ@army.mil
Keywords: UGS, sensors, acoustics, seismic, Detection, Vehicle, speed

The DEVCOM Army Research Laboratory (ARL) is developing new approaches for next-generation unattended ground sensors (UGSs). Low-level signal processing algorithms are needed to demonstrate these approaches on prototypes. Many detection and estimation algorithms are already implemented on existing UGSs, but the source code is usually proprietary. To address this issue, threshold-based detection algorithms were developed and evaluated for passive acoustic or seismic modalities that support implementation on low-size, weight, power and cost (SWaP-C) devices. Results from the algorithms are presented using post-processed data from acoustic and seismic measurements for several vehicles.

Energy-based techniques were developed, coded and evaluated to detect ground vehicles, estimate the time of arrival of vehicles to the closest point of approach (CPA), detect multiple vehicles in a convoy and estimate their speed using a single microphone or geophone. The algorithms filter the data using either a single-pole and/or moving average filters, then estimated the CPA and speed of the vehicles using statistical models. Convoys are detected by summing the number of single target detections or CPA events over a fixed time period, then comparing the result to a threshold. The speed of a vehicle is estimated by minimizing the errors in spherical spreading attenuation and constant-speed Doppler shift models. These algorithms are being transitioned to prototype UGSs for testing and evaluation.

Effective Properties and Acoustic Absorption for a Sierpiński-like Fractal Willis Metamaterial

Carl R. Hart[1,*], Michael B. Muhlestein[1], Cody M. Best[1], Matthew G. Blevins[2], and D. Keith Wilson[1]

[1]U.S. Army Engineer Research Development Center, Cold Regions Research and Engineering Laboratory, 72 Lyme Rd., Hanover, NH 03755

[2]U.S. Army Engineer Research Development Center, Construction Engineering Research Laboratory, 2902 Newmark Dr, Champaign, IL 61822

**Corresponding Author Email: carl.r.hart@usace.army.mil*

Keywords: effective properties, asymmetric absorption, Willis coupling, fractal geometry, metamaterial

Willis materials are a class of metamaterials exhibiting mass-momentum coupling. The coupling arises from hidden degrees of freedom that are asymmetrical with respect to the boundaries of an isolated element. Resonant Willis metamaterials incorporate resonators, e.g., a Helmholtz resonator, along with material asymmetry to effectively obtain Willis coupling over a narrow frequency band. By incorporating fractal geometry into the resonator shapes, Willis coupling can be obtained over multiple frequency bands. Measurements and modeling of resonant Willis metamaterials based on fractal geometry are reported herein. Measurements are obtained with a transmission impedance tube, and predictions are based on a lumped-element analysis. With resonator volume shapes based on the Sierpiński triangle, Willis coupling is obtained over several frequency bands in the range of 500 to 1500 Hz. For a subset of the resonators, Willis coupling is tuned by mirroring the asymmetric location of some resonator necks across the element's midplane. Directionally-dependent acoustic absorption is observed, along with tuning of the absorption curves by introducing non-uniformity to the internal sample asymmetry.

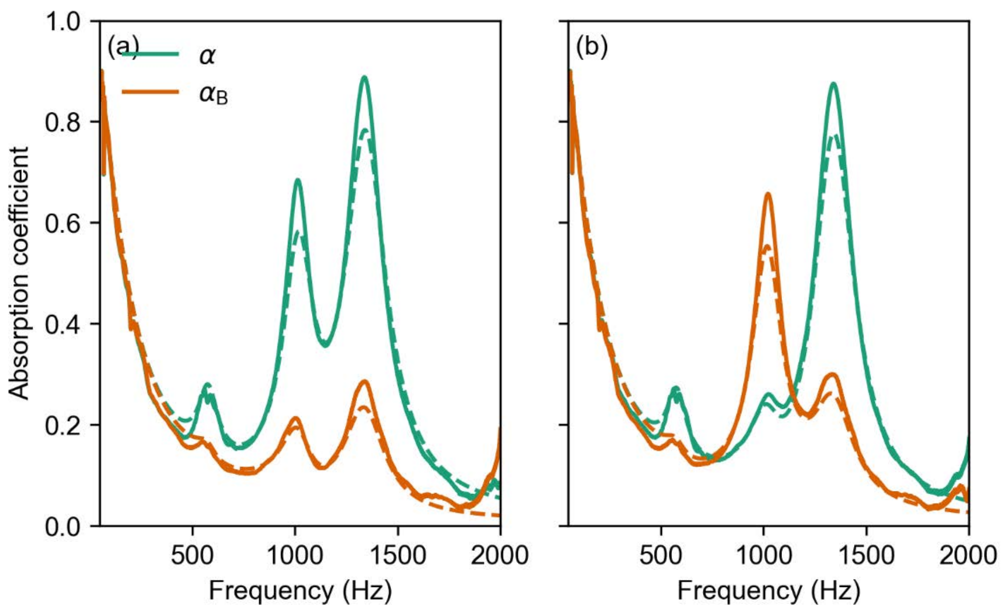

Fig. 1 – Acoustic absorption coefficient for forward (α) and backward (α_{B}) sample orientations. (a) Sample S1, and (b) sample S2. Solid lines correspond to measurements and dashed lines to predictions.

Observations and predictions of directionally-dependent acoustic absorption are shown in Fig. 1. By modifying the relative placement of resonator necks (sample S1 vs. S2), the magnitude of the acoustic absorption can be modified within a frequency band corresponding to a specific cavity resonance. Due to inherent asymmetry within the sample, sound absorption is sensitive to the direction of incidence. As indicated by lumped-element analysis, resonance frequencies can also be sensitive to the direction of incidence.

Dirac-like Spectrum for Surface Waves in an Ultrasonic Crystal

Nicholas T. Gangemi[1,*], Caleb F. Sieck[1], Joseph F. Vignola[2], Diego Turo[2], Jeffrey W. Baldwin[1], Steven W. Liskey[1], Aaron D. Edmunds[1], William B. Wilson[1], Douglas M. Photiadis[1], and Bernard R. Matis[1]

[1]*Acoustics Division, U.S. Naval Research Laboratory, 4555 Overlook Avenue SW, Washington, D.C. 20375, USA*

[2]*Department of Mechanical Engineering, The Catholic University of America, 620 Michigan Avenue NE, Washington, D.C. 20064, USA*

**Corresponding Author Email: nicholas.t.gangemi.civ@us.navy.mil*

Keywords: "ultrasonic crystals, surface waves, dispersion, Dirac-like physics".

Absent of dissipation, wave energy transport occurs with the group velocity. In this talk we demonstrate how to exploit this principle to resolve the Dirac cone at the Brillouin-zone edge for ultrasonic surface waves in a hexagonal lattice of resonant cavities.

Acoustic analogues of condensed-matter systems provide a unique opportunity to conduct experimental studies of various phenomena without the difficulty of working with atomic-scale components. A honeycomb array of cavities in a flat plate is known to support subsonic acoustic modes at the interface exhibiting Dirac cones, analogous to electronic graphene. The open nature of this system enables detailed measurements of unique wave phenomena.

In this talk, wave propagation measurements along varying real-space lattice angles are shown to resolve dispersion along the Dirac cone in reciprocal space where the band structure gradient is oriented along the angle for which energy propagation is measured. Through the Dirac point, we measure group and phase velocities, and the Dirac-point frequency, in agreement with finite-element modeling. The results demonstrate how one-dimensional line-scan measurements can resolve targeted reciprocal space dispersion about a specific high-symmetry point for a two-dimensional crystal, and opens the door for applying Dirac-like physics to the development of acoustic twistronics, novel wave manipulation, and sub-wavelength spatial control of sound propagation.

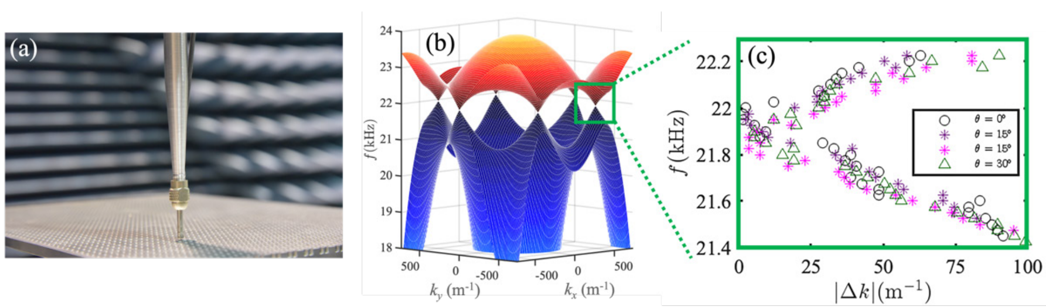

Fig 1. (a) measurement microphone positioned above the ultrasonic crystal (b) 3D FEM-predicted band structure for the ultrasonic crystal showing six Dirac points at the Brillouin zone edge where the upper (red) and lower (blue) bands touch at f = 22.01 kHz. (c) Experimentally measured Dirac-like spectrum using line scans along varying real-space lattice angles θ. The values of the wavenumber k are projected and shifted such that the Dirac point for each θ is at |Δk| = 0.

Funding: This work was funded by the Office of Naval Research

References:

[1] N. T. Gangemi, C. F. Sieck, J. F. Vignola, D. Turo, J. W. Baldwin, S. W. Liskey, A. D. Edmunds, W. B. Wilson, D. M. Photiadis and B. R. Matis, "Dirac-like spectrum for surface waves in an ultrasonic crystal," *Phys. Rev. Applied.*, vol. 22, no. 044008, Oct. 2024.

[2] N. T. Gangemi, C. F. Sieck, J. F. Vignola, D. Turo, J. W. Baldwin, S. W. Liskey, A. D. Edmunds, W. B. Wilson, D. M. Photiadis and B. R. Matis, "Frequency-dependent surface wave suppression at the Dirac point of an acoustic graphene analog," *Phys. Rev. B.*, vol. 106, no. 064301 Aug. 2022.

Rapid Distortion Theory for Modeling Turbulent Flow and Internal Pressures of Windscreens

Gordon M. Ochi[1,*], Carl R. Hart[2]
[1]U.S. Army Engineer and Research Development Center, Construction Engineering Research Laboratory, 2902 Newmark Dr, Champaign, IL 61821
[2]U.S. Army Engineer and Research Development Center, Cold Regions Research and Engineering Laboratory, 72 Lyme Road, Hanover, NH 03755
**Corresponding Author Email: Gordon.M.Ochi@usace.army.mil*
Keywords: Turbulence, Acoustics, Rapid Distortion, Infrasound.

Current models for the wind noise reduction (WNR) of microphone windscreens in atmospheric turbulence generally assume a homogeneous surface pressure averaging process. The surface pressures average in such a way that the noise spectrum at low turbulence wavenumbers, relative to the windscreen dimension, should approach that of an unscreened microphone. In contrast, past experiments show a significant WNR at low wavenumbers.

In this work, we examine a rapid distortion theory model for linking turbulent distortion to the unsteady pressure received inside the windscreen. Rapid distortion theory proposes a linear approximation to the momentum equations for an incompressible flow under the assumptions that the upstream turbulence is weak, the integral scale of the upstream turbulence is large, and the time scale of the distortion is much smaller than the time scale of the turbulence [1]:

$$\frac{\partial \omega_i}{\partial t} + U_i \frac{\partial \omega_i}{\partial x_i} + u_i \frac{\partial \Omega_i}{\partial x_i} = \omega_i \frac{\partial U_i}{\partial x_i} + \Omega_i \frac{\partial u_i}{\partial x_i} \tag{1}$$

where $U_i = \bar{u}_i/\bar{u}_{i,\infty}$, $\bar{u}_i$ is the mean flow, $u_i = u_i'/u_{i,\infty}'$ with a prime denoting the fluctuating flow, subscript ∞ indicating the flow far upstream of the body. The coordinates are normalized by the body dimension $(x, y, z, t) = (x^*, y^*, z^*, t^*\bar{u}_\infty)/a$, a being the body dimension, and the vorticity terms are $\Omega = \nabla \times U$ and $\omega = \nabla \times u$. The theoretical background and underlying assumptions of rapid distortion theory for a 2D cylinder (Fig. 1) are examined in detail, along with extensions to surface [2] and internal pressures. Then, results for the case of both impermeable and permeable cylinders are presented.

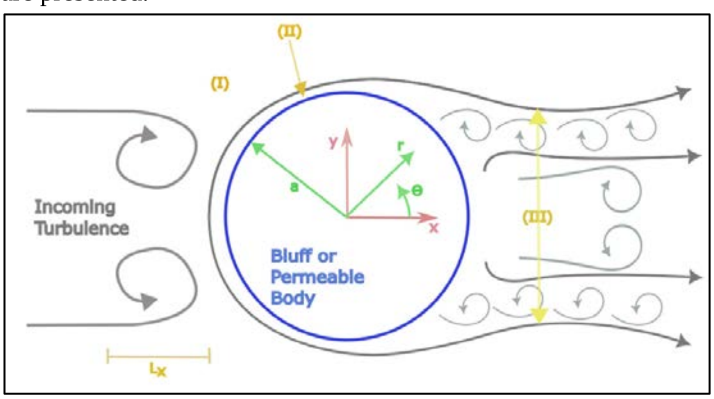

Fig. 1: Depiction of Rapid Distortion theory applied to a cylindrical body for a turbulent flow moving from left to right. Region (I) is an external region where the flow is irrotational, while Region (II) is a thin boundary layer on the body, and Region (III) is the turbulent wake. Coordinate systems are centered on the cylindrical body (blue), with analysis non-dimensionalized by the integral scale of the upstream turbulence (L_x) and the body radius (a). Rapid distortion theory allows for a linear approximation of the turbulent distortion due to the body, and by extending the method, the resulting surface and internal pressures.

References:

[1] R. Zamponi, S. Moreau, and C. Schram, "Rapid distortion theory of turbulent flow around a porous cylinder," *Journal of Fluid Mechanics*, vol. 915, p. A27, 2021. doi:10.1017/jfm.2021.8

[2] J.C.R. Hunt, "A theory of turbulent flow round two-dimensional bluff bodies", *Journal of Fluid Mechanics*, vol. 61, p. 625-706.

Acoustic Cavities for 100GHz Frequency Range: Optical Mode of Operation

M.K. Zalalutdinov[1,*], J.T. Robinson[1], C.D Cress[1], J.J. Fonseca[1], S.W. LaGasse[1,2], I. Welland[1,3], T. Reinecke[1], S. Dey[1], J.C. Culbertson[1]

[1]Naval Research Laboratory, 4555 Overlook Ave. S.W. Washington, DC 20375

[2]Current address: Laboratory for Physical Science 8050 Greenmead Drive, College Park, MD 20740

[3]Current address: Naval Surface Warfare Center 9500 MacArthur Blvd. West Bethesda, MD 20817-5700

**Corresponding Author Email: Maxim.K.Zalalutdinov.civ@us.navy.mil*

Keywords: "Acoustic, cavity, phonons, photoelastic, ultrafast".

The interaction of incoming photons with longitudinal coherent acoustic phonons (CAP) trapped in 100 GHz range acoustic cavities based on 2D transition metal dichalcogenides (TMD)[1,2] will be discussed. Exciton-driven photoelastic effects in 2D semiconductors will be presented as means of enhancing photon-phonon interaction, leading to orders of magnitude improvements in the efficiency of optical readout, as well as extending functionality of TMD-based high frequency acoustic cavities.

While the resonant behavior of acoustic cavities provides a foundation for frequency-selective components in phonon-based signal processing, extending operation into the 100GHz frequency range represents a significant challenge, as physical dimensions of the cavities (defined by the wavelength of the sound) enter the nanometer range and necessitate a transition from electronic to optical means of communicating with the cavity. In this work we present an optical mode of operation based on an ultrafast pump-probe system for cavities implemented as ultrathin suspended TMD films, where strain-sensitive 2D excitonic features couple probe light to the out-of-plane sound waves trapped between atomically flat free surfaces acting as acoustic mirrors.

In WSe_2 acoustic cavities we demonstrate over two orders of magnitude in tunability range for the amplitude of optical readout, attainable through temperature-driven bandgap narrowing that provides a control over relative alignment between the energy of the probe photons and the position of the K-K valley excitonic peak (Fig. 1). We show that the phase of the optical readout can be tuned over 180^o range in the vicinity of critical points (Fig. 1b). Continuously tunable phase shift attainable in WSe_2-based cavities will be contrasted with a polarization-controlled set of discrete phase values demonstrated for birefringent ReS_2 and will be discussed in the context of extending cavity functionality.

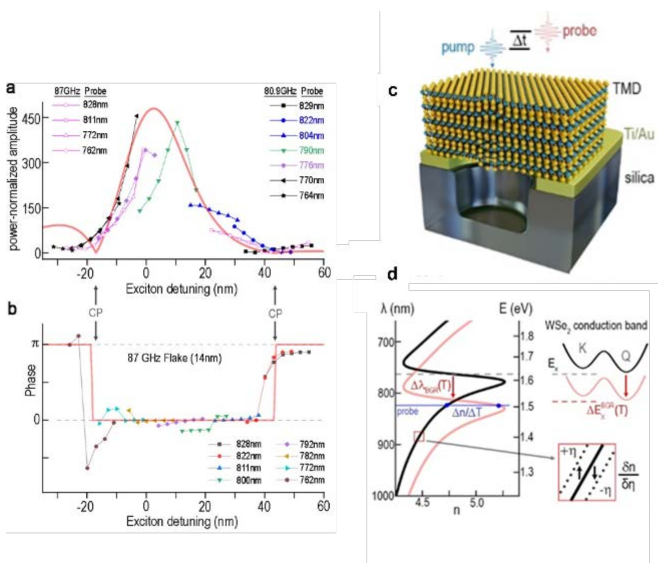

Fig. 1 – Amplitude (a) and phase (b) of the optical modulation imposed on the probe beam by the out-of-plane longitudinal CAP in an 87GHz, 14nm-thick WSe_2 acoustic cavity (shown schematically in (c)). The effect of temperature and mechanical strain on band alignment and excitonic features in TMD dispersion shown in (d).

Funding: This work was supported by the Office of Naval Research.

References: [1] M.K. Zalalutdinov et al., "Acoustic cavities in 2D heterostructures", Nature Communications, 12, 3267 (2021).
[2] J.T. Robinson et al., "Tunable exciton-driven photoelasticity in 2D material acoustic cavities", ACS Nano 19 (10), 10059-10069 (2025)

Investigating Inter-Ferroelectric Phase Switching and Domain Dynamics for a High-Gain Sound Projector Transduction Modality

Margo Staruch[1], Thomas Mion[1]and Peter Finkel[1]*

Materials Science and Technology Division, U.S. Naval Research Laboratory, Washington, DC 20375

**Corresponding Author Email: peter.finkel.civ@us.navy.mil*

Keywords: ferroelectric, acoustic, transducers

The development of highly efficient, compact-sized sound projectors for high-power, low-frequency applications necessitates a new generation of materials with superior electromechanical properties. Domain-engineered relaxor ferroelectric single crystals with compositions near a morphotropic phase boundary (MPB) are particularly promising due to their exceptionally large piezoelectric response. This work investigates a transduction modality based on inter-ferroelectric transitions in mechanically clamped, domain-engineered single crystals poised near a phase instability. This approach leverages strain levels significantly exceeding those achievable via the linear piezoelectric effect, which is attributed to the presence of intermediate monoclinic and/or orthorhombic ferroelectric states facilitating enhanced polarization rotation between the rhombohedral and tetragonal phases. We utilized [110]-poled domain-engineered $xPb(In_{1/2}Nb_{1/2})O_3$-$(1-x-y)Pb(Mg_{1/3}Nb_{2/3})O_3$-$yPbTiO_3$ (PIN-PMN-PT) relaxor single crystals, demonstrating their ability to be dynamically and reversibly driven by a time variable electric field through a ferroelectric-ferroelectric phase transition, exhibiting a highly enhanced piezoelectric response across a broad frequency range. To elucidate the phase switching dynamics, including domain reconfiguration times and critical field which are crucial for maximizing the switching frequency in next-generation high-speed electro-optic applications, we performed *in situ* synchrotron X-ray diffraction studies on [011]-poled PIN-PMN-PT single crystals with compositions near the MPB [1]. Time-resolved diffraction experiments were conducted as a function of an applied electric field to investigate this transient phase transition and commensurate structural phases switching path. Quantitative analysis of the diffraction peaks indicates the presence of intermediate monoclinic phases during the inter-ferroelectric phase transition, which can be induced by a relatively small electric field (≤ 0.2 kV/mm). Furthermore, we demonstrated compact broadband sound projectors based on Tonpilz [2] and Class IV flextensional transducers utilizing this modality, achieving a 10 to 15 dB higher sound pressure level over two and a half octaves compared to their linear piezoelectric mode counterparts [2]. This abstract will discuss implications of these results and advances in the fundamental understanding of this transduction modality and device physics in details.

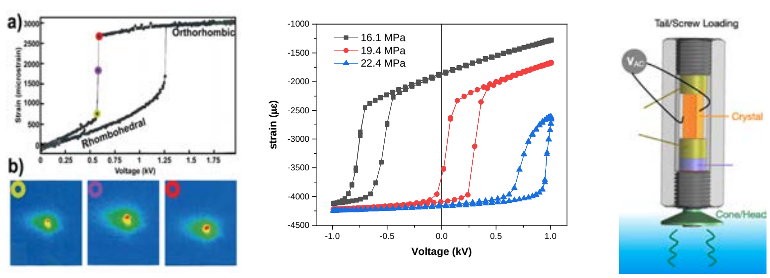

Fig. 1. In-situ measurements of a) voltage – strain during diffraction measurements where colored spots correlate to diffraction images in b) obtained with high-speed camera observing phase transition and intermediate phases. c) strain vs electric field as a function of prestress. d) Schematic of the Tonpiltz-type transducer with the crystal placement and application of mechanical bias.

Funding: This work was sponsored by the Office of Naval Research.

References:

[1] Finkel et al., *Adv. Mater*. 34, 2106827 (2022)

[2] Patterson et al., *Appl. Phys. Lett. 116, 222903 (2020)*

Ultrasonic Propagation and Slow Dynamic Nonlinear Elasticity in Saturated Glass Bead Packs

Dr. John Yoritomo[1,*], Ms. Grace Burkholder[2], and Dr. Benjamin Dzikowicz[1]

[1]*Acoustics Division, U.S. Naval Research Laboratory, 4555 Overlook Ave. SW, Washington, DC 20375*

[2]*Department of Physics, Bethel University, 3900 Bethel Dr., St. Paul, MN 55112*

**Corresponding Author Email: john.y.yoritomo.civ@us.navy.mil*

Keywords: Nonlinear Elasticity, Slow Dynamics, Granular Physics, Sediment Acoustics.

Nonlinear Mesoscopic Elasticity (NME) refers to a class of materials that display nonlinear elastic behaviors that cannot be captured by the classical theory, where the stress field is related to powers of the strain field. The designation "mesoscopic" indicates that NME materials are composed of grain elements that are large compared to the atomic scale (and thus can be contrasted with materials like aluminum or quartz that have atomic elasticity) but small compared to sample size [1]. Of the NME behaviors, slow dynamic nonlinear elasticity, or simply "slow dynamics" (SD), has received particular attention. There is a prevailing thought that moisture plays a key role in SD. Some models predict that the SD response should disappear in a saturated material [2]. To test this prediction, we probe saturated glass bead packs with ultrasound and assess changes using coda wave interferometry. Saturation increases the cutoff frequency [3], i.e., the Debye frequency, of the bead pack (Fig. 1a). SD is induced using a low frequency harmonic pump. Our results are compared with similar measurements of dry packs. We find that saturated bead packs also exhibit SD and, with some caveats, the SD response is unaffected by saturation (Fig. 1b).

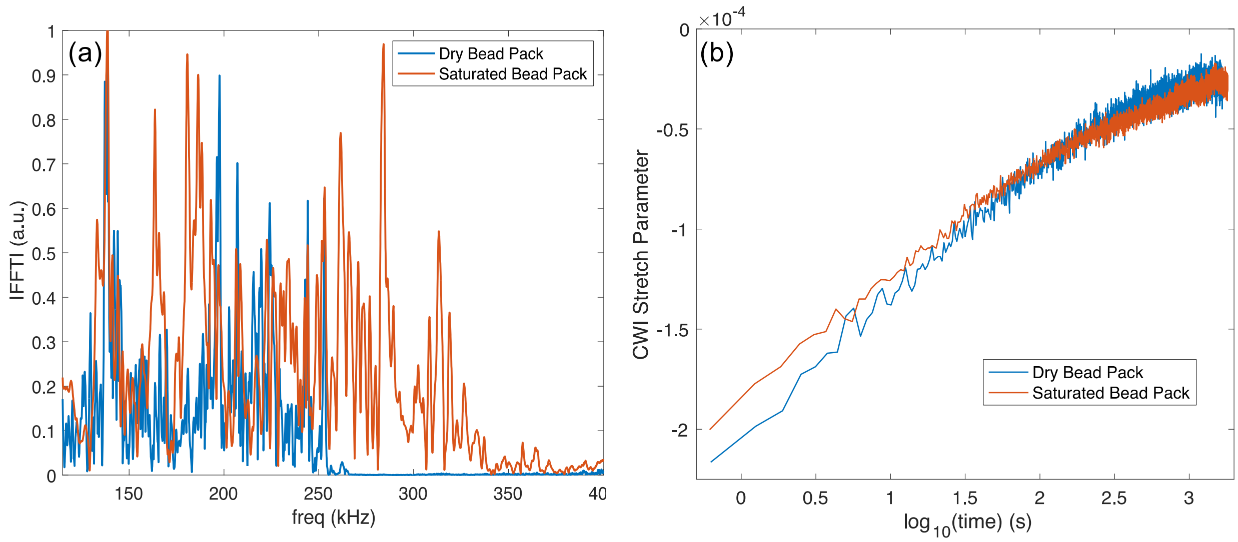

Fig. 1 – Panel (a) plots the spectrum of an ultrasonic signal that propagated through a dry (blue curve) and saturated (red curve) glass bead pack. The cutoff frequency for the dry case is near 250 kHz, while the one for the saturated case is near 350kHz. Panel (b) displays the slow dynamic log(t) relaxation for the dry (blue curve) and saturated (red curve) bead packs. It is clear that SD is still present in saturated materials.

Funding: Office of Naval Research, NRL Base Program 6.1 Funding, Work Unit #991AE6

References:

[1] R. A. Guyer and P. A. Johnson, "Nonlinear Mesoscopic Elasticity: Evidence for a New Class of Materials," Physics Today, vol. 52, no. 4, pp. 30–36, Apr. 1999.

[2] J. A. Bittner and J. S. Popovics, "Mechanistic diffusion model for slow dynamic behavior in materials," Journal of the Mechanics and Physics of Solids, vol. 150, p. 104355, May 2021.

[3] J. Y. Yoritomo and R. L. Weaver, "Slow dynamic nonlinearity in unconsolidated glass bead packs," Phys. Rev. E, vol. 101, no. 1, p. 012901, Jan. 2020.

16. Topic: Mathematical Sciences

Efficient Pseudometrics for Data-Driven Comparisons of Nonlinear Dynamical Systems

Bryan Glaz
DEVCOM Army Research Laboratory, Aberdeen Proving Ground, MD 21005
Corresponding Author Email: bryan.j.glaz.civ@army.mil
Keywords: Nonlinear Dynamics, Topological Conjugacy, Data-Driven Dynamics, Koopman Eigenfunctions, Dissimilarity Measures

Computationally efficient solutions for pseudometrics quantifying deviation from topological conjugacy between dynamical systems based on diagonalizable data-driven Koopman operators are presented. Deviation from conjugacy is quantified in a Pareto optimal sense that accounts for spectral properties of Koopman operators as well as trajectory geometry. Theoretical justification is provided for computing such pseudometrics in Koopman eigenfunction space rather than observable space. Furthermore, it is shown that theoretical consistency with topological conjugacy can be maintained when restricting the search for optimal transformations between systems to the unitary group. The benefits of considering operator and trajectory geometry based dissimilarity measures in a unified and consistent formalism are demonstrated. Overall, the deviation from conjugacy pseudometrics provide practical advantages in terms of computational efficiency and scalability, while maintaining theoretical consistency.

Data-driven and machine learning approaches are becoming increasingly prevalent for modeling, predicting, controlling, and designing complex nonlinear dynamical systems across a variety of scientific and technical fields [1]. Quantitative comparisons (dissimilarity measures) between nonlinear dynamical systems based on data are particularly important for a variety of machine learning and optimization tasks. As a result, it is desirable for data-driven dissimilarity measures to (a) be computationally efficient such that the approach is scalable when analyzing multiple combinations of systems and (b) respect the inherent features of the dynamical system that generated the data. The latter condition is achieved here by maintaining theoretical consistency with topological conjugacy, while the former condition is achieved by showing that computationally efficient analytical solutions for unitary transformations in Koopman eigenfunction space can describe deviation from conjugacy between dynamical systems [2]. Fig. 1 illustrates the deviation from conjugacy pseudometrics, *d*, in objective function space spanned by conjugacy residuals, *r*. Example results for comparisons between two nonlinear dynamical systems are shown in which the systems are topologically conjugate for α and $\beta = 1$, and non-conjugate otherwise. Overall, results presented demonstrate substantial advantages in terms of theoretical consistency and computational efficiency. See [2] for details.

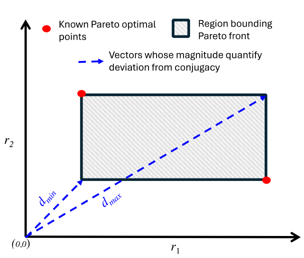

$$r_1 = \left\| \Phi_g - C\Phi_f \right\|_F / \left\| \Phi_{ref} \right\|_F$$

and

$$r_2 = \left\| \Lambda_f - C^{-1}\Lambda_g C \right\|_F / \left\| \Lambda_{ref} \right\|_F$$

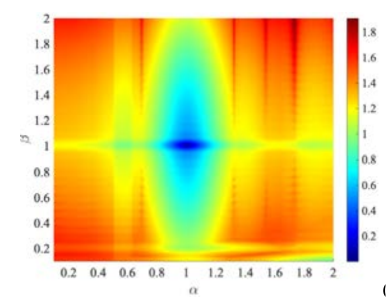

Fig. 1 – Left: Deviation from conjugacy pseudometrics in objective function space, Center: Conjugacy residuals for systems f and g in terms of Koopman eigenfunctions Φ, Koopman eigenvalues Λ, and unitary transformation C, Right: Example results for comparison between two nonlinear dynamical systems.

References:

[1] S. Brunton and J. Kutz, Data-driven science and engineering: Machine learning, dynamical systems, and control, Cambridge, UK: Cambridge University Press, 2019.
[2] B. Glaz, “Efficient pseudometrics for data-driven comparisons of nonlinear dynamical systems,” Nonlinear Dyn, vol. 113, 2025.

Leveraging Hamilton-Jacobi Partial Differential Equations for Scientific Machine Learning to Enhance Autonomous Warfighting Capabilities

Paula Chen[1*]

[1]Naval Air Warfare Center Weapons Division, China Lake, 1 Administration Circle, China Lake, CA 93555

**Corresponding Author Email: paula.x.chen.civ@us.navy.mil*

Keywords: Hamilton-Jacobi PDEs, optimal control, scientific machine learning, nonlinear dynamics identification

The overall objective of this work is to enhance the Navy's autonomous warfighting capabilities via the development of intelligent, reactive systems. In particular, we seek to develop data-driven technology that improves as more data becomes available and adapts to complex, ever-changing environments. To achieve these objectives, we establish new mathematical theory that shows that solving certain optimization problems arising from scientific machine learning (SciML) is equivalent to solving a Hamilton-Jacobi partial differential equation (HJ PDE) with time-dependent Hamiltonian. This novel theoretical connection allows us to reinterpret incremental updates to learned models as the time evolution of an associated HJ PDE and optimal control problem, where all previously incorporated information is intrinsically encoded in the solution to the HJ PDE. As a result, we create new efficient training approaches for SciML based on existing HJ PDE solvers that naturally coincide with continual learning, while inherently avoiding catastrophic forgetting. We then demonstrate how these new training approaches can be applied to (1) canonical SciML test problems to illustrate the potential computational and memory advantages of these new approaches and (2) nonlinear dynamics identification problems in support of the improved maneuverability and controllability of UAVs. Finally, we discuss extensions of this new mathematical theory to HJ PDEs with nonconvex Hamiltonians and differential games. This work summarizes the results of a SMART Scholarship-for-Service SEED Grant, including the work published in [1] as well as some new results.

Funding: SMART Scholarship-for-Service SEED Grant

References:

[1] P. Chen, T. Meng, Z. Zou, J. Darbon, & G. E. Karniadakis, "Leveraging Hamilton-Jacobi PDEs with time-dependent Hamiltonians for continual scientific machine learning," in 6th Annual Learning for Dynamics & Control Conference, Proceedings of Machine Learning Research, June 2024.

Multimodal Deep Learning for Segmentation of Geospatial Imagery

Katherine Wall[1*]

[1]National Geospatial-Intelligence Agency, 7500 GEOINT Drive, Springfield, VA 22150
**Corresponding Author Email: Katherine.E.Wall@nga.mil*
Keywords: computer vision, multimodal, fusion, neural networks

The majority of neural network models for computer vision (CV) artificial intelligence (AI) applications rely on unimodal inputs. In other words, they generate predictions using only one source of information: for instance, a satellite image. However, the wealth of contextual information known about aerial collection, stored as metadata, goes unutilized. Bringing these contextual measures into image analysis is necessary for human analysts, and existing research suggests the same approach may improve CV approaches. The purpose of this manuscript is to demonstrate a neural network architecture that adapts, and, ultimately, enhances CV model performance in semantic segmentation by integrating multiple modes of information. Training, testing, and tuning was performed using 50,000 instances of synthetic imagery and binary masks of plane objects from the Rare Planes dataset. Segmentation results accounting for known rendering parameters, such as solar characteristics, ground resolve distance, ground vegetation, and other tabular measures, were assessed, on the basis of Jaccard index and Dice score. Backbone architectures included Meta's Segment Anything 2 (SAM2) with weights pre-trained on ImageNet. Fusing tabular and image features for network prediction has the potential to augment a range of CV solutions and improve model performance.

Funding: This research is funded by the Department of Defense Science, Mathematics, and Research for Transformation (SMART) SEED Grant.

MapperEEG: A Topological Approach to Brain State Clustering in EEG Recordings

Brittany Story[1,*], Zhibin Zhou[2], Ramesh Srinivasan[2], and Piotr J. Franaszczuk[1,3]
[1]DEVCOM Army Research Laboratory, 7101 Mulberry Point Rd., Aberdeen Proving Ground, MD 21005
[2]University of California, Irvine, 3151 Social Sciences Plaza, Irvine, CA 92617
[3]Johns Hopkins University School of Medicine, 733 N. Broadway, Baltimore, MD 21205
**Corresponding Author Email: brittany.m.story.civ@army.mil*
Keywords: Clustering brain states, functional structure, topological signal processing, EEG clustering

Electrical potential scalp recordings (Electroencephalograms-EEGs) are a common tool used to investigate brain activity. EEG is routinely used in clinical applications as well as in research studies thanks to its noninvasive nature, relatively inexpensive equipment, and high temporal resolution. But EEG is prone to contamination from movement artifacts and signals from external sources. Thus, it requires advanced signal processing and mathematical analysis methods in tasks requiring brain state identification. Recently, tools from topological data analysis have been used successfully across many domains, including brain research, however these uses have been limited to fMRI datasets [1, 3, 4]. We introduce the topological tool MapperEEG (M-EEG) and provide an example of its ability to separate different brain states during a simple finger tapping teaming task without any pre-labeling or prior knowledge. M-EEG uses the power spectral density applied to traditional EEG frequency bands combined with the Mapper algorithm from topological data analysis to capture the underlying structure of the data and represent that structure as a graph in two-dimensional space [5, 6]. This tool provides clear separation (clustering) of states during different conditions of the experiment (syncopated vs. synchronized) and we demonstrate that M-EEG outperforms other clustering methods when applied to EEG data [2].

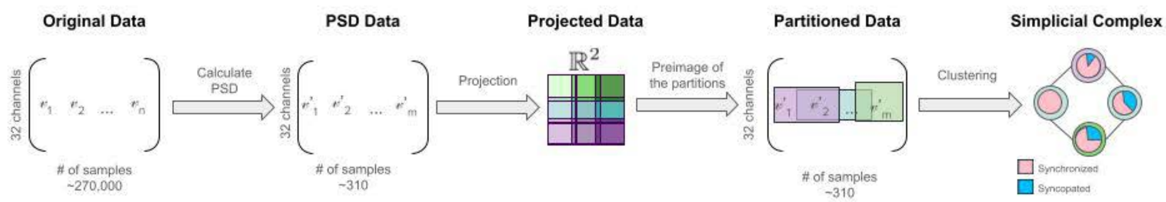

Fig. 1 – An example of the Mapper algorithm with projection function $tSNE: \mathbb{R} \to \mathbb{R}^2$. We cover the 2-dimensional plane with boxes that overlap a certain amount. Then, we cluster points in $\mathbb{R}^2$ based off the label assigned to the each of the points in the projection space and clustering-based distance. If points fall into two clusters, we denote this by connecting those clusters. Thus, we represent the structure of the data as the simplicial complex on the right side of the figure, which captures the relevant topological information.

Funding: Research was accomplished under Cooperative Agreement Number W911NF-24-2-0013.

References:

[1] Hasegan, D., Geniesse, C., Chowdhury, S., & Saggar, M. (2024). Deconstructing the mapper algorithm to extract richer topological and temporal features from functional neuroimaging data. *Network Neuroscience*.

[2] Pinto, I. I. L. D., Zhou, Z., Garcia, J. O., & Srinivasan, R. (2025). Symbolic dynamics of joint brain states during dyadic coordination. Chaos: An Interdisciplinary Journal of Nonlinear Science, 35(1), 013110. https://doi.org/10.1063/5.0234902

[3] Saggar, M., Shine, J. M., Liégeois, R., & et al. (2022). Precision dynamical mapping using topological data analysis reveals a hub-like transition state at rest. *Nature Communications*, *13*, 4791.

[4] Saggar, M., Sporns, O., Gonzalez-Castillo, J., & et al. (2018). Towards a new approach to reveal dynamical organization of the brain using topological data analysis. *Nature Communications*, *9*, 1399.

[5] Singh, G., Memoli, F., & Carlsson, G. (2007). Topological methods for the analysis of high dimensional data sets and 3D object recognition. In M. Botsch, R. Pajarola, B. Chen, & M. Zwicker (Eds.), *Eurographics Symposium on Point-Based Graphics*. The Eurographics Association.

[6] van Veen, H. J., Saul, N., Eargle, D., & Mangham, S. W. (2020). Kepler Mapper: A flexible Python implementation of the Mapper algorithm.

1 (PDF)	DEFENSE TECHNICAL INFORMATION CTR DTIC OCA
1 (PDF)	DEVCOM ARL FCDD RLB CI TECH LIB